

**Inflammation-dependent differentiation of two  
distinct regulatory T cell populations in the  
visceral adipose tissue shapes systemic  
metabolism**

**Stalin Santiago Valle Torres**

ORCID ID:  
0000-0003-1430-6716

from Quito, Ecuador

Submitted in total fulfilment of the requirements of the joint  
degree of Doctor of Philosophy (PhD)

of

The Medical Faculty

The Rheinische Friedrich-Wilhelms-Universität Bonn

and

The Department of Microbiology and Immunology

The University of Melbourne

Bonn/Melbourne, 2023

Performed and approved by The Medical Faculty of The Rheinische Friedrich-Wilhelms-Universität Bonn and The University of Melbourne

- 1. Supervisor: Prof. Christoph Wilhelm, PhD
- 2. Supervisor: Prof. Dr. Axel Kallies
- Co-Supervisors: Dr. Marc Beyer  
Dr. Ajithkumar Vasanthakumar

Original thesis submission: September 2022

Oral examination: November 2023

Institute for Clinical Chemistry and Clinical Pharmacology

Director: Prof. Dr. med. Gunther Hartmann

## Table of Contents

<b>Abbreviations</b> .....	<b>IV</b>
<b>List of Tables</b> .....	<b>VI</b>
<b>List of Figures</b> .....	<b>VII</b>
<b>Abstract</b> .....	<b>X</b>
<b>Declaration</b> .....	<b>XI</b>
<b>Preface</b> .....	<b>XII</b>
<b>Acknowledgements</b> .....	<b>XIII</b>
<b>Publications</b> .....	<b>XV</b>
<b>Chapter 1 – Introduction</b> .....	<b>1</b>
<b>1.1 Adipose tissue</b> .....	<b>1</b>
1.1.1 Adipose tissue distribution and function .....	1
1.1.2 Sexual divergence in the VAT .....	3
1.1.3 VAT inflammation and immunity in health and disease .....	5
<b>1.2 Regulatory T cells</b> .....	<b>7</b>
1.2.1 Treg cell function .....	8
1.2.2 Treg cell development and differentiation .....	8
1.2.3 Treg cell diversity and plasticity .....	9
<b>1.3 VAT Treg cells</b> .....	<b>15</b>
1.3.1 VAT Treg cell phenotype and function .....	15
1.3.2 VAT Treg cell regulation .....	16
1.3.3 VAT Treg cell precursors .....	17
1.3.4 VAT Treg cell in humans and obesity .....	18
<b>1.4 Study Aims</b> .....	<b>19</b>
<b>Chapter 2 – Material &amp; Methods</b> .....	<b>20</b>
<b>2.1 Buffers and Media</b> .....	<b>20</b>
<b>2.2 Animal Models</b> .....	<b>21</b>
2.2.1 Mice .....	21
2.2.2 Bone marrow reconstitution of chimeric mice .....	22
2.2.3 Adoptive transfer .....	23
2.2.4 High-fat diet (HFD) .....	23
2.2.5 Treg cell recovery .....	23
2.2.6 IL-33 treatment .....	23
2.2.7 Glucose Tolerance Test .....	23
2.2.8 Metabolic Cages .....	24
2.2.9 Body Composition Analysis .....	24

<b>2.3 Procedures for cellular immunology</b> .....	<b>25</b>
<b>2.3.1 Processing explanted organs for lymphocyte isolation and/or analysis</b> .....	<b>25</b>
<b>2.3.2 Cell culture</b> .....	<b>26</b>
<b>2.3.3 Ex vivo restimulation of T cells</b> .....	<b>26</b>
<b>2.3.4 Antibodies and flow cytometry</b> .....	<b>26</b>
<b>2.3.5 Intravascular staining</b> .....	<b>29</b>
<b>2.4 Procedure of molecular immunology</b> .....	<b>30</b>
<b>2.4.1 Polymerase chain reaction for PCR genotyping</b> .....	<b>30</b>
<b>2.4.2 RNA-sequencing and bioinformatic analysis</b> .....	<b>31</b>
<b>2.4.3 Single-cell RNA-Seq and bioinformatics</b> .....	<b>32</b>
<b>2.5 Statistics</b> .....	<b>35</b>
<b>Chapter 3 – Cellular characterization of regulatory T cells in male and female VAT</b> .....	<b>36</b>
<b>3.1 VAT harbours a heterogenous population of Treg cells</b> .....	<b>36</b>
<b>3.2 ST2 and CXCR3 define two distinct mature VAT Treg cell populations</b> .....	<b>39</b>
<b>3.3 CXCR3+ VAT Treg cells are tissue resident</b> .....	<b>42</b>
<b>3.4 CD62L+ (DN) VAT Treg cells are precursors for CXCR3+ and ST2+ VAT Treg cells</b> .....	<b>43</b>
<b>3.5 Development of the VAT Treg cell compartment</b> .....	<b>48</b>
<b>3.6 CXCR3+ and ST2+ VAT Treg cells correlate differently to body and VAT weight</b> .....	<b>52</b>
<b>3.7 Variation in weight gain and metabolic phenotype of high fat diet fed mice</b> .....	<b>54</b>
<b>3.8 High-fat diet has little impact on VAT Treg cell composition</b> .....	<b>56</b>
<b>3.9 VAT Treg cell composition in other adipose tissue depots and mouse models</b> .....	<b>59</b>
<b>3.10 Characterization of immune and non-immune cell populations in the VAT</b> .....	<b>61</b>
<b>Chapter 4 – Molecular regulation of ST2+ and CXCR3+ VAT Treg cells</b> ...	<b>65</b>
<b>4.1 PPAR<math>\gamma</math> is required for ST2+ but not CXCR3+ VAT Treg cell differentiation</b> .....	<b>65</b>
<b>4.2 PPAR<math>\gamma</math> impacts Treg cells in other lymphoid and non-lymphoid organs</b> .....	<b>69</b>
<b>4.3 GATA3 promotes the differentiation of ST2+ VAT Treg cells</b> .....	<b>74</b>
<b>4.4 Loss of GATA3 impacts Treg cells in other lymphoid and non-lymphoid organs</b> .....	<b>77</b>
<b>4.5 T-bet depletion results in expansion of ST2+ VAT Treg cells in female mice</b> .....	<b>82</b>

4.6 T-bet expression in Treg cells is required for CXCR3+ VAT Treg cell differentiation .....	88
4.7 Sirt1 contributes to ST2+ VAT Treg cell differentiation.....	93
4.8 Treg specific ablation of TGF $\beta$ R2 significantly impairs VAT Treg cell differentiation and function.....	97
<b>Chapter 5 – Interplay between VAT Treg cells and the VAT microenvironment.....</b>	<b>103</b>
5.1 Cytokines and chemokines shape sex differences in the VAT.....	103
5.2 IFN- $\gamma$ deficiency leads to ST2+ VAT Treg cell expansion and T cell infiltration .....	110
5.3 IFN $\alpha$ R2 deficiency induces minor changes in VAT T cell composition .....	116
5.4 IL-33 shapes both, ST2+ and CXCR3+ VAT Treg cells and regulates CD8+ T cell infiltration .....	119
5.8 High-fat diet induces TNF and IFN- $\gamma$ production in males but not T cell infiltration .....	123
<b>Chapter 6 – Functions of ST2+ and CXCR3+ VAT Treg cells .....</b>	<b>128</b>
6.1 Elevated T cell infiltration and IFN- $\gamma$ expression in the VAT after systemic Treg depletion .....	128
6.2 GATA3 dependent ST2+ VAT Treg cells are required to regulate T cell infiltration and cytokine production .....	131
6.3 Depletion of CXCR3+ but not ST2+ VAT Treg cells significantly impact T cell and cytokine homeostasis in the VAT.....	134
6.5 Loss of IFN- $\gamma$ impacts adiposity but not metabolism in males.....	144
6.6 Treg cell specific PPAR $\gamma$ and GATA-3 but not T-bet depletion results in impaired glucose tolerance in male mice .....	150
<b>Chapter 7 – Discussion .....</b>	<b>155</b>
7.1 VAT Treg cell heterogeneity.....	157
7.2 Environmental factors that affect VAT Treg cell composition.....	159
7.3 Development of VAT Treg cells .....	163
7.4 Molecular regulation and function of VAT (tissue) Treg cells .....	165
7.5 ST2+ and CXCR3+ VAT Treg cells in obesity .....	169
7.6 Conclusion.....	170
<b>References.....</b>	<b>171</b>

## Abbreviations

T2D	Type 2 Diabetes
AT	Adipose tissue
WAT	White adipose tissue
BAT	Brown adipose tissue
SAT	Subcutaneous adipose tissue
VAT	Visceral adipose tissue
pnAT	Perinephric adipose tissue
IL	Interleukin
TNF	Tumour necrosis factor
UCP1	Uncoupling protein 1
PPAR	Peroxisome proliferator-activated receptor
IFN	Interferon
GATA3	GATA binding protein 3
T-bet	T box expressed in T cell
ICOS	Inducible co-stimulator
KLRG1	Killer cell lectin like receptor G1
ST2	Suppression of tumorigenicity 2
TGF $\beta$	Transforming growth factor $\beta$
ILC	Innate lymphoid cell
NK	Natural killer
T <sub>H</sub>	T helper
MIP	Macrophage inflammatory protein
MCP	Monocyte chemoattractant protein
ER	Estrogen receptor
SVF	Stromovascular fraction
IPEX	Immunodysregulation polyendocrinopathy enteropathy X-linked syndrome
Foxp3	Forkhead box P3
Tconv	Conventional T cells

Treg	Regulatory T cells
CTLA-4	Cytotoxic T-lymphocyte-associated protein 4
TCR	T cell receptor
CCR	Chemokine receptor
GITR	Glucocorticoid-induced tumor necrosis factor receptor
IRF4	Interferon regulatory factor 4
Blimp1	B lymphocyte induced maturation protein 1
Gzmb	Granzyme B
ROR	Retinoid orphan receptor
STAT4	Signal transducer and activator of transcription 4
eTreg	Effector Treg
pTreg	Peripheral Treg
nTreg	Natural Treg
iTreg	Inducible Treg
DC	Dendritic cells
Nrp1	Neuropilin1
BATF	Basic leucine zipper ATF-like transcription factor
MSC	Mesenchymal stromal cell
scRNASeq	Single cell RNA sequencing
DT	Diphtheria toxin
DTR	Diphtheria toxin receptor
TCF-1	T cell factor 1
ND	Normal diet
HFD	High-fat diet

**List of Tables**

<b>Table 1</b>   Mouse lines .....	21
<b>Table 2</b>   Antibody list .....	27
<b>Table 3</b>   List of primer for genotyping .....	30

## List of Figures

Figure 1   Molecular and cellular mediators of VAT inflammation. ....	17
Figure 2   VAT harbours a heterogenous population of Treg cells. ....	39
Figure 3   ST2+ and CXCR3+ VAT Treg cells display different enrichment and phenotype in male and female mice. ....	42
Figure 4   CXCR3+ Treg cells are VAT resident cells. ....	43
Figure 5   CXCR3+ and ST2+ VAT Treg cells have different developmental trajectories. ....	46
Figure 6   CXCR3+ and CD62L+ Treg cells emerge first after Treg depletion. ....	47
Figure 7   VAT Treg cell composition is different in young adult mice. ....	49
Figure 8   VAT Treg cell population do not change significantly with progressing age. ....	51
Figure 9   ST2+ VAT Treg cells positively correlate with adiposity. ....	54
Figure 10   High-fat diet induces different phenotypes in glucose metabolism. ....	55
Figure 11   High-fat diet has a different impact on Treg cells in female and male mice. ....	58
Figure 12   VAT Treg cell distribution in other adipose tissue compartments and mouse models. ....	60
Figure 13   Stromal cell composition in the VAT is similar in C57BL/6 and Balb/c mouse models. ....	63
Figure 14   Myeloid cells in the VAT. ....	64
Figure 15   PPAR $\gamma$ is required for ST2+ but not CXCR3+ VAT Treg cells. ....	68
Figure 16   PPAR $\gamma$ impacts GATA3 expression in male VAT Treg cells. ....	68
Figure 17   KLRG1 and Foxp3 expression are affected in splenic Treg cells that lack PPAR $\gamma$ . ....	70
Figure 18   PPAR $\gamma$ -depleted mice have a reduced ROR $\gamma$ t+ Treg cell compartment in the gut. ....	72
Figure 19   CXCR3 and Ki67 expression is impacted by PPAR $\gamma$ depletion in gut resident Treg cells. ....	73
Figure 20   GATA3 is essential for the differentiation of ST2+ VAT Treg cells. ....	75
Figure 21   Loss of GATA3 induces proliferation of CXCR3+ VAT Treg cells. ....	76
Figure 22   GATA3 depletion leads to expansion of splenic Treg cells in males and females. ....	78
Figure 23   Gut resident ROR $\gamma$ t+ Treg cells expand in absence of GATA3. ....	80
Figure 24   GATA3 is required for KLRG1+ but not CXCR3+ lung resident Treg cells. ....	82
Figure 25   T-bet is expressed predominantly in CXCR3+ Treg cells in VAT and spleen. ....	85
Figure 26   ST2+ VAT Treg cells emerge in females in response to whole body depletion of T-bet. ....	86

Figure 27   KLRG1+ and ST2+ splenic Treg cells expand in absence of T-bet.....	87
Figure 28   <i>Tbx21</i> <sup>-/-</sup> cells accumulate as DN Treg cells in mixed bone marrow chimeric mice.....	89
Figure 29   ST2+ VAT Treg cells are increased in <i>Tbx21</i> <sup>fl/fl</sup> <i>Foxp3</i> <sup>Cre</sup> female mice.....	90
Figure 30   ST2+ VAT Treg cells emerge from infiltrating cells in female <i>Tbx21</i> <sup>fl/fl</sup> <i>Foxp3</i> <sup>Cre</sup> mice.....	92
Figure 31   Splenic KLRG1+ Treg cell population is increased in female <i>Tbx21</i> <sup>fl/fl</sup> <i>Foxp3</i> <sup>Cre</sup> mice.....	93
Figure 32   Treg cell specific <i>Sirt1</i> ablation impacts ST2+ and CXCR3+ VAT Treg cells modestly.....	95
Figure 33   Splenic Treg cells are unaltered in <i>Sirt1</i> <sup>fl/fl</sup> <i>Foxp3</i> <sup>Cre</sup> mice.....	96
Figure 34   TGFβ promotes ST2+ but restrains the differentiation of CXCR3+ VAT Treg cells.....	100
Figure 35   CD8+ T cells are significantly reduced in male <i>Tgfb2</i> <sup>fl/fl</sup> <i>Foxp3</i> <sup>Cre</sup> mice.....	102
Figure 36   T <sub>H</sub> 1 and T <sub>H</sub> 2 type cytokines are differentially expressed in male and female mice.....	106
Figure 37   Cytokine production in young adult mice is different from mature mice.....	107
Figure 38   CXCR3 ligands CXCL9 and CXCL10 production is higher in female mice compared to male mice.....	109
Figure 39   IFN-γ depletion induces expansion of ST2+ VAT Treg cells in female and male mice.....	111
Figure 40   ST2+ <i>Foxp3</i> <sup>-</sup> cells expand in absence of IFN-γ in both sexes.....	114
Figure 41   IL-5 production is significantly enhanced in <i>Ifng</i> <sup>-/-</sup> mice.....	116
Figure 42   VAT Treg cell numbers are increased in <i>Ifnar2</i> <sup>-/-</sup> male mice.....	117
Figure 43   IFNαR2 ablation leads to the reduction of CD8+ and CXCR3+ <i>Foxp3</i> <sup>-</sup> VAT cells.....	118
Figure 44   IL-33 signalling promotes ST2+ and inhibits CXCR3+ VAT Treg cell differentiation.....	121
Figure 45   CD8+ T cells expand in absence of IL-33-dependent signalling.....	123
Figure 46   Cellular infiltration is not substantially altered in high-fat diet fed mice.....	125
Figure 47   TNF, IL5 and IL13 cytokine production is reduced upon high-fat diet.....	127
Figure 48   T cell infiltration and IFN-γ production is substantially increased in the VAT after Treg cell depletion.....	130
Figure 49   Treg cell specific ablation of GATA3 leads to increased T cell infiltration and inflammatory cytokine production.....	134
Figure 50   CD8+ T cells expand in <i>Tbx21</i> <sup>fl/fl</sup> <i>Foxp3</i> <sup>Cre</sup> but not <i>Pparg</i> <sup>fl/fl</sup> <i>Foxp3</i> <sup>Cre</sup> mice.....	136
Figure 51   TNF production is reduced in <i>Tbx21</i> <sup>fl/fl</sup> <i>Foxp3</i> <sup>Cre</sup> mice.....	138
Figure 52   CXCR3+ but not ST2+ VAT Treg depletion leads to increased VAT inflammation.....	142

<b>Figure 53   Depletion of CXCR3+ Treg cells blunt the sex-specific transcriptional differences in VAT .....</b>	<b>144</b>
<b>Figure 54   Male <i>Ifng</i><sup>-/-</sup> mice have reduced VAT and body weight compared to controls. ....</b>	<b>145</b>
<b>Figure 55   Male <i>Ifng</i><sup>-/-</sup> mice have reduced lean mass compared to controls. ....</b>	<b>147</b>
<b>Figure 56   <i>Ifng</i><sup>-/-</sup> mice have reduced lean and fat mass compared to controls on a high-fat diet. ....</b>	<b>149</b>
<b>Figure 57   ST2+ and CXCR3+ VAT Treg cells regulate different aspects of VAT physiology and metabolism. ....</b>	<b>151</b>
<b>Figure 58   GATA-3 but not TGFβR2 depletion affects glucose metabolism .....</b>	<b>153</b>
<b>Figure 59   VAT Treg cell development, phenotype, and function. ....</b>	<b>156</b>

**Abstract**

Visceral adipose tissue (VAT) is an endocrine organ critical for energy storage and metabolic homeostasis. It harbours a plethora of immune cells, which play an important role in maintaining tissue homeostasis. A large body of work has shown that type 2 immune cells including T helper (T<sub>H</sub>2) cells, type 2 innate lymphoid cells (ILC2) and anti-inflammatory macrophages are associated with a healthy VAT and metabolic state. On the other hand, infiltration of inflammatory immune cells, such as CD8<sup>+</sup> T cells, pro-inflammatory macrophages, and T<sub>H</sub>1 cells, result in type 1 inflammation and ultimately lead to insulin resistance and development of metabolic disease.

Foxp3<sup>+</sup> regulatory T (Treg) cells are critical to restrain VAT inflammation and preserve glucose tolerance. We and others have previously demonstrated that VAT Treg cells are dependent on the adipogenesis transcription factor PPAR $\gamma$  and the cytokine IL-33 for their differentiation and maintenance. Further, we have shown that VAT Treg cells display sexual dimorphism on a cellular and transcriptional level. These differences are orchestrated by IL-33 and sex hormones that underpin VAT inflammation and metabolic phenotype. How precisely VAT inflammation and microenvironment shape Treg cell differentiation and function in males and females, however, is still insufficiently known. Here we uncover that the VAT harbours two distinct Treg cell populations, prototypical ST2<sup>+</sup> Treg cells, that are enriched in males and depend on IL-33 and PPAR $\gamma$ , and a previously uncharacterized population of VAT Treg cells that express the chemokine receptor CXCR3, are enriched in females and depend on the transcription factor T-bet and cytokine IFN- $\gamma$ . We also reveal that the transcription factor GATA3 promoted differentiation of ST2<sup>+</sup> VAT Treg cells and together with PPAR $\gamma$  and IL-33 repressed the differentiation of CXCR3<sup>+</sup> Treg cells. We further show that CXCR3<sup>+</sup> VAT Treg cells developed from naïve Treg cells in a cytokine IFN- $\gamma$  dependent manner. Finally, we demonstrate that ST2<sup>+</sup> Treg cells controlled blood glucose levels, while CXCR3<sup>+</sup> Treg cells limited VAT inflammation. Overall, this study establishes the developmental trajectories of two molecularly and functionally distinct Treg cell types in the VAT that act in a sex-specific manner.

**Declaration**

The work that is presented in this thesis was conducted at The University of Melbourne and The Rheinische Friedrich-Wilhelms-Universität Bonn in the laboratories of Professor Axel Kallies (The Peter Doherty Institute, Melbourne) and Dr Marc Beyer (German Centre for Neurodegenerative Diseases, Bonn). I was supported by the Melbourne International Research Scholarship and the Melbourne International Fee Remission Scholarship.

This is to certify that

- I. the thesis comprises only my original work towards the PhD except where indicated in the Preface,
- II. due acknowledgement has been made in the text to all other material used,
- III. the thesis is less than 100,000 words in length, exclusive of tables, maps, bibliographies and appendices.

Santiago Valle Torres

## **Preface**

I acknowledge the important contributions of others to experiments presented herein.

## **Chapter 3**

Single-cell RNASeq experiments and analyses were performed by Tarek ElMazzahi in Dr Marc Beyer's laboratory. Data derived from this analysis is used in **chapter 5**.

## **Chapter 6**

Bioinformatic analysis of bulk RNA-Seq data was performed by Dr David Chisanga from the Olivia Newton John Cancer Research Institute.

Metabolic cage measurements were performed by Dr Vanessa Haynes from the Melbourne Mouse Metabolic Phenotyping Platform

## **Acknowledgements**

I want to thank my Melbourne-supervisor Prof Axel Kallies for giving me the opportunity to work in his lab and be involved in a very interesting and exciting project. I also want to thank my co-supervisor Dr Ajith Vasanthakumar for guiding me through the first months of my PhD and giving me important practical advice. And lastly, I would like to thank both of my supervisors for your support, encouragement, patience, wisdom and compassion which has been very important during the pandemic. This has helped me tremendously to grow on a professional and personal level.

Thank you to Prof Matthew Watt and Prof Sammy Bedoui for your helpful advice and assistance in navigating my PhD which have been instrumental for my completion.

I am grateful to Dr Marc Beyer and Tarek for the single-cell RNASeq analysis and intellectual input to this project.

I also want to thank the administrative team Dr Marie Greyer, Dr Annabelle Blum and Lucie Delforge for the organisation and implementation of the Bonn&Melbourne Graduate School.

I would like to thank Dr Vanessa Haynes for their assistance with metabolic cage setup and analysis.

I would also like to thank Dr Joanna Groom for providing T-bet reporter and floxed mice and Dr Nancy Wang for IFN- $\gamma$  KO mice.

Furthermore, I would like to thank the Kallies group for creating a great work environment that included fun conversations, lunches or pub nights. I would like to specially thank Teisha for your extensive support in the lab but also for moral support and lab shenanigans

Also, many thanks to my friends in Melbourne in and out of the lab that made this experience so much easier.

Y finalmente quiero agradecer a mi familia con la cual no estaria en la posicion actual. Muchas gracias por el apoyo incondicional que me ha ayudado ha realizar este doctorado y ver partes del mundo que no crei seria posible. Gracias.

## **Publications**

Vasanthakumar A, Chisanga D, Blume J, Gloury R, Britt K, Henstridge DC, Zhan Y, **Torres SV**, Liene S, Collins N, Cao E, Sidwell T, Li C, Spallanzani RG, Liao Y, Beavis PA, Gebhardt T, Trevaskis N, Nutt SL, Zajac JD, Davey RA, Febbraio MA, Mathis D, Shi W, Kallies A. Sex-specific adipose tissue imprinting of regulatory T cells. *Nature*. 2020 Mar;579(7800):581-585. doi: 10.1038/s41586-020-2040-3. Epub 2020 Feb 26.

## **Chapter 1 – Introduction**

### **1.1 Adipose tissue**

Globally obesity has risen drastically which has increased the incidence of associated metabolic morbidities such as type 2 diabetes mellitus (T2D), kidney, eye and liver injury among others (The Emerging Risk Factors, 2010). According to the international diabetes foundation, in 2021 more than 537 million people were living with diabetes worldwide, with a higher prevalence in men compared to women. Accumulation of white adipose tissue, particularly in the visceral region, is accompanied by increased secretion of inflammatory mediators by local immune cells enhancing inflammation that effectively poses a higher risk for the development of T2D and other obesity associated diseases (Cildir, Akincilar, & Tergaonkar, 2013). Therefore, it is crucial to understand the interplay between adipose tissue (AT), metabolism and the immune system to help design efficient therapies to counteract obesity induced diseases.

#### **1.1.1 Adipose tissue distribution and function**

White adipose tissue (WAT) is classically regarded as the main site to store energy in form of lipids. White adipocytes are large round cells that store lipids in the form of triglycerides in large unilocular lipid droplets. The WAT is distributed in discrete locations throughout the body. However, subcutaneous (SAT) and visceral adipose tissue (VAT) depots are the most abundant in mammals and has relevance to systemic metabolism. The most prominent SAT depots in humans are located in the abdominal and gluteofemoral area, of which the latter is most prominent in mice. In the peritoneal cavity, omental, mesenteric, pericardial and retroperitoneal AT depots conform the main human VAT (Chusyd, Wang, Huffman, & Nagy, 2016; Cinti, 2012). To explore VAT biology, most studies have made use of rodent models. The best investigated depot in mice is the perigonadal AT, that is also present but significantly smaller in humans. It is located around the testes in male and along the uterus in female mice near the intestinal tract. Since perigonadal AT is the best studied depot in rodents and the

focus in the current study, perigonadal AT will be referred to as VAT for the rest of the study.

A clear distinction between SAT and VAT is important as they have different impact on systemic metabolism (Galic, Oakhill, & Steinberg, 2010). SAT is generally regarded as beneficial to systemic metabolism demonstrated by transplantation of SAT in the peritoneum of rodents that improves metabolic health (Tran & Kahn, 2010). Conversely, VAT is regarded as deleterious, corroborated by VAT lipectomy that has the same effect as SAT transplantation (Gabriely et al., 2002; Lu et al., 2012; Muzumdar et al., 2008). Typically, SAT expands through hyperplasia (cell proliferation) whereas VAT expands through hypertrophy (cell size increase). This might be a contributing factor as hyperplasia prevents cell death, inflammation and metabolic dysfunction in the former (Q. A. Wang, Tao, Gupta, & Scherer, 2013). Increased resistance to adipocyte cell death and differential release of adipokines are potential factors that contribute to these opposing functions in metabolism (Clegg, Brown, Woods, & Benoit, 2006; Karastergiou et al., 2013; Manolopoulos, Karpe, & Frayn, 2010; Murano et al., 2008; Tran, Yamamoto, Gesta, & Kahn, 2008; Woods, 2003).

Adipokines are referred to as a group of molecules, secreted by adipocytes or other cells within the AT. To this group belong hormones such as leptin and adiponectin, that have opposing roles in nutrition and fatty acid homeostasis (Kautzky-Willer, Harreiter, & Pacini, 2016), and inflammatory cytokines such as interleukin (IL)1- $\beta$ , IL-6 and tumour necrosis factor (TNF). Adipokines exert their function by targeting neural pathways, local adipocytes, adipocyte progenitors, endothelial cells and local immune cells (E. D. Rosen & Spiegelman, 2014). They have a significant impact on metabolic health since systemic adipokine levels rise with increasing fat mass, ultimately leading to metabolic dysfunction (Fontana, Eagon, Trujillo, Scherer, & Klein, 2007).

Adipocytes also have a high degree of plasticity. Apart from white adipocytes, most mammals have brown adipocytes that have different function compared to white adipocytes. Adipocytes can differentiate and de-differentiate between brown and white state (Vitali et al., 2012). As opposed to white adipocytes, brown adipocytes are smaller polygonal cells that store lipids in multiple droplets

(Giordano, Frontini, & Cinti, 2016). Reports have shown that brown adipocytes are found together with white adipocytes in most depots and are not used as energy reservoirs but rather serve to dissipate energy in the form of heat (Morrison, Madden, & Tupone, 2014). This is mediated via uncoupling protein-1 (UCP1) which is uniquely found in mitochondria of adipocytes with thermogenic function (Vitali et al., 2012). In response to cold exposure or caloric restriction, thermogenesis is induced in UCP1-expressing cells. They are regarded as beneficial for metabolic health. Studies have shown that obesity resistant mice have up to five times more brown adipocytes than obesity prone mice (Vitali et al., 2012).

Thus, the relationship between metabolism and AT is complex as multiple factors such as location, inflammation and adipocyte composition affect it. A large body of work has demonstrated that most of these factors show sex-specific differences in mouse and human which in turn influences their metabolic phenotype.

### **1.1.2 Sexual divergence in the VAT**

Sexual differences in general adipose tissue biology and metabolism have been described in various studies. Inherent sexual/hormonal differences affect AT distribution and size. Women have higher adiposity that mainly collects in SAT depots around the gluteofemoral region. In contrast, men tend to accumulate VAT which is deleterious to metabolism with increasing size (Arnetz, Rajamand Ekberg, & Alvarsson, 2014; Fuente-Martín, Argente-Arizón, Ros, Argente, & Chowen, 2013a; Karastergiou, Smith, Greenberg, & Fried, 2012; Kautzky-Willer et al., 2016; Mauvais-Jarvis, Clegg, & Hevener, 2013).

Accordingly, incidence of T2D is higher in males compared to females suggesting the importance of sex-specific factors in development of metabolic disease. Indeed, AT distribution is considered an important factor to predict susceptibility to develop T2D. Obese individuals with gynoid (female-like) obesity, have lower risk to develop T2D and are considered metabolically healthy, as opposed to individuals with android (man-like) obesity independent of their sex (Arnetz et al.,

2014; Fuente-Martín, Argente-Arizón, Ros, Argente, & Chowen, 2013b; Jensen, Haymond, Rizza, Cryer, & Miles, 1989; Karastergiou et al., 2012; Kautzky-Willer et al., 2016; Koster et al., 2010; Manolopoulos et al., 2010; Mauvais-Jarvis et al., 2013; White & Tchoukalova, 2014; Woods, 2003). This is also concordant with an increased occurrence of T2D in older individuals since redistribution of AT, more specifically depletion of SAT and accumulation of VAT are hallmarks of ageing in rodents and humans (Tchkonina et al., 2010).

Furthermore, hormones play a significant role in regulating adipose tissue formation and distribution. Estradiol can suppress food intake as shown in women that eat significantly less when estradiol levels peak during the menstrual cycle (Palmer & Clegg, 2015). The distinct function and distribution of estrogen receptors (ER)  $\alpha$  and  $\beta$  also plays a role in adiposity. ER $\alpha$  functions to reduce adiposity through lipolysis while ER $\beta$  opposes that function (Gavin, Cooper, Raymer, & Hickner, 2013; Lindberg et al., 2002; Tramunt et al., 2020). In line with this notion, ER $\alpha$ /ER $\beta$  ratio is higher in female VAT compared to SAT to prevent AT accumulation in the former. Since ER $\alpha$  expression is relatively low in the VAT of males, they lack this protective mechanism (Davis et al., 2013; Gavin, Cooper, & Hickner, 2013). In agreement with this notion, conditions that result in severe hormonal imbalance including obesity, menopause or androgen deprivation therapy, contribute to accumulation of VAT and development of metabolic disease (Camhi et al., 2011; Goodman-Gruen & Barrett-Connor, 1996; Varghese, Griffin, & Singer, 2017). This is supported by studies that linked hormone expression and signalling to metabolic health. Multiple studies have shown that estrogens protect against adiposity, dampen inflammatory signalling and improve insulin activity (Brussaard et al., 1997; Evans, Eckert, Lai, Adelman, & Harnish, 2001; C. C. Lee, Kasa-Vubu, & Supiano, 2003; Ribas et al., 2010; Sun, Keller, Stebler, & Ershler, 1998). Furthermore, estrogen receptor  $\alpha$  and  $\beta$  activation directly impacts cellular metabolism (J.-Q. Chen, Cammarata, Baines, & Yager, 2009) and also regulates the expression of glucose intake receptor Glut4 and Peroxisome proliferator activated receptor (PPAR) $\gamma$  (Rüegg et al., 2011; H. Zhang, Chen, & Sairam, 2012) which has protective effects on metabolic health in both sexes (Heine, Taylor, Iwamoto, Lubahn, & Cooke, 2000; Ribas et al.,

2010; Smith et al., 1994). Androgen signalling however appears to act in a sex-specific manner to regulate metabolic health. Androgen administration positively impacts insulin sensitivity in male but induces the opposite effects in female AT (Corbould, 2007; Varlamov et al., 2012). Furthermore, females with higher androgen levels have heightened body weight (Elbers, Asscheman, Seidell, Megens, & Gooren, 1997), whereas men with lower testosterone levels, in part due to accelerated conversion of testosterone to oestradiol (aromatization), have an increased risk to develop T2D (Ding, Song, Malik, & Liu, 2006; Kautzky-Willer et al., 2016). Additionally, AT specific depletion of the androgen receptor prevents male mice from becoming obese (Macotela, Boucher, Tran, & Kahn, 2009; Varlamov et al., 2012).

Intact adipocytes, advantageous AT distribution and anti-inflammatory microenvironment are therefore crucial for a healthy metabolism. Although adipocytes can produce adipokines and contribute to VAT inflammation, it is mainly local immune cells that shape the inflammatory environment by secretion of high levels of cytokines. The non-adipocyte part of the VAT stromovascular fraction (SVF) is composed of multiple cell types including mesenchymal stromal cells, endothelial cells, and immune cells. Crosstalk between these cell types determines the function of VAT and therefore central to preserve systemic metabolism.

### **1.1.3 VAT inflammation and immunity in health and disease**

In lean mice the VAT is characterized by type 2 inflammation with a predominance of T (helper)  $T_H2$  cells, innate lymphoid cell (ILC)2 and anti-inflammatory macrophages (Diane Mathis, 2013; Shu, Benoist, & Mathis, 2012). Cytokines associated with type 2 inflammation include IL-4, IL-5 and IL-13 that are largely produced by  $T_H2$  cells and ILC2 (Licona-Limón, Kim, Palm, & Flavell, 2013). Furthermore, lean VAT is enriched in regulatory T (Treg) cells, which are potent suppressors of inflammation (Markus Feuerer et al., 2009). Increase in AT mass, particularly in VAT, is accompanied by increased adipokine secretion which induces sustained low-grade inflammation in VAT, and effectively poses a

higher risk for the development of T2D and other obesity associated diseases (Cildir et al., 2013; Xu et al., 2003).

The type 2 environment reigning in lean subjects switches to a type 1 inflammatory phenotype by infiltration and expansion of pro-inflammatory macrophages, neutrophils, ILC1, B cells,  $T_H1$  and  $CD8^+$  T cells (Boulenouar et al., 2017; DeFuria et al., 2013; Ferrante, 2013; Michael J.; Kraakman et al., 2015; Carey N. Lumeng, Bodzin, & Saltiel, 2007; C. N. Lumeng, Deyoung, Bodzin, & Saltiel, 2007; O'Sullivan et al., 2016; Osborn & Olefsky, 2012; Weisberg et al., 2003; Xu et al., 2003). Pro-inflammatory macrophages form crown-like structures around dead adipocytes marking the exacerbation of inflammation in VAT (Murano et al., 2008; Weisberg et al., 2003). Macrophages and obese AT also secrete pro-inflammatory cytokines including, interferon (IFN), TNF, monocyte chemoattractant protein (MCP)-1, Rantes, macrophage inflammatory protein (MIP)-1 $\alpha$  and IL1- $\beta$  which accelerate further recruitment of inflammatory immune cells and causing chronic inflammation. This results in increased kinase activity and inhibitory phosphorylation of insulin receptor substrate (IRS) proteins ultimately leading to the development of insulin resistance (DeFronzo et al., 2015). If left untreated, T2D can lead to microvascular complications (retinopathy and nephropathy), development of hypertension and a higher risk of cardiovascular diseases.

Prevention and treatment of T2D include weight loss and exercise or administration of drugs that aid in managing insulin availability and sensitivity such as metformin (DeFronzo et al., 2015). To increase insulin sensitivity more recent treatment approaches have used pioglitazone and rosiglitazone, two strong activators of PPAR $\gamma$ , a transcription factor that has been in the focus of the VAT Treg cell field and the present thesis (DeFronzo et al., 2015, Feuerer et al., 2009). Furthermore, obesity induced inflammation in the VAT could be reverted by administration of IL-33 (M. Feuerer et al., 2009; M. J. Kraakman et al., 2015; A. Vasanthakumar et al., 2015; Ajithkumar Vasanthakumar et al., 2015). Increase in  $T_H1/T_H2$  and  $T_H1/Treg$  cell ratio ( $T_H1/T_H2$  switch) also contributes to insulin resistance and metabolic dysfunction (Markus Feuerer et al., 2009; C. N. Lumeng et al., 2007). This is referred to as the  $T_H1/T_H2$  paradigm

in obesity which has implications in human pathology (Winer et al., 2009). IFN- $\gamma$ , a key player downstream of T box expressed in T cells (T-bet), is directly implicated in VAT inflammation (Stolarczyk et al., 2013). IFN- $\gamma$  dysregulates insulin signalling, represses adipocyte differentiation and directly promotes pro-inflammatory macrophage differentiation. Conversely, depletion of IFN- $\gamma$  in obese mice results in improved insulin sensitivity and glucose tolerance (McGillicuddy et al., 2009; O'Rourke et al., 2012; Rocha et al., 2008; Wong et al., 2011). In humans, analyses of VAT T cells in obese individuals have shown that they display a T<sub>H1</sub>/T<sub>H17</sub> skewed phenotype with elevated IFN- $\gamma$  and IL1- $\beta$  production which may impact insulin sensitivity (Bertola et al., 2012; Dalmas et al., 2014; Ioan-Facsinay et al., 2013).

Despite the complications lymphocytes cause during obesity, they are crucial to maintain metabolic health as demonstrated by experiments with *Rag2*<sup>-/-</sup> mice that do not have B or T cells. These mice show increased weight gain and insulin resistance highlighting the importance of adaptive immune cells, including VAT Treg cells, in metabolic regulation (Cipolletta et al., 2012; Markus Feuerer et al., 2009; Stolarczyk et al., 2013; Winer et al., 2009). Dissecting the molecular mechanisms and environmental cues that regulate Treg cell development, differentiation, maintenance and function in the VAT is therefore crucial.

## 1.2 Regulatory T cells

Treg cells have been described more than 30 years ago as cells of adaptive immune system that limit immune cell activity (S. Sakaguchi, Fukuma, Kuribayashi, & Masuda, 1985; S. Sakaguchi, Sakaguchi, Asano, Itoh, & Toda, 1995). This specialized CD4<sup>+</sup> T cell lineage makes up 10-20% of the CD4<sup>+</sup> T cell population in lymphoid tissues and is dependent on the expression of the master regulator forkhead box P3 (Foxp3) (Fontenot, Gavin, & Rudensky, 2003; Hill et al., 2007; Hori, Nomura, & Sakaguchi, 2003; Josefowicz, Lu, & Rudensky, 2012). The Foxp3 gene is located in the X chromosome and is essential for Treg cell stability and function (Derry et al., 1995; Schubert, Jeffery, Zhang, Ramsdell, & Ziegler, 2001). Disruption of Foxp3 protein expression results in fatal

lymphoproliferative disorder and IPEX (Immunodysregulation polyendocrinopathy enteropathy X-linked) syndrome in mice and human, respectively (Bennett et al., 2001; Brunkow et al., 2001).

### **1.2.1 Treg cell function**

Treg cells have a crucial function in inhibition of immune response through various mechanisms. Expressing the high affinity IL-2 receptor  $\alpha$  chain (CD25), Treg cells are efficient in sequestering IL-2 and making it unavailable to Tconv cells, which require IL-2 for expansion during immune responses (Shimon Sakaguchi, Yamaguchi, Nomura, & Ono, 2008; Tang & Bluestone, 2008; Teh, Vasanthakumar, & Kallies, 2015; James B. Wing & Sakaguchi, 2012). Other mechanisms include secretion of anti-inflammatory cytokine IL-10, and receptor-mediated inhibition through cytotoxic T-lymphocyte-associated protein 4 (CTLA-4). In an inflammatory environment, Treg cells express high levels of CD39 and CD73 which are membrane-bound enzymes that convert extracellular ATP to immunosuppressive adenosine (Borsellino et al., 2007).

Therefore, mutations in *Foxp3* or ablation of Treg cells results in fatal autoimmunity underpinning their importance in mice and human (Ohkura, Kitagawa, & Sakaguchi, 2013).

### **1.2.2 Treg cell development and differentiation**

There are two main pathways for Treg cell generation. Thymic-derived (t)Treg cells are directly generated in the thymus which contributes to immune tolerance. Alternatively, CD4<sup>+</sup>Foxp3<sup>-</sup> conventional T(conv) cells in peripheral organs can differentiate into peripheral (p)Treg cells upon T cell receptor (TCR) stimulation and co-stimulatory signals from IL-2 and transforming growth factor (TGF)- $\beta$ .

Functionally, Treg cells could be grouped as central (cTreg) and effector Treg (eTreg) cells based on their activation status and localization. cTreg cells express high levels of lymphoid homing receptors, such as CD62L (L-selectin) and chemokine receptor CCR7 and display a naïve phenotype (Liston & Gray, 2014;

Smigiel et al., 2014). When activated by TCR signaling, cTreg cells undergo differentiation process by down-regulating CD62L and CCR7 and upregulation of the activation marker CD44 to become eTreg cells. This differentiation process is underpinned by unique transcriptional changes that reflects in the unique phenotype of eTreg cells. Compared to their cTreg cell counterparts, eTreg cells display a distinct effector phenotype characterized by the expression of glucocorticoid-induced tumor necrosis factor receptor (GITR), killer-cell lectin like receptor G1 (KLRG1), Tigit, inducible T cell co-stimulator (ICOS), and IL-10 (E. Cretney et al., 2011; Panduro, Benoist, & Mathis, 2016; Vasanthakumar et al., 2017; A. Vasanthakumar et al., 2015; J. M. Weiss et al., 2012). This differentiation program is driven by TCR induced transcription factors interferon regulatory factor 4 (IRF4) and Batf, which are also critical for the homeostasis of eTreg cells in non-lymphoid organs (Erika Cretney, Kallies, & Nutt, 2013b; E. Cretney et al., 2011).

### **1.2.3 Treg cell diversity and plasticity**

Treg cells reside in a wide variety of lymphoid and non-lymphoid tissues. To be able to populate unique tissue niches, Treg cells employ tissue specific mechanisms that facilitate their migration and residency. Inflammation also impacts the identity of Treg cells and compromises their function. Treg cell differentiation follows a multi-step change of the transcriptional profile allowing Treg cells to divert into various subsets if the microenvironment provides the appropriate cues. Studies focused on Treg cells in peripheral tissues such as skin, liver and colon have shown how Treg cells adjust their transcriptional signature in a tissue-specific manner (M. Delacher et al., 2020; Michael Delacher et al., 2017; C. Li, A. R. Munoz-Rojas, et al., 2021; Miragaia et al., 2019). Unpublished results in our lab have also demonstrated a progressive evolution of naïve cTreg cells to eTreg cells is mediated via Blimp1. Furthermore, there is increasing evidence of Treg cells co-opting T helper T cell specific transcriptional machinery to suppress cognate T helper subsets ( $T_H1$ ,  $T_H2$ ,  $T_H17$  etc.) These additional layers of Treg cell specialization increase their precision in

immunosuppression and confer on them non-canonical functions (Munoz-Rojas & Mathis, 2021; Shi & Chi, 2019).

Under conditions of excessive inflammation, Treg cells gain an activated and often pathogenic memory phenotype and lose Foxp3 expression and suppressive functions, which may be restored once inflammation recedes (Bin Dhuban, Kornete, Mason, & Piccirillo, 2014; Zhou et al., 2009). Several reports have shown this phenomenon and Treg cell mediated pro-inflammatory cytokine production in mice and human with inflammatory diseases such as psoriasis, rheumatoid arthritis and inflammatory bowel disease (Hovhannisyan, Treatman, Littman, & Mayer, 2011; Komatsu et al., 2009; Voo et al., 2009; X. O. Yang et al., 2008). However, this model is disputable as Treg cells have reported to expand in scenarios of increased inflammation such as chronic infection and serve as targets for drugs in tumor immunotherapy (Belkaid & Tarbell, 2009; Hu et al., 2021; McHugh et al., 2002; Piconese, Valzasina, & Colombo, 2008; Punkosdy et al., 2011).

#### *1.2.3.1 Treg cells adapt to specific inflammatory milieus*

Differentiation of T<sub>H</sub> cells requires TCR and CD28 co-stimulation. T<sub>H</sub> cell fate decision, however, depends on tertiary signals including cytokines. T<sub>H</sub>1 cells are essential for immune responses against intracellular pathogens and do so by assisting or 'helping' CD8<sup>+</sup> T cells and innate immune cells. T<sub>H</sub>2 cells are involved in immune responses against parasitic infections, required for humoral immunity and drive allergic inflammatory responses in different tissues (Burzyn, Benoist, & Mathis, 2013; Chaudhry & Rudensky, 2013; Erika Cretney et al., 2013b).

At the molecular level T<sub>H</sub>1 cells require interleukin (IL)-12 and/or IFN- $\gamma$ , to induce transcriptional reprogramming mediated by transcription factor T-bet. T-bet stabilizes T<sub>H</sub>1 commitment and is required for efficient CD8<sup>+</sup> cytotoxic T cell (CTL) responses. It does so by directly promoting the expression of chemokine receptor CXCR3, IFN- $\gamma$ , perforin and Granzyme B (Gzmb) (Glimcher, Townsend, Sullivan, & Lord, 2004; Lord et al., 2005; B. M. Sullivan, Juedes, Szabo, Von

Herrath, & Glimcher, 2003; Szabo et al., 2000; Szabo, Sullivan, Peng, & Glimcher, 2003). Simultaneously, it represses GATA-3 and Retinoid orphan receptor (ROR)γt function directly, thereby inhibiting T<sub>H</sub>2 and T<sub>H</sub>17 commitment, respectively (Hwang, Szabo, Schwartzberg, & Glimcher, 2005; Lazarevic et al., 2011). Ablation of T-bet arrests CTL formation, affects natural killer (NK) and NKT cell formation, dampens IFN-γ production and increases levels of type 2 cytokine IL-4 and anti-inflammatory cytokine IL-10 (Glimcher et al., 2004; B. M. Sullivan et al., 2003; Townsend et al., 2004). Mice deficient for T-bet are less susceptible to type 1 autoimmunity driven diseases such as inflammatory bowel disease, Type 1 diabetes (T1D), arthritis and systemic lupus erythematosus (Lazarevic et al., 2011). Conversely, these mice are more susceptible to spontaneous allergic inflammation due to dysregulated type 2 cytokine expression (Finotto et al., 2002; Szabo et al., 2003). Treg cells can also acquire a T<sub>H</sub>1-like phenotype. Studies have shown the existence of CXCR3, IFN-γ and T-bet expressing Treg cells in various tissues (Koch et al., 2009; Tan, Mathis, & Benoist, 2016; Yu, Sharma, Edwards, Feigenbaum, & Zhu, 2015). These Treg cells either differentiate during homeostatic conditions or in response to infections or tumours (Colbeck et al., 2015). Importantly, T-bet and CXCR3 expression gradually increase across the Treg cell population supporting the heterogenous nature of Treg cells (Levine et al., 2017).

The zinc finger transcription factor GATA-3 is crucial for early T cell development, ILC2 development and, along with IL-4, T<sub>H</sub>2 commitment (Ting, Olson, Barton, & Leiden, 1996; Yamamoto et al., 1990; D.-H. Zhang, Cohn, Ray, Bottomly, & Ray, 1997; W.-P. Zheng & Flavell, 1997). Furthermore, it is also essential for CD8<sup>+</sup> T cell survival, proliferation and Treg cell function (Rudra et al., 2012; Yunqi Wang, Maureen, & Yisong, 2011; Y. Wang et al., 2013). GATA-3 is activated downstream of the TCR, inducing its nuclear localization to regulate the expression of various molecules that include IL-10, IL-20, IL-4, CCR5 and ST2 (Jones & Flavell, 2005; Kanhere et al., 2012; Wei et al., 2011). GATA-3 also suppresses T-bet mediated IFN-γ production and dampens the expression of signal transducer and activator of transcription (STAT) 4 and IL12-R subunit, both

important for  $T_H1$  induction (Ouyang et al., 1998; Usui et al., 2006). GATA-3 is also important for the activation and function of ILC2s during allergic inflammation such as asthma. Together with  $T_H2$  cells, ILC2s produce high amounts of IL-5 and IL-13 that amplify asthmatic allergic inflammation (Kleinjan et al., 2014).  $T_H2$ -specific Treg cells are therefore essential to restrict excessive type 2 inflammation. These are characterized by increased GATA3, IRF4, IL-4 and IL-13 expression (Jin, Park, Elly, & Liu, 2013; Krishnamoorthy et al., 2012; Noval Rivas et al., 2015; Rudra et al., 2012). IRF4 in this case has a dual function: it suppresses pro-inflammatory  $T_H2$  gene expression while also forming a complex with Foxp3 to drive eTreg cell differentiation (Levine, Arvey, Jin, & Rudensky, 2014; Vasanthakumar et al., 2017; Y. Zheng et al., 2009).

In human blood, Treg cells with  $T_H1$ - and  $T_H2$ -like properties have also been reported mostly sustaining Helios and CTLA-4 expression and their suppressive function (Duhén, Duhén, Lanzavecchia, Sallusto, & Campbell, 2012; Halim et al., 2017). In autoimmune diseases and cancer, these Treg cell types are found in peripheral tissues (J. B. Wing, Tanaka, & Sakaguchi, 2019). Thus, the study of tissue Treg cells is crucial as they serve as potential targets for immunotherapy.

#### *1.2.3.2 Tissue Treg cells*

Treg cells are found in most organs, but enriched in barrier organs such as the skin and gut as well as the VAT. Non-lymphoid tissues are predominantly populated by eTreg cells and only very few if any cTreg cells (Erika Cretney et al., 2013b; E. Cretney et al., 2011). In these tissues, eTreg cells help to maintain homeostasis by preventing autoimmune reactions, assisting in tissue repair and assuming tissue specific functions (Burzyn et al., 2013; Erika Cretney, Kallies, & Nutt, 2013a; Teh et al., 2015). The maintenance of the effector phenotype is crucial to perform these functions. Indeed, Treg cell specific ablation of IRF4, which is important for eTreg formation, results in fatal autoimmunity within a few months due to lower expression of IL-10, ICOS and Granzyme B resulting in exacerbated IL-4 and IL-5 production and tissue inflammation (Chensue et al., 2001; Ho, Lo, & Glimcher, 1998; Lohning et al., 1998; Y. Zheng et al., 2009).

Furthermore, IL-33 can induce GATA-3 expression in Treg cells in skin, gut, lung and VAT, maintain Foxp3 and CD25 expression (Cayrol & Girard, 2018; Schiering et al., 2014; Wohlfert et al., 2011). Several studies have shown that Treg cells in tissues share a common gene signature. For example, Treg cells residing in the VAT, skin, liver, lung, gut and skeletal muscle express GATA3, c-Maf, IL-10, ST2, KLRG1 and amphiregulin (Areg) (Michael Delacher et al., 2017; Wilson Kuswanto et al., 2016; Miragaia et al., 2019; Ohnmacht et al., 2015; Wohlfert et al., 2011). While all tissue Treg cells share a core transcriptional signature, Treg cells in distinct tissues express unique molecules specific to the tissue microenvironment.

#### *Skin*

As a barrier tissue, an adequate Treg cell response against infection, injury and allergy is crucial to reduce skin damage. Skin resident Treg cells express high levels of arginase 2 (Arg2), which they use to enhance cellular metabolism (Lowe et al., 2019). Additionally, they are characterized by expression of signaling molecule Jagged 1 and require proenkephalin, an opioid precursor, as well as Amphiregulin to maintain tissue homeostasis (Ali et al., 2017; Shime et al., 2020). Skin Treg cells are essential to suppress profibrotic immune responses and restrain allergic inflammation via ROR $\alpha$  expression (Kalekar et al., 2019; Malhotra, 2018).

#### *Gut*

The intestinal tract is another barrier organ that offers a large contact area with food, commensal and pathogenic bacteria and is therefore a highly immunologically active organ. In colon and small intestine (SI), there are two Treg cell subtypes that can be distinguished based on the expression of GATA3 and ROR $\gamma$ t transcription factors, which are mutually exclusive (Wohlfert et al., 2011). Commensal microbiota induce ROR $\gamma$ t<sup>+</sup> pTreg cell differentiation in the SI and colon. This happens through microbial-derived short-chain fatty acids (SCFA), retinoic acid, IL-6, IL-23, TGF $\beta$  and microbial antigen presentation by local dendritic cells (DC) (Nutsch et al., 2016; Ohnmacht et al., 2015). ROR $\gamma$ t<sup>+</sup> Treg

cells are essential to suppress IL-17 and IFN- $\gamma$  expression and thereby control inflammation (Sefik et al., 2015). ROR $\gamma$ t<sup>+</sup> Treg cells are mostly located in the colon while most of Treg cells in the SI are ROR $\gamma$ t<sup>-</sup> (Atarashi et al., 2011; Geuking et al., 2011; B. H. Yang et al., 2016). In the SI, ROR $\gamma$ t<sup>+</sup> Treg cell induction mainly depends on dietary antigens such as retinoic acid, which is converted from Vitamin A (Coombes et al., 2007; Jaensson-Gyllenback et al., 2011; Kang, Lim, Andrisani, Broxmeyer, & Kim, 2007; K. Kim et al., 2016).

In contrast, GATA3<sup>+</sup> tTreg cells are independent from microbiota and are the main population in germ free mice (Geuking et al., 2011). IL-33 promotes accumulation and function of GATA3<sup>+</sup> Treg cells that express high levels of KLRG1 and CD103 and are important for tissue repair (Ohnmacht et al., 2015; Schiering et al., 2014). Previous reports have shown that Neuropilin 1 (Nrp1) and Helios are expressed in GATA3<sup>+</sup> tTreg cells and therefore can be utilised as additional markers for discrimination (Thornton et al., 2010; J. Weiss et al., 2012).

### *Lung*

In the airways, type 2 inflammation is typically responsible for allergic inflammation and asthma (Kleinjan et al., 2014; Morita et al., 2015). Accordingly, Treg cells in the lung display high GATA3 expression along with surface expression of KLRG1 and ST2. Furthermore, a subset of CD103<sup>hi</sup> Treg cells is instrumental to prevent Tconv mediated fibrosis in lung in response to fungal infection (Ichikawa et al., 2019)

### *Other tissues*

Transcriptional analysis of pancreatic Treg cells showed increased T-bet and CXCR3 expression enabling them to suppress type 1 inflammation (Tan et al., 2016). Occurrence of CXCR3<sup>+</sup>/T-bet<sup>+</sup> Treg cells have also been reported in the intestinal lamina propria, lung and brain (Koch et al., 2009; McPherson, Turner, Mair, O'Connor, & Anderton, 2015; Yu et al., 2015). The central nervous system (CNS) itself is devoid of Treg cells under homeostatic conditions. Upon injury, Treg cells are recruited which express the typical 'tissue Treg' cell markers (GATA3, ST2, KLRG1 and Areg) but also show elevated expression of PPAR $\gamma$

and the serotonin receptor 5-HT7 (Ito et al., 2019; Korn et al., 2007). Furthermore, these Treg cells also secrete CCN3, a growth regulatory protein that promotes tissue regeneration, remyelination and tissue repair in the brain (Dombrowski et al., 2017). Overall, the functional specialization of Treg cells within different tissues is accompanied by their differentiation and adaptation to the local environment. As mentioned previously, this is also important for Treg cells found in the VAT.

### **1.3 VAT Treg cells**

#### **1.3.1 VAT Treg cell phenotype and function**

Treg cells are enriched (up to 50% of CD4 T cells) in the VAT where they restrain inflammation and maintain local and systemic metabolic health (J. R. DiSpirito & D. Mathis, 2015; D. Kolodin et al., 2015; D. Mathis, 2013; A. Vasanthakumar et al., 2015). Apart from the effector markers such as IL-10, KLRG1, ICOS and PD-1, murine VAT Treg cells also express CCR2 and ST2 which are required for migration and IL-33 signalling, respectively (Sagar P. Bapat et al., 2015; Cipolletta et al., 2012; E. Cretney et al., 2011; A. Vasanthakumar et al., 2015). Recent reports also have shown that VAT Treg cells express hydroxyprostaglandin dehydrogenase (HPGD), which catabolizes prostaglandin E<sub>2</sub> (PGE<sub>2</sub>) into 15-keto PGE<sub>2</sub>, to suppress Tconv activity, which is dependent on PPAR $\gamma$  (Schmidleithner et al., 2019). Despite displaying a very different phenotype, VAT Treg cells maintain a specific core eTreg-signature (CTLA-4, GITR, CD44 etc.) and are functional in T cell suppression assays (Markus Feuerer et al., 2009). In line with stimulus-specific differentiation theory, VAT Treg cells acquire a T<sub>H</sub>2-like phenotype through expression of GATA-3 which is enriched in VAT but not splenic Treg cells (Sagar P. Bapat et al., 2015; Cipolletta, Cohen, Spiegelman, Benoist, & Mathis, 2015; Cipolletta et al., 2012; Han et al., 2015). Previous studies have demonstrated that VAT Treg cells have very low T-bet and IFN- $\gamma$  expression, while VAT Tconv cells display a strong T<sub>H</sub>1 polarization and high TNF production (Markus Feuerer et al., 2009).

### 1.3.2 VAT Treg cell regulation

VAT Treg cells are dependent on IRF4, basic leucine zipper ATF-like transcription factor (BATF) and IL-33 for differentiation and survival (M. Feuerer et al., 2009; A. Vasanthakumar et al., 2015; Y. Zheng et al., 2009). The latter is a nuclear cytokine from the IL-1 family that can regulate gene expression or act as an alarmin when released to elicit immune responses and assist in tissue repair (Cayrol & Girard, 2018; Liew, Girard, & Turnquist, 2016). IL-33 can promote T<sub>H</sub>2, ILC2 and cytotoxic T cell differentiation and is particularly found in peripheral tissues (Bonilla et al., 2012; Licona-Limón et al., 2013; Ari B. Molofsky et al., 2013; Moro et al., 2010; Schmitz et al., 2005). Within tissues, it is abundantly expressed by endothelial, epithelial and mesenchymal cells in homeostatic and inflammatory conditions (Spallanzani et al., 2019). Our recent study has shown that IL-33 is produced exclusively by gp38<sup>+</sup> mesenchymal stromal cells (MSCs) in the VAT in a sex-specific manner (Vasanthakumar et al., 2020). Sex hormones regulate the differentiation of these specialized MSCs, which play a pivotal role in maintaining VAT homeostasis and insulin sensitivity by promoting the survival and expansion of local anti-inflammatory ILC2 and VAT Treg cells (Brestoff et al., 2015; Burzyn et al., 2013; Jackson-Jones et al., 2016; W. Kuswanto et al., 2016; Nishimura et al., 2013; A. Vasanthakumar et al., 2015). In keeping with this, IL-33 administration is sufficient to expand VAT Treg cells and ILC2 (*in vivo* and *in vitro*) and notably revert glucose intolerance in genetic and diet induced obese/diabetic mouse models (Brestoff et al., 2015; Han et al., 2015; D. Kolodin et al., 2015; W. Kuswanto et al., 2016; Miller et al., 2010; Moro et al., 2010; A. Vasanthakumar et al., 2015). The mechanism by which IL-33 rescues the obese phenotype might not only rely on VAT Treg cell expansion but also on direct changes of the transcriptional signature of VAT Treg cells.

VAT Treg cells acquire their tissue specific signature in part by expressing PPAR $\gamma$ , which is the master regulator of adipogenesis, a potent promotor of systemic insulin sensitivity and expressed in other VAT resident immune cells (Cipolletta et al., 2012; Odegaard et al., 2007; E. D. S. Rosen, B. M., 2013). Indeed, the dependence of VAT Treg cells on PPAR $\gamma$  has been demonstrated

using *Pparg<sup>fl/fl</sup>Foxp3<sup>Cre</sup>* mice, that lack PPAR $\gamma$  only in Treg cells. Treg cell populations in these mice are depleted in the VAT but not the spleen (Cipolletta et al., 2012).

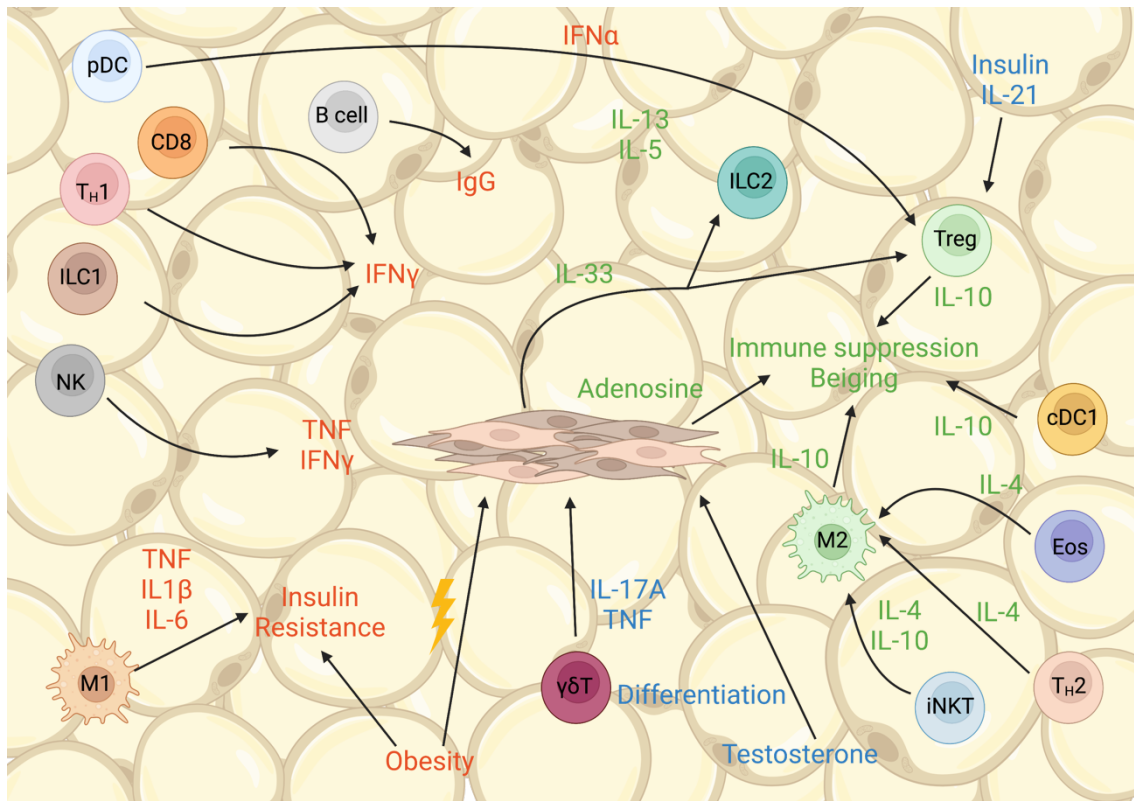


**Figure 1 | Molecular and cellular mediators of VAT inflammation.** Lean adipose tissue is enriched in immune cells that contribute to a T<sub>H</sub>2-dominant environment, including Treg cells, T<sub>H</sub>2 cells,  $\gamma\delta$  T cells, M2 macrophages, ILC2s, NKT cells and eosinophils whose activity has anti-inflammatory effects and are crucial in preserving insulin sensitivity. Also non-immune cells such as PDGFR $\alpha$ + mesenchymal stromal cells contribute to immune suppression in the adipose tissue. Hormones, IL17-A and TNF promote differentiation and IL-33 production by stromal cells which is pivotal for ILC2 and Treg cell maintenance, survival, and activation. Obesity impairs this fine-tuned environment through recruitment of inflammatory immune cells that includes CD8+ T cells, ILC1s, B cells, T<sub>H</sub>1 cells, NK cells and M1 macrophages. This effect is mediated at least in part by hypoxic and ER stress signals, as well as inflammatory chemokines and cytokines.

### 1.3.3 VAT Treg cell precursors

Despite the thorough investigation of VAT Treg cells over the past decade, only recently the search for a VAT Treg cell precursor has intensified. Li and colleagues identified a subpopulation of splenic eTreg cells that display marginal

PPAR $\gamma$  expression and upon adoptive transfer populate the VAT among other tissues, to become ST2<sup>+</sup> VAT Treg cells (C. Li et al., 2018; C. Li, A. R. Munoz-Rojas, et al., 2021). A different study showed that Treg cells undergo step-wise transcriptional changes from naïve (Nfil3-KLRG1<sup>-</sup>), over intermediate (Nfil3+KLRG1<sup>-</sup>) to eTreg cells (Nfil3+KLRG1<sup>+</sup>), of which the latter are capable to populate the VAT, skin, colon among other tissues (M. Delacher et al., 2020). Additionally, our group has shown that VAT Treg cell precursors in the spleen constitute a population of Blimp1+KLRG1<sup>+</sup> Treg cells that migrate to the VAT in a CCR2-CCL2 dependent manner (Vasanthakumar et al., 2020). Thus, according to the current model, Treg cells are derived from splenic precursors and can be characterized as Nfil3+KLRG1+Blimp1+PPAR $\gamma$ <sup>lo</sup> Treg cells.

### 1.3.4 VAT Treg cell in humans and obesity

Previous studies have indirectly shown the presence of Treg cells in human adipose through mRNA expression of Foxp3 (Sagar P. Bapat et al., 2015; Eller et al., 2011; Markus Feuerer et al., 2009). In obese human subjects, Treg cells from the omental fat express high levels of ST2 and display an activated CD25<sup>+</sup>CD69<sup>+</sup> phenotype (Deiuliis et al., 2011; Travers, Motta, Betts, Bouloumié, & Thompson, 2015; Wouters et al., 2017), unlike their counterparts found in blood. Therefore, tissue specific VAT Treg cells potentially also play a role in humans and potentially serve as therapeutic targets to treat diabetes and metabolic disease.

Several studies have shown that Treg cell are significantly depleted during obesity (Cipolletta et al., 2012; M. Feuerer et al., 2009; Man, Kallies, & Vasanthakumar, 2022). Additionally, obesity induces changes in the VAT Treg transcriptional signature (levels of *Ccr2*, *Il1rl1*, *Klrg1*, *Gata3* and *Pparg*) (Cipolletta et al., 2015; A. Vasanthakumar et al., 2015). This would suggest a change in local inflammatory environment considering the ability of eTreg cells to mirror the type of immune response they are suppressing. However, their role in obesity and its associated morbidities have remained controversial (S. P. Bapat

et al., 2015; Beppu et al., 2021; Cipolletta et al., 2012; M. Feuerer et al., 2009; Man et al., 2022; Wu et al., 2020)

#### **1.4 Study Aims**

Previous research has shown the importance of Treg cells in regulating VAT homeostasis and metabolic function. However, most studies have focused on the PPAR $\gamma$ -dependent ST2<sup>+</sup> population of VAT Treg cells that are abundant in males. Our recent publication laid the groundwork for this study by revealing sexual dimorphism in VAT Treg cells that is driven by distinct VAT microenvironment in females and males.

The current project aims to integrate multiple aspects of VAT biology in order to thoroughly understand the cellular and molecular differences between male and female VAT Treg cells. Furthermore, this project aims to assess the impact of inflammation on VAT Treg cells and vice versa and define mechanisms that drive dietary and sexual differences in VAT immunity and systemic metabolism.

Specific aims of the present study were:

1. To understand the molecular mechanisms that dictate VAT Treg cell differentiation and maintenance.
2. To characterize VAT inflammation in males and females and assess the impact on VAT immunity and metabolism.
3. To determine how diet and age influences VAT Treg cell composition and inflammation in males and females

## Chapter 2 – Material & Methods

### 2.1 Buffers and Media

#### *Type 1 ultrapure water*

Distilled water further filtered using a Milli-Q Gradient A10 unit, to a final resistance above 1.2 MΩ at 25 °C. Hereafter 'Milli-Q water'.

#### *Red cell removal buffer (RCRB)*

155.8 g NH<sub>4</sub>Cl, 0.74 g ethylenediaminetetraacetic acid (EDTA)-disodium salt and 20 g NaHCO<sub>3</sub> dissolved in Milli-Q water and adjusted to pH 7.3.

#### *Fluorescence-activated cells sorting (FACS) buffer*

Phosphate buffered saline (PBS) was supplemented with 0.1 % bovine serum albumin (BSA).

#### *Magnetic-activated cell sorting (MACS) buffer*

FACS buffer was supplemented with 2 mM EDTA.

#### *T cell medium*

Iscove's modified Dulbecco's medium (gibco) was supplemented with 1 x non-essential amino acids (Sigma), 1 mM sodium pyruvate, 10 mM HEPES (Sigma), 2 mM L-glutamine, 50 µg/ml gentamycin (Sigma), 50 mM β-mercaptoethanol (Sigma), and 10 % fetal calf serum (FCS) and sterile filtered.

#### *Hanks 2% FCS*

Hanks balanced salt sodium (HBSS) with glucose, no calcium and no magnesium (Gibco) was supplemented with 2 % FCS.

#### *Fat digestion buffer*

2 mg/ml Collagenase IV (Gibco) in Dulbecco's Modified Eagle Medium (DMEM) (Gibco).

### *Gut digestion buffer*

1 µg/ml DNase1 (Roche), 200µg/ml Dispase (Gibco), 1.4 mg/ml Collagenase III (Worthington) and 10 % heat-inactivated FCS in Roswell Park Memorial Institute (RPMI) 1640 medium (Gibco).

## 2.2 Animal Models

### 2.2.1 Mice

Mice were maintained in the Biological Resources facility (BRF) of the Peter Doherty Institute in accordance with the guidelines of the University of Melbourne Animal Ethics Committee.

**Table 1** shows details on the origin and location of different mouse strains.

**Table 1** | Mouse strains used in this study:

Mouse strain	Location	Source
<i>Blimp1<sup>Foxp3Cre</sup></i>	PDI	<i>Prdm1<sup>fl/fl</sup></i> (Jax stock #008100) were from Jax
<i>Foxp3<sup>DTR</sup></i>	PDI	Jax (Jax stock #016958)
<i>Il33<sup>-/-</sup></i>	PDI	Obtained from Susumi Nakae (Oboki et al., 2010)
<i>Foxp3<sup>Cre</sup></i> (Ly5.1)	PDI	<i>Foxp3<sup>CreI</sup></i> mice (Jax stock # 016959) mice were from Jax
<i>Gata3<sup>Foxp3Cre</sup></i>	PDI	<i>Gata3<sup>fl/fl</sup></i> (Jax stock # 028103) were obtained from Monash University
<i>HobitTom<sup>Cre</sup></i>	PDI	
<i>Ifnar2<sup>-/-</sup></i>	PDI	
<i>Ifng<sup>-/-</sup></i>	PDI	Strugnell Group (Jax stock #002287)
<i>Ifng<sup>eYFP</sup></i>	PDI	Strugnell Group (Jax stock #017581)

<i>Pparg<sup>fl/fl</sup>Foxp3<sup>Cre</sup></i>	PDI	<i>Pparg<sup>fl/fl</sup></i> (Jax stock # 004584) mice were from Jax
<i>RAG1<sup>-/-</sup></i>	PDI	ARC (Jax stock # 002216)
REX3	WEHI	
<i>Sirt1<sup>Foxp3Cre</sup></i>	PDI	
<i>I1r1<sup>-/-</sup></i>	PDI	
<i>Tbx21<sup>-/-</sup></i>	PDI	
<i>Tbx21<sup>Foxp3Cre</sup></i>	PDI	<i>Tbx21<sup>fl/fl</sup></i> (Jax stock #022741) were from WEHI
<i>Tbx21<sup>zsGreen</sup></i>	WEHI	Obtained from Joanna Groom, originally from Jinfang Zhu, NIAD (Zhu et al., 2012)
<i>TgfbRII<sup>Foxp3Cre</sup></i>	PDI	

*Gata3<sup>fl/fl</sup>*, *Prdm1<sup>fl/fl</sup>*, *Tbx21<sup>fl/fl</sup>* and *Pparg<sup>fl/fl</sup>* mice were intercrossed with *Foxp3<sup>Cre</sup>* (Jax stock #016959) mice. Possible germline deletion was tested for by genotyping (data not shown). All mouse lines were maintained on a C57BL/6J (Ly5.2) background, except *I133<sup>-/-</sup>*, which is on a C57BL/6N background. Mice were analyzed at 25-30 weeks of age unless specified.

### 2.2.2 Bone marrow reconstitution of chimeric mice

Mixed bone marrow chimeras were generated from lethally irradiated (2 doses of 550Rad each) Ly5.1xLy5.2 F1, *Rag2<sup>-/-</sup>* or Ly5.1 mice reconstituted with a mixture of mutant or control F1, Ly5.1 or Ly5.2 bone marrow as indicated and allowed to reconstitute for a minimum of 6 weeks. Irradiated mice were provided with ampicillin (Sigma) supplemented drinking water.

### **2.2.3 Adoptive transfer**

*Rag1*<sup>-/-</sup> mice were injected intraperitoneally (i.p.) with 10 million purified splenic CD4<sup>+</sup> T cells from a mixture of mutant or control Ly5.1 and Ly5.2 mice. Mice were analysed six- or 16-weeks post-transfer.

### **2.2.4 High-fat diet (HFD)**

Mice were kept on standard diet from weaning till 6-12 weeks of age. High fat diet (SF14-154, 45 or 60 % energy from fat) replaced standard chow for up to 25 weeks. The diet is produced by Specialty Feeds Pty Ltd.

### **2.2.5 Treg cell recovery**

To achieve punctual depletion of Treg cells, *Foxp3*<sup>DTR</sup> mice were injected intraperitoneally with diphtheria toxin (DT, 50 µg/kg) and analysed 3-, 10- and 30-days post-injection.

### **2.2.6 IL-33 treatment**

0.5 µg of recombinant murine IL-33 in PBS (R&D systems) were intraperitoneally injected to mice in a maximum 200 µl volume every second day for a total of up to 4 times.

### **2.2.7 Glucose Tolerance Test**

Mice were fast overnight for a period of 6-7 hours. Mice were weighed and a very small nick at the tip of the tail made with scissors. This involved removing the very tip of the tail (<1 mm). 1-2 drops of blood (10 µl) will be collected. Then, 1.75-2 g/kg glucose was given by intraperitoneal injection with a 26G or 27.5G needle (this dose is achieved by delivering 10uL per g body weight of a 175 g-200g/l solution in PBS) and repeated tail vein samples of 10 µl were collected from the tail after 15, 30, 60, 120 minutes. This was done without making any further

incisions but rather by gently squeezing the tip of the tail. After the last bleed, mice were killed by CO<sub>2</sub> inhalation, or rested and allowed to recover. If the glucose tolerance test needs to be repeated, or if an insulin tolerance test needs to be performed, a second sequence of bleeds may be taken 7-14 days after the first bleeds from the tail.

### **2.2.8 Metabolic Cages**

To measure food intake, water intake, activity, oxygen consumption and carbon dioxide production in individual mice over a 48 hour period we used the Promethion Metabolic System from Sable (Nevada, USA).

Mice from PDI were placed in a clean mouse cage with food pellets and gel for hydration. The box was placed in 2 paper bags, which allows adequate ventilation and protects the mice from exposure to pathogens while outside the building. Bagged mice were transported with a trolley across Grattan Street to the BSAF in the Medical Building. There the mice were transferred to the facility's own group housing cages (same caging system as PDI, but without automatic watering) and allowed to acclimatize for at least a week. In their new home cages the mice were brought into a surgery room within the BSAF (W936) in the Medical Building. One by one, mice were weighed and transferred into Promethion cages with food, water and bedding. Mice were housed individually in the Promethion for a period of 2.5 days. This is the minimal time required for accurate assessment of energy expenditure, food intake and activity. The first 12 hours is to allow acclimation of the mouse to the new cage, and the subsequent 48 hour period is required in order to obtain stable values and differentiate between energy expenditure, food intake and activity during night (active) time and day (resting) time.

### **2.2.9 Body Composition Analysis**

To measure the fat mass, lean mass and free liquid composition of an awake mouse a Bruker LF50 MiniSpec scanner was used. The MiniSpec uses Time Domain Nuclear Magnetic Resonance (TD-NMR) to measure body composition

(fat mass, lean mass and free fluid) in conscious mice without the need of anaesthesia.

The mouse in its home cage will be brought into a surgery room within the BSAF (W905) and acclimatized for at least 15 minutes. After acclimatization the mouse will be gently guided into the restrainer and the plunger locked behind it. Restriction is achieved by lowering the plunger until the mouse is confined to the 'frosted' section of the tube.

After the mouse is confined, the restrainer is inserted into the MiniSpec and the scan is initiated automatically. The scan is completed after approximately 2 minutes upon which the restrainer is removed, and the mouse placed back into its original cage.

## **2.3 Procedures for cellular immunology**

### **2.3.1 Processing explanted organs for lymphocyte isolation and/or analysis**

Spleens, lymph nodes and lungs were dissociated to single cell suspensions by being gently worked through a 70  $\mu$ m filter (Falcon) using the end of a syringe plunger in the presence of PBS. Erythrocytes were lysed from spleens by resuspension in 1 ml of RCRB and incubation for 3 minutes at room temperature (rt) and washed with FACS buffer.

To isolate lamina propria lymphocytes, guts were flushed with chilled PBS and kept moist with Hanks 2 % FCS while Peyer's patches were manually removed. Gut tissue was cut into 3-5 mm pieces and washed twice by vortexing in PBS. Gut pieces were transferred into 20 ml Hanks 2% FCS with 5 mM EDTA, vortexed, and incubated shaking (230 rpm) at 37 °C for 40 minutes, vortexed before, at 20 minutes of, and after incubation. Supernatant and gut pieces were transferred through a 70  $\mu$ m strainer and 30 ml Hanks 2% FCS added to neutralize digestive enzymes.

To isolate lymphocytes from VAT, tissue was placed in a 10 mm petri dish and minced into small pieces with a scalpel in 1 ml fat digestion buffer. Residual fat pieces were washed with 2-4 ml (based on VAT weight) digestion medium. All

minced tissue as transferred to a 50 ml tube (Falcon) and incubated shaking (180 rpm) at 37 °C for 50 minutes. After incubation tube was topped up to 40 ml with ice-cold FACS buffer and vortexed for 15s until well mixed. Samples were centrifuged at 800 x g for 15 min at 4 °C, supernatant discarded and resuspended in RCRB and incubated for one minute at rt and washed with FACS buffer. To remove cell debris, cell suspension was run through a 100 µm filter. Cells were resuspended in FACS buffer for antibody labelling and analysis.

### **2.3.2 Cell culture**

T cells were cultured in T cell medium at 37 °C in 5% CO<sub>2</sub>. For stimulated conditions, naïve CD4<sup>+</sup>CD25<sup>+</sup> T cells were activated using 10 µg/ml plate-bound anti-CD3 (2C11, produced in house) and soluble anti-CD28 (37.51, produced in house), in the presence of 100 U/ml recombinant human IL-2 (rhIL-2) (Peprotech) for neutral conditions. The following cytokines were included for stimulatory conditions 20 ng/ml IL-4 (R&D Systems), 0.5 ng/ml TGF-β (eBioscience), 10 ng/ml IL-6 (eBioscience), IL-27 ( ), IL-33 (Peprotech), IFN-γ ( ), IL-12 (Peprotech). Stromal cells were cultured in DMEM supplemented with 10% FCS and 1% PenStrep (Gibco) at 37 °C in 5% CO<sub>2</sub>.

### **2.3.3 *Ex vivo* restimulation of T cells**

Restimulation for cytokine production was performed using phorbol 12-myristate 12-acetate (PMA, 50 mg/ml) and ionomycin (0.5 mg/ml) (Sigma) in the presence of Brefeldin A (Sigma) in T cell medium for four hours at 37 °C in 5% CO<sub>2</sub>. The Invitrogen Bioscience Fixation and Permeabilization kit was used for intracellular analysis of cytokines, according to manufacturer's instructions.

### **2.3.4 Antibodies and flow cytometry**

Fluorochrome-conjugated antibodies that recognize the following mouse antigens were used for flow cytometry analysis.

**Table 2 | Antibody list**

<b>Antibodies</b>	<b>Clone</b>	<b>Manufacturer</b>	<b>Dilution</b>
CXCR3-BV421	CXCR3-173	Invitrogen/eBioscience	1:200
CXCR3-APC	CXCR3-173	Invitrogen/eBioscience	1:200
CD11b-BUV737	N418	BioLegend	1:200
CD11c-BV711	M1/70	BD	1:200
CD206-BV421	C068C2	BioLegend	1:200
CD206-FITC	C068C2	BioLegend	1:200
CD25-PECy7	PC61.5	Invitrogen/eBioscience	1:200
CD31-BV421	390	BioLegend	1:200
CD34-APC	RAM34	BD	1:100
CD38-PEDazzle594	90	BioLegend	1:200
CD39-BV605	24DMS1	Invitrogen/eBioscience	1:200
CD39-PECy7	24DMS1	Invitrogen/eBioscience	1:200
CD4-BUV496	GK1.5	BD	1:200
CD4-FITC	GK1.5	WEHI Antibody Facility	1:400
CD44-BUV395	IM7	BD	1:100
CD44-FITC	IM7	BD	1:200
CD45.2-Biotin	104	WEHI Antibody Facility	1:400
CD45.2-PacBlue	104	WEHI Antibody Facility	1:1600
CD45.2-BUV395	104	BD	1:100
CD45.2-BV605	104	BioLegend	1:200
CD49a-BV711	Ha31/8	BD	1:200
CD49a-PE	Ha31/8	BD	1:200
CD49b-APC	HMa2	BD	1:200
CD49b-PE	HMa2	BD	1:200
CD62L-BV605	DREG-56	BioLegend	1:800
CD62L-PECy7	MEL-14	Invitrogen/eBioscience	1:800
CD64-APC	X54-5/7.1	BioLegend	1:200
CD69-BV711	H1.2F3	BioLegend	1:200
CD69-PECy7	H1.2F3	Invitrogen/eBioscience	1:200

CD73-APC	TY/11.8	BioLegend	1:200
CD73-PE	TY/11.8	BioLegend	1:200
CD8a-BUV737	53-5.7	BD	1:400
CD90.2-FITC	30-H12	Invitrogen/eBioscience	1:200
CD90.2-PerCPeFluor710	30-H12	Invitrogen/eBioscience	1:200
F4/80-FITC	BM8	BioLegend	1:200
Foxp3-eFluor450	FJK-16s	Invitrogen/eBioscience	1:200
Foxp3-PE	FJK-16s	Invitrogen/eBioscience	1:200
Foxp3-PEeFluor610	FJK-16s	Invitrogen/eBioscience	1:200
GATA3-PE	TWAJ	Invitrogen/eBioscience	1:200
GATA3-PECy7	L50-823	BD	1:200
gp38-PECy7	eBio8.1.1	Invitrogen/eBioscience	1:200
GranzymeB-APC	GB12	Invitrogen/eBioscience	1:200
GranzymeB-PE	GB12	Invitrogen/eBioscience	1:200
IFN- $\gamma$ -PECy7	XMG1.2	Invitrogen/eBioscience	1:200
IL5-PE	TRFK5	Invitrogen/eBioscience	1:200
IL13-PECy7	eBio13A	Invitrogen/eBioscience	1:200
IL17A-PE	TC11-18H10	BD	1:200
IL17A-PerCPCy5.5	TC11-18H10	BD	1:200
Ki67-FITC	B56	BD	1:200
KLRG1-BV711	2F1	Invitrogen/eBioscience	1:200
KLRG1-FITC	2F1	BD	1:200
mCCR2-A700		R&D Systems	1:100
MHCII-APCCy7	M5/114.15.2	BioLegend	1:200
Neuropilin-SuperBright436	3DS304M	Invitrogen/eBioscience	1:200
NK1.1-BV605	PK136	BD	1:200
NKp46-PECy7	29A1.4	Invitrogen/eBioscience	1:200
SA-BUV395	n/a	BD	1:200
ST2-APC	RMST2-2	Invitrogen/eBioscience	1:200
ST2-PerCPeFluor710	RMST2-2	Invitrogen/eBioscience	1:200

TCF1-APC	C63D9	Cell Signalling Technologies	1:200
TCR $\beta$ -BV510	H57-597	BD	1:200
Ter119-A700	TER-119	BioLegend	1:200
Tigit-APC	GIGD7	Invitrogen/eBioscience	1:200
Tigit-PerCPeFluor710	GIGD7	Invitrogen/eBioscience	1:200
TNF-APC	MP6-XT22	BD	1:200
XCR1-BV650	ZET	BioLegend	1:200

For cell surface staining, antibodies were diluted at indicated concentrations and incubated with cells in PBS with 2% BSA on ice or 4 degrees for 30 mins. SytoxBlue (Invitrogen) or fixable viability dyes (ThermoFisher) were used to exclude dead cells. Intracellular staining was performed using the Foxp3 staining kit (eBioscience) according to manufacturer's protocols. In some experiments Treg cells were enriched prior to analysis or culture using antibodies against CD8 (53.6.7) and B220 (), followed by depletion with Goat anti-Rat magnetic beads (Polyscience). Or flow cytometrically using the BD FACSAria II or BD FACSAria Fusion. Flow cytometric analysis performed on the BD LSRFortessa, BD LSRFortessa X-20 or BD FACSCanto II (BD Biosciences).

### 2.3.5 Intravascular staining

Intravascular labelling was performed according to a published protocol (Anderson et al., 2014). Briefly, 3 $\mu$ g of CD45.2 – PacBlue was prepared in 300 $\mu$ l 1 x PBS and injected in the tail vein. The mice were euthanised with CO<sub>2</sub> 3 min post-injection for approx. 3min.

## 2.4 Procedure of molecular immunology

### 2.4.1 Polymerase chain reaction for PCR genotyping

PCR was performed using GoTaq Green Master Mix (Promega). Sequences (5'-3') of primers (Geneworks) for genotyping various genetic knock-out and transgenic mouse strains are listed in **Table 3**.

**Table 3** | List of primer for genotyping

Allele	Forward	Reverse
Foxp3-RFP	CAAAACCAAGAAAAGG TGGGC	Wild type: CAGTGCTGTTGCTGTG TAAGGGTC Reporter: GGAATGCTCGTCAAGA AGACAGG
Gata3-flox	TGTCAGGGCACTAAGG GTTG	WT/Flox: CACAGTGGGGTAGAGG TTGC Deletion: TTAAATCTCTGGCCCCT GTG
Ifng-null	Wild type: AGAAGTAAGTGGAAGG GCCCAGA Knockout: CCTTCTATCGCCTTCTT GACG	AGGGAACTGGGAGAG GAGAAATA
Il33-GFP	CACTAAGACTACTCAG CCTCAG	Wild type: CGGTGATGCTGTGAAG TCTG

		Reporter/Knock in: GTGTTCTGCTGGTAGT GGTCG
Pparg-flox	TGGCTTCCAGTGCATA AGTT	TGTAATGGAAGGGCAA AAGG
Sirt1-flox	GGTTAAGATTAGCCCA TTAAAGC	AGGAATCCCACAGGAG ACAG
Il1r1-null	AGGTGGATTATGACGT TGTGCTCATGG	Wild type: GCCCTCCGTAAGTGC AAATACATGGG Knock-out: ATCGCCTTCTATCGCCT TCTTGACGAG
Tbx21-flox	AGTCCCCCTGGAAGAA CACT	TGAAGGACAGGAATGG GAAC
Tbx21-null	Wild type: GACTGAAGCCCCGACC CCCCTCCTAA Knockout: GCGCGAAGGGGCCAC CAAAGAACGGAG	TGGGCATACAGGAGGC AGCAACAAATA

#### 2.4.2 RNA-sequencing and bioinformatic analysis

RNA was extracted from VAT using Qiagen RNeasy lipid tissue mini kit as per manufacturers protocol. VAT was pooled from 2 mice per sample. In each biological condition two samples were generated from a male and female mouse respectively. Library preparation was performed using the Illumina workflow according to TruSeq RNA Sample Preparation v2 Guide (Illumina). Briefly, mRNA was poly-A selected, fragmented and mixed with random primers. cDNA first and second strand synthesis was performed, followed by an end-repair reaction, phosphorylation and A-tailing. Samples were ligated to unique adapters and run

on a bioanalyser (Agilent) prior to pooling and sequencing on the NextSeq platform (Illumina).

All samples were sequenced on an Illumina NextSeq 500 generating 65 bp paired end reads. Reads were aligned to the mouse reference genome GRCm38/mm10 using the Subread aligner (Rsubread version 2.10.1) (Liao, Smyth, & Shi, 2013). Mapped reads were assigned to NCBI RefSeq mouse genes (build 38.1) and genewise counts were produced by using featureCounts (Liao, Smyth, & Shi, 2014). Genes that failed to achieve a CPM (counts per million mapped reads) value of 1 in at least 4 libraries were excluded from downstream analysis. Read counts were converted to log<sub>2</sub>-CPM, quantile normalized and precision weighted with the voom function of the limma package (Law, Chen, Shi, & Smyth, 2014; Ritchie et al., 2015). A linear model was fitted to each gene and batch effect was corrected during model fitting. Empirical Bayes moderated *t*-statistics were used to assess differences in expression (McCarthy & Smyth, 2009). Raw p values were adjusted to control the global FDR across all comparisons using the 'global' option in decideTests function in the limma package. Genes were called differentially expressed if they achieved a false discovery rate (FDR) less than 0.15. Enrichment analysis of Gene Ontology (GO) terms on the DE genes was performed using the goana function within the limma package<sup>63</sup>. Pathway enrichment against the Kyoto Encyclopedia of Genes and Genomes (KEGG) pathways on the DE genes was performed using the kegga function also implemented in the limma package.

### **2.4.3 Single-cell RNA-Seq and bioinformatics**

Equivalent amounts of a unique hashtag oligo (HTO)-conjugated anti-CD45 antibody (BD Mouse Immune Single-Cell Multiplexing Kit, #633793) and fluorescently labelled CD45 antibody were added to each sample. An initial round of low-purity, high-yield presorting of live single CD45<sup>+</sup> CD3<sup>+</sup> cells was followed by a high-purity sort of CD4<sup>+</sup> T cells. Sorted CD4<sup>+</sup> T cells were then loaded on a BD Rhapsody cartridge (BD Bioscience, #400000847) using a BD Rhapsody Express Single-Cell Analysis System. In total, 5 cartridges were used across 5

experimental days, and each cartridge was loaded with cells pooled from male and female mice after HTO-multiplexing. Cell and bead loading, cell lysis, recovery of mRNA-bound beads, reverse transcription, and exonuclease treatment were performed according to the manufacturer's instructions (BD Biosciences). Whole-transcriptome library preparation, based on the random-priming strategy, and index PCR steps were performed using the BD Rhapsody mRNA Whole Transcriptome Analysis and Sample Tag Library Preparation Protocol, as per the manufacturer's recommendations (BD Biosciences). Quantification of the cDNA libraries was performed using a Qubit Fluorometer with the Qubit dsDNA HS Kit (ThermoFisher), whereas the size distribution of the libraries was assessed using the Agilent High-Sensitivity D5000 assay on a TapeStation 4200 system (Agilent Technologies). Paired-end sequencing (2\*75 cycles) was performed on a NextSeq 500 System (Illumina) using NextSeq 500/550 High Output Kit v2.5.

Raw bcl files were demultiplexed using the Bcl2fastq2\_ V2.20 from Illumina. Sequencing adapters were trimmed and sequencing reads with a PHRED score >20 were filtered in using Cutadapt 1.16. Subsequently, STAR aligner (Dobin et al., 2013) was used to align reads against GENCODE vM16 mouse reference genome. Drop-seq tools 2.0.0 was used to generate a UMI-corrected gene expression count matrix. HTO sequences were added to the reference genome to simultaneously allow for their retrieval during alignment.

The dataset was filtered using the barcodeRanks() function to exclude cells with unique molecular identifier (UMI) counts below the inflection point, which represents the sharp transition in UMI counts between cell-containing wells and empty wells(Lun et al., 2019). Downstream analysis was performed using the Seurat R package(Stuart et al., 2019). The dataset was further filtered to exclude cells expressing less than 200 genes, more than 2000 genes, or cells whose mitochondrial reads account for more than 10% of their transcriptomes. After such filtration, 12,469 cells were included for further analysis. Normalization and scaling were performed using the SCTransform function(Hafemeister & Satija, 2019). The dataset comprised data generated from two separate sets of experiments, and a preliminary analysis on the composite data revealed a cross-

experiment batch effect. Hence, batch-effect correction and data integration were performed using the canonical correlation analysis method from Seurat. Specifically, after applying `SCTransform()` on the data from each set of experiments separately, the data was then integrated by sequentially running the following functions: `SelectIntegrationFeatures()`, `PrepSCTIntegration()`, `FindIntegrationAnchors()`, and `IntegrateData()`, selecting `nFeatures` of 3000 and setting the normalization method argument to `SCT`.

Downstream analysis was performed using the Seurat package. Principal component analysis (PCA) was applied using the `RunPCA()` function, and – based on elbow plot and the inspection of the individual PCs and their contribution to the variance in the data – the first 24 PCs were used for clustering. Clustering and non-linear dimensionality reduction were performed using the `FindClusters()` and `RunUMAP()` functions, respectively, using a resolution value of 0.8. Differential expression (DE) analysis was performed using the `FindAllMarkers()` function, setting both `min.pct` and `logfc.threshold` to 0.25.

The initial round of analysis showed an impact on clustering by differential expression of X- and Y-chromosome genes, cellular stress-related genes (van den Brink et al., 2017), and ribosome protein small (*Rps*) and large (*Rpl*) subunit genes. Hence, the following genes were excluded from the expression matrix (Soh et al., 2014; van den Brink et al., 2017): *Xist*, *Ddx3y*, *Eif2s3y*, *Kdm5d*, *Uty*, *Hsp\**; and *Rps\** and *Rpl\**, and the analysis steps were repeated.

Cluster annotation based on expression of canonical markers revealed the presence of small clusters containing mainly  $\gamma\delta$  T and myeloid cells. After exclusion of these two contaminating cell clusters, a total of 11,735 CD4<sup>+</sup> T cells were included in the further analysis. The aforementioned analysis steps were then applied on the subsetted CD4<sup>+</sup> T cells (with the exception of `SCTransform()` being applied on the entire dataset prior to integration). For Treg subclustering, the two Treg clusters described in – comprising 3304 cells – were subsetted and subjected to the same pipeline described above, with the following modifications: use of 10 PCs for clustering, and a resolution value of 0.2 in `FindClusters()`. For heatmap generation, clusters 3, 4, and 5 were merged, and DEG call was repeated using `FindAllMarkers()` function setting `min.pct` to 0.1 and

logfc.threshold to 0.25. Subsequently, the averages of gene-expression values per cluster were computed using the AverageExpression() function from Seurat. Heatmap was plotted using the pheatmap package (version 1.0.12), downsampling each cluster to 100 cells. All plotted genes passed the p value threshold of 0.05 except for Tcf7 and Prdm1.

Trajectory inference was conducted using the Monocle3 package (v0.2.3) (J. Cao et al., 2019). To set the root of the trajectory, the entropy of each cell cluster was calculated using the perCellEntropy function from the TSCAN package (v1.28.0) (Ji & Ji, 2016). The underlying assumption is that less-differentiated cells would exhibit a greater transcriptional diversity – and hence a higher entropy – compared to terminally differentiated cells. Accordingly, the *Sell*-expressing Treg cluster 1 was set as the root of the trajectory. The cluster\_cells() package from Monocle3 was used while setting k nearest neighbor to 35 and using “Louvain” as the clustering method. Histograms were generated using the dittoSeq package (Bunis, Andrews, Fragiadakis, Burt, & Sirota, 2020) in R.

## **2.5 Statistics**

If not stated otherwise, paired or unpaired Student's t test as appropriate were performed to test for statistical significance. P-values are two-tailed with a confidence level of 95% and statistical significance is defined as  $P < 0.05$ . 2-way ANOVA analysis was used to analyze populations over time, using Turkey's test for multiple comparisons with a 95% confidence interval. Calculations for statistical significance were performed using Graphpad Prism software.

## Chapter 3 – Cellular characterization of regulatory T cells in male and female VAT

### 3.1 VAT harbours a heterogenous population of Treg cells

Treg cells can adapt to diverse tissue environments where they not only perform canonical immune suppressive function, but also execute non-canonical functions to preserve tissue homeostasis (Cipolletta et al., 2012; Han et al., 2015; A. Vasanthakumar et al., 2015). VAT inflammation is driven by extrinsic and intrinsic factors such as diet and hormones (Cipolletta et al., 2015; Hotamisligil, Shargill, & Spiegelman, 1993; Carey N. Lumeng et al., 2007; Varghese et al., 2017; Vasanthakumar et al., 2020). Therefore, it was hypothesized that distinct Treg cell types with the ability to suppress unique inflammatory cues may exist in the VAT. To test this idea, single cell RNA sequencing (scRNAseq) of CD4<sup>+</sup> T cells (CD45<sup>+</sup>TCR $\beta$ <sup>+</sup>CD4<sup>+</sup>) isolated from the VAT from 22-week-old male and female C57BL/6 mice was performed (**Figure 2a**). Combined analysis identified several clusters, including conventional CD4<sup>+</sup> T cells with T<sub>H</sub>1 and T<sub>H</sub>2 transcriptional profiles and two clusters of Treg cells that expressed *Foxp3* and differed significantly by the expression of ST2 (**Figure 2b**). To dissect Treg cell heterogeneity in further detail, focused analysis of *Foxp3* expressing cells was performed which revealed five distinct clusters (**Figure 2c**). Surprisingly, two populations were identified that did not express canonical VAT Treg cell transcripts. In cluster 1 increased levels of *Lrrc32* and *Nrp1* expression were detected but also enriched expression of transcripts associated with naïve T cells, such as *Tcf7* and *Sell*. While cluster 2 was defined by transcripts associated with a T<sub>H</sub>1-like phenotype including *Tbx21*, *Cxcr3* and *Ifng* (**Figure 2d**), clusters 3, 4 and 5 were characterised by expression of prototypical VAT Treg cell transcripts, including *Il1r11*, *Ccr2* and *Klrg1* (**Figure 2d**). Furthermore, a higher amount of *Il10* transcripts were observed in clusters 4 and 5. Cluster 5 could be further defined by a distinctly high expression of *Gzmb* compared to the other clusters while cluster 4 was characterised by elevated *Areg* and *Cxcl2* transcript levels (**Figure 2c**). All the above clusters were represented in male and female mice, however,

cluster 1 and 2 dominate in females while cluster 3,4 and 5 made up a large proportion of the male VAT Treg cell population (**Figure 2e**). Hence, analysis revealed a heterogenous VAT Treg cell population that was enriched in a sex-dependent manner.

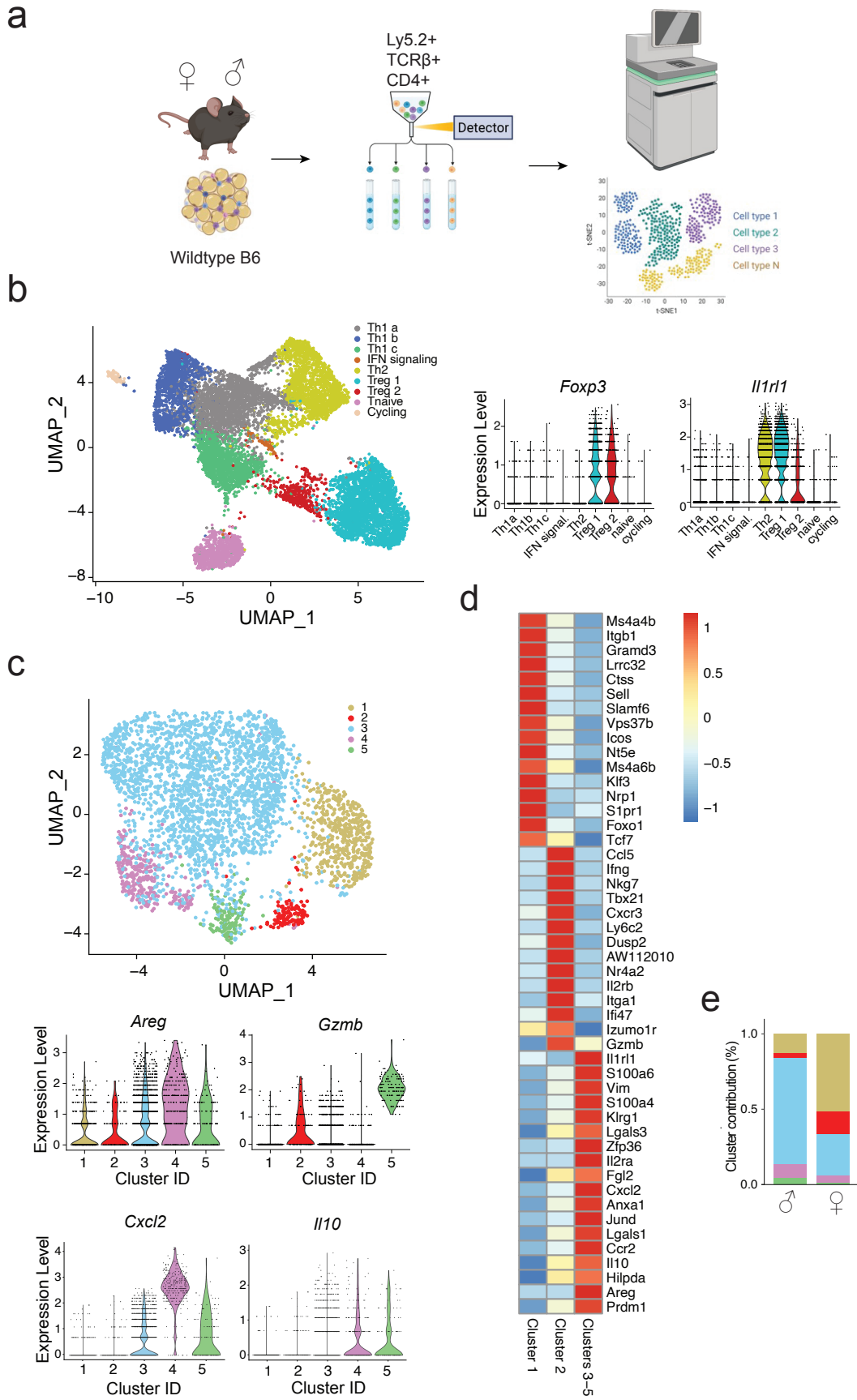


**Figure 2 | VAT harbours a heterogeneous population of Treg cells.** **a**, Schematic overview of experimental method. Briefly, CD45<sup>+</sup>CD3<sup>+</sup>CD4<sup>+</sup> VAT lymphocytes were sorted from 22-week-old male and female mice for single-cell RNA-Seq analysis. **b**, UMAP plot showing cell clusters of CD4<sup>+</sup> T cells and violin plots indicating *Foxp3* and *Il1rl1* expression. **c**, UMAP plot showing cell clusters among Foxp3<sup>+</sup> Treg cells and violin plots indicating *Areg*, *Gzmb*, *Cxcl2* and *Il10* and expression. **d**, Heatmap showing average expression of signature transcripts for VAT Treg cell (*Foxp3* expressing) clusters 1, 2 and 3-5. **e**, Bar graph showing percentages of cell clusters in the Treg cell compartment in male and female mice identified by single cell RNA sequencing.

### 3.2 ST2 and CXCR3 define two distinct mature VAT Treg cell populations

To further explore the heterogeneity of VAT Treg cells at the phenotypic level, flow cytometry was employed. Different VAT Treg cell populations were identified that could be compartmentalized into three distinct populations based on ST2 and CXCR3 expression. In line with the scRNA-Seq data, ST2<sup>+</sup> VAT Treg cells dominated in male mice and expressed high levels of KLRG1 and CCR2. Additionally, high IL-10 levels were detected in male mice only (**Figure 3a, b**). In contrast, proportions of DN (ST2-CXCR3<sup>-</sup>) and CXCR3<sup>+</sup> Treg cells were dominant in female and largely lacked KLRG1, CCR2 and IL-10 expression. However, there was no difference in cell numbers between both sexes in DN or CXCR3<sup>+</sup> cells (**Figure 3a**). Further characterisation of these three populations revealed that ST2<sup>+</sup> VAT Treg cells expressed higher levels of CD44, CD25, CD69 and PD-1. In contrast, DN and CXCR3<sup>+</sup> VAT Treg cells displayed higher expression of Nrp1 compared to ST2<sup>+</sup> cells (**Figure 3b**). DN Treg cells could be further defined by expression of CD62L, T cell factor (TCF)1 and CD73 which is in line with our scRNA-Seq data. Additionally, the proliferative capacity of the different Treg cell types was investigated by assessing Ki67 expression. Analysis showed that VAT Treg cells in female have a higher proportion of Ki67<sup>+</sup> cells compared to male mice (**Figure 3c, d**). The results showed that CXCR3<sup>+</sup> VAT Treg cells harboured the largest Ki67<sup>+</sup> cell population followed by DN, ST2<sup>+</sup> Treg cells (**Figure 3c, d**). Overall, the data corroborated the findings from scRNA-Seq analysis, showing two mature VAT Treg cell populations, ST2<sup>+</sup> and CXCR3<sup>+</sup>

cells, and a naïve-like population, all residing in the VAT but at proportions in males and females.

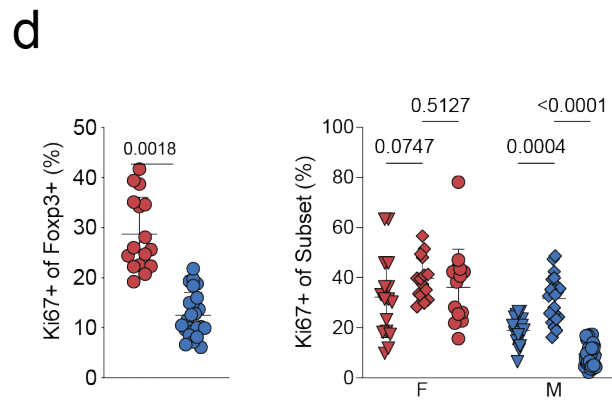
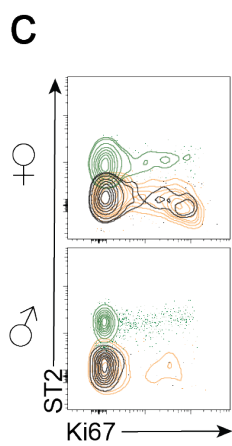
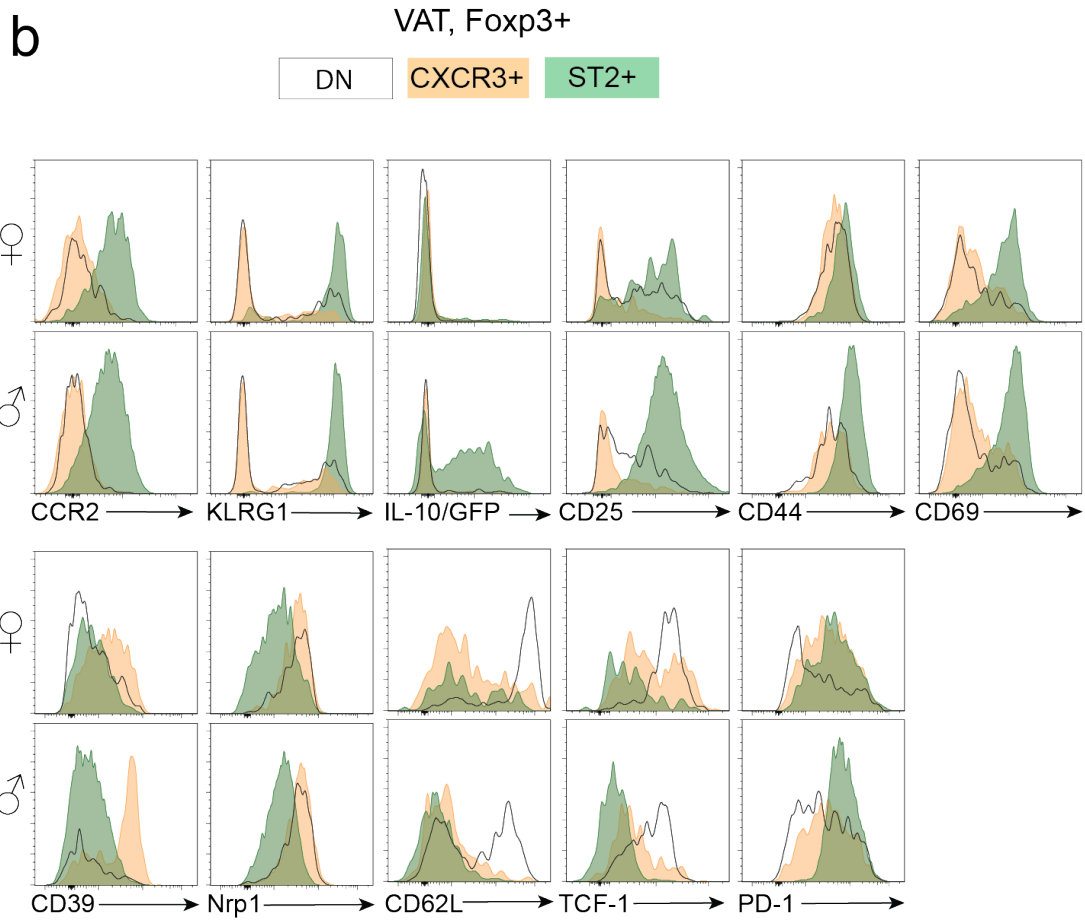
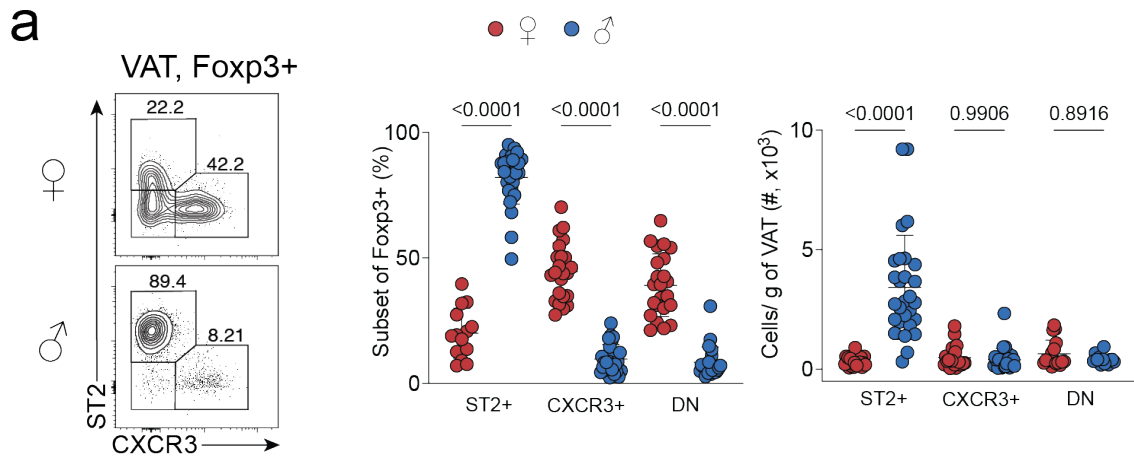


**Figure 3 | ST2<sup>+</sup> and CXCR3<sup>+</sup> VAT Treg cells display different enrichment and phenotype in male and female mice.** **a**, Flow cytometric analysis of 25-week-old male and female C57BL/6 mice showing ST2 versus CXCR3 expression among VAT Treg cells and quantification of ST2<sup>+</sup>, CXCR3<sup>+</sup> and DN VAT Treg cell proportion and numbers among total VAT Treg cells in female (red) and male (blue) mice. **b**, Expression of CCR2, KLRG1, *Il10*<sup>GFP</sup>, CD25, CD44, CD69, CD39, Nrp1, CD62L, PD1 and TCF-1 among ST2<sup>+</sup> (green), CXCR3<sup>+</sup> (orange) and DN (black line) VAT Treg cells in female (top) and male (bottom) mice. **c, d**, FACS plots (**c**) depicting Ki67 expression and quantification (**d**) in ST2<sup>+</sup> (green), CXCR3<sup>+</sup> (orange) and DN (black line) VAT Treg cells in female (top) and male (bottom) mice. Quantification of Ki67<sup>+</sup> cells among ST2<sup>+</sup>, CXCR3<sup>+</sup> and DN Treg cells. Symbols represent individual mice (**a**); horizontal lines indicate means (**a**). Data are representative (**b, c**) or pooled (**a**) from a minimum of two independent experiments. Error bars indicate the standard deviation. Statistical analyses were performed using two-way ANOVA (**d**).

### 3.3 CXCR3<sup>+</sup> VAT Treg cells are tissue resident

Prior to examining the function, kinetics and properties of the two new VAT Treg cell populations, DN and CXCR3<sup>+</sup> cells, the question arose whether these cells are tissue resident or cells derived from the vasculature. To separate resident and circulating immune cells, an intravascular staining technique was employed (Anderson et al., 2014). First, the effectiveness of the technique was assessed by looking at the overall contribution of circulating cells in blood (positive control) and lymph node (LN) (negative control). All Treg cells in the blood were stained by the intravascular antibody while Treg cells in the pLN remained negative for that antibody (**Figure 4a**). The vast majority of Treg cells in the VAT (approx. 90%) were iv<sup>-</sup>, and therefore tissue resident (**Figure 4a**). In male mice less than 3% ST2<sup>+</sup> VAT Treg cells were of intravascular origin. The contribution of circulating cells was approx. 12% in CXCR3<sup>+</sup> cells and more than 25% in DN cells in males. In females, DN cells had the highest proportion of circulating cells (approx. 22%) while they made up between 5-9% in ST2<sup>+</sup> and CXCR3<sup>+</sup> VAT Treg cells (**Figure 4b, c**). CD62L expression is typically associated with migrating and circulatory lymphocytes. CD62L expression was detected mostly in DN Treg cells in the VAT while its expression was absent or marginal in ST2<sup>+</sup> and CXCR3<sup>+</sup> VAT Treg cells (**Figure 4c**). These data show that CXCR3<sup>+</sup> and ST2<sup>+</sup>

are tissue resident while DN cells harbour a large proportion of naïve-like cells that are partly blood-borne characterized by CD62L expression.

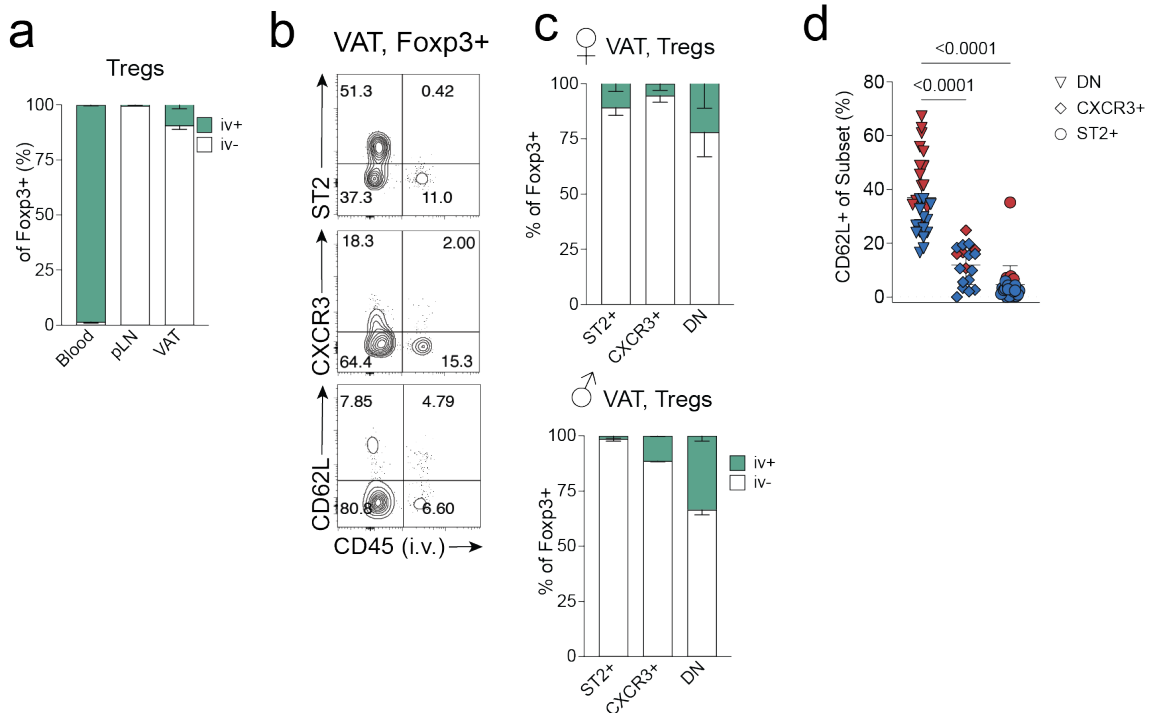


**Figure 4 | CXCR3<sup>+</sup> Treg cells are VAT resident cells.** Circulatory cells in male mice were stained with an intravascular (CD45, i.v.) antibody. **a**, Frequencies of intravascularly labelled (iv<sup>+</sup>) and non-labelled (iv<sup>-</sup>) VAT Treg cells. **b**, ST2, CXCR3 and CD62L expression versus CD45 (i.v.) expression in VAT Treg cells. **c**, Frequencies of iv<sup>+</sup> and iv<sup>-</sup> DN, CXCR3<sup>+</sup> and ST2<sup>+</sup> VAT Treg cells. **d**, Quantification of CD62L<sup>+</sup> among DN, CXCR3<sup>+</sup> and ST2<sup>+</sup> VAT Treg cells in female (red) and male (blue) mice. Symbols represent individual mice (**d**); horizontal lines indicate means (**d**). Data are representative (**b**) or pooled (**a**, **c**, **d**) from a minimum of two independent experiments. Error bars indicate the standard deviation. Statistical analyses were performed using two-way ANOVA (**d**).

### 3.4 CD62L<sup>+</sup> (DN) VAT Treg cells are precursors for CXCR3<sup>+</sup> and ST2<sup>+</sup> VAT Treg cells

Previous studies have shown that ST2<sup>+</sup> VAT Treg cells develop from tissue Treg cell precursors that express low amounts of PPAR $\gamma$ , KLRG1, BATF and Blimp1 (C. Li, A. R. Munoz-Rojas, et al., 2021). Furthermore, insulin signalling has recently been shown to be a major driver of their differentiation (Y. Li et al., 2021). To better understand the developmental trajectory of CXCR3<sup>+</sup> VAT Treg cells

and their relationship to ST2<sup>+</sup> VAT Treg cell population, trajectory inference using monocle3 was performed using our single cell data set. The trajectory analysis suggested that VAT Treg cells start at the cluster 1 (DN stage), which then bifurcates into ST2<sup>+</sup> and CXCR3<sup>+</sup> subpopulations (**Figure 5a**). In line with their circulatory origin and elevated expression of CD62L and TCF-1, these cells might constitute uncommitted Treg cells in circulation or *en route* to seed the VAT and act as precursors to mature VAT Treg populations. Elevated expression of CD73 DN Treg cells supported this notion (**Figure 5b, c**). Furthermore, it was determined that CD73<sup>+</sup> Treg cells partly co-expressed CD62L which further sets them apart from the mature ST2<sup>+</sup> and CXCR3<sup>+</sup> VAT Treg cells (**Figure 5c**). Importantly, however, trajectory inference analysis does not guarantee that pseudotime and chronological time have a linear relationship and the analysis does not specify whether the cells maintain plasticity or not, which should be considered in the interpretation of these results (van den Berge et al, 2020).

Another method used to test for VAT Treg cell trajectory was to deplete Treg cells in the VAT, requiring new cells to fill the niche. For this purpose, *Foxp3<sup>DTR</sup>* mice were used which allowed for punctual Treg cell depletion (J. M. Kim, Rasmussen, & Rudensky, 2007). Treg cell depletion was induced with a single DT injection leading to systemic Treg cell death. Analyses were subsequently performed 3-, 10- and 30-days post DT treatment to follow gradual VAT Treg cell recovery (**Figure 6a**). Mice analysed on day-3 were devoid of Treg cells in the spleen and VAT, whereas Treg cells had gradually re-populated these tissues by days 10 and 30 post DT treatment (**Figure 6b**). In line with transfer experiments into *Rag1<sup>-/-</sup>* mice described above, analysis of VAT Treg cells at day 10 post DT treatment revealed a dominance of CD62L<sup>+</sup> and CXCR3<sup>+</sup> Treg cells in male and female DT treated mice (**Figure 6c-e**). However, CD62L<sup>+</sup> and CXCR3<sup>+</sup> Treg cell numbers were only elevated in female DT treated mice while the numbers in male mice were equal to controls. In contrast, ST2<sup>+</sup> Treg cells were only detectable 30 days post treatment, but specifically in male DT treated mice.

It is noteworthy to mention that DT treatment induces an artificial inflammatory state that might not reflect the status at early age considering that the microflora is also

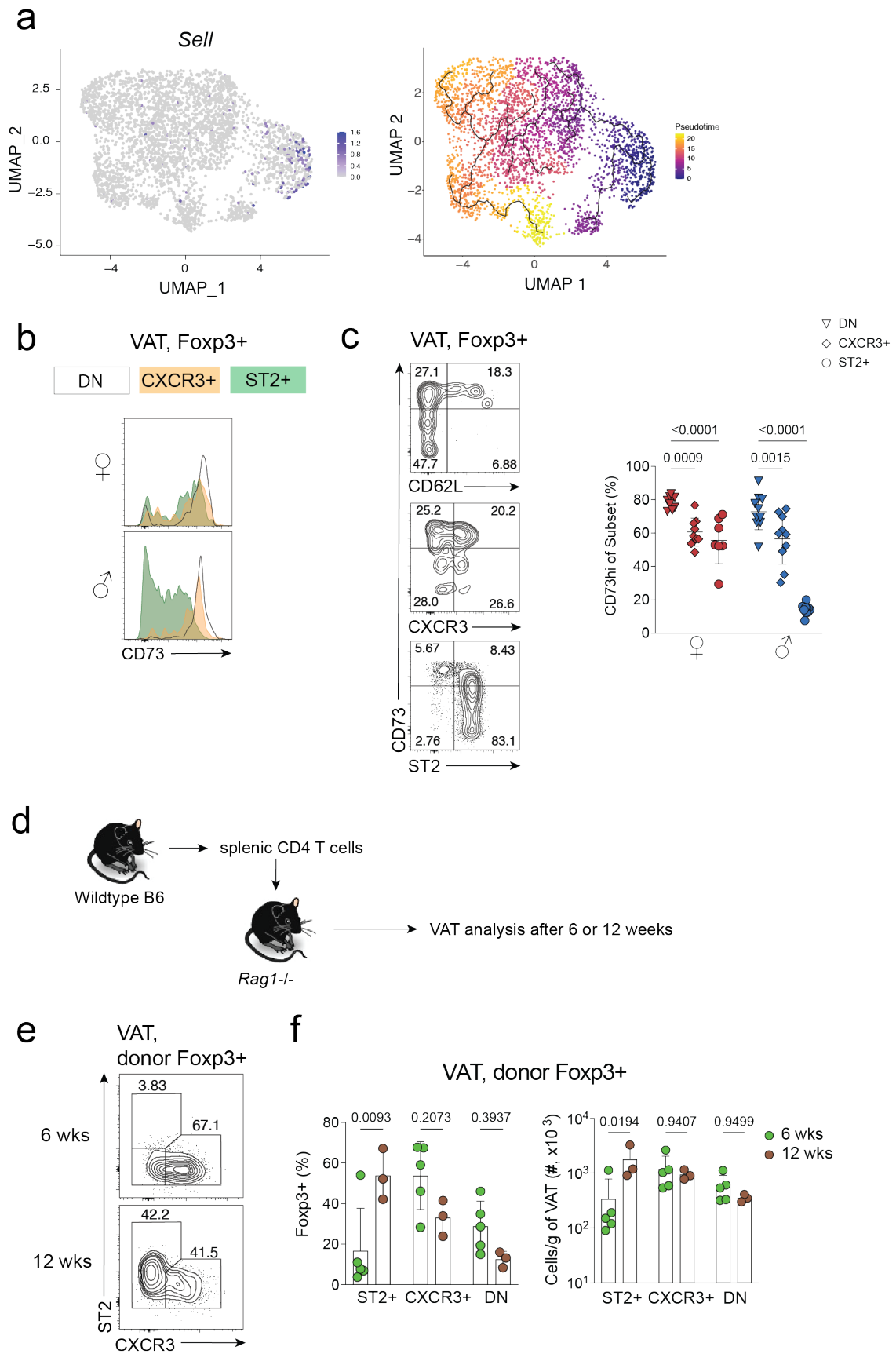


**Figure 5 | CXCR3<sup>+</sup> and ST2<sup>+</sup> VAT Treg cells have different developmental trajectories.** **a**, UMAP plot showing *Sell* expression within Treg cells (left) and trajectory-based differential gene expression along different cell stages as a function of pseudotime through Monocle analysis (right). **b**, Expression of CD73 among double negative (DN; black line), ST2<sup>+</sup> (green) and CXCR3<sup>+</sup> (orange) VAT Treg cells in female (top) and male (bottom) adult mice. **c**, Flow cytometry plots showing CD73 versus CD62L, CXCR3 and ST2 expression in female and male VAT Treg cells (left) and quantification of CD73 expression (right). **d-f**, CD4<sup>+</sup> cells were transferred into sex-matched male *Rag1*<sup>-/-</sup> mice. **d**, Schematic of experiment. **e**, ST2 and CXCR3 expression on VAT Treg cells in *Rag1*<sup>-/-</sup> mice 6 (top) and 12 (bottom) weeks post-transfer. **f**, Frequencies (left) and absolute numbers (right) of DN, CXCR3<sup>+</sup> and ST2<sup>+</sup> VAT Treg cells 6- and 12-weeks post-transfer. Symbols represent individual cells (**a**) or mice (**c**, **h**); horizontal lines indicate means (**c**). Data are representative (**b**, **c**, **e**) or pooled (**c**, **f**) from a minimum of two independent experiments. Error bars indicate the standard deviation. Statistical analyses were performed using two-way ANOVA (**c**, **h**).

Overall, findings from the above experiments suggest that CD62L, TCF-1 and CD73 expressing naïve Treg cells populate the VAT and are directed to differentiate into CXCR3<sup>+</sup> and ST2<sup>+</sup> VAT Treg cells *in situ*. Chronologically, CXCR3<sup>+</sup> VAT Treg cell differentiation appears to precede ST2<sup>+</sup> cells suggesting distinct and temporal tissular signals might facilitate the differentiation of these two Treg cell types in the VAT.

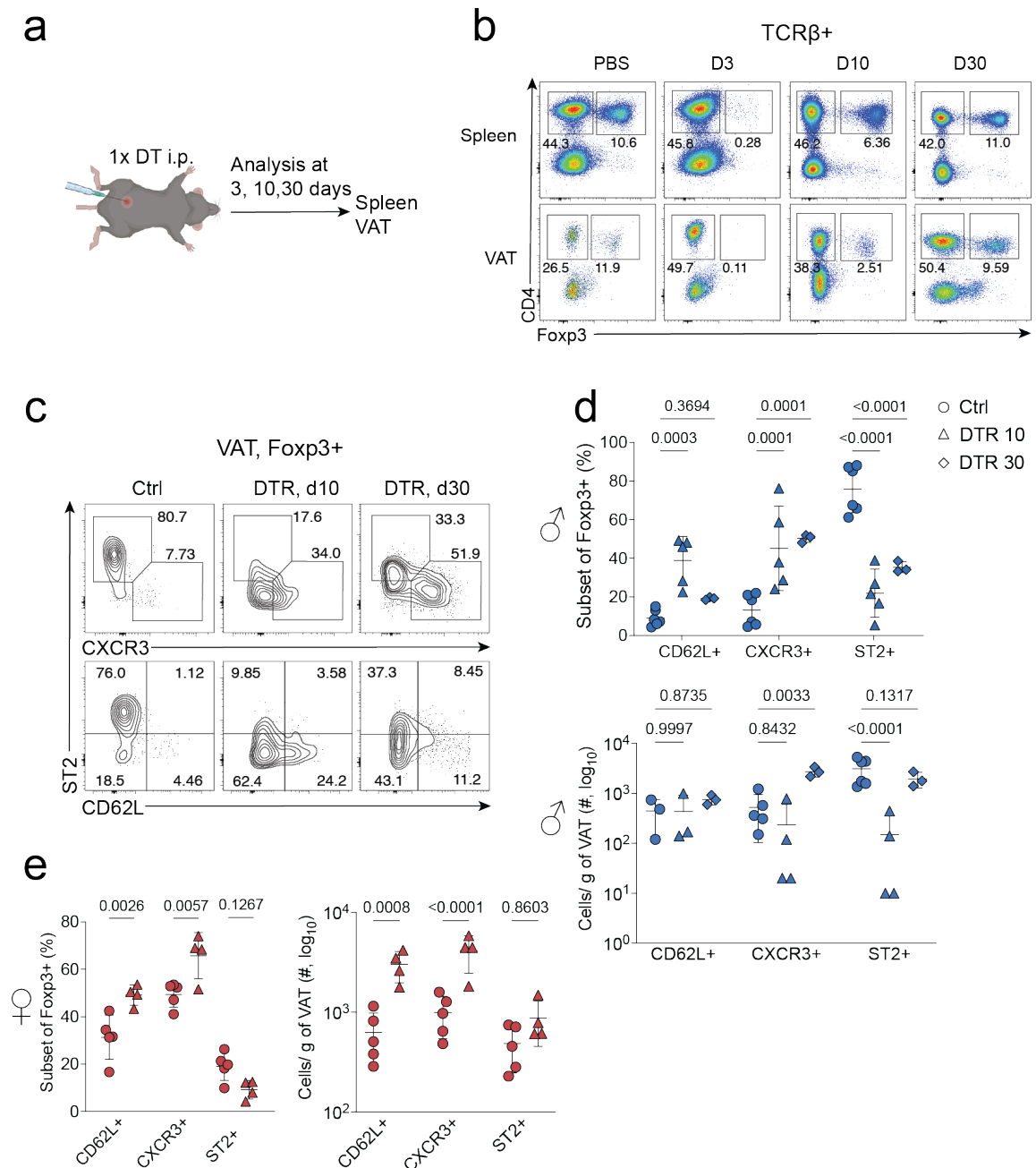


**Figure 6 | CXCR3<sup>+</sup> and CD62L<sup>+</sup> Treg cells emerge first after Treg depletion.**

**a-e**, *Foxp3<sup>DTR</sup>* and control mice were administered a single dose of diphtheria toxin (DT) and left to recover. **a**, Schematic of the experiment. **b**, Flow cytometry plots showing expression CD4 and Foxp3 in CD4<sup>+</sup> T cells from spleen (top) and VAT (bottom) in control mice (PBS) or in *Foxp3<sup>DTR</sup>* mice 3, 10 and 30-days post DT administration. **c**, Flow cytometry plots showing ST2, CXCR3 and CD62L expression in VAT Treg cells in control and *Foxp3<sup>DTR</sup>* mice 10- and 30-days post-treatment. **d-e**, Frequencies and numbers of ST2<sup>+</sup>, CXCR3<sup>+</sup> and CD62L<sup>+</sup> cells among VAT Treg cells in male (blue) and female (red) mice. Symbols represent individual mice; horizontal lines indicate means. Data are representative (**b, c**) or pooled (**d, e**) from at least two independent experiments; FACS plots are

representative. Error bars indicate the standard deviation. Statistical analyses were performed using two-way ANOVA.

### 3.5 Development of the VAT Treg cell compartment

To assess the developmental kinetics of the VAT Treg cell subtypes, male and female mice of different age groups were analysed. Notably, there was no sex-dependent dichotomy in total Treg proportion and numbers in young adult mice (7-weeks-old) (**Figure 7a**). There were also similar proportions of ST2<sup>+</sup> and CXCR3<sup>+</sup> subsets in young male and female mice (**Figure 7b**). Furthermore, expression of prototypical VAT Treg cell molecules CCR2 and KLRG1 were highest in ST2<sup>+</sup> Treg cells from 7-week-old mice comparable to aged mice (see **Fig. 2; Fig. 5c**). The expression pattern of markers that delineate naïve lymphocytes such as CD73 and CD62L were also investigated. Analysis showed similar CD73 expression levels in ST2<sup>+</sup> and DN cells of female mice. (**Figure 7c, d**). Surprisingly, CXCR3<sup>+</sup> Treg cells showed the lowest CD73 expression, which contrasts with what we observed in adult females. On the other hand, male DN Treg cells expressed the highest amount of CD73 compared to CXCR3<sup>+</sup> and ST2<sup>+</sup> populations, in line with the expression pattern in adult male mice (**Figure 7d**). Measurement of CD62L expression revealed that the majority of CD62L<sup>+</sup> Treg cells were within the DN population and mirrored the results of mature adult mice of both sexes. CD44 expression was significantly higher in ST2<sup>+</sup> cells compared to DN and CXCR3<sup>+</sup> Treg cells, in line with the phenotype of adult Treg cells (**Figure 7d**).

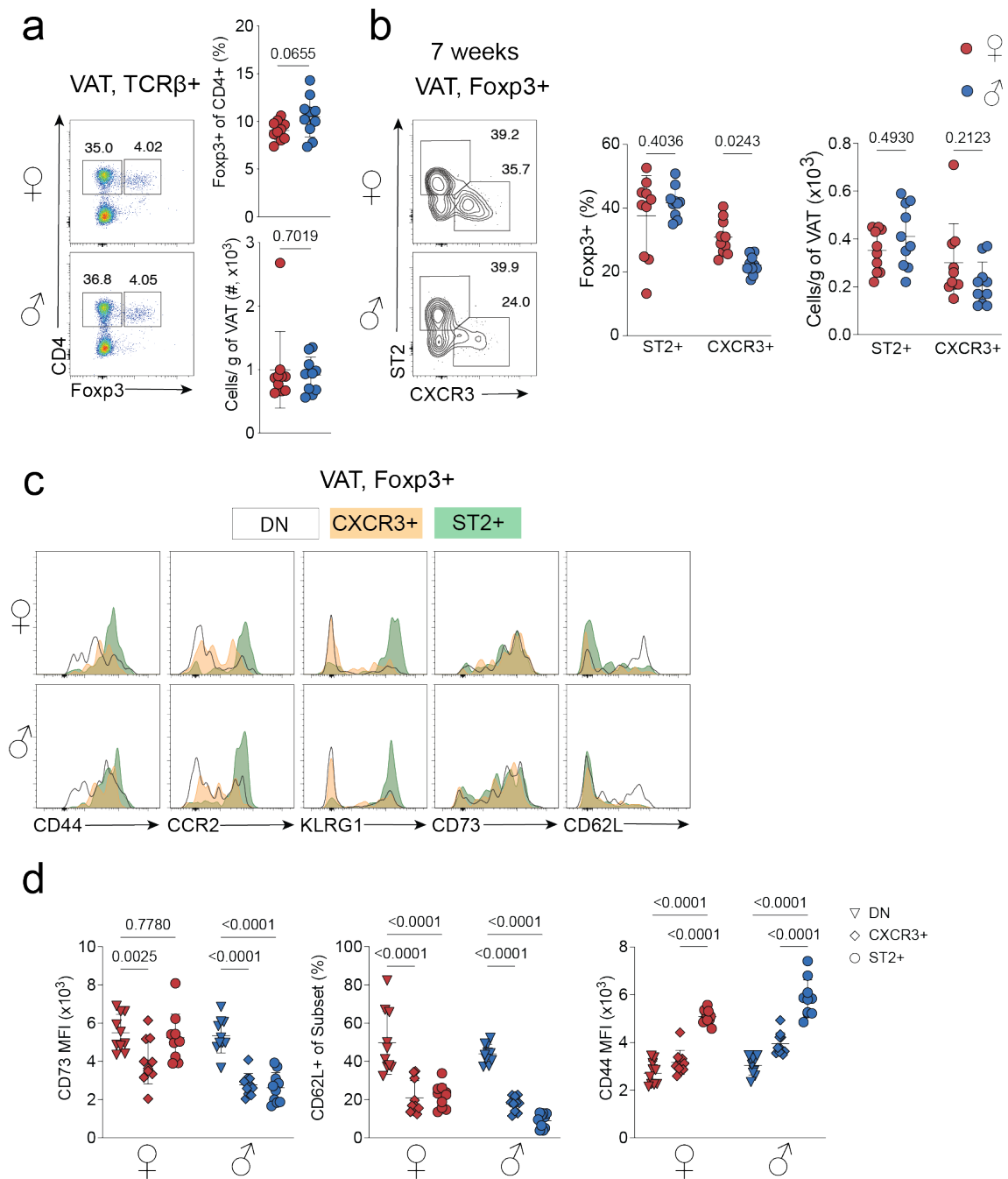


**Figure 7 | VAT Treg cell composition is different in young adult mice.** VAT Treg cells from young (7-week-old) male and female mice were analysed. **a**, CD4 and Fcpx3 expression of VAT TCR $\beta$ + T cells (left). Frequencies (top) and numbers (bottom) of Treg cells. **b**, ST2 and CXCR3 expression of VAT Treg cells in male and female mice (left). Frequencies (centre) and numbers (right) of ST2+ and CXCR3+ cells. **c**, Expression of CD44, CCR2, KLRG1, CD73 and CD62L among (DN; black line), ST2+ (green) and CXCR3+ (orange) VAT Treg cells in female (top) and male (bottom) adult mice. **d**, Quantification of CD62L+ cells (right) and CD73 (left) and CD44 MFI (centre) among DN, CXCR3+ and ST2+ VAT Treg cells. Symbols represent individual mice; horizontal lines indicate

means. Data are representative (a, **b**, **c**) or pooled (a, b, **d**) from at least two independent experiments; FACS plots are representative. Error bars indicate the standard deviation. Statistical analyses were performed using two-way ANOVA (**b**, **d**) or unpaired, two-tailed Student's *t*-test (**a**).

Consistent with the published studies, our analysis also showed that the proportion of total VAT Treg cells increases over time, but only in male mice (**Figure 8a**) (Cipolletta et al., 2015). Further investigation revealed that ST2<sup>+</sup> and CXCR3<sup>+</sup> Treg cell proportions start at similar levels in male and female mice (**Fig. 3.7b**). At 15 weeks however, sexual dimorphism was observed that continued up to 30-weeks of age. Beyond this period, proportion of female ST2<sup>+</sup> VAT Treg cells gradually increased until about 40 weeks of age, but still stayed significantly lower than males. Percentage of ST2<sup>+</sup> cells showed minimal decrease beyond 40 weeks to approx. 74% in male and 35% in female mice (**Figure 8b**). Similarly, CXCR3<sup>+</sup> VAT Treg cells were approximately 20 and 30% in 7-week-old male and female mice, respectively, which then increased in females but decreased in male VAT (Fig. 3.7b). After dipping at around 33 weeks of age, the proportion of CXCR3<sup>+</sup> cells increased at 40 weeks in males, but still much lower compared to females. At approximately one-year of age, CXCR3<sup>+</sup> cells on average contribute to 20% and 40% of male and female VAT Treg cells, respectively (**Fig. 3.7b**).

Analysis of the VAT in 50-55w old mice revealed that the distribution of Treg cell subtypes was largely sex-specific. VAT Treg cells were higher in proportion and numbers in male mice compared to female mice (**Figure 8c**). Furthermore, ST2<sup>+</sup> VAT Treg cells were still dominant in males, while CXCR3<sup>+</sup> and DN cells were dominant in female mice (**Figure 8d**). Next, the proliferative capacity of Treg cells was investigated by Ki67 expression and found that it is higher in females compared to males (**Figure 8e**). This was particularly the case in female ST2<sup>+</sup> VAT Treg cells which expressed significantly higher amounts of Ki67 compared to their male counterparts (**Fig. 3.7f**). Ki67 expression did not differ in DN and CXCR3<sup>+</sup> cells between both sexes and there was also no difference in the number of Ki67-expressing cells in any of the Treg cell subtypes. Overall, the data shows the distinct developmental kinetics of ST2<sup>+</sup> and CXCR3<sup>+</sup> VAT Treg

cells, which showed sex-specific distribution of Treg cell subsets even in 1 year old male and female mice.

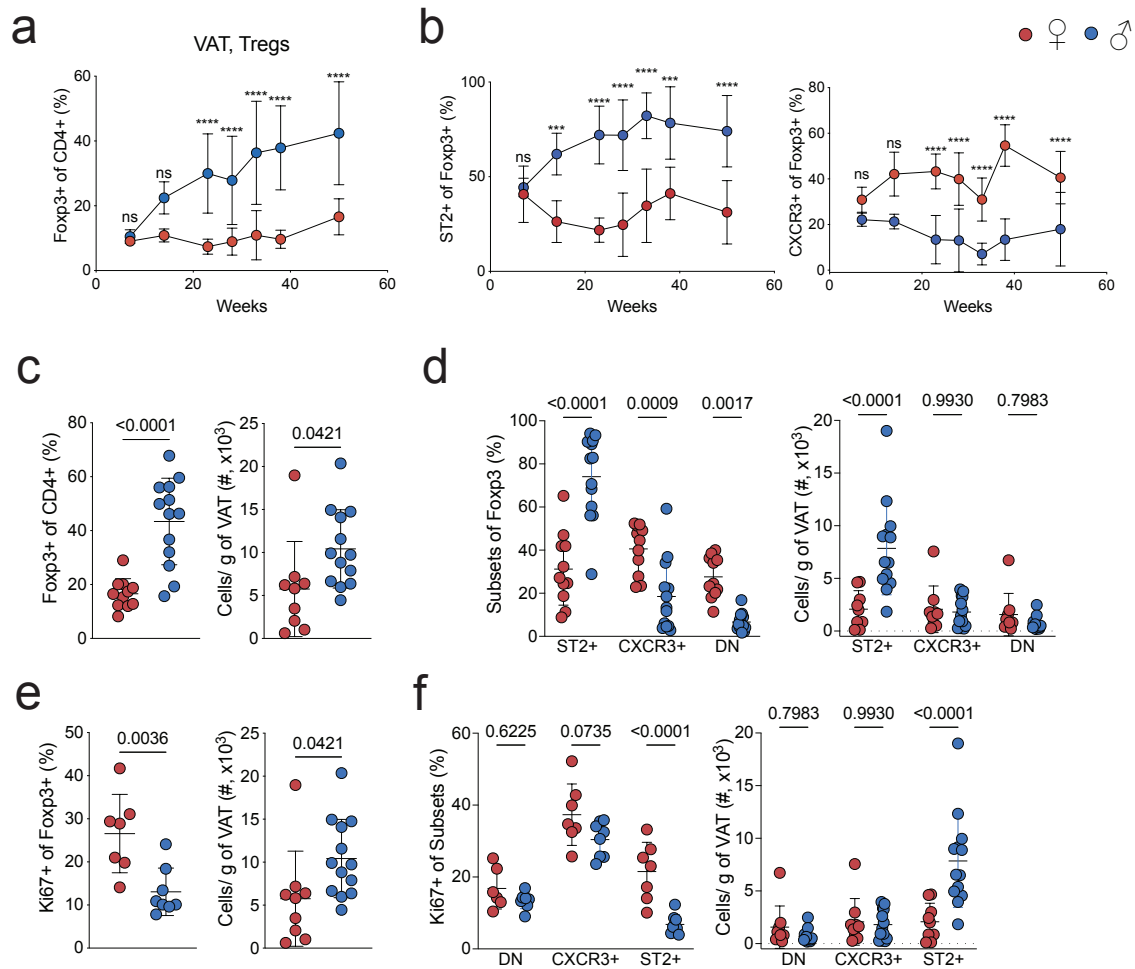


**Figure 8 | VAT Treg cell population do not change significantly with progressing age. a, b,** Frequencies of total (a) or ST2+ (b, left) and CXCR3+ (b, right) VAT Treg cells from female (red) and male (blue) mice at different ages. **c-f,** Mice at 50-55 weeks of age were analysed. **c, d,** Frequency and numbers of total (c) and ST2+, CXCR3+ and DN (d) VAT Treg cells. Quantification of Ki67+ cells in total (e) and ST2+, CXCR3+ and DN (f) VAT Treg cells. Symbols represent individual mice (c-f) or the means (a, b) of at least two biological replicates. Error bars indicate the standard deviation. Data are representative pooled from at least two independent experiments. Error bars indicate the standard deviation. Statistical analyses were performed using two-way ANOVA (d, f) or unpaired, two-tailed Student's *t*-test (a-c, e).

### 3.6 CXCR3<sup>+</sup> and ST2<sup>+</sup> VAT Treg cells correlate differently to body and VAT weight

Despite the clear differences between sexes in ST2<sup>+</sup> and CXCR3<sup>+</sup> VAT Treg cell composition, a substantial degree of biological variation was observed. ST2<sup>+</sup> cells ranged between 5-40% in females and between 70-95% in males. On the other hand, CXCR3<sup>+</sup> cells contributed between 30-65% in females and 0-30% in males (see **Fig. 2b**). Given the large variation among mice of the same age, Treg cell proportions were correlated to body and VAT weight of individual mice. First, a positive correlation between body weight and frequency of total Treg cells was observed in pooled samples from both sexes (**Figure 9a**). The data showed the same for numbers of total Treg cells, which significantly correlated to body weight. Correlation between VAT weight and proportion and numbers of Treg cells followed the same trend, although the slope and  $R^2$  of the regression curve were smaller than the curves of the body weight data (**Figure 9b**). Furthermore, ST2<sup>+</sup> VAT Treg cells correlated with increasing body weight in a positive manner, both in proportion and numbers (**Figure 9c**). The correlation of ST2<sup>+</sup> Treg cells to VAT weight mirrored the data observed in total Treg cells: positive correlation with a relatively small  $R^2$  (**Figure 9d**). Unlike total and ST2<sup>+</sup> VAT Treg cells, the proportion of CXCR3<sup>+</sup> cells correlated negatively with body and VAT weight (**Figure 9e, f**). In contrast to ST2<sup>+</sup> Treg cells, numbers of CXCR3<sup>+</sup> VAT Treg cells did not correlate with body or VAT weight. Taken together, total and ST2<sup>+</sup> VAT Treg cells expanded with increasing body and VAT mass, while CXCR3<sup>+</sup> VAT Treg cell proportions negatively correlated with body and VAT mass.

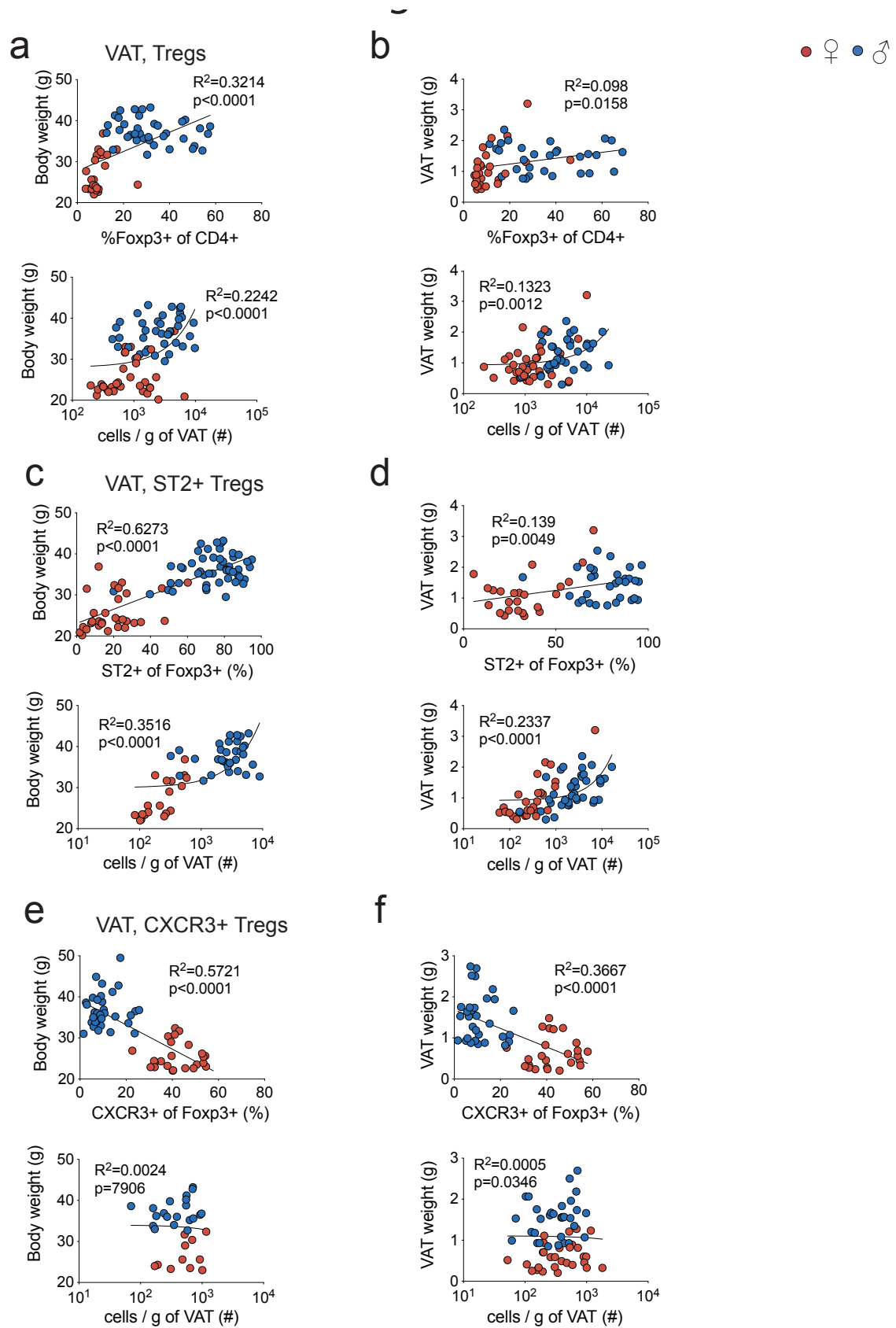


**Figure 9 | ST2+ VAT Treg cells positively correlate with adiposity.** Correlation between body weight (**a, c, e**) or VAT weight (**b, d, f**) and total, (**a, b**), ST2+ (**c, d**) and CXCR3+ (**e, f**) VAT Treg cells in 25–30-week-old mice. Symbols represent individual mice. Data are pooled from a minimum of two independent experiments. Statistical analyses were performed using a linear regression model.

### 3.7 Variation in weight gain and metabolic phenotype of high fat diet fed mice

It is well documented that high-fat diet (HFD) affects VAT Treg cells and the VAT microenvironment. To understand the effect of HFD on adiposity, Treg cell distribution and systemic metabolism, male and female C57BL/6 mice were fed a HFD for the duration of 20-25 weeks. Weight gain was tracked over the period; VAT weight and glucose tolerance were recorded at the experimental endpoint. There was significant variation across experiments; hence two experiments were compared to exemplify the different outcomes that were observed. In the first experiment ND and HFD fed females gained approx. 180% of their start weight at the experimental endpoint (**Figure 10a**). In contrast, female mice from experiment 2 gained approx. 165% and 200% when fed a ND and HFD, respectively. In male mice, weight gain of HFD mice was similar in both experiments, yet ND males from experiment 1 gained more weight compared to ND males in experiment 2 (160% vs 140%). In line with the weight gain, VAT mass from HFD fed females was not different from ND females in the first experiment while HFD females in the second experiment had significantly increased VAT mass. VAT weight was higher in HFD compared to ND in male mice of both experiments (**Figure 10b**).

In line with these observations, glucose tolerance testing also revealed different outcomes. In experiment 1, only males on HFD were glucose intolerant compared to male controls while there was no difference between ND and HFD females (**Figure 10c**). In contrast, only females on HFD were glucose intolerant compared to controls in experiment 2. No difference between ND and HFD males was observed in this case.

Overall, the results showed a significant degree of variance after HFD making it difficult to draw any conclusions on sex-bias in adiposity and glucose tolerance upon HFD feeding.

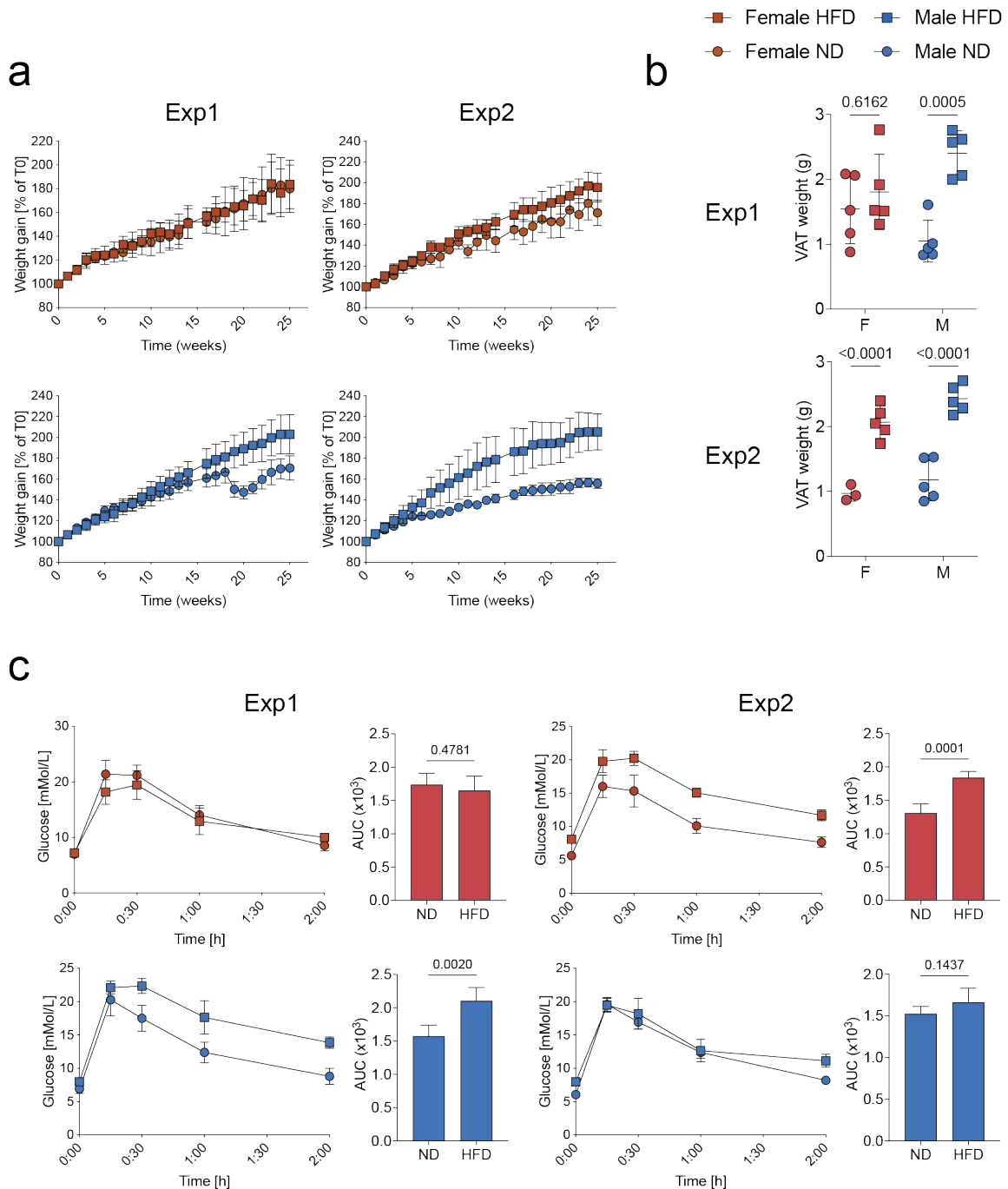


**Figure 10 | High-fat diet induces different phenotypes in glucose metabolism.** C57BL/6 female and male mice were subjected to high-fat diet for 25 weeks. **a, b**, Curves depicting weight gain (**a**) and graphs showing VAT weight (**b**) of ND and HFD mice out of two independent experiments. **c**, Glucose

tolerance tests of female and male mice on ND and HFD and quantification of area under the curve. Symbols represent individual mice (**b**) or mean of 3-5 mice (**a**, **c**); horizontal lines indicate means (**b**). Data are from two separate experiments. Error bars indicate the standard deviation (**a**, **b**) or s.e.m. (**c**). Statistical analyses were performed using two-way ANOVA (**b**) unpaired, two-tailed Student's *t*-test (**c**).

### 3.8 High-fat diet has little impact on VAT Treg cell composition

VAT Treg cells are known to promote or protect against glucose intolerance in a context specific manner (S. P. Bapat et al., 2015; Beppu et al., 2021; Cipolletta et al., 2012; M. Feuerer et al., 2009; Man et al., 2022; Wu et al., 2020). These conflicting findings could be due to the different experimental approaches or animal models used by the research groups and therefore more evidence is required to fully understand the function of Treg cells in VAT. Loss of Treg cells in the VAT is generally associated with exacerbation of inflammation and attributed to their protective function. The aim of the present section was to assess changes in VAT Treg cells in mice fed a high-fat diet (HFD) compared to sex-matched mice on normal chow (ND).

Surprisingly, analysis of ST2<sup>+</sup> and CXCR3<sup>+</sup> VAT Treg cell populations did not show difference in proportion or numbers between males that were on ND or fed HFD for 25 weeks (**Figure 11a, b**). In contrast, ST2<sup>+</sup> Treg cells expanded in HFD fed females but CXCR3<sup>+</sup> VAT Treg cells were reduced in proportion compared to ND females. Yet, total number of VAT Treg cells remained unchanged in HFD females compared to their ND fed counterparts. However, across all experiments a high degree of variation between individual mouse was observed. Therefore, to better understand the relation between Treg cell populations and weight gain, percentages and numbers of ST2<sup>+</sup> and CXCR3<sup>+</sup> VAT Treg cells were correlated to body and VAT weight of the corresponding mouse. Unexpectedly, correlation between ST2<sup>+</sup> VAT Treg cell proportions and weight was similar in both, ND and HFD mice, suggesting no diet induced changes. The same observation was made when correlating ST2<sup>+</sup> VAT Treg cell numbers with body weight (**Figure 11c**). Furthermore, correlation of CXCR3<sup>+</sup> VAT Treg cell percentage and numbers with body weight was not significantly different between ND and HFD

mice (**Figure 11d**). ST2<sup>+</sup> or CXCR3<sup>+</sup> VAT Treg cell proportions were positively and negatively correlated with VAT weight, respectively, yet no diet specific impact was observed in either case (**Figure 11e**).

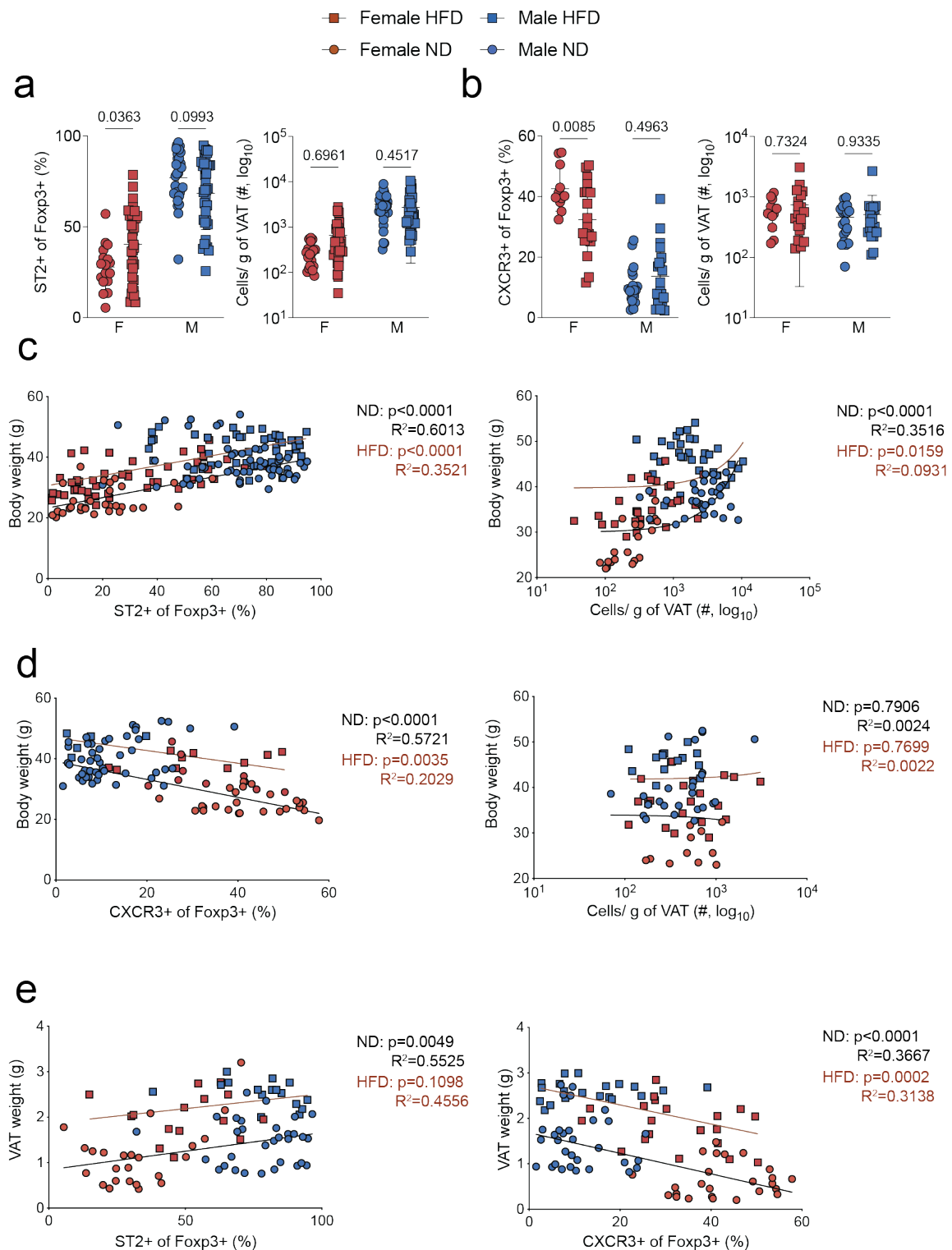


**Figure 11 | High-fat diet has a different impact on Treg cells in female and male mice.** C57BL/6 female and male mice were subjected to high-fat diet for 25 weeks and VAT was analysed. **a, b** Quantification of frequencies and numbers of ST2+ (**a**) and CXCR3+ (**b**) VAT Treg cells in HFD mice and controls on normal diet. **c, d**, Correlation between body weight and frequencies (left) and numbers (right) of ST2+ (**c**) and CXCR3+ (**d**) VAT Treg cells in 25–30-week-old mice on

ND or HFD. Symbols represent individual mice; horizontal lines indicate means (**a, b**). Data are pooled from a minimum of two independent experiments. Error bars indicate the standard deviation. Statistical analyses were performed using two-way ANOVA (**a, b**) or a linear regression model (**c-e**).

### **3.9 VAT Treg cell composition in other adipose tissue depots and mouse models**

Compared to other AT depots, Treg cells in the VAT are unique in displaying sexual dimorphism (Vasanthakumar et al., 2020). However, Treg cell heterogeneity in other AT depots remain unexplored. Here, different AT depots in male and female mice were analysed, to assess the distribution of CXCR3<sup>+</sup> and ST2<sup>+</sup> VAT Treg cells. Flow cytometric analysis showed that Treg cell enrichment in males is unique to VAT and was not observed in scAT, pnAT nor mAT (**Figure 12a**) (Vasanthakumar et al., 2020). Assessment of Treg cell subsets showed that CXCR3<sup>+</sup> Treg cells were present to varying degrees in other AT depots but in similar proportions in both sexes (**Figure 12b, c**). Surprisingly, sex-dependent distribution of ST2<sup>+</sup> VAT Treg cells was observed in pnAT, but not in scAT nor mAT.

To assess strain specific differences, mice from different genetic backgrounds were analysed to confirm whether sex dependent Treg cell enrichment was conserved in other mouse models. C57BL/6 mice are known to have T<sub>H</sub>1-dominant immune responses whereas, T<sub>H</sub>2 immunity is dominant in Balb/c mice (Heinzel, Sadick, Holaday, Coffman, & Locksley, 1989; Hsieh, Macatonia, O'Garra, & Murphy, 1995). Hence, we explored whether these differences also affect the phenotypic diversity of VAT Treg cells. Unlike C57BL/6 mice, 30–33-week-old Balb/c mice did not display sexual dimorphism in the total VAT Treg cell population in proportion or in numbers (**Figure 12d, e**). Notably, however, CXCR3<sup>+</sup> VAT Treg cells were more prevalent in female mice compared to males, while no difference was detected in ST2<sup>+</sup> VAT Treg cell distribution (**Figure 12f, g**). In conclusion we only observed partial sex-bias in Treg cell phenotypes in pnAT depot but no strain specific differences when comparing C57BL/6 and Balb/c mice.

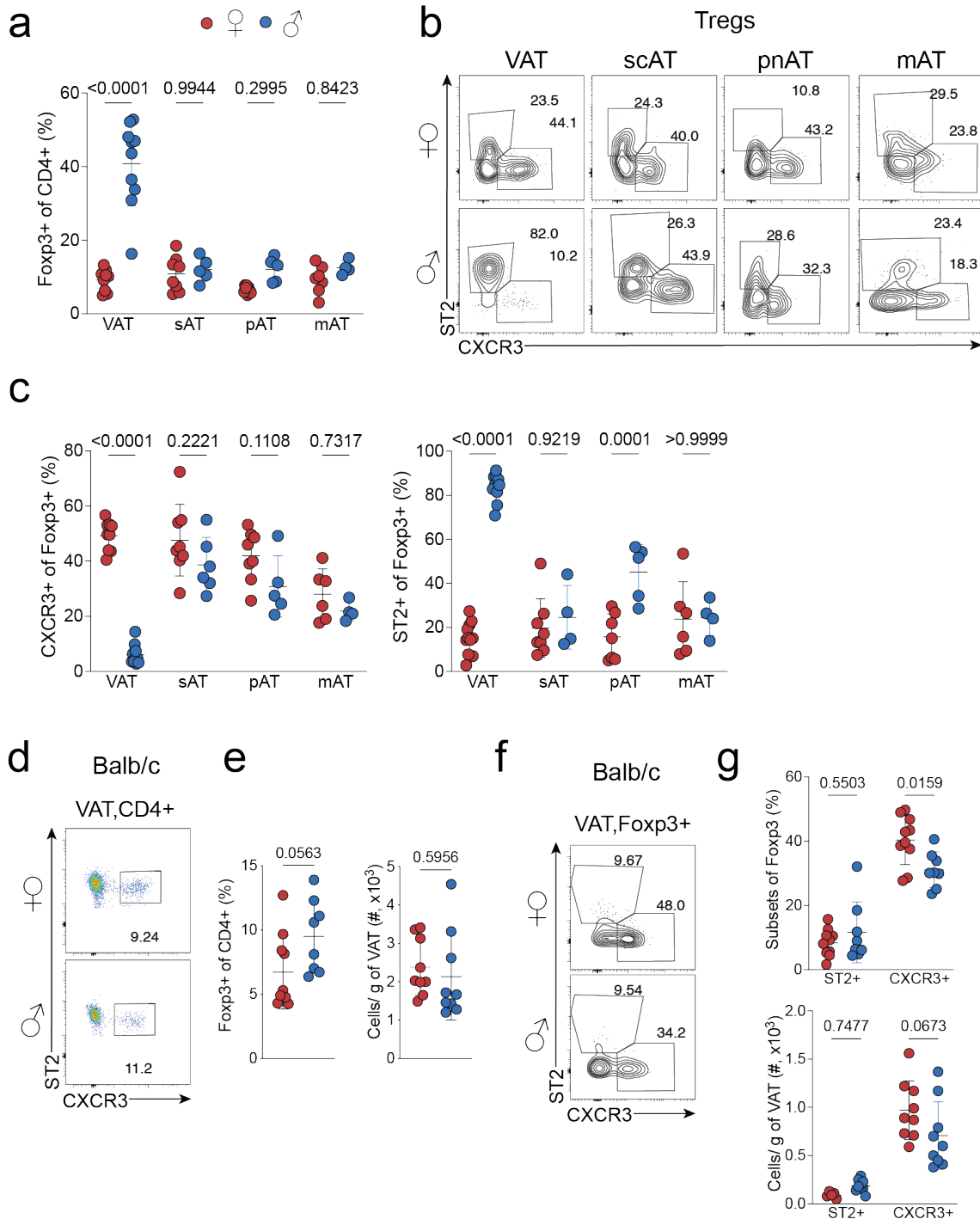


**Figure 12 | VAT Treg cell distribution in other adipose tissue compartments and mouse models.** **a**, Frequencies of Fcpx3+ Treg cells in VAT, sAT, pAT and mAT of female and male mice. **b**, **c** FACS plots displaying ST2 against CXCR3 expression (**b**) in different adipose tissue depots and quantification (**c**) of CXCR3+ (left) and ST2+ (right) VAT Treg cell proportions. **d-g**, VAT of 30–35-week-old Balb/c mice were analysed. **d**, FACS plots displaying CD4 vs Fcpx3 expression in CD4+ T cells. **e**, Frequencies (left) and numbers (right) of VAT Treg

cells in female and male mice. **f**, Flow cytometric analysis showing ST2 versus CXCR3 expression in VAT Treg cells. **g**, Frequencies (top) and numbers (bottom) of ST2<sup>+</sup> and CXCR3<sup>+</sup> VAT Treg cells. Symbols represent individual mice; horizontal lines indicate means. Data are representative (**b, d, f**) or pooled (**a, c, e, g**) from a minimum of two independent experiments. Error bars indicate the standard deviation. Statistical analyses were performed using two-way ANOVA (**a, c, g**) or unpaired, two-tailed Student's *t*-test (**e**).

### 3.10 Characterization of immune and non-immune cell populations in the VAT

While adipocytes constitute most of the VAT volume, other immune and non-immune cells that are numerically abundant in the VAT play critical roles in tissue function and homeostasis (Joanna R. Dispirito & Diane Mathis, 2015; Kershaw & Flier, 2004). The cellular composition of VAT was investigated in male and female mice using the gating strategy depicted in Figure 3.10a. Mesenchymal stromal cells (MSCs) were analysed by selecting Ly5.2-CD31-Ter119-gp38<sup>+</sup> cells (**Figure 13a**). No difference in the proportion and numbers of gp38<sup>+</sup> cells was observed between both sexes (**Figure 13b**). Within the gp38 expressing population, the MSCs were divided into four main populations based on CD90 and CD73 expression. As we have demonstrated recently (Vasanthakumar et al., 2020), both CD73<sup>+</sup>CD90<sup>+</sup> and CD73<sup>+</sup>CD90<sup>-</sup> MSC populations were proportionally higher in males compared to female mice (**Figure 13c**). Overall, CD73<sup>+</sup>CD90<sup>+</sup> MSCs were abundant in the VAT of male mice compared to females. On the other hand, females harboured more CD73<sup>-</sup>CD90<sup>+</sup> and CD73<sup>-</sup>CD90<sup>-</sup> cells both in proportion and in numbers within the gp38<sup>+</sup> population of MSCs (**Figure 13c**).

Furthermore, CD34 expression in MSCs was measured, as CD34 has been reported to define 'true adipocyte progenitors' and is also associated with better metabolic health (Rodeheffer, Birsoy, & Friedman, 2008). The data showed higher CD34 MFI in female mice compared to male mice and an increased number of CD34 expressing cells within the gp38<sup>+</sup> MSC population (**Figure 13d**). Further compartmentalization of the stromal population showed that CD34 expression is higher in female across most subpopulations except CD90<sup>+</sup>CD73<sup>-</sup> cells (**Figure 13d**).

Stromal cell populations were also analysed in Balb/c mice. The data showed no significant differences in proportion or numbers of gp38<sup>+</sup> stromal cells between female and male Balb/c mice (**Figure 13f**). However, the CD73<sup>+</sup> population was higher in proportion but not in numbers in male mice compared to females (**Figure 13g**). On the other hand, CD90<sup>+</sup>CD73<sup>-</sup> stromal cells represented the largest population in female mice and were higher in proportion and numbers compared to males (**Figure 13g**). Additionally, a basic analysis of VAT resident macrophages (Macs) and dendritic cells (DCs) was performed. For this purpose, the gating strategy depicted in **Figure 14a** was employed. While our data indicates higher numbers of Macs and DCs in males compared to females (**Figure 14b**), DC subpopulations did not show any differences between male and female mice.

Overall, our data revealed sex-specific differences in immune and non-immune cells in the VAT and suggest that sex-specific distribution of stromal cells is conserved between different mouse strains.

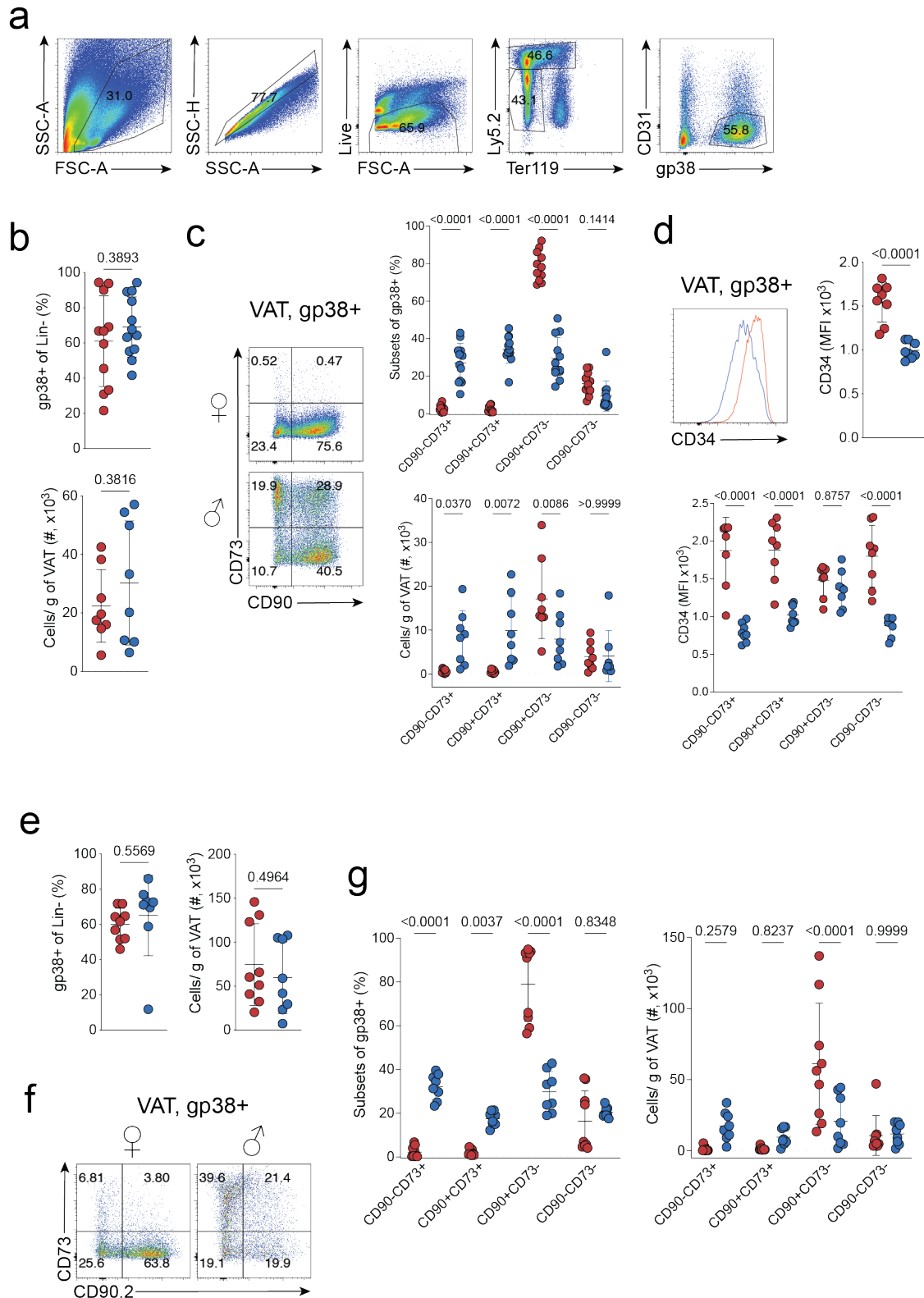


**Figure 13 | Stromal cell composition in the VAT is similar in C57BL/6 and Balb/c mouse models.** Mesenchymal stromal cell populations were analysed in VAT of C57BL/6 (**b-d**) and Balb/c (**e-g**) mice. **a**, Gating strategy to identify gp38+ MSCs in the VAT. **b**, Frequency (top) and numbers (bottom) of gp38+ MSCs. **c**,

FACS plots displaying CD73 versus CD90 expression (left) and frequencies (top) and numbers (bottom) of CD90-CD73+, CD90+CD73+, CD90+CD73- and CD90-CD73- MSCs in female and male VAT. **d**, Histogram displaying CD34 expression in gp38+ cells (top left). Quantification of CD34 MFI in gp38+ cells (top right) and gp38+ MSC subpopulations in female and male VAT. **e**, Frequency (top) and numbers (bottom) of gp38+ MSCs. **f**, FACS plots displaying CD73 versus CD90 expression. **g**, Quantification of frequencies (left) and numbers (right) of CD90-CD73+, CD90+CD73+, CD90+CD73- and CD90-CD73- MSCs in female and male VAT. Symbols represent individual mice; horizontal lines indicate means. Data are representative (**a, d, f**) or pooled (**b, c, d, e, g**) from a minimum of two independent experiments. Error bars indicate the standard deviation. Statistical analyses were performed using two-way ANOVA (**c, d, g**) or unpaired, two-tailed Student's *t*-test (**b, d, e**).

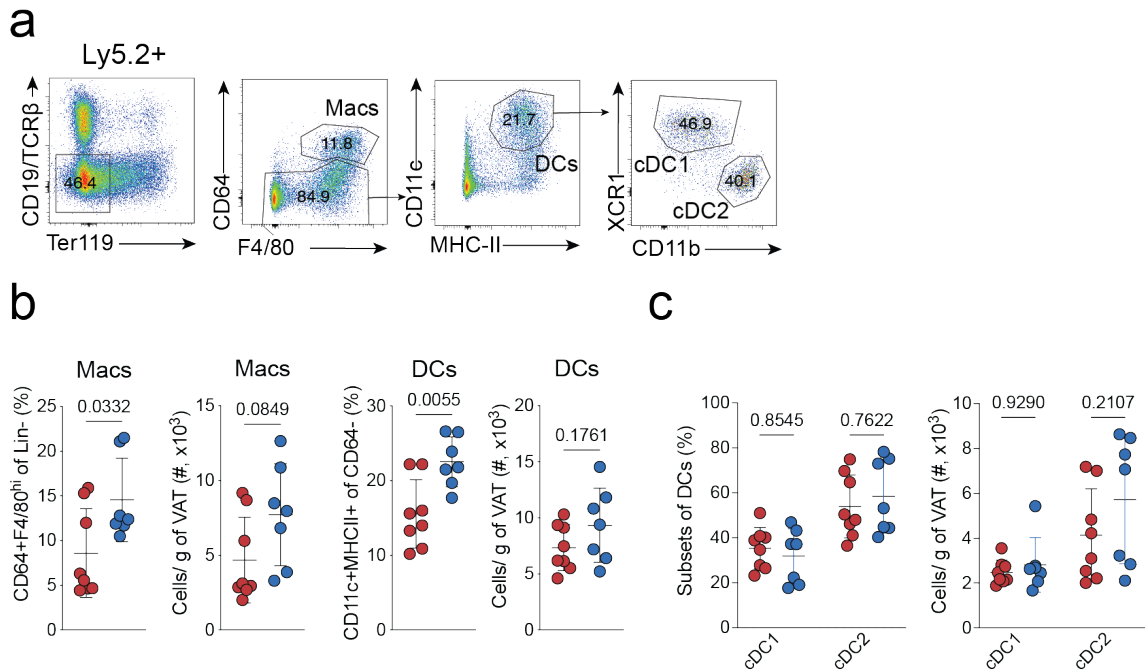


**Figure 14 | Myeloid cells in the VAT.** **a**, Gating strategy to identify macrophages and DCs in the VAT. **b**, Frequencies and numbers of VAT-derived macrophages and DCs. **c**, Frequencies (left) and numbers (right) of cDC1 and cDC2 in female and male VAT. Symbols represent individual mice; horizontal lines indicate means. Data are representative (**a**) or pooled (**b, c**) from a minimum of two independent experiments. Error bars indicate the standard deviation. Statistical analyses were performed using two-way ANOVA (**c**) or unpaired, two-tailed Student's *t*-test (**b**).

## Chapter 4 – Molecular regulation of ST2<sup>+</sup> and CXCR3<sup>+</sup> VAT Treg cells

### 4.1 PPAR $\gamma$ is required for ST2<sup>+</sup> but not CXCR3<sup>+</sup> VAT Treg cell differentiation

Our results uncovered VAT Treg cells of different phenotype and developmental trajectory suggesting distinct molecular pathways might regulate the differentiation and function of these subsets. Therefore, we investigated the impact of various molecular regulators on ST2<sup>+</sup> and CXCR3<sup>+</sup> VAT Treg cell differentiation.

The role of PPAR $\gamma$  in VAT Treg cells is very well established (Cipolletta et al., 2015; Cipolletta et al., 2012). Therefore, the potential role of this transcription factor in the development of CXCR3<sup>+</sup> and ST2<sup>+</sup> VAT Treg cells was assessed. In line with previous reports (Cipolletta et al., 2015; Cipolletta et al., 2012), total VAT Treg cell populations were significantly reduced in proportion and numbers in *Pparg<sup>fl/fl</sup>Foxp3<sup>Cre</sup>* mice (**Figure 15a**). Importantly, however, this was only observed in males, while female VAT Treg cell populations remained unchanged. A significant decrease in Foxp3 expression within VAT Treg cells was observed in *Pparg<sup>fl/fl</sup>Foxp3<sup>Cre</sup>* compared to control mice as measured through Foxp3 MFI (**Figure 15b**). Furthermore, ST2<sup>+</sup> VAT Treg cells were reduced in proportion and numbers in male *Pparg<sup>fl/fl</sup>Foxp3<sup>Cre</sup>* mice compared to controls (**Figure 15c, d**). CXCR3<sup>+</sup> Treg cells on the other hand expanded in the VAT of these mice. (**Figure 15c, d**). In females, both VAT Treg cell populations remained unchanged. Next, the proliferative capacity of both subpopulations were assessed through Ki67 expression analysis. The proportion of Ki67<sup>+</sup> cells was higher in *Pparg<sup>fl/fl</sup>Foxp3<sup>Cre</sup>* male mice compared to controls, while Ki67 levels in female mice remained unaltered (**Figure 15e, f**). Within ST2<sup>+</sup> and CXCR3<sup>+</sup> VAT Treg cell populations, the percentage of Ki67<sup>+</sup> cells did not change significantly between genotypes. However, the overall number of Ki67-expressing cells decreased in ST2<sup>+</sup> and increased in CXCR3<sup>+</sup> VAT Treg cells of male mice (**Figure 15f**).

We and others have previously shown that GATA3 is highly expressed in ST2+ VAT Treg cells and it is known to stabilize Foxp3 expression in order to maintain Treg cell identity (Vasanthakumar et al., 2020; Wohlfert et al., 2011). High GATA3 expression was confirmed in ST2+ Treg cells, while expression was lower in the CXCR3+ VAT Treg cell compartment (**Figure 16a**). Analysis of scRNA-Seq revealed similar results. Clusters 3 and 4 had higher amount of *Gata3* transcripts compared to other groups, with cluster 4 having the highest number of transcripts (**Figure 16b**). However, Clusters 2 and 5 displayed very similar *Gata3* expression levels while Cluster 1 had the least. The ability of PPAR $\gamma$  to control ST2+ VAT Treg cell identity by modulating GATA3 expression was tested. Flow cytometric analysis showed that GATA3 expression was significantly reduced in male but not female VAT Treg cells which is in line with the overall sex-specific phenotype we see *Pparg<sup>fl/fl</sup>Foxp3<sup>Cre</sup>* mice (**Figure 16c**).

Overall, we showed that PPAR $\gamma$  promotes ST2+ VAT Treg cell formation and suppresses differentiation of CXCR3+ cells in a sex-specific manner through modulation of proliferation and GATA3 expression.

**a** ● ♀ Ctrl ● ♂ Ctrl  
○ ♀ *Pparg<sup>Foxp3cre</sup>* ○ ♂ *Pparg<sup>Foxp3cre</sup>*

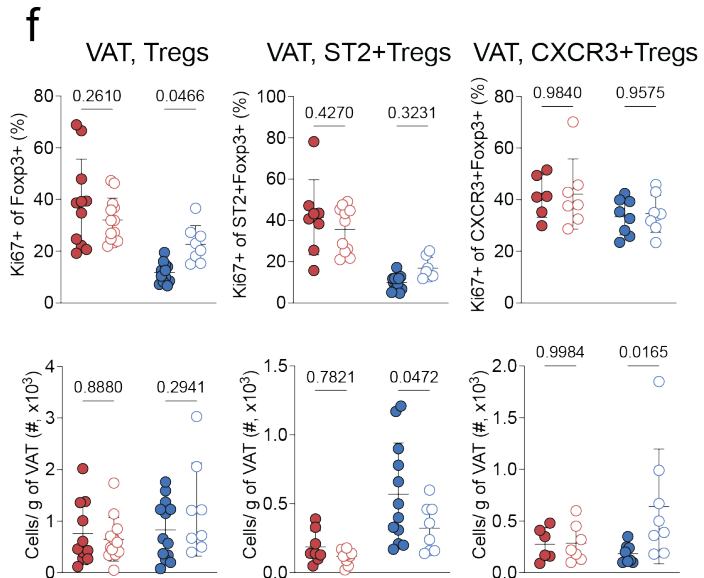
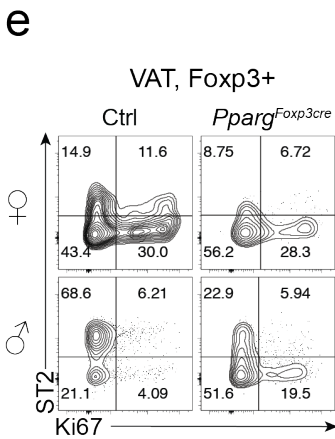
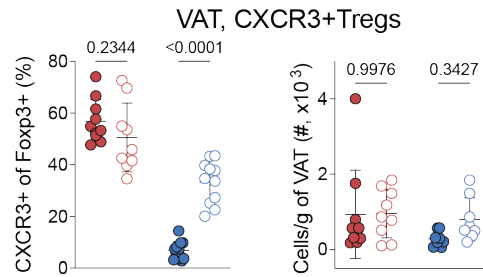
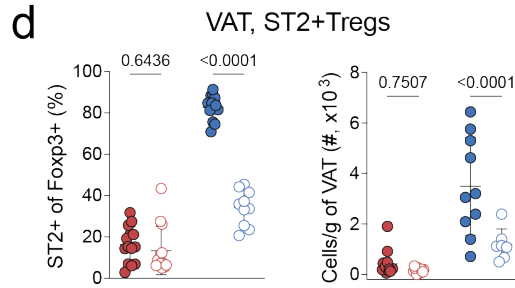
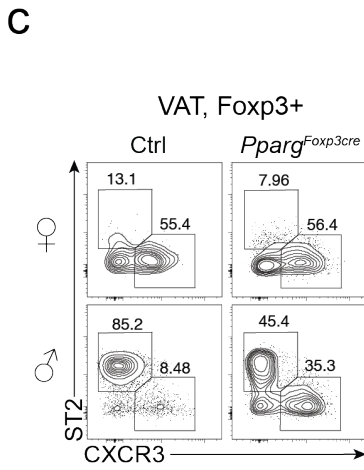
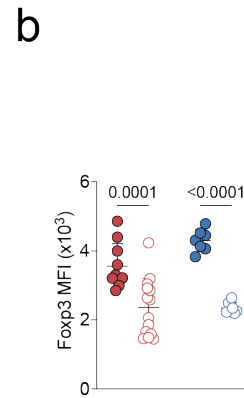
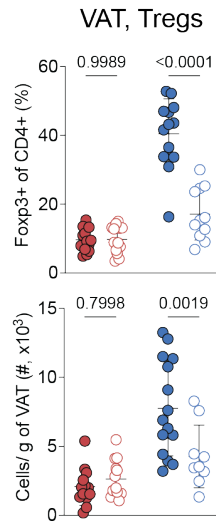
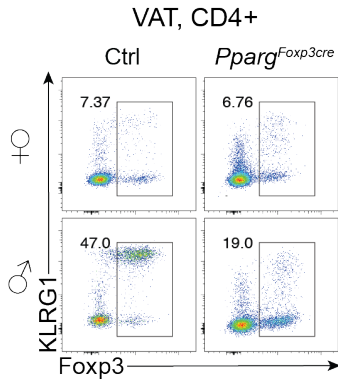


**Figure 15 | PPAR $\gamma$  is required for ST2+ but not CXCR3+ VAT Treg cells.** VAT from 20–28-week-old *Pparg<sup>fl/fl</sup>Foxp3<sup>Cre</sup>* and control (wildtype and *Foxp3<sup>Cre</sup>*) mice was analysed and compared. **a**, FACS plots showing Foxp3 and KLRG1 expression in CD4+ T cells (left). Quantification of proportion (top) and cell numbers (bottom) of total VAT Treg cell population. **b**, Quantification of Foxp3 MFI in total VAT Treg cells. **c, d**, Flow cytometry plots (**c**) showing ST2 and CXCR3 expression and quantification (**d**, frequencies left, numbers right) of VAT Treg cells in *Pparg<sup>fl/fl</sup>Foxp3<sup>Cre</sup>* and control mice. **e, f**, Flow cytometry plots (**e**) showing ST2 and Ki67 expression and quantification (**f**, frequencies top, numbers bottom) of total, ST2+ and CXCR3+ VAT Treg cells in *Pparg<sup>fl/fl</sup>Foxp3<sup>Cre</sup>* and control mice. Symbols represent individual mice; horizontal lines indicate means. Data are representative (**a, c, e**) or pooled (**a, b, d, f**) from a minimum of two independent experiments. Error bars indicate the standard deviation. Statistical analyses were performed using two-way ANOVA.

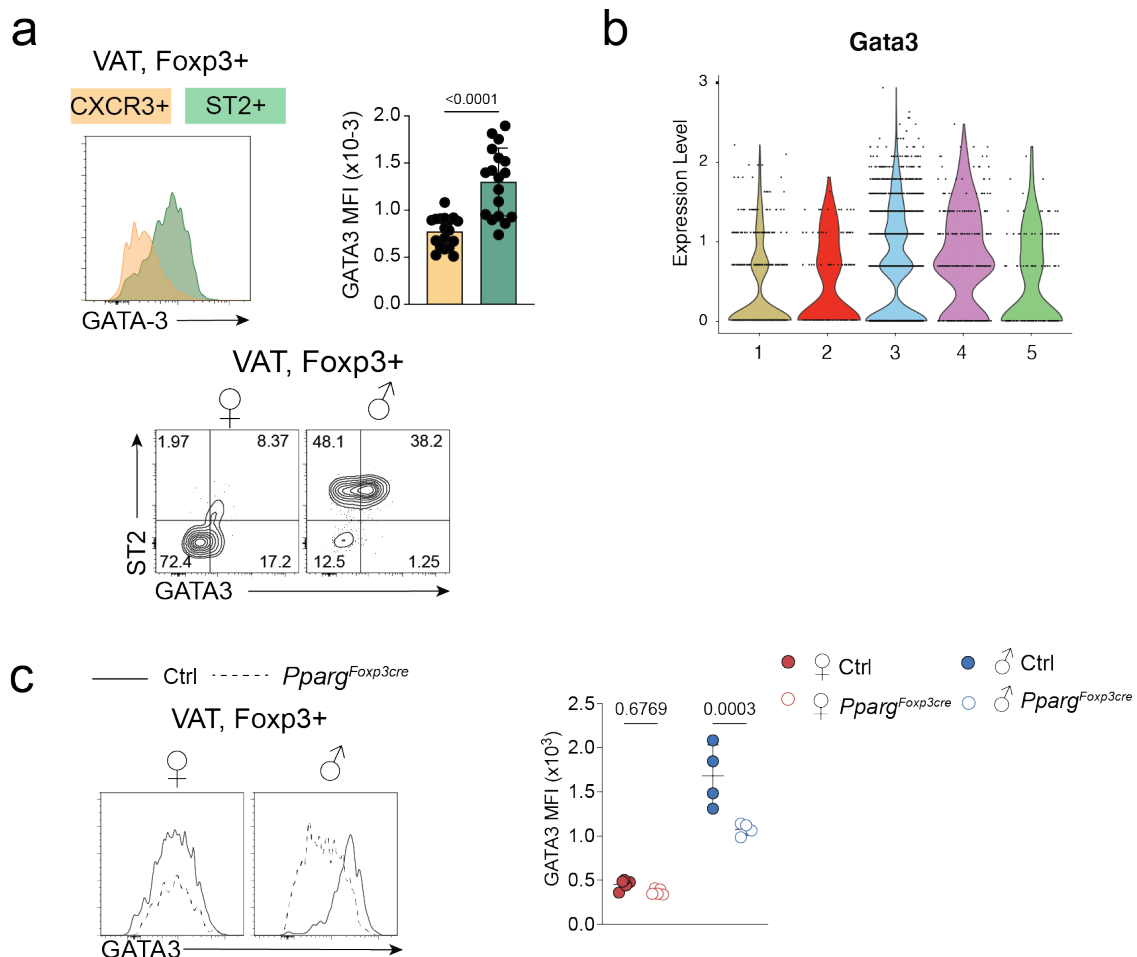


**Figure 16 | PPAR $\gamma$  impacts GATA3 expression in male VAT Treg cells.** **a**, Histogram (top left) depicting GATA3 expression and quantification of GATA3 MFI (top right) in ST2+ (green) and CXCR3+ (orange) VAT Treg cells. FACS plots (bottom) showing expression of ST2 versus GATA3 in female and male VAT Treg cells. **b**, Violin plots showing *Gata3* transcript levels in VAT Treg cell clusters from

single-cell RNA-Seq data. **c**, Histograms displaying GATA3 expression in female and male *Pparg<sup>fl/fl</sup>Foxp3<sup>Cre</sup>* and control mice (left) and quantification of GATA3 MFI (right). Symbols represent individual mice; horizontal lines indicate means. Data are representative (**a**, **c**) or pooled (**a**) from a minimum of two independent experiments. Error bars indicate the standard deviation. Statistical analyses were performed using two-way ANOVA (**c**) or unpaired, two-tailed Student's *t*-test (**a**).

## 4.2 PPAR $\gamma$ impacts Treg cells in other lymphoid and non-lymphoid organs

We extended the investigation to other organs to assess the impact of PPAR $\gamma$  deletion in Treg cells on a systemic level. Analysis of splenocytes revealed elevated total Treg cell population in *Pparg<sup>fl/fl</sup>Foxp3<sup>Cre</sup>* mice compared to control mice (**Figure 17a**). As shown in the VAT, Foxp3 expression levels were substantially reduced *Pparg<sup>fl/fl</sup>Foxp3<sup>Cre</sup>* mice compared to control mice (**Figure 17b**). Surprisingly, however, GATA3 expression levels were enhanced in *Pparg<sup>fl/fl</sup>Foxp3<sup>Cre</sup>* male mice, while they remained unaltered in females (**Figure 17c**). Further analysis of splenic Treg cell subpopulations showed that KLRG1+ Treg cells were significantly reduced in absence of PPAR $\gamma$ , especially in male mice, while there was an increase of activated Treg cells (CD44<sup>hi</sup>CD62L<sup>-</sup>) specifically in female mice (**Figure 17d, e**). Analysis of CXCR3+ Treg cells in the spleen revealed no difference between *Pparg<sup>fl/fl</sup>Foxp3<sup>Cre</sup>* and control mice.

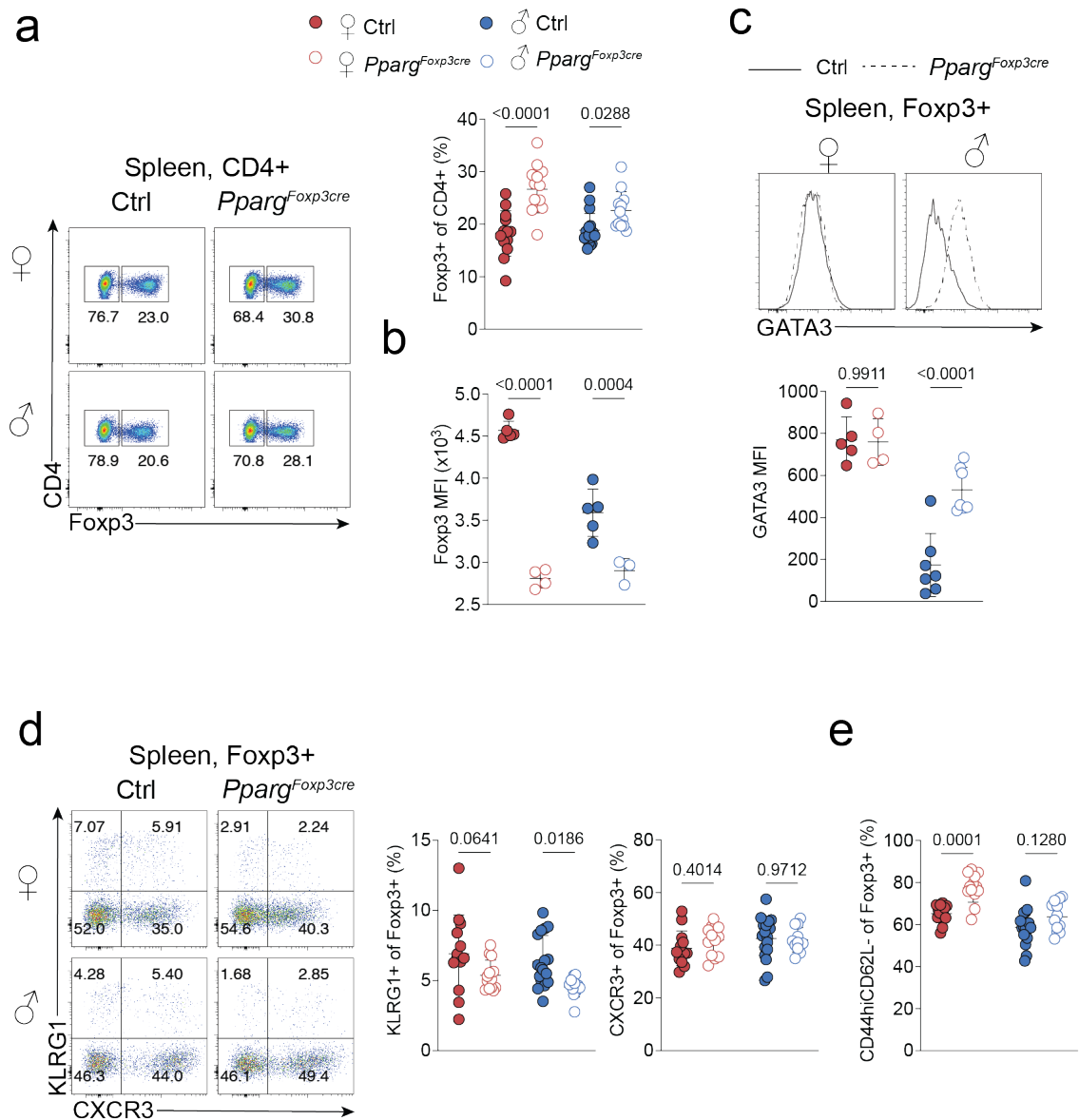


**Figure 17 | KLRG1 and Fxp3 expression are affected in splenic Treg cells that lack PPAR $\gamma$ .** Spleens from 20–28-week-old *Pparg<sup>fl/fl</sup>Foxp3<sup>Cre</sup>* and control (wildtype and *Foxp3<sup>Cre</sup>*) mice were analysed and compared. **a**, FACS plots showing Fxp3 and CD4 expression in CD4+ T cells (left). Frequency of total splenic Treg cell population (top right). **b**, Quantification of Fxp3 MFI in splenic Treg cells. **c**, Histograms displaying GATA3 expression in female and male *Pparg<sup>fl/fl</sup>Foxp3<sup>Cre</sup>* and control mice (top) and quantification of GATA3 MFI (bottom). **d**, Flow cytometry plots showing KLRG1 versus CXCR3 expression and quantification of KLRG1+ and CXCR3+ splenic Treg cells in *Pparg<sup>fl/fl</sup>Foxp3<sup>Cre</sup>* and control mice. **e**, Frequencies of CD44<sup>hi</sup>CD62L<sup>-</sup> Treg cells in *Pparg<sup>fl/fl</sup>Foxp3<sup>Cre</sup>* and control mice. Symbols represent individual mice; horizontal lines indicate means. Data are representative (**a**, **c**, **d**) or pooled (**a-e**) from a minimum of two independent experiments. Error bars indicate the standard deviation. Statistical analyses were performed using two-way ANOVA.

Analysis of Treg cells in the small intestine of *Pparg<sup>fl/fl</sup>Foxp3<sup>Cre</sup>* mice revealed substantial increase of total Treg cells in proportion and numbers in both sexes compared to control mice. The increase however was pronounced in females (**Figure 18a**). Similar to splenic Treg cells, Foxp3 expression was also reduced in PPAR $\gamma$ -deficient SI Treg cells compared to their controls (**Figure 18b**). More detailed analysis of Treg cells revealed no difference in the proportion of GATA3+ Treg cells *Pparg<sup>fl/fl</sup>Foxp3<sup>Cre</sup>* mice compared to controls in both male and female mice (**Figure 18c**). However, absolute numbers of GATA3+ cells were increased in *Pparg<sup>fl/fl</sup>Foxp3<sup>Cre</sup>* mice compared to controls, which was only significant in females. ROR $\gamma$ t+ Treg cells were reduced in proportion but not in numbers in both male and female *Pparg<sup>fl/fl</sup>Foxp3<sup>Cre</sup>* mice (**Figure 18c**). Additionally, we noted that PPAR $\gamma$  depletion led to a proportional reduction in CXCR3+ Treg cell population in the gut while KLRG1+ Treg cells remained unchanged in both sexes (**Figure 19a**). Absolute numbers of KLRG1+ and CXCR3+ Treg cells were increased in both cases in *Pparg<sup>fl/fl</sup>Foxp3<sup>Cre</sup>* mice compared to their controls. However, as the CXCR3 staining was not optimal, these results need confirmation. Next, Ki67 expression was measured to assess whether proliferation was affected by PPAR $\gamma$  depletion. Treg cells in *Pparg<sup>fl/fl</sup>Foxp3<sup>Cre</sup>* mice displayed enhanced Ki67 expression in both sexes compared to controls (**Figure 19b**). Furthermore, the number of Ki67+ cells were higher in PPAR $\gamma$ -deficient mice. In keeping with this observation, Ki67+ cells were elevated in GATA3+ and ROR $\gamma$ t+ Treg cells in the small intestine of male and female *Pparg<sup>fl/fl</sup>Foxp3<sup>Cre</sup>* mice compared to controls (**Figure 19b**).

Overall, the data shows that PPAR $\gamma$  functions as a regulator of Treg cell differentiation and proliferation in spleen and SI, suggesting that it has immune and tissue specific functions across various organs.

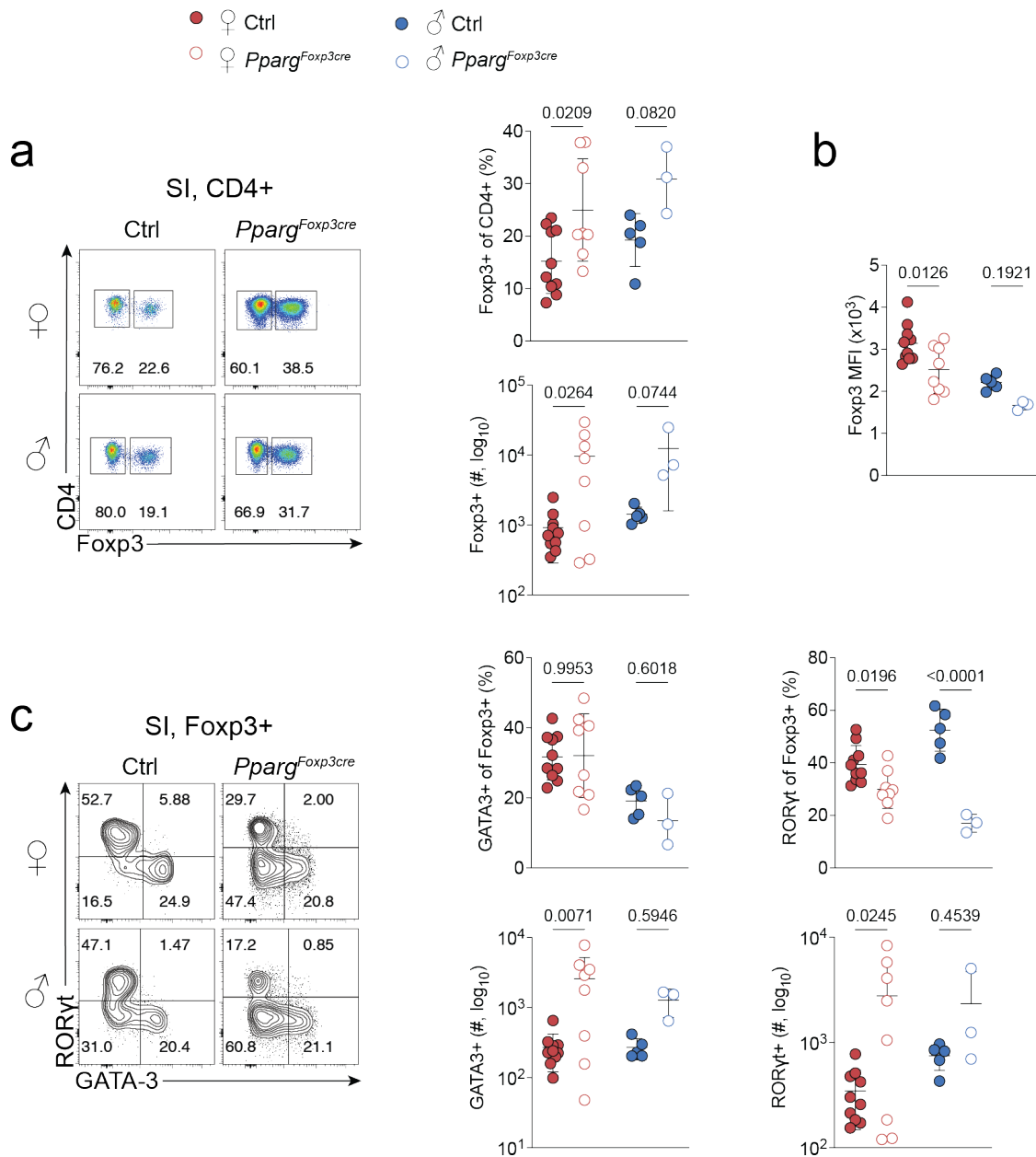


**Figure 18 | PPAR $\gamma$ -depleted mice have a reduced ROR $\gamma$ t<sup>+</sup> Treg cell compartment in the gut.** Small intestine from 20–28-week-old *Pparg*<sup>fl/fl</sup>*Foxp3*<sup>Cre</sup> and control (wildtype and *Foxp3*<sup>Cre</sup>) mice were analysed and compared. **a**, FACS plots showing Foxp3 and CD4 expression in CD4<sup>+</sup> T cells (left). Frequency (top) and total cell numbers (bottom) of gut resident Treg cell population (top right). **b**, Quantification of Foxp3 MFI in intestinal Treg cells. **c**, Flow cytometry plots showing GATA3 versus ROR $\gamma$ t expression and frequencies (top) and numbers (bottom) of GATA3<sup>+</sup> and ROR $\gamma$ t<sup>+</sup> intestinal Treg cells in *Pparg*<sup>fl/fl</sup>*Foxp3*<sup>Cre</sup> and control mice. Symbols represent individual mice; horizontal lines indicate means. Data are representative (**a**, **c**) or pooled (**a-c**) from a minimum of two independent experiments. Error bars indicate the standard deviation. Statistical analyses were performed using two-way ANOVA.

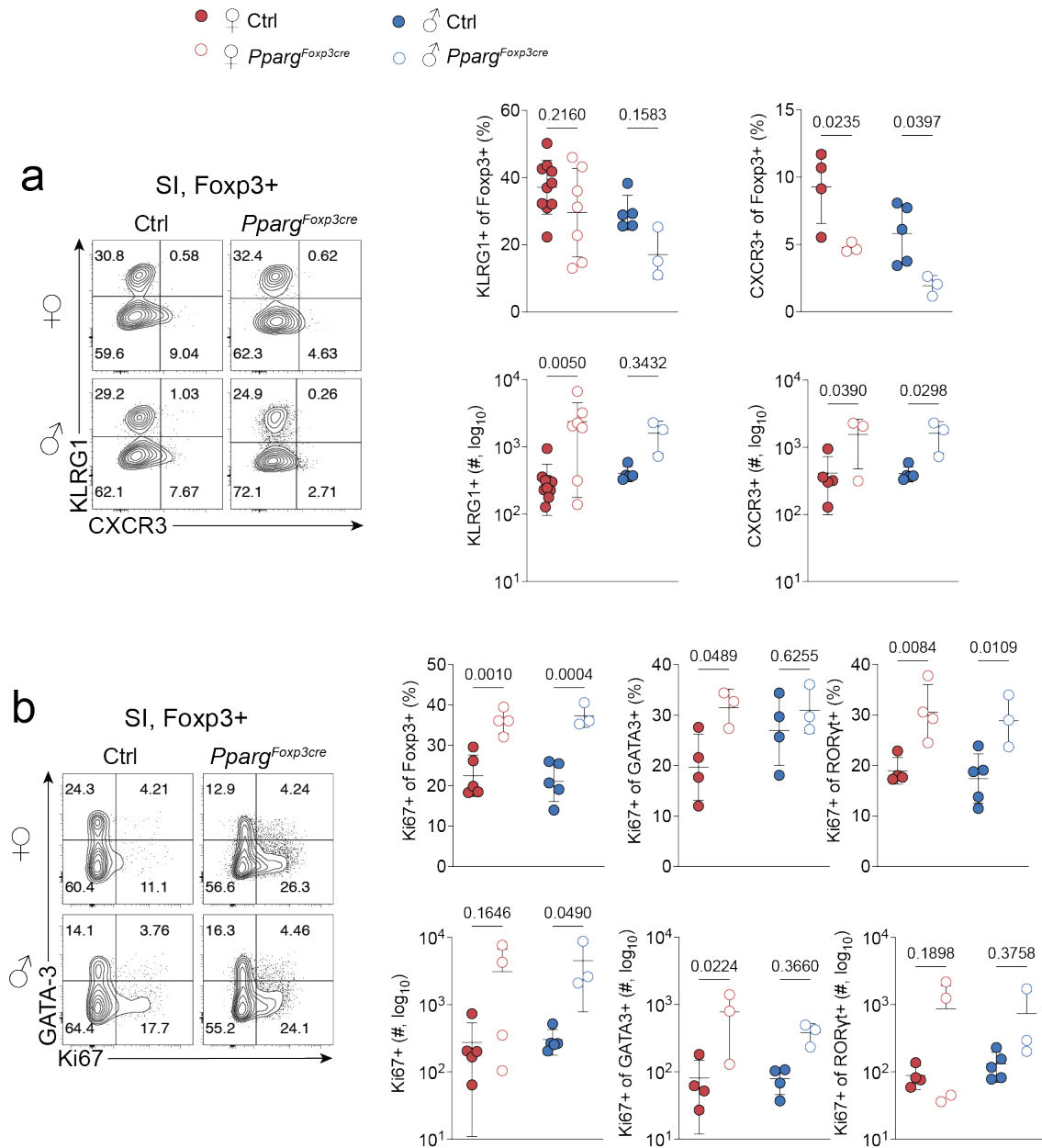


**Figure 19 | CXCR3 and Ki67 expression is impacted by PPAR $\gamma$  depletion in gut resident Treg cells. a**, Flow cytometry plots showing KLRG1 and CXCR3 expression and frequencies (top) and numbers (bottom) of KLRG1+ and CXCR3+ intestinal Treg cells in *Pparg<sup>fl/fl</sup>Foxp3<sup>Cre</sup>* and control mice. **b**, Flow cytometry plots showing GATA3 and Ki67 expression and frequencies (top) and numbers (bottom) of Ki67+ cells among total (left), GATA3+ (centre) and ROR $\gamma$ t+ (right) intestinal Treg cells in *Pparg<sup>fl/fl</sup>Foxp3<sup>Cre</sup>* and control mice. Symbols represent individual mice; horizontal lines indicate means. Data are representative or pooled (a) from a minimum of two independent experiments. Error bars indicate the standard deviation. Statistical analyses were performed using two-way ANOVA.

### 4.3 GATA3 promotes the differentiation of ST2+ VAT Treg cells

T<sub>H</sub>2 immunity has been associated with tissue Treg cell development (Michael Delacher et al., 2017). In line with this notion, the T<sub>H</sub>2 specific transcription factor GATA3 has been implicated in the formation of skin- and gut-specific tissue Treg cells and overall stability of Treg cell identity (Kalekar et al., 2019; Yunqi Wang et al., 2011; Wohlfert et al., 2011).

To examine the role of GATA3 in the generation and diversification of VAT Treg cells, *Gata3<sup>fl/fl</sup>Foxp3<sup>Cre</sup>* mice were generated to deplete GATA3 selectively in Treg cells. As expected, we observed Treg cell specific loss of GATA3, while it was enhanced in Foxp3<sup>-</sup> cells (**Figure 20a**). Analysis of VAT from *Gata3<sup>fl/fl</sup>Foxp3<sup>Cre</sup>* mice showed a significant decrease in the total VAT Treg cell population in male mice (**Figure 20b, c**). In contrast, the proportion of female VAT Treg cells was increased in *Gata3<sup>fl/fl</sup>Foxp3<sup>Cre</sup>* mice (**Figure 20c**). In line with its role in regulating Foxp3 expression, GATA3-deficient Treg cells showed substantially decreased Foxp3 MFI compared to controls, in both sexes (**Figure 20d**). Analysis of Treg cell subsets revealed a significant loss of ST2+ cells in *Gata3<sup>fl/fl</sup>Foxp3<sup>Cre</sup>* mice in both males and females compared to the control group (**Figure 20e, f**). This however was accompanied by a substantial increase in CXCR3+ VAT Treg cells in males but not female *Gata3<sup>fl/fl</sup>Foxp3<sup>Cre</sup>* mice. The absolute number of CXCR3+ VAT Treg cells were also significantly increased in *Gata3<sup>fl/fl</sup>Foxp3<sup>Cre</sup>* females compared to controls while this was not observed in male mice (**Figure 20e, f**).

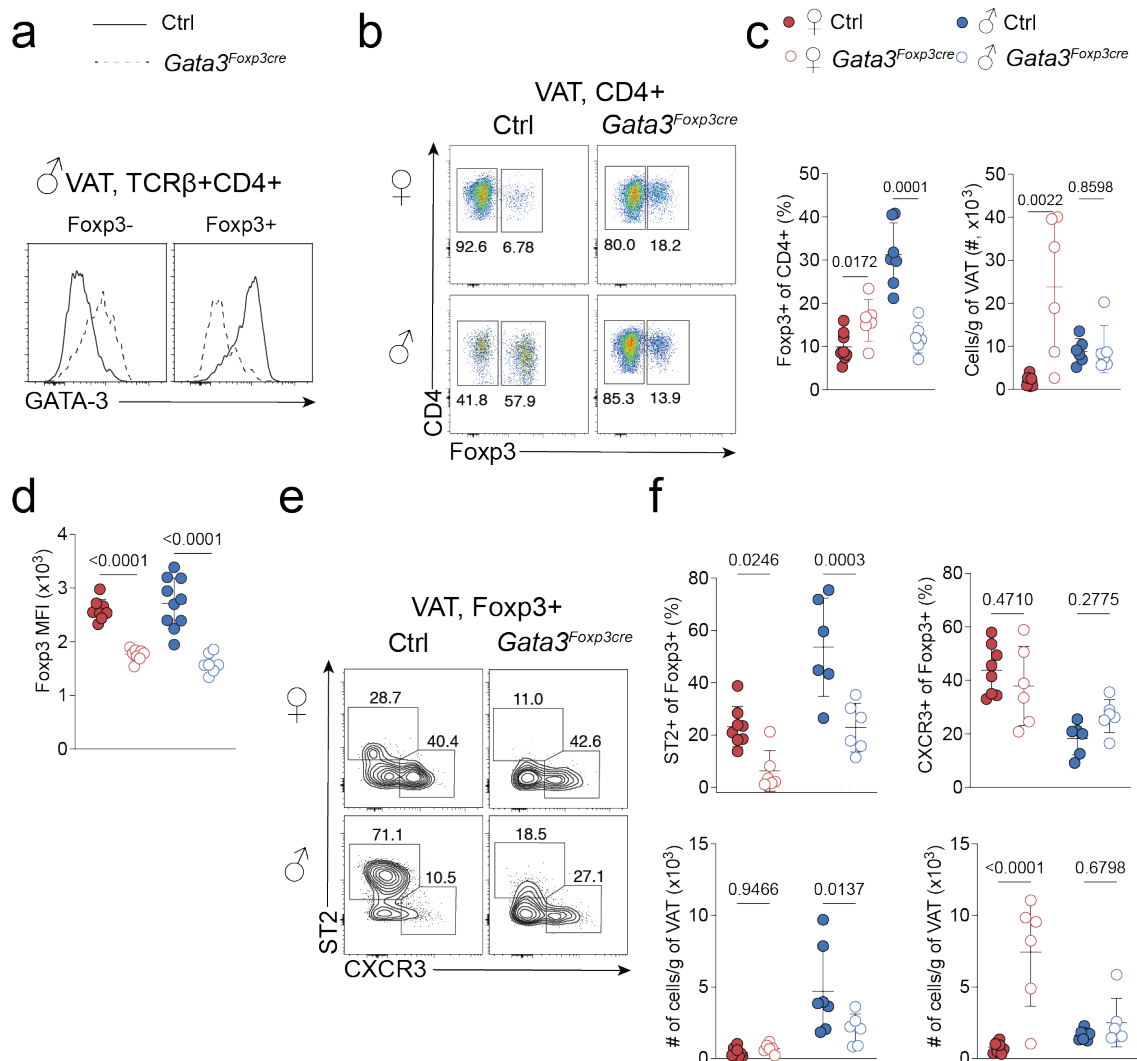


**Figure 20 | GATA3 is essential for the differentiation of ST2+ VAT Treg cells.** Analysis of VAT from 22-28-week-old male and female *Gata3<sup>fl/fl</sup>Foxp3<sup>Cre</sup>*, wildtype (n=6) and *Foxp3<sup>Cre</sup>* (n=8) mice. **a**, Histograms displaying GATA3 expression in Foxp3+ and Foxp3- negative cells of male *Gata3<sup>fl/fl</sup>Foxp3<sup>Cre</sup>* and *Foxp3<sup>Cre</sup>* control mice. **b, c**, Flow cytometry plots (**b**) and quantification (**c**) of total VAT Treg cells of indicated genotypes. **d**, Quantification of Foxp3 MFI in VAT Treg cells of *Gata3<sup>fl/fl</sup>Foxp3<sup>Cre</sup>* and *Foxp3<sup>Cre</sup>* control mice. **e, f**, Flow cytometry plots (**e**) showing ST2 and CXCR3 expression and quantification (**f**, frequencies top, numbers bottom) of total, ST2+ and CXCR3+ VAT Treg cells in *Gata3<sup>fl/fl</sup>Foxp3<sup>Cre</sup>* and control mice. Symbols represent individual mice; horizontal lines indicate means. Data are representative (**a, b, e**) or pooled (**c, d, f**) from a minimum of two independent experiments. Error bars indicate the standard deviation. Statistical analyses were performed using two-way ANOVA.

Since Treg cell numbers were altered in female mice, proliferation of Gata3 deficient VAT Treg cells were assessed by Ki67 expression. Proportion of Ki67+ cells were increased in total VAT Treg cells in males but not female mice (**Figure**

**21a).** Furthermore, Ki67 expression was enhanced in CXCR3+ Treg cells of both, male and female mice. ST2+ VAT Treg cells, however, had elevated Ki67 expression only in male mice (**Figure 21a**). Furthermore, Treg cells in the VAT displayed an increased activated phenotype in *Gata3<sup>fl/fl</sup>Foxp3<sup>Cre</sup>* mice marked by high PD1 expression in VAT Treg cells of male mice (**Figure 21b**).

Together our results demonstrate that GATA3 is required specifically for the maintenance of ST2+ Treg cells, Foxp3 stability, proliferation and possibly activation of VAT Treg cells.

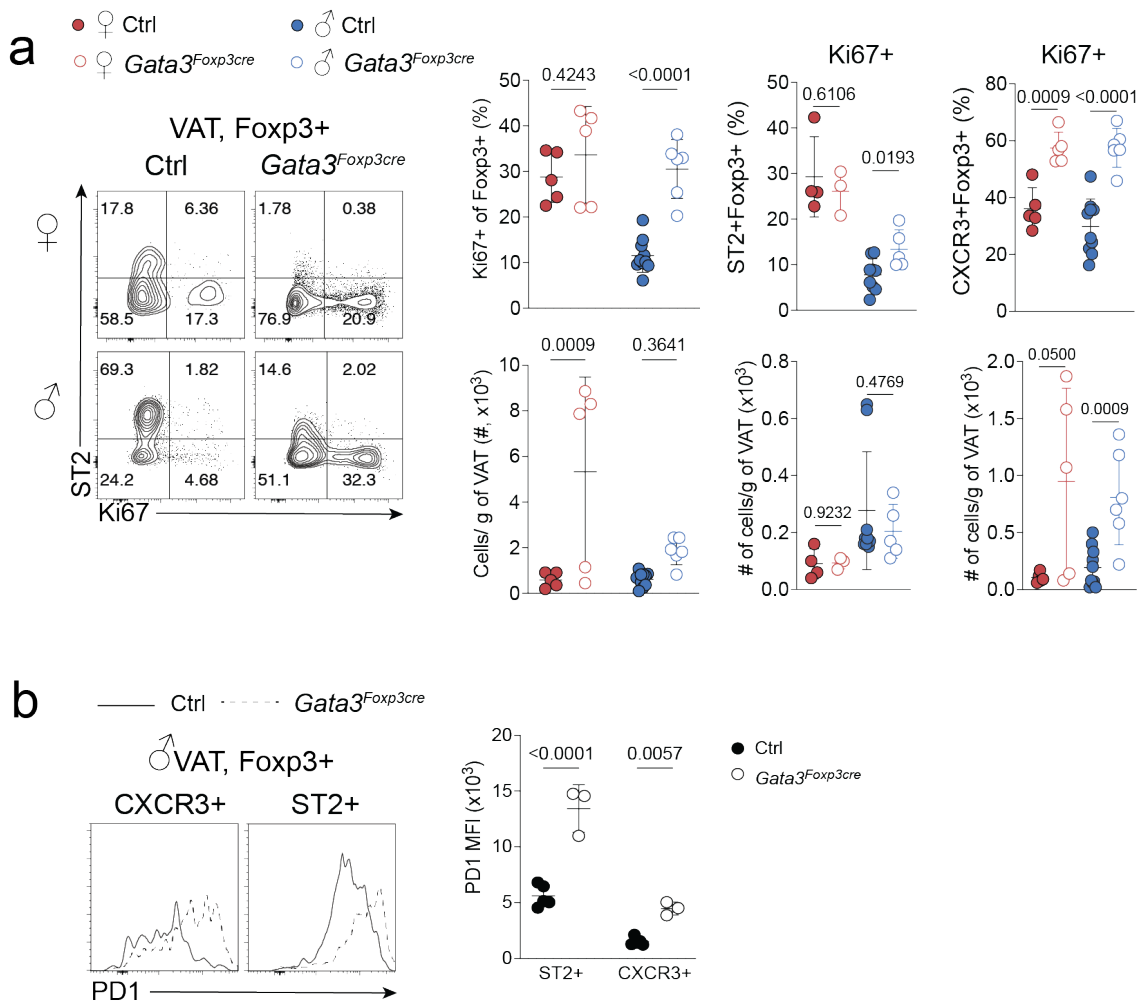


**Figure 21 | Loss of GATA3 induces proliferation of CXCR3+ VAT Treg cells.**  
**a,** Flow cytometry plots showing ST2 versus Ki67 expression and quantification (frequencies top, numbers bottom) of total, ST2+ and CXCR3+ VAT Treg cells in *Gata3<sup>fl/fl</sup>Foxp3<sup>Cre</sup>*, wildtype (n=6) and *Foxp3<sup>Cre</sup>* (n=8) mice. **b,** Histograms depicting PD1 expression (left) and PD1 MFI quantification (right) in CXCR3+ and ST2+ VAT Treg cells of male *Gata3<sup>fl/fl</sup>Foxp3<sup>Cre</sup>* and control mice. Symbols

represent individual mice; horizontal lines indicate means. Data are representative (**b**) or pooled (**a**) from a minimum of two independent experiments. Error bars indicate the standard deviation. Statistical analyses were performed using two-way ANOVA.

#### 4.4 Loss of GATA3 impacts Treg cells in other lymphoid and non-lymphoid organs

To understand the broader impact of GATA3 on Treg cell differentiation, analysis of Treg cells in other tissues of *Gata3<sup>fl/fl</sup>Foxp3<sup>Cre</sup>* mice was performed. Analysis of the spleen revealed that the proportion of Treg cells was increased in *Gata3<sup>fl/fl</sup>Foxp3<sup>Cre</sup>* mice compared to controls (**Figure 22a**). As observed in VAT Treg cells, splenic Treg cells also had reduced Foxp3 expression (**Figure 22b**). Further analysis of the Treg cell compartment showed a significant reduction of KLRG1+ Treg cells in GATA3-deficient mice when compared of controls in both sexes (**Figure 22c**). Similar to VAT Treg cells, CXCR3 expression was elevated in GATA3-deficient Treg cells of female mice (**Figure 22c**). Additionally, *Gata3<sup>fl/fl</sup>Foxp3<sup>Cre</sup>* Treg cells displayed increased CD44 expression and increased proliferation, based on Ki67 staining, which is reminiscent of the VAT Treg cell phenotype (**Figure 22d, e**).

Analysis of the small intestine (SI) of *Gata3<sup>fl/fl</sup>Foxp3<sup>Cre</sup>* and control mice revealed no difference between sexes and therefore data from male and female mice are pooled for this section. Measurement of SI length revealed that GATA3-deficient mice have longer SI compared to controls (**Figure 23a**). Furthermore, SI Treg cell population in *Gata3<sup>fl/fl</sup>Foxp3<sup>Cre</sup>* mice was significantly larger in proportion and in numbers compared to control mice (**Figure 23b**). In line with observations from other organs, we also observed a significant decrease in Foxp3 expression (**Figure 23c**). Further investigation of the Treg cell compartment showed, as expected, no GATA3+ Treg cells in *Gata3<sup>fl/fl</sup>Foxp3<sup>Cre</sup>* mice compared to controls (**Figure 23d**). In contrast, ROR $\gamma$ t+ Treg cells expanded in absence of GATA3 both in proportion and in numbers. Moreover, KLRG1+ Treg cells disappeared in *Gata3<sup>fl/fl</sup>Foxp3<sup>Cre</sup>* mice while the proportion but not the numbers of Helios+ROR $\gamma$ t- Treg cells were reduced in GATA3-deficient mice (**Figure 23d**). Here it is important to note that GATA3 and Helios expression overlap in most Treg cells

(Figure 23d). Strikingly a population of ROR $\gamma$ t+Helios+ Treg cells emerged in *Gata3<sup>fl/fl</sup>Foxp3<sup>Cre</sup>* mice, which does not exist in control mice (Figure 23d).

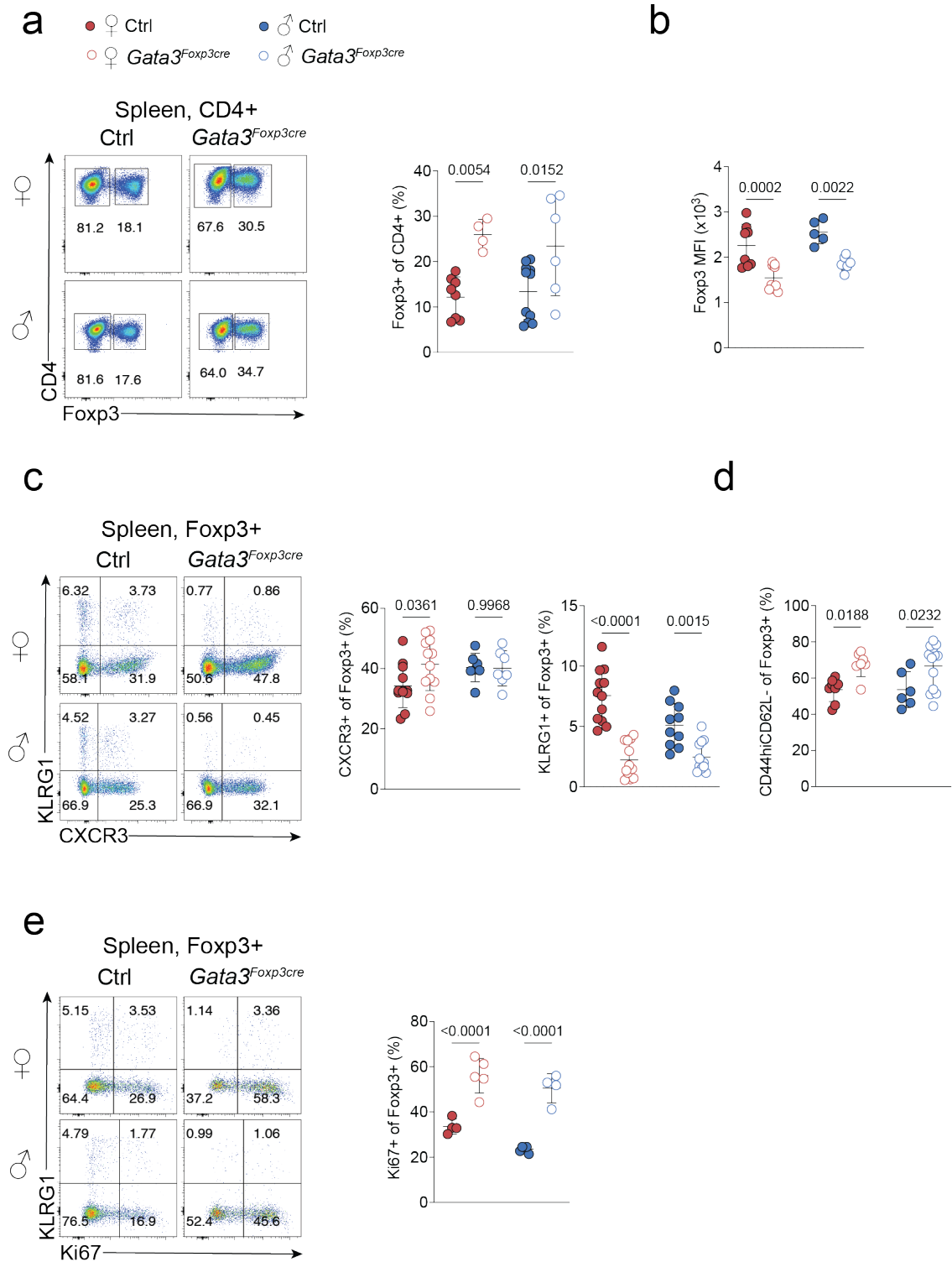


**Figure 22 | GATA3 depletion leads to expansion of splenic Treg cells in males and females.** Analysis of spleens from 22-28-week-old male and female

*Gata3<sup>fl/fl</sup>Foxp3<sup>Cre</sup>*, wildtype (n=6) and *Foxp3<sup>Cre</sup>* (n=8) mice. **a**, FACS plots showing Foxp3 and CD4 expression in CD4<sup>+</sup> T cells (left). Frequency of total splenic Treg cell population (right). **b**, Quantification of Foxp3 MFI in splenic Treg cells. **c**, Flow cytometry plots showing KLRG1 and CXCR3 expression and quantification of KLRG1<sup>+</sup> and CXCR3<sup>+</sup> splenic Treg cells in *Gata3<sup>fl/fl</sup>Foxp3<sup>Cre</sup>* and control mice. **d**, Frequencies of CD44<sup>hi</sup>CD62L<sup>-</sup> Treg cells in *Gata3<sup>fl/fl</sup>Foxp3<sup>Cre</sup>* and control mice. **e**, Flow cytometry plots showing KLRG1 and Ki67 expression and quantification of Ki67<sup>+</sup> splenic Treg cells in *Gata3<sup>fl/fl</sup>Foxp3<sup>Cre</sup>* and control mice. Data are representative (**a**, **c**, **e**) or pooled (**a-e**) from a minimum of two independent experiments. Error bars indicate the standard deviation. Statistical analyses were performed using two-way ANOVA.

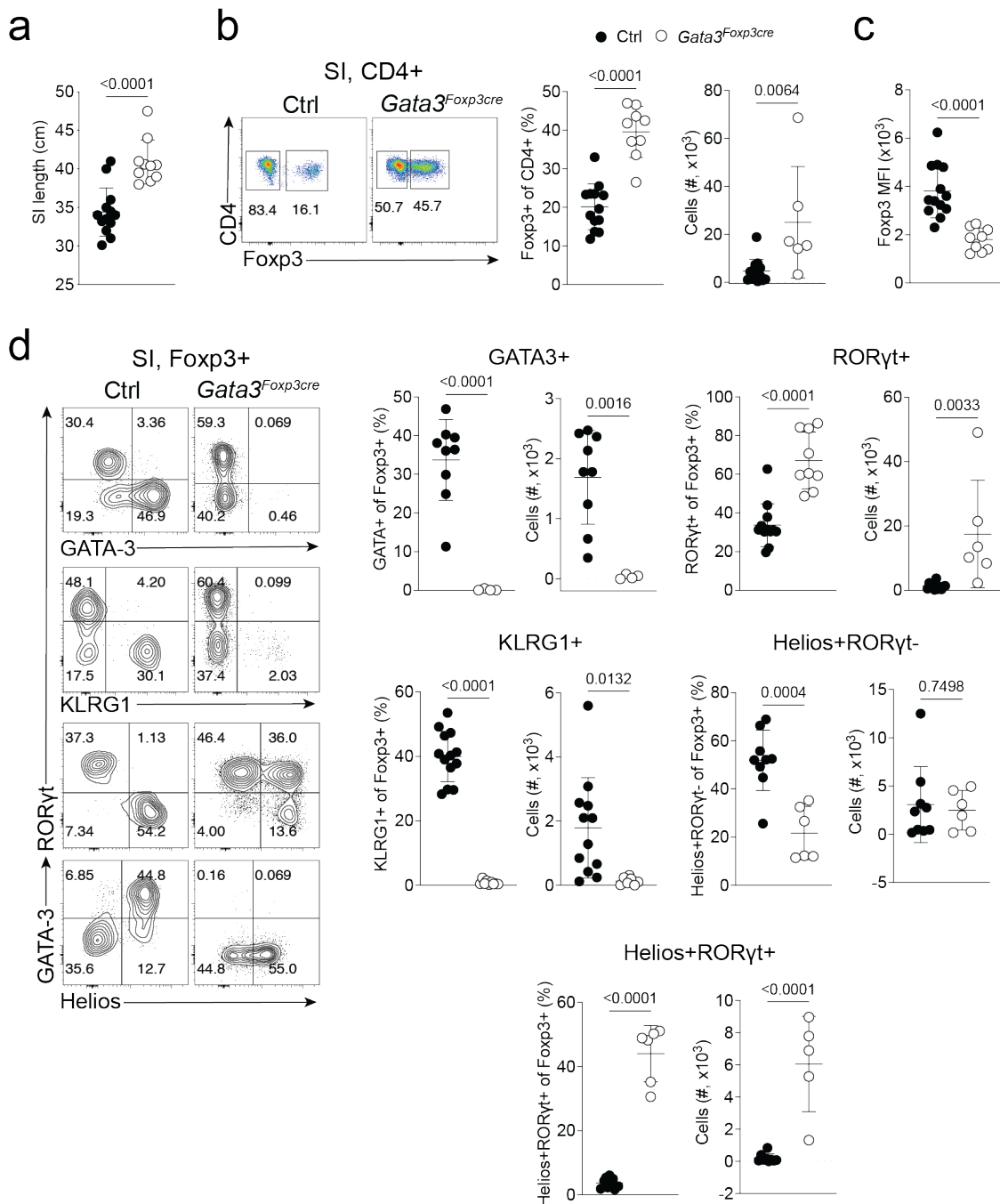


**Figure 23 | Gut resident ROR $\gamma$ t<sup>+</sup> Treg cells expand in absence of GATA3.** Small intestine from 20–28-week-old *Gata3<sup>fl/fl</sup>Foxp3<sup>Cre</sup>*, wildtype (n=6) and *Foxp3<sup>Cre</sup>* (n=8) mice were analysed and compared. **a**, Quantification of SI length in *Gata3<sup>fl/fl</sup>Foxp3<sup>Cre</sup>* and control (wildtype and *Foxp3<sup>Cre</sup>*) mice. **b**, FACS plots showing Foxp3 and CD4 expression in CD4<sup>+</sup> T cells (left). Frequency (centre) and numbers (right) of total intestinal Treg cell population. **c**, Quantification of Foxp3 MFI in splenic Treg cells. **d**, Flow cytometry plots showing ROR $\gamma$ t versus GATA3, KLRG1 and Helios expression and frequencies and numbers of GATA3<sup>+</sup>, ROR $\gamma$ t<sup>+</sup>, KLRG1<sup>+</sup>, Helios<sup>+</sup> and Helios+ROR $\gamma$ t<sup>+</sup> intestinal Treg cells in *Gata3<sup>fl/fl</sup>Foxp3<sup>Cre</sup>* and control mice. Symbols represent individual mice; horizontal

lines indicate means. Data are pooled from a minimum of two independent experiments. FACS plots are representative. Error bars indicate the standard deviation. Statistical analyses were performed using unpaired, two-tailed Student's *t*-test.

We then analysed the impact of GATA3 depletion on Treg cells in the lung as several studies have demonstrated the role of Gata3 in lung resident Treg cells (Ichikawa et al., 2019; Kleinjan et al., 2014; Morita et al., 2015). As observed in other organs, Treg cells are increased in proportion and numbers in the lungs of *Gata3<sup>fl/fl</sup>Foxp3<sup>Cre</sup>* mice compared to controls (**Figure 24a**). Consistent with other organs, Foxp3 MFI is also decreased in the absence of GATA3 in lung Treg cells (**Figure 24b**). Detailed analysis of the Treg cell compartment showed a proportional decrease in KLRG1+ and ST2+ Treg cells in the lung (**Figure 24c**). However, the numbers of KLRG1+ cells did not change while an increased number of ST2+ Treg cells was observed. In contrast, both, proportion and numbers of CXCR3+ Treg cells increased in the absence of GATA3.

Together, our results demonstrate the importance of GATA3 for Treg cell function. The data shows that GATA3 depletion has a universal impact on development, differentiation and proliferation of CXCR3+ Treg cells and KLRG1+/ST2+ Treg cells across multiple organs.

Notably, however, due to suboptimal CXCR3 and ST2 staining in SI and lung, the present results require further confirmation.

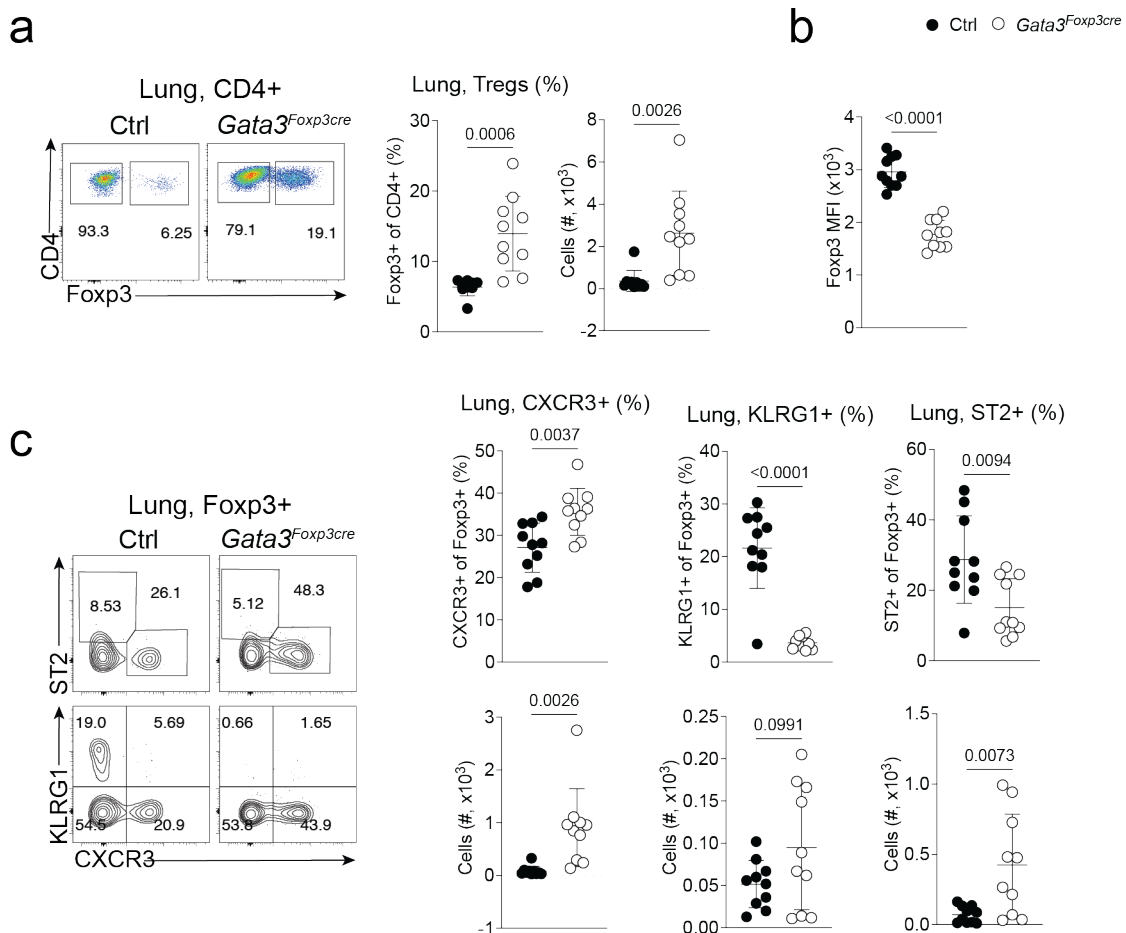


**Figure 24 | GATA3 is required for KLRG1+ but not CXCR3+ lung resident Treg cells.** Lungs from 20–28-week-old  $Gata3^{fl/fl}Foxp3^{Cre}$ , wildtype (n=6) and  $Foxp3^{Cre}$  (n=8) mice were analysed and compared. **a**, FACS plots showing Foxp3 and CD4 expression in CD4+ T cells (left). Frequency (centre) and numbers (right) of total lung Treg cell population. **b**, Quantification of Foxp3 MFI in splenic Treg cells. **c**, Flow cytometry plots showing CXCR3 versus ST2 and KLRG1 and frequencies (top) and numbers (bottom) of CXCR3+, KLRG1+ and ST2+ lung Treg cells in  $Gata3^{fl/fl}Foxp3^{Cre}$  and control mice. Symbols represent individual mice; horizontal lines indicate means. Data are pooled from a minimum of two independent experiments. FACS plots are representative. Error bars indicate the standard deviation. Statistical analyses were performed using unpaired, two-tailed Student's *t*-test.

#### 4.5 T-bet depletion results in expansion of ST2+ VAT Treg cells in female mice

Having established the crucial role GATA3 plays in VAT Treg cell development we investigated how its counterpart, T-bet, affects VAT Treg cells. The  $T_H1$  transcription factor T-bet, encoded by *Tbx21*, is a critical regulator of *Cxcr3*

expression (Szabo et al., 2000). First, the expression pattern of T-bet in the VAT and spleen was measured in both sexes using *Tbx21*-reporter mice (Zhu et al., 2012). Analysis of the entire CD45<sup>+</sup> compartment revealed higher T-bet expression in female mice compared to males (**Figure 25a, b**). This characteristic could be attributed to CD4<sup>+</sup> T cells that displayed higher T-bet expression in female mice. Analysis of the VAT Treg cell compartment revealed that females express higher T-bet levels compared to their male counterparts (**Figure 25c, d**). A significant proportion of ST2-negative VAT Treg cells expressed *Tbx21*, which was restricted to CXCR3<sup>+</sup> Treg cells both in males and females (**Figure 25c, d**). In the spleen, T-bet expression was higher in T cells from female mice compared to male mice (**Figure 25e**). Furthermore, T-bet expression was higher in conventional (Foxp3<sup>-</sup>) CD4<sup>+</sup> T cells in females compared to males (**Figure 25f, g**). However, T-bet expression was similar in Treg cells of both female and male mice and restricted to CXCR3<sup>+</sup> population (**Figure 25g**).

Considering the sexually divergent expression pattern of T-bet in both VAT and spleen, *Tbx21*<sup>-/-</sup> mice were analysed to assess how T-bet ablation influences the Treg cell compartment. In the VAT, the entire Treg cell compartment was proportionally larger in *Tbx21*<sup>-/-</sup> compared to controls, in both sexes (**Figure 26a**). However, the number of Treg cells was similar in *Tbx21*<sup>-/-</sup> and WT mice (**Figure 26b**). Assessment of Foxp3 expression also showed no difference across all groups (**Figure 26c**). Further analysis of the Treg cell compartment showed a significant increase of ST2<sup>+</sup> cells. This was particularly striking in female mice where the proportion of ST2<sup>+</sup> VAT Treg cells increase to male-like levels (**Figure 26d, e**). However, ST2<sup>+</sup> VAT Treg cell numbers were increased only in male *Tbx21*<sup>-/-</sup> mice and not in female mice. Given CXCR3<sup>+</sup> Treg cells are diminished upon T-bet depletion, the entire ST2<sup>-</sup> Treg cell compartment was analysed as surrogate for CXCR3<sup>+</sup> Treg cells. ST2<sup>-</sup> Treg cell proportions were reduced in both sexes, but numbers were only reduced in female *Tbx21*<sup>-/-</sup> mice compared to their respective controls (**Figure 26d, e**), indicating the sex-specific impact of T-bet on VAT Treg cells.

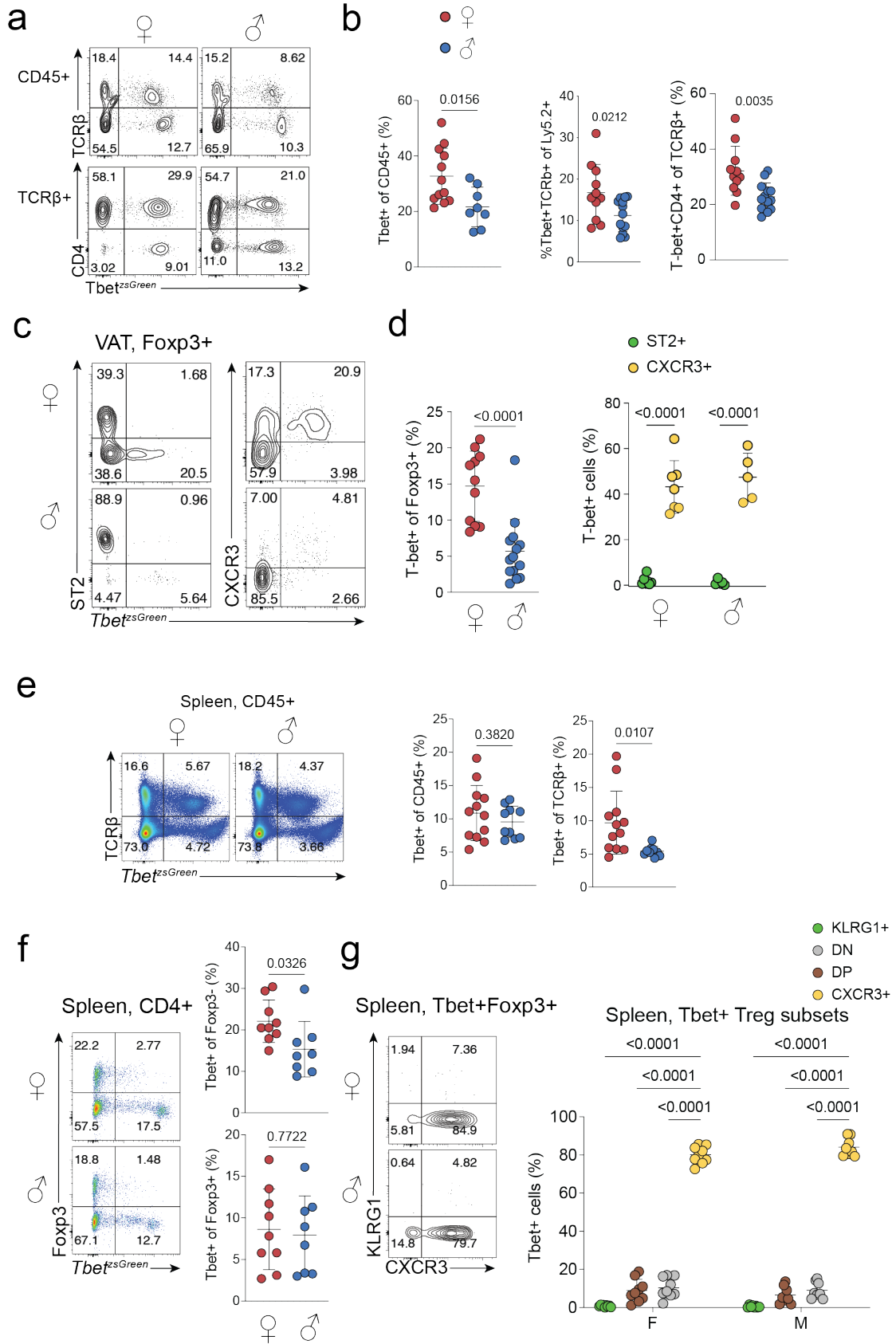


**Figure 25 | T-bet is expressed predominantly in CXCR3+ Treg cells in VAT and spleen.** **a-d**, VAT from 30–36-week-old *Tbet<sup>tsGreen</sup>* female and mice were analysed and compared. **a**, FACS plots showing *Tbet<sup>tsGreen</sup>* versus TCR $\beta$  and CD4 in CD45+ and TCR $\beta$ + VAT cells, respectively. **b**, Frequencies of T-bet+ cells among CD45+ (left), CD45+TCR $\beta$ + (centre) and TCR $\beta$ +CD4+ cells. **c**, FACS plots depicting *Tbet<sup>tsGreen</sup>* against ST2 and CXCR3 expression in VAT Treg cells of female and male mice. **d**, Quantification of T-bet+ cells among total (left), CXCR3+ and ST2+ (right) Treg cells in male and female mice. **e-g**, Spleens from 30–36-week-old *Tbet<sup>tsGreen</sup>* female and mice were analysed and compared. **e**, FACS plots (left) showing *Tbet<sup>tsGreen</sup>* versus TCR $\beta$  expression in CD45+ splenic cells. Frequencies of T-bet+ cells among CD45+ (centre), TCR $\beta$ + (right) cells. **f**, FACS plots (left) showing *Tbet<sup>tsGreen</sup>* versus Foxp3 expression in CD4+ splenic T cells. Frequencies of T-bet+ cells among Foxp3- (top) and Foxp3+ (bottom) cells. **g**, FACS plots (left) showing CXCR3 versus KLRG1 expression in T-bet+Foxp3+ splenic cells. Frequencies of KLRG1+ (green), DN (grey), DP (brown) and CXCR3+ (yellow) cells among T-bet+Foxp3+ splenic cells. Symbols represent individual mice; horizontal lines indicate means. Data are representative (**a, c, e-g**) or pooled (**b, d e-g**) from a minimum of two independent experiments. Error bars indicate the standard deviation. Statistical analyses were performed using unpaired, two-tailed Student's *t*-test (**b, d-f**) or two-way ANOVA (**d, g**).

Analysis of the spleen revealed expansion of Treg cells in both male and female mice deficient for T-bet (**Figure 27a, b**). This was accompanied by enhanced Foxp3 expression, but only in female mice (**Figure 27c**). More detailed analysis of the splenic Treg cell compartment revealed that ST2+ and KLRG1+ VAT Treg cells were enriched in male and female *Tbx21<sup>-/-</sup>* mice compared to their WT counterparts (**Figure 27d, e**).

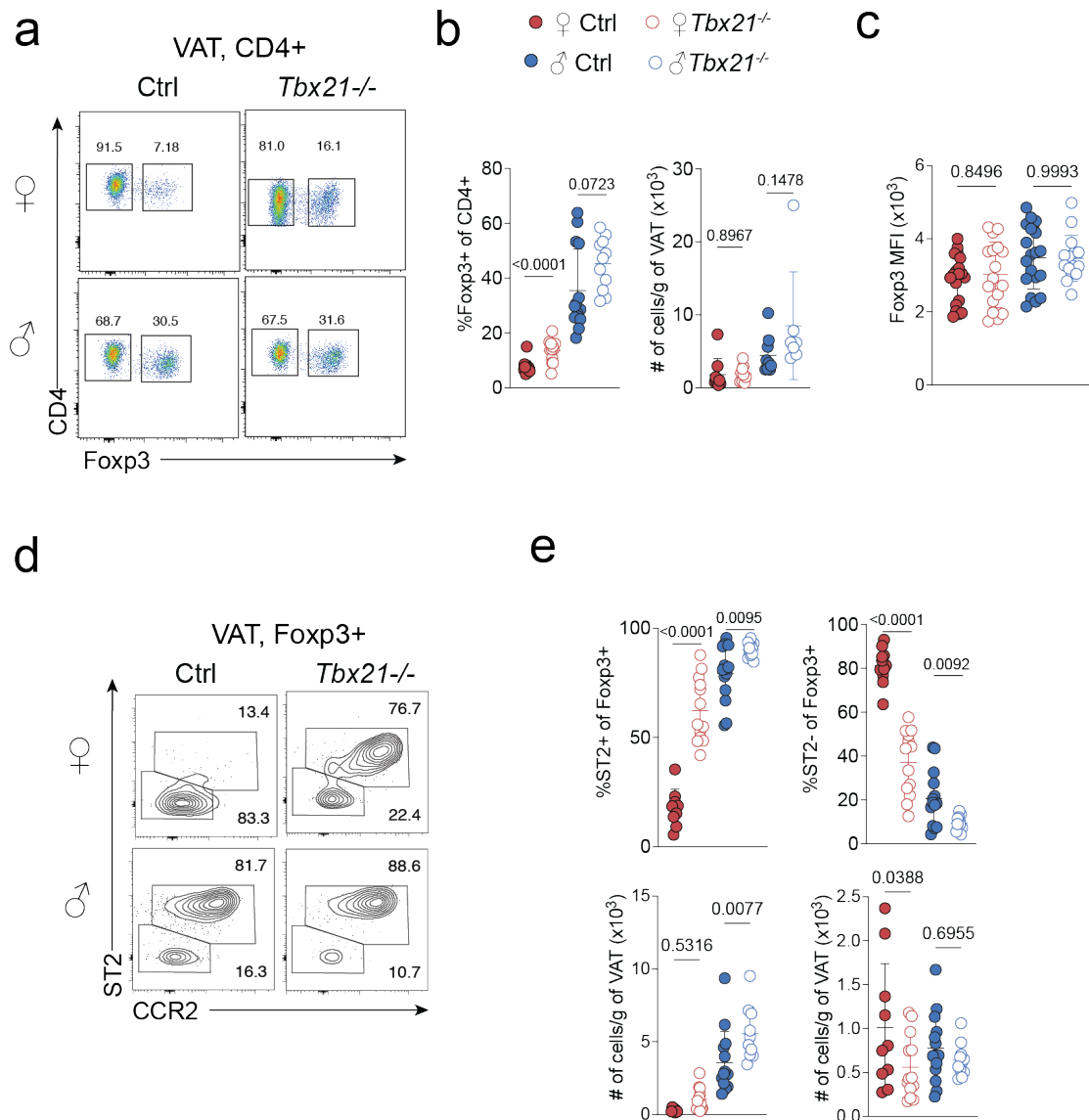


**Figure 26 | ST2<sup>+</sup> VAT Treg cells emerge in females in response to whole body depletion of T-bet.** VAT from 30–36-week-old *Tbx21*<sup>-/-</sup> and control (WT) female and mice were analysed and compared. **a**, **b**, FACS plots (**a**) depicting CD4 versus Fxp3 expression in CD4<sup>+</sup> T cells and quantification (**b**) of frequencies and numbers of total VAT Treg cells in *Tbx21*<sup>-/-</sup> and control mice. **c**, Quantification of Fxp3 MFI in *Tbx21*<sup>-/-</sup> and control mice. **d**, **e**, FACS plots (**d**) depicting CD4 versus Fxp3 expression in CD4<sup>+</sup> T cells and quantification (**e**) of frequencies and numbers of ST2<sup>+</sup> and ST2<sup>-</sup> VAT Treg cells in *Tbx21*<sup>-/-</sup> and control mice. Symbols represent individual mice; horizontal lines indicate means. Data are representative (**a**, **d**) or pooled (**b**, **c**, **e**) from a minimum of two independent experiments. Error bars indicate the standard deviation. Statistical analyses were performed using two-way ANOVA.

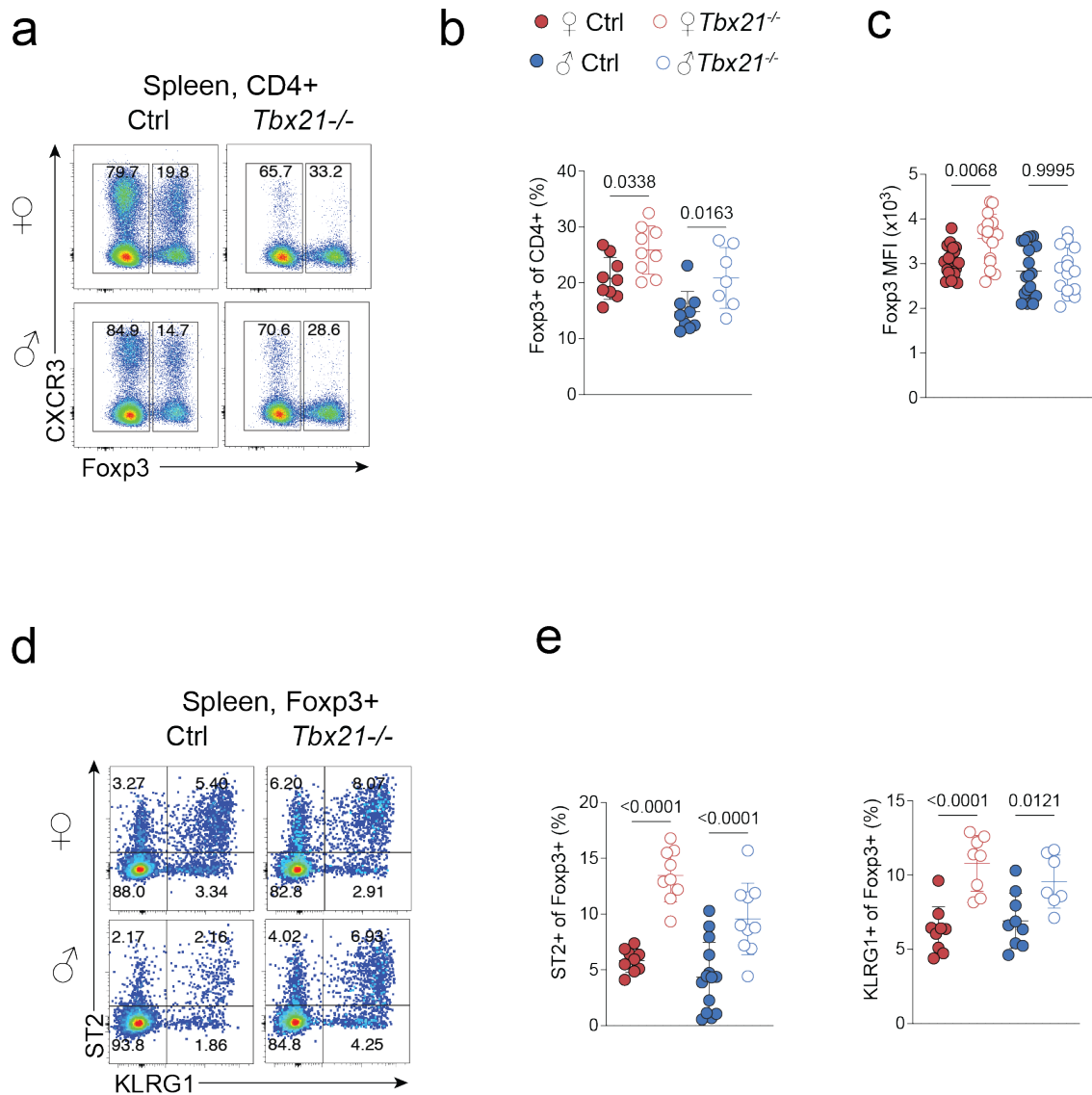


**Figure 27 | KLRG1<sup>+</sup> and ST2<sup>+</sup> splenic Treg cells expand in absence of Tbet.** Splensins from 30–36-week-old *Tbx21*<sup>-/-</sup> and control (WT) female and mice were analysed and compared. **a, b**, FACS plots (**a**) depicting CXCR3 versus Foxp3 expression in CD4<sup>+</sup> T cells and quantification (**b**) of frequencies of total splenic Treg cells in *Tbx21*<sup>-/-</sup> and control mice. **c**, Quantification of Foxp3 MFI in *Tbx21*<sup>-/-</sup> and control mice. **d, e**, FACS plots (**d**) depicting ST2 versus KLRG1 expression in splenic Treg cells and quantification (**e**) of ST2<sup>+</sup> and KLRG1<sup>+</sup> Treg cells in *Tbx21*<sup>-/-</sup> and control mice. Symbols represent individual mice; horizontal lines indicate means. Data are representative (**a, d**) or pooled (**b, c, e**) from a minimum of two independent experiments. Error bars indicate the standard deviation. Statistical analyses were performed using two-way ANOVA.

## 4.6 T-bet expression in Treg cells is required for CXCR3<sup>+</sup> VAT Treg cell differentiation

Analysis of *Tbx21*<sup>-/-</sup> mice showed that T-bet expression affects the Treg cell compartment significantly in the VAT. Considering it is a full body knockout, to examine Treg-intrinsic effect of T-bet loss, mixed bone marrow chimeras were generated that harbour WT and *Tbx21*<sup>-/-</sup> immune cells, which then can be discriminated based on a congenic marker. With the help of this model, the relative contribution of each genotype to CXCR3<sup>+</sup>, DN and ST2<sup>+</sup> VAT Treg cell compartment was assessed. The indicated gating strategy was employed, to exclude radio-resistant host cells from analysis (**Figure 28a**). In both experiments, *Tbx21*<sup>-/-</sup> cells did not contribute to the CXCR3<sup>+</sup> Treg cell compartment. The DN Treg cell compartment proportionally increased in male and female mice, although only reaching significance in females (**Figure 28c**). Furthermore, ST2<sup>+</sup> VAT Treg cell proportions were increased in the first experiment but not in the second experiment (**Figure 28b**).

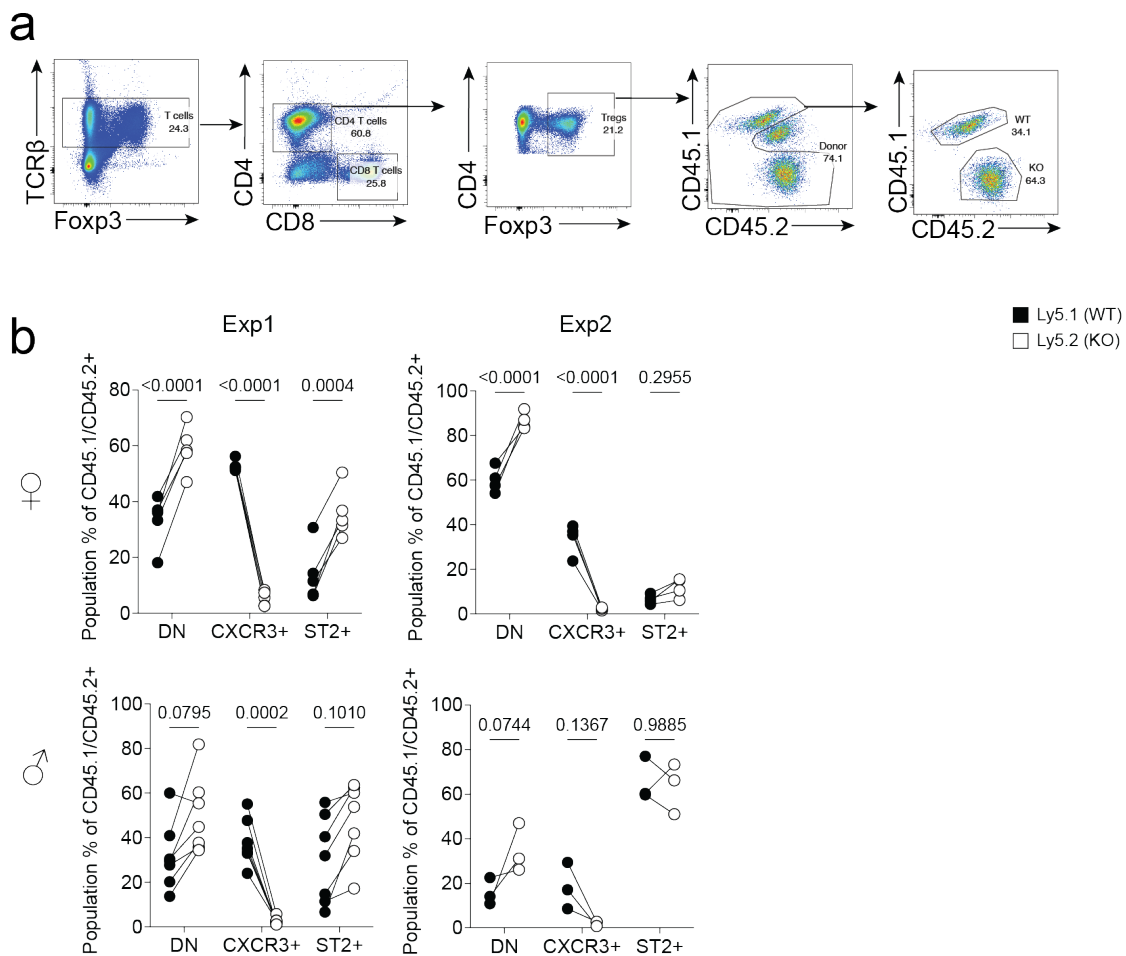


**Figure 28 | *Tbx21*<sup>-/-</sup> cells accumulate as DN Treg cells in mixed bone marrow chimeric mice.** To generate bone marrow chimeras, 6-8-week-old F1 (CD45.1/CD45.2) female and male mice were irradiated and reconstituted with a mix of WT (CD45.1) and *Tbx21*<sup>-/-</sup> (CD45.2) bone-marrow derived cells. VAT was analysed 20-22 weeks post-reconstitution. **a**, Gating strategy used for analysis. **b**, Frequencies of WT (CD45.1+) and *Tbx21*<sup>-/-</sup> (CD45.2+) cells among DN, CXCR3+ and ST2+ VAT Treg cell populations in female and male mice from two different experiments (Exp1 & Exp2). Symbols represent individual mice. Statistical analyses were performed using two-way ANOVA.

To fully understand the Treg cell intrinsic role of T-bet, *Tbx21*<sup>fl/fl</sup>*Foxp3*<sup>Cre</sup> mice that lack T-bet expression specifically in Treg cells were generated. First, the specificity of this mouse model was confirmed by showing that CXCR3 expression was only reduced in *Foxp3*<sup>+</sup> T cell, while *Foxp3*<sup>-</sup> T cells maintained CXCR3 expression (**Figure 29a**). Analysis of the total VAT Treg cell compartment showed no difference between control and *Tbx21*<sup>fl/fl</sup>*Foxp3*<sup>Cre</sup> mice (**Figure 29b**). Surprisingly, we found reduced *Foxp3* expression in Treg cells devoid of T-bet in

both sexes (**Figure 29c**). Additionally, Treg-specific T-bet depletion resulted in expansion of ST2<sup>+</sup> VAT Treg cells, which was specific to females. In contrast, ST2<sup>-</sup> VAT Treg cell proportions were reduced in females but remained unchanged in male mice (**Figure 29d, e**).

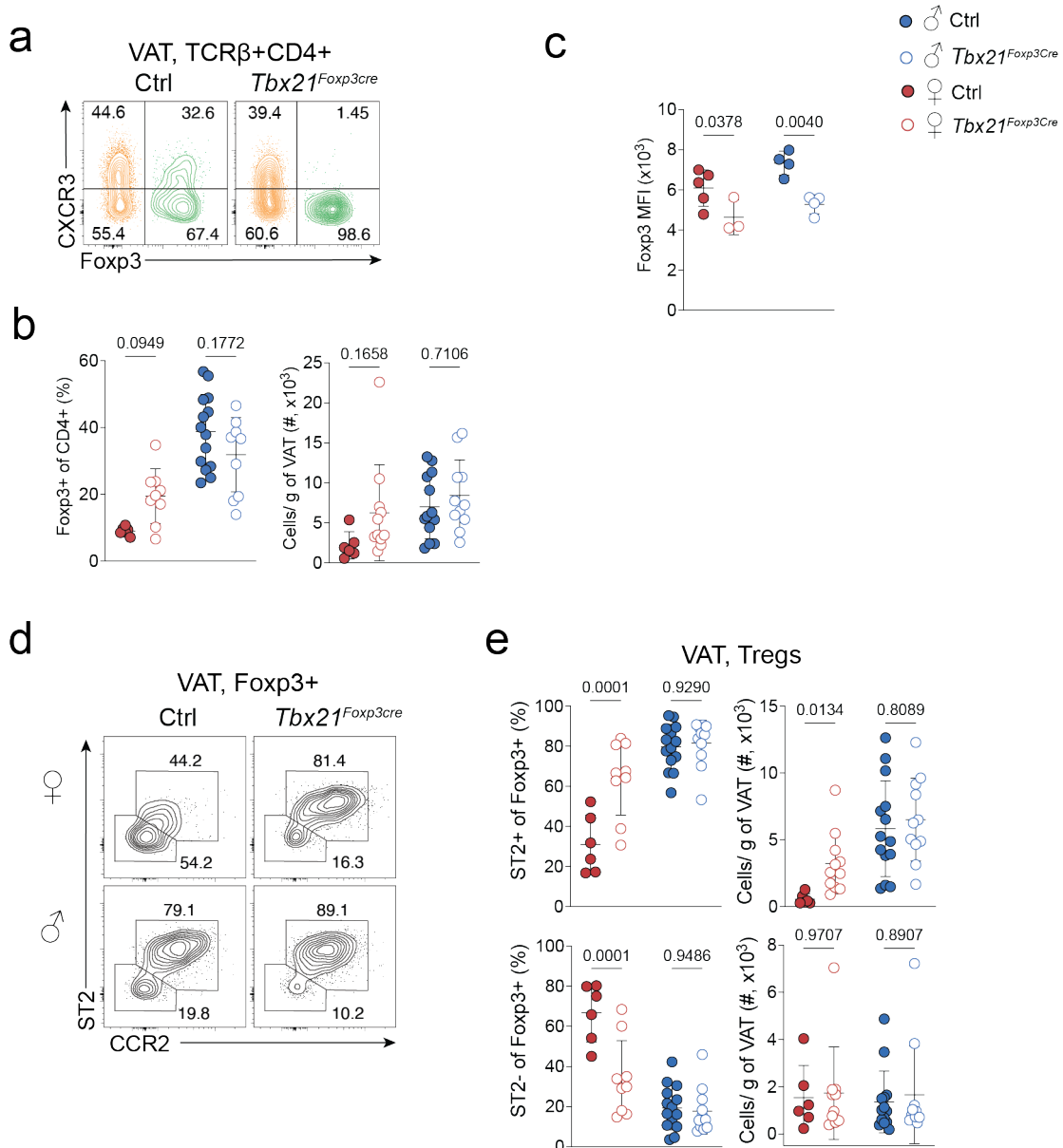


**Figure 29 | ST2<sup>+</sup> VAT Treg cells are increased in *Tbx21<sup>fl/fl</sup>Foxp3<sup>Cre</sup>* female mice.** Analysis of VAT from 26-32-week-old male and female *Tbx21<sup>fl/fl</sup>Foxp3<sup>Cre</sup>* and control (WT and *Foxp3<sup>Cre</sup>*) mice. **a**, Combined flow cytometry plots showing CXCR3 versus Fcγ3 expression among CD4<sup>+</sup> T cells (orange, left) and Treg cells (green, right) in VAT. Numbers represent percentages among Fcγ3<sup>-</sup> (left) or Fcγ3<sup>+</sup> (right) cells. **b**, Quantification of frequencies (left) and numbers (right) of total VAT Treg cell population in *Tbx21<sup>fl/fl</sup>Foxp3<sup>Cre</sup>* and control mice. **c**,

Quantification of Foxp3 MFI in VAT Treg cells. **d, e**, Flow cytometry plots (**d**) showing ST2 and CCR2 expression and quantification (**e**, frequencies left, numbers right) of ST2+ and CXCR3+ VAT Treg cells in *Tbx21<sup>fl/fl</sup>Foxp3<sup>Cre</sup>* and control mice. Symbols represent individual mice; horizontal lines indicate means. Data are representative (**a, d**) or pooled (**b, c, e**) from a minimum of two independent experiments. Error bars indicate the standard deviation. Statistical analyses were performed using two-way ANOVA.

To test whether the enrichment in ST2+ Treg cells in females was due to recruitment or proliferation, Ki67 staining was performed, to stain for actively dividing cells. Total Ki67+ Treg cell proportions were reduced in female *Tbx21<sup>fl/fl</sup>Foxp3<sup>Cre</sup>* mice compared to control mice in total Treg cells (**Figure 30a**) but unaffected in males. Further analysis of the ST2+ and ST2- VAT Treg cell compartments revealed less Ki67+ cells in *Tbx21<sup>fl/fl</sup>Foxp3<sup>Cre</sup>* mice compared to controls in female mice, suggesting that Treg cell enrichment in female *Tbx21<sup>fl/fl</sup>Foxp3<sup>Cre</sup>* mice was not due to enhanced proliferation (**Figure 30b**). Furthermore, CD25 expression was measured in male mice as a measure of activation status (Ferenczi, Burack, Pope, Krueger, & Austin, 2000). CD25 expression was reduced in T-bet deficient ST2+ VAT Treg cells while and remained unchanged ST2- Treg cells (**Figure 30c**).

In the spleen, the total population of Treg cells remained unchanged in male and female *Tbx21<sup>fl/fl</sup>Foxp3<sup>Cre</sup>* mice despite displaying lower Foxp3 expression than their respective controls (**Figure 31a-c**). Analysis of splenic KLRG1+ Treg cell subsets mirrored the VAT phenotype. KLRG1+ splenic Treg cells were increased in female but not male *Tbx21<sup>fl/fl</sup>Foxp3<sup>Cre</sup>* mice compared to their controls (**Figure 31d, e**). Additionally, no difference in Ki67 expression was observed in T-bet-deficient mice compared to controls.

Overall, our results reveal that T-bet is required for the differentiation of CXCR3+ VAT Treg cells but simultaneously repressed ST2+ population.

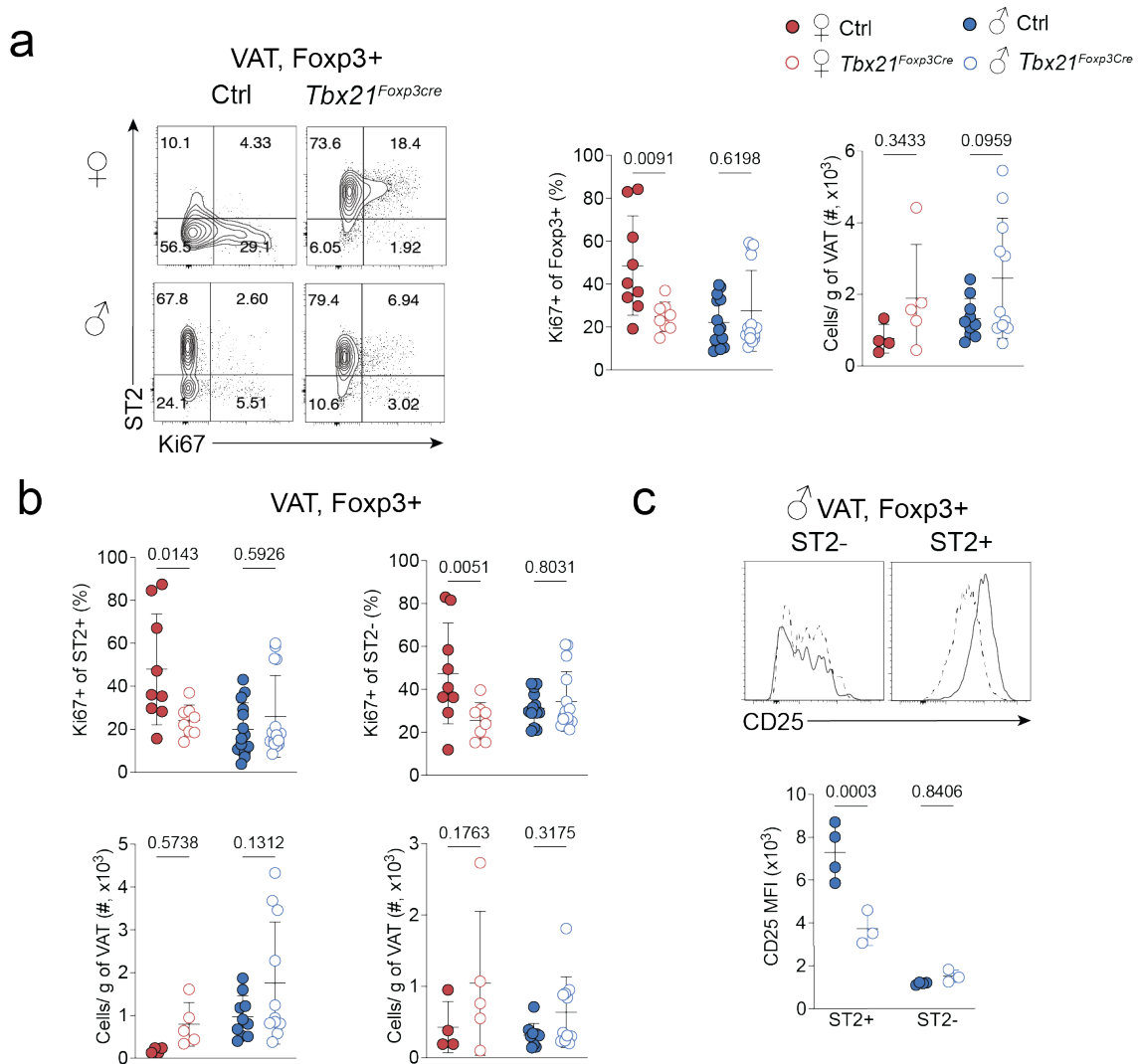
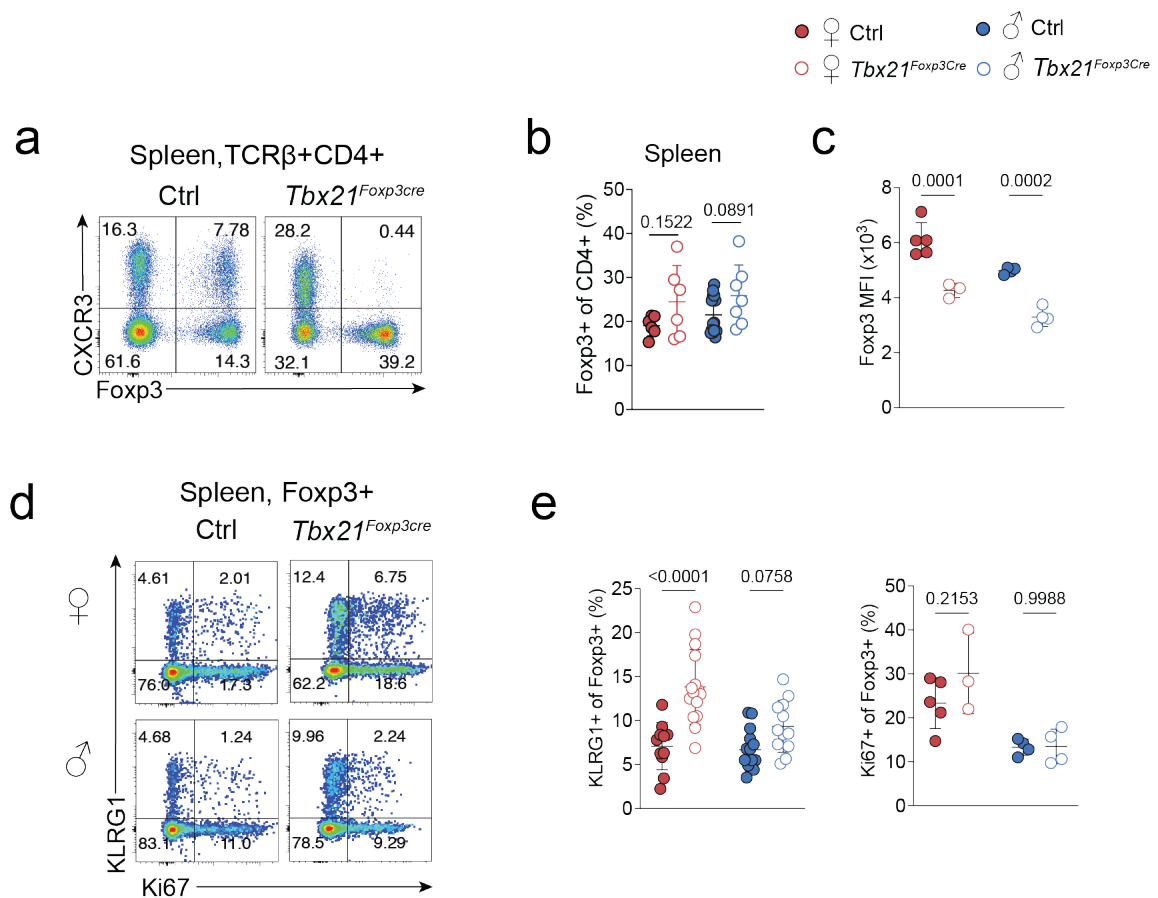


**Figure 30 | ST2<sup>+</sup> VAT Treg cells emerge from infiltrating cells in female *Tbx21<sup>fl/fl</sup>Foxp3<sup>Cre</sup>* mice.** Analysis of VAT from 26-32-week-old male and female *Tbx21<sup>fl/fl</sup>Foxp3<sup>Cre</sup>* and control (WT and *Foxp3<sup>Cre</sup>*) mice. **a, b**, Flow cytometry plots (**a**) showing ST2 versus Ki67 expression and quantification (frequencies and numbers) of total (**a**) and ST2<sup>+</sup> and CXCR3<sup>+</sup> (**b**) VAT Treg cells in *Tbx21<sup>fl/fl</sup>Foxp3<sup>Cre</sup>* and control mice. **c**, Histograms displaying CD25 expression (top) and CD25 MFI quantification (bottom) in male *Tbx21<sup>fl/fl</sup>Foxp3<sup>Cre</sup>* and control mice. Symbols represent individual mice; horizontal lines indicate means. Data are representative (**a, c**) or pooled (**a-c**) from a minimum of two independent experiments. Error bars indicate the standard deviation. Statistical analyses were performed using two-way ANOVA.



#### 4.7 Sirt1 contributes to ST2+ VAT Treg cell differentiation

The above experiments have shown the imperative role of PPAR $\gamma$ , GATA3 and T-bet transcription factors in VAT Treg cell biology. These transcription factors also seem to influence the expression of the Treg lineage specific transcription factor Fcpx3. Sirt1 is a deacetylase which has been shown to regulate the stability

of PPAR $\gamma$  (Picard et al., 2004; Qiang et al., 2012; van Loosdregt et al., 2011; van Loosdregt et al., 2010). Given the essential role of PPAR $\gamma$  in VAT Treg cells, we analysed the role of Sirt1 specifically in Treg cells using the *Sirt1<sup>fl/fl</sup>Foxp3<sup>Cre</sup>* mice. Foxp3 expression was lower in male Sirt1-depleted VAT Treg cells compared to controls, while it was unaffected in female Treg cells (**Figure 32c**). In keeping with this, total VAT Treg cells in male mice were proportionally reduced compared to their controls (**Figure 32a, b**). Female Treg cells however remained unaffected. Further analysis of the Treg cell compartment revealed that ST2<sup>+</sup> VAT Treg cells were reduced in proportion in male *Sirt1<sup>fl/fl</sup>Foxp3<sup>Cre</sup>* mice compared to controls (**Figure 32d, e**). However, ST2<sup>+</sup> Treg cells in female *Sirt1<sup>fl/fl</sup>Foxp3<sup>Cre</sup>* mice and controls were comparable. CXCR3<sup>+</sup> VAT Treg cells were increased in proportion in both sexes. However, CXCR3<sup>+</sup> cell numbers were enriched only in male *Sirt1<sup>fl/fl</sup>Foxp3<sup>Cre</sup>* mice compared to controls (**Figure 32d, e**).

Additionally, expression of CCR2, KLRG1 and CD73 was measured but no significant difference was detected between controls and *Sirt1<sup>fl/fl</sup>Foxp3<sup>Cre</sup>* mice. Analysis of CD44 expression showed decreased CD44 MFI in *Sirt1<sup>fl/fl</sup>Foxp3<sup>Cre</sup>* males compared to controls. In the spleen, Sirt1 depletion did not affect the Treg cell compartment (**Figure 33a, b**). Yet, a decrease in Foxp3 expression in Treg cells of *Sirt1<sup>fl/fl</sup>Foxp3<sup>Cre</sup>* mice compared to controls was observed (**Figure 33c**). Analysis of Treg cell subsets showed no significant difference between *Sirt1<sup>fl/fl</sup>Foxp3<sup>Cre</sup>* and control mice in KLRG1<sup>+</sup> or CXCR3<sup>+</sup> Treg cells (**Figure 33d, e**).

Overall, our data demonstrates that SIRT1 has little impact on splenic Treg cells but supports the differentiation of ST2<sup>+</sup> Treg cells in the VAT.

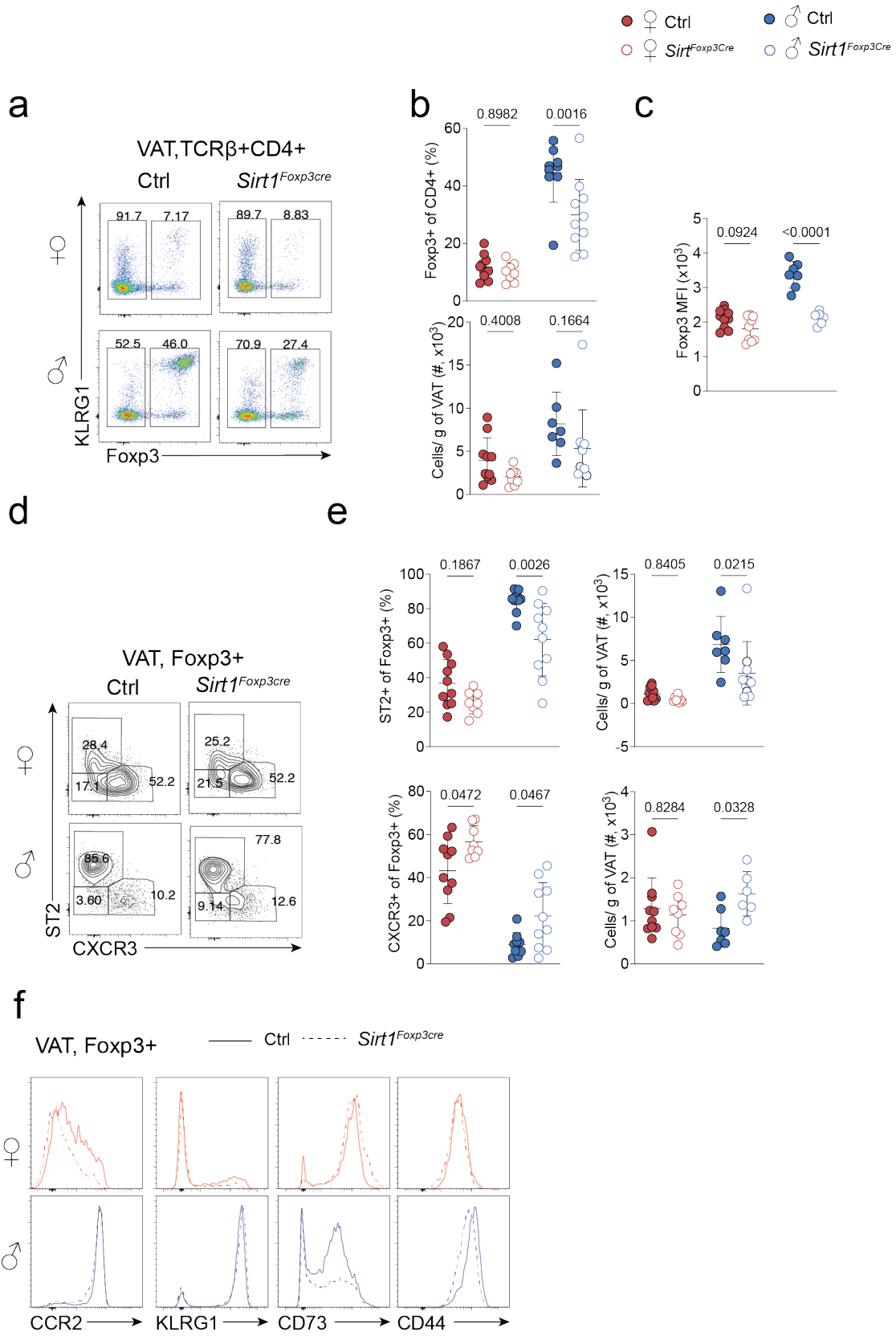


**Figure 32 | Treg cell specific *Sirt1* ablation impacts ST2+ and CXCR3+ VAT Treg cells modestly. Analysis of VAT from 28-32-week-old male and female**

*Sirt1<sup>fl/fl</sup>Foxp3<sup>Cre</sup>*, wildtype (n=10) and *Foxp3<sup>Cre</sup>* (n=7) mice. **a, b**, Flow cytometry plots showing KLRG1 versus Foxp3 expression (**a**) and quantification (**b**) frequencies and numbers of total VAT Treg cells in *Sirt1<sup>fl/fl</sup>Foxp3<sup>Cre</sup>* and control mice. **c**, Quantification of Foxp3 MFI in VAT Treg cells. **d, e**, Flow cytometry plots showing ST2 versus CXCR3 expression (**d**) and quantification (**e**, frequencies top, numbers bottom) of ST2+ and CXCR3+ VAT Treg cells in *Sirt1<sup>fl/fl</sup>Foxp3<sup>Cre</sup>* and control mice. **f**, Histograms showing CCR2, KLRG1, CD73 and CD44 in female and male *Sirt1<sup>fl/fl</sup>Foxp3<sup>Cre</sup>* and control mice. Symbols represent individual mice; horizontal lines indicate means. Data are representative (**a, d, f**) or pooled (**b, c, e**) from a minimum of two independent experiments. Error bars indicate the standard deviation. Statistical analyses were performed using two-way ANOVA.

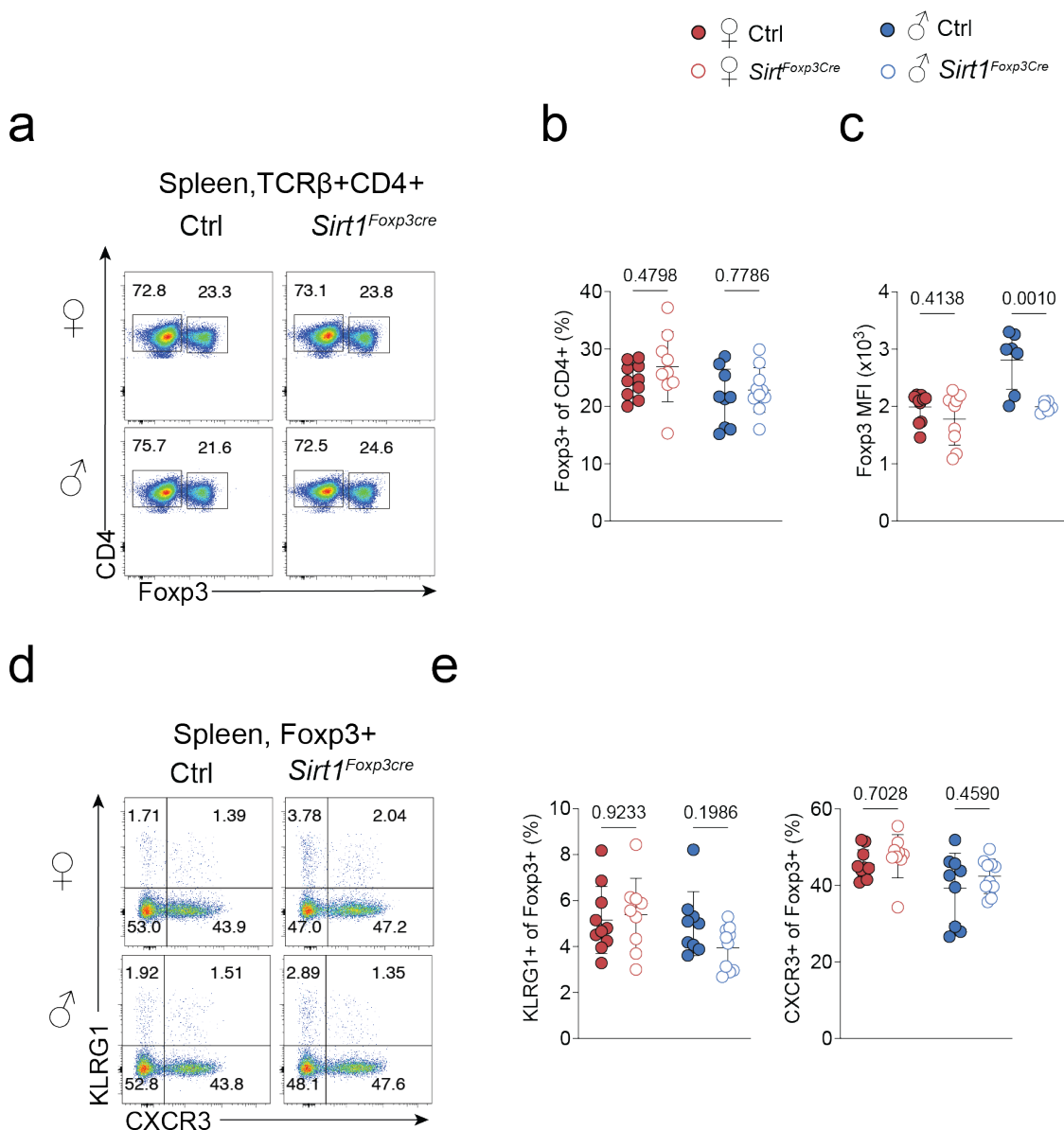


**Figure 33 | Splenic Treg cells are unaltered in *Sirt1<sup>fl/fl</sup>Foxp3<sup>Cre</sup>* mice.** Analysis of spleens from 28-32-week-old male and female *Sirt1<sup>fl/fl</sup>Foxp3<sup>Cre</sup>*, wildtype

(n=10) and *Foxp3<sup>Cre</sup>* (n=7) mice. **a, b**, Flow cytometry plots showing CD4 versus Foxp3 expression (**a**) and frequencies (**b**) of total splenic Treg cells in *Sirt1<sup>fl/fl</sup>Foxp3<sup>Cre</sup>* and control mice. **c**, Quantification of Foxp3 MFI in splenic Treg cells. **d, e**, Flow cytometry plots showing KLRG1 versus CXCR3 expression (**d**) and frequencies (**e**) of KLRG1+ and CXCR3+ splenic Treg cells in *Sirt1<sup>fl/fl</sup>Foxp3<sup>Cre</sup>* and control mice. Symbols represent individual mice; horizontal lines indicate means. Data are representative (**a, d**) or pooled (**b, c, e**) from a minimum of two independent experiments. Error bars indicate the standard deviation. Statistical analyses were performed using two-way ANOVA.

#### 4.8 Treg specific ablation of TGFβR2 significantly impairs VAT Treg cell differentiation and function

TGFβ is a cytokine with pleiotropic functions in immunity (Batlle & Massague, 2019; M. O. Li, Wan, Sanjabi, Robertson, & Flavell, 2006). Among its immunomodulatory functions, it is required for the generation of pTreg cells, and several reports have also shown its involvement in tissue Treg cell function and maintenance (Konkel et al., 2017; Moreau et al., 2021; Worthington et al., 2015). However, its influence on VAT Treg cell biology remains unknown. To dissect the role of TGFβ in VAT Treg cells, *Tgfbr2<sup>fl/fl</sup>Foxp3<sup>Cre</sup>* mice were generated and analysed.

First, specific deletion of TGFβR2 in Treg cells could be indirectly shown through expression of CD73 and CD103, both targets of TGFβ signalling (S. Chen et al., 2019; Duhon et al., 2018). CD73 was significantly downregulated in Foxp3+ but not Foxp3- VAT T cells (**Figure 34a**). Similarly, CD103 which was completely absent in Treg cells of *Tgfbr2<sup>fl/fl</sup>Foxp3<sup>Cre</sup>* mice but not controls (**Figure 34b**). Notably, the total VAT Treg cell population was substantially increased in *Tgfbr2<sup>fl/fl</sup>Foxp3<sup>Cre</sup>* mice compared to controls in female and in male mice, both in proportion and in numbers (**Figure 34c, d**). Detailed analysis of ST2+ VAT Treg cells showed their significant drop in absence of TGFβ-mediated signalling in female and male mice (**Figure 34e, f**). Yet, the number of ST2+ Treg cells were reduced only in male *Tgfbr2<sup>fl/fl</sup>Foxp3<sup>Cre</sup>* mice compared to controls. In contrast, percentage and numbers of CXCR3+ VAT Treg cells were strikingly higher in *Tgfbr2<sup>fl/fl</sup>Foxp3<sup>Cre</sup>* mice compared to controls in both sexes (**Figure 34e, f**). Measurement of Treg cell proliferation revealed that Ki67 expression did not

change in absence of TGF $\beta$  signalling. However, this has only been done in male mice so far.

Analysis of the conventional T cell compartment showed that percentages of Tconv cells were reduced in female *Tgfb2<sup>fl/fl</sup>Foxp3<sup>Cre</sup>* mice while the percentages of CD8+ T cells were significantly lower in *Tgfb2<sup>fl/fl</sup>Foxp3<sup>Cre</sup>* mice in both sexes. However, only males displayed lower cell CD8+ T cell numbers (**Figure 35a, b**). No major differences in CXCR3+ or ST2+ conventional CD4 T cells were observed when comparing *Tgfb2<sup>fl/fl</sup>Foxp3<sup>Cre</sup>* and control mice (**Figure 35c, d**). Moreover, Ki67 expression showed no significant differences in either CD4+Foxp3- or CD8+ T cells of male *TgfbR2<sup>Foxp3<sup>Cre</sup></sup>* mice (**Figure 35e, f**). Analysis of the TCR $\beta$ - compartment also showed no significant changes in ILC2 or Ki67 expression in absence of TGF $\beta$  signalling (**Figure 35g, h**).

Taken together, our results reveal that TGF $\beta$  signalling promotes ST2+ Treg cell differentiation and limits overall Treg infiltration to the VAT. However, further analysis is required to dissect the precise role of TGF $\beta$  in a more detailed manner.

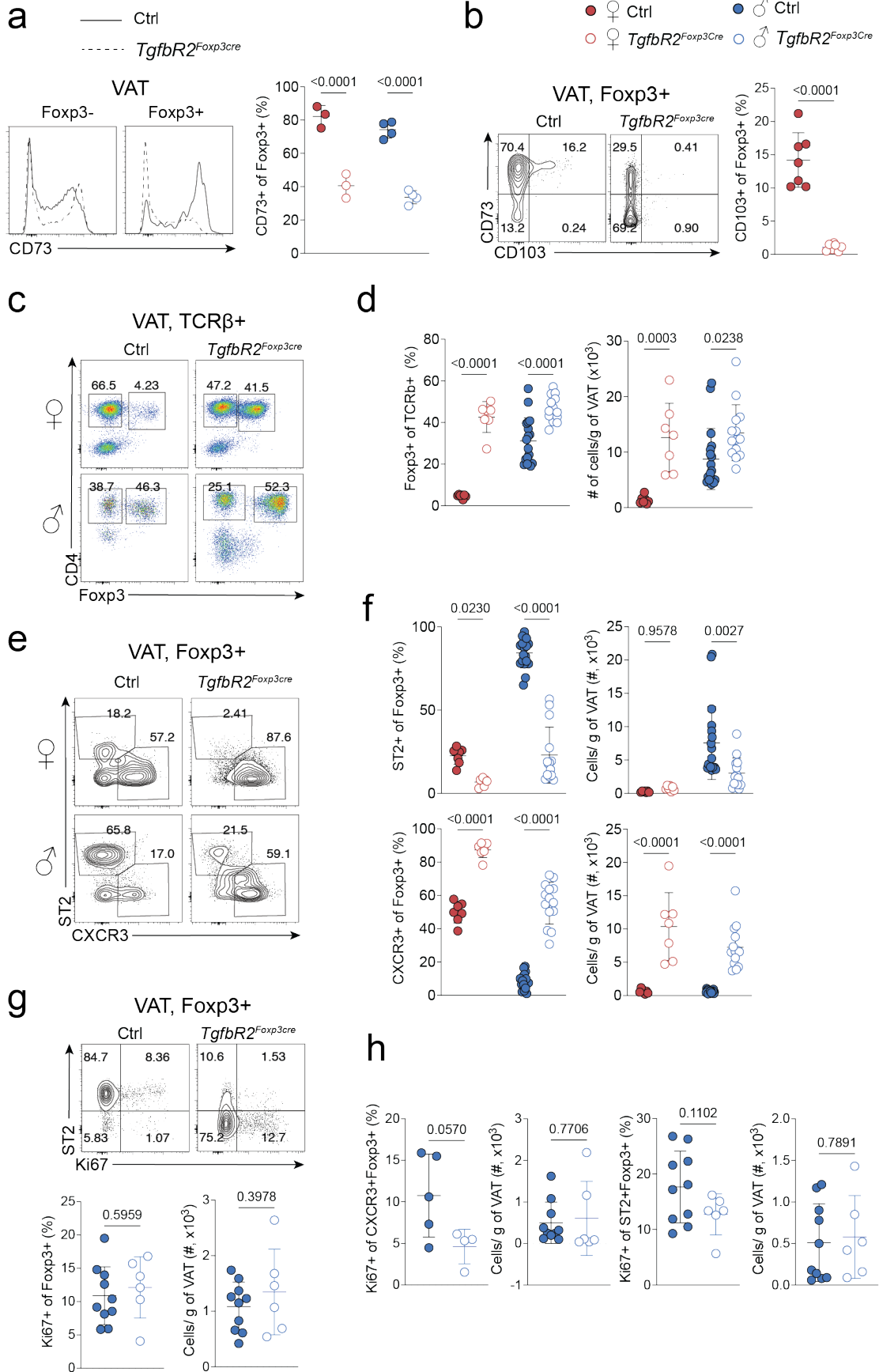


**Figure 34 | TGF $\beta$  promotes ST2+ but restrains the differentiation of CXCR3+ VAT Treg cells.** Analysis of VAT from 29-32-week-old male and female *Tgfbr2<sup>fl/fl</sup>Foxp3<sup>Cre</sup>*, wildtype (n=20) and *Foxp3<sup>Cre</sup>* (n=4) mice. **a**, Histograms displaying CD73 expression (left) and quantification of CD73 MFI (right) in Foxp3- and Foxp3+ in *Tgfbr2<sup>fl/fl</sup>Foxp3<sup>Cre</sup>* and control mice. **b**, Flow cytometry plots depicting CD73 against CD103 expression and quantification of CD103+ cells in VAT Treg cells of *Tgfbr2<sup>fl/fl</sup>Foxp3<sup>Cre</sup>* and control mice. **c, d**, Flow cytometry plots showing CD4 versus Foxp3 expression in TCR $\beta$ + cells (**c**) and quantification (**d**) of frequencies and numbers of total VAT Treg cells in *Tgfbr2<sup>fl/fl</sup>Foxp3<sup>Cre</sup>* and control mice. **e, f**, Flow cytometry plots showing ST2 versus CXCR3 expression (**e**) and quantification (**f**, frequencies top, numbers bottom) of ST2+ and CXCR3+ VAT Treg cells in *Tgfbr2<sup>fl/fl</sup>Foxp3<sup>Cre</sup>* and control mice. **g, h**, Flow cytometry plots showing ST2 versus Ki67 expression (**g**) and quantification of frequencies and numbers of Ki67+ cells among total (**g**), ST2+ and CXCR3+ (**h**) VAT Treg cells in male *Tgfbr2<sup>fl/fl</sup>Foxp3<sup>Cre</sup>* and control mice. Symbols represent individual mice; horizontal lines indicate means. Data are representative (**a-c, e, g**) or pooled (**b, d, f-h**) from a minimum of two independent experiments. Error bars indicate the standard deviation. Statistical analyses were performed using two-way ANOVA (**a, d, f**) or unpaired, two-tailed Student's *t*-test (**b, g, h**).

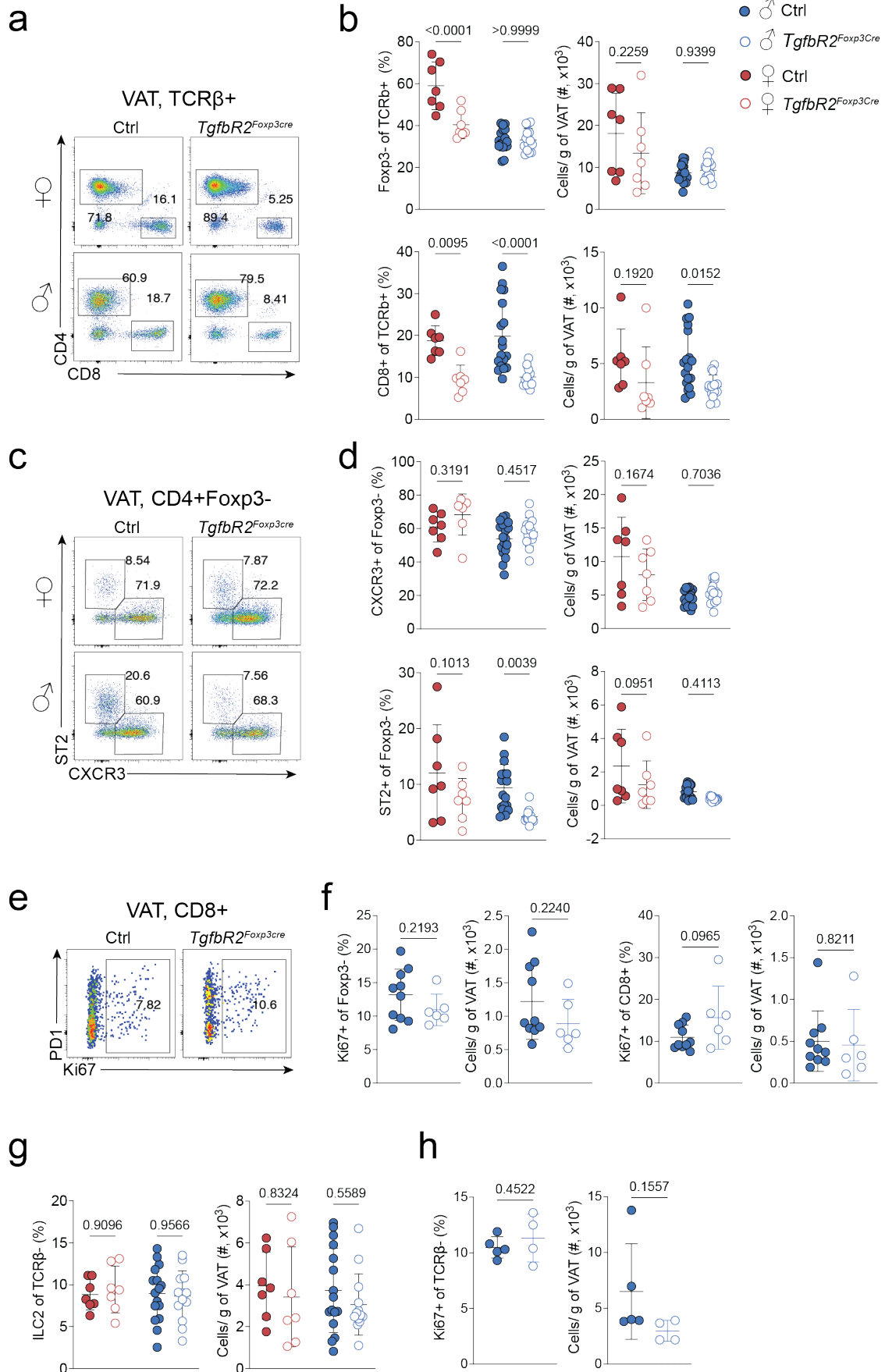


**Figure 35 | CD8+ T cells are significantly reduced in male *Tgfbr2<sup>fl/fl</sup>Foxp3<sup>Cre</sup>* mice.** Analysis of VAT from 29-32-week-old male and female *Tgfbr2<sup>fl/fl</sup>Foxp3<sup>Cre</sup>*, wildtype (n=20) and *Foxp3<sup>Cre</sup>* (n=4) mice. **a, b**, Flow cytometry plots showing CD4 versus CD8 expression in TCR $\beta$ + cells (**a**) and quantification (**b**) of frequencies and numbers of CD4+Foxp3- and CD8+ T cells in *Tgfbr2<sup>fl/fl</sup>Foxp3<sup>Cre</sup>* and control mice. **c, d**, Flow cytometry plots showing ST2 versus CXCR3 expression in CD4+Foxp3- cells (**c**) and quantification (**d**) of frequencies and numbers of ST2+ and CXCR3+ cells in *Tgfbr2<sup>fl/fl</sup>Foxp3<sup>Cre</sup>* and control mice. **e, f**, Flow cytometry plots showing PD1 versus Ki67 expression in CD8+ cells (**e**) and quantification (**f**) of frequencies and numbers of Ki67+ cells among CD4+Foxp3- and CD8+ cells in male *Tgfbr2<sup>fl/fl</sup>Foxp3<sup>Cre</sup>* and control mice. **g, h**, Quantification of frequencies and cell numbers of ILC2 (**g**) and Ki67+ cells (**h**) in TCR $\beta$ - cells. Symbols represent individual mice; horizontal lines indicate means. Data are representative (**a, c, e**) or pooled (**b, d, f-h**) from a minimum of two independent experiments. Error bars indicate the standard deviation. Statistical analyses were performed using two-way ANOVA (**b, d, g**) or unpaired, two-tailed Student's *t*-test (**f, h**).

## Chapter 5 – Interplay between VAT Treg cells and the VAT microenvironment

### 5.1 Cytokines and chemokines shape sex differences in the VAT

Local VAT inflammation has been linked to a metabolic disease, especially during obesity or conditions of nutritional excess (Hotamisligil et al., 1993; Xu et al., 2003). Recently, we have shown that VAT inflammatory parameters are different in male and female mice (Vasanthakumar et al., 2020). However, a deeper understanding of the steady state cytokine landscape in both males and females is still lacking.

To evaluate inflammation on a population level, VAT SVF from male and female C57BL/6 mice was stimulated with PMA/Ionomycin to quantify cytokine production via antibody staining. Expression of IL-5 and IL-13 in total immune cells (CD45+) did not show a significant difference between the sexes (**Figure 36a**). T cells (TCR $\beta$ +) however expressed higher levels of IL-13 in female mice compared to males (**Figure 36b**). IL-5 expression on the other hand was not different between males and females. In contrast, type 1 inflammatory cytokines such as IFN- $\gamma$  and TNF were increased in T cells of female mice compared to males (**Figure 36a, b**). However, expression of the above cytokines in T cells was indistinguishable between female and male mice. Due to its involvement in fibrosis and tissue repair, we also assessed IL-17 expression in the VAT of male and female mice by staining for its subunit IL-17A. However, IL-17A+ cell proportion and numbers were similar between male and female mice in T cells (**Figure 36a, b**). Analysis of IFN- $\gamma$  and TNF production in TCR $\beta$ - cells showed no major difference between both sexes, although male mice had slightly more TNF-producing cells than female mice (**Figure 36c**). Furthermore, IFN- $\gamma$  MFI was higher in TCR $\beta$ + and TCR $\beta$ - cells in female mice while TNF MFI was only higher in TCR $\beta$ + cells compared to males (**Figure 36d**). IL5, IL13 and IL17A levels were significantly higher in male mice compared to female mice in TCR $\beta$ - cells. Yet the number of cells producing these cytokines was also similar in both sexes (**Figure 36c**). IL17A production, however, was both proportionally and numerically higher in TCR $\beta$ - cells of male mice compared to female mice (**Figure 36c**). Analysis of,

*Ifng*<sup>eYFP</sup> reporter mice could confirm the results stated above. Overall, female VAT contained more cells expressing *Ifng*<sup>eYFP</sup> that also expressed a higher amount of *Ifng* transcripts per cell as measured by MFI (**Figure 36e-g**).

Taken together, cytokine measurements showed increased expression of type 1 inflammatory cytokines in VAT TCR $\beta$ <sup>+</sup> cells of female mice, while elevated levels of IL-5, IL-13 and IL-17A were measured in TCR $\beta$ <sup>-</sup> cells of male mice.

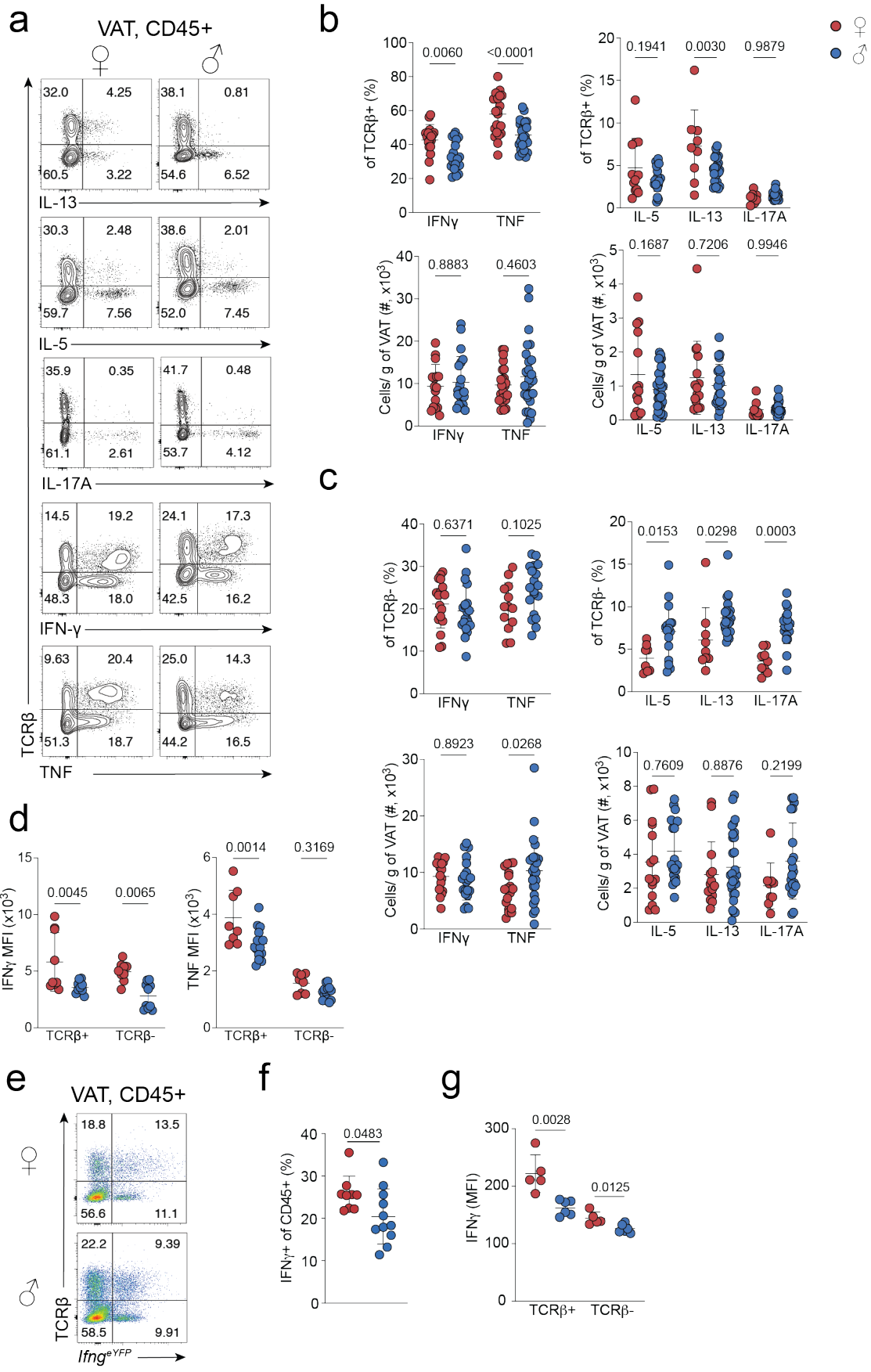


**Figure 36 | T<sub>H</sub>1 and T<sub>H</sub>2 type cytokines are differentially expressed in male and female mice.** **a-d**, VAT SVF from 25-30-week-old female and male WT mice was restimulated with PMA/Ionomycin for 4 hours to measure cellular cytokine production. **a-c**, Flow cytometric plots displaying TCR $\beta$  versus IL-13, IL-5, IL17A, IFN- $\gamma$  and TNF expression (**a**) in CD45<sup>+</sup> cells and quantification of frequencies (top) and cell numbers (bottom) of cytokine producing cells in TCR $\beta$ <sup>+</sup> (**b**) and TCR $\beta$ <sup>-</sup> (**c**) cells in male and female mice. **d**, Quantification of IFN- $\gamma$  and TNF MFI in TCR $\beta$ <sup>+</sup> and TCR $\beta$ <sup>-</sup> cells. **e-g**, VAT SVF from 25-30-week-old female and male *Ifng*<sup>eYFP</sup> mice was restimulated with PMA/Ionomycin for 4 hours to measure cellular cytokine production. **e, f**, FACS plots displaying TCR $\beta$  versus *Ifng*<sup>eYFP</sup> expression (**e**) and quantification (**f**) of IFN- $\gamma$ <sup>+</sup> cells in CD45<sup>+</sup> in female and male mice. **g**, Quantification of *Ifng*<sup>eYFP</sup> MFI in TCR $\beta$ <sup>+</sup> and TCR $\beta$ <sup>-</sup> cells. Symbols represent individual mice; horizontal lines indicate means. Data are representative (**a, e**) or pooled (**b-d, f, g**) from a minimum of two independent experiments. Error bars indicate the standard deviation. Statistical analyses were performed using two-way ANOVA.

Considering the increased IFN- $\gamma$  levels in female adult mice, it was conceivable that the observed sexual dichotomy in CXCR3<sup>+</sup> VAT Treg cells was at least partially driven by IFN- $\gamma$ . Thus, the cytokine milieu in younger mice (7 weeks) was measured, considering the sex-specific difference in ST2<sup>+</sup> and CXCR3<sup>+</sup> VAT Treg cells is not observable at that age (see **Figure 7**). Results showed that proportion and amount of IFN- $\gamma$  and TNF-producing T cells was higher in male mice compared to female mice, which contrasted the phenotype in older mice (**Figure 37a, b**). No significant differences in the proportions or numbers of IL-5, IL-13 and IL-17A<sup>+</sup> cells were observed. Further analysis showed that IFN- $\gamma$ , TNF, IL5 and IL13 production was similar in TCR $\beta$ <sup>-</sup> cells of male and female mice (**Figure 37c**). However, as seen in older mice, the proportion and number of IL17A-producing cells was substantially higher in male mice compared to female mice.

Hence, the results showed that IFN- $\gamma$  expression aligns with CXCR3<sup>+</sup> VAT Treg cell proportions. However, analyses at more timepoints are required, to establish a firm correlation between IFN- $\gamma$  expression levels and CXCR3<sup>+</sup> VAT Treg cell proportions.

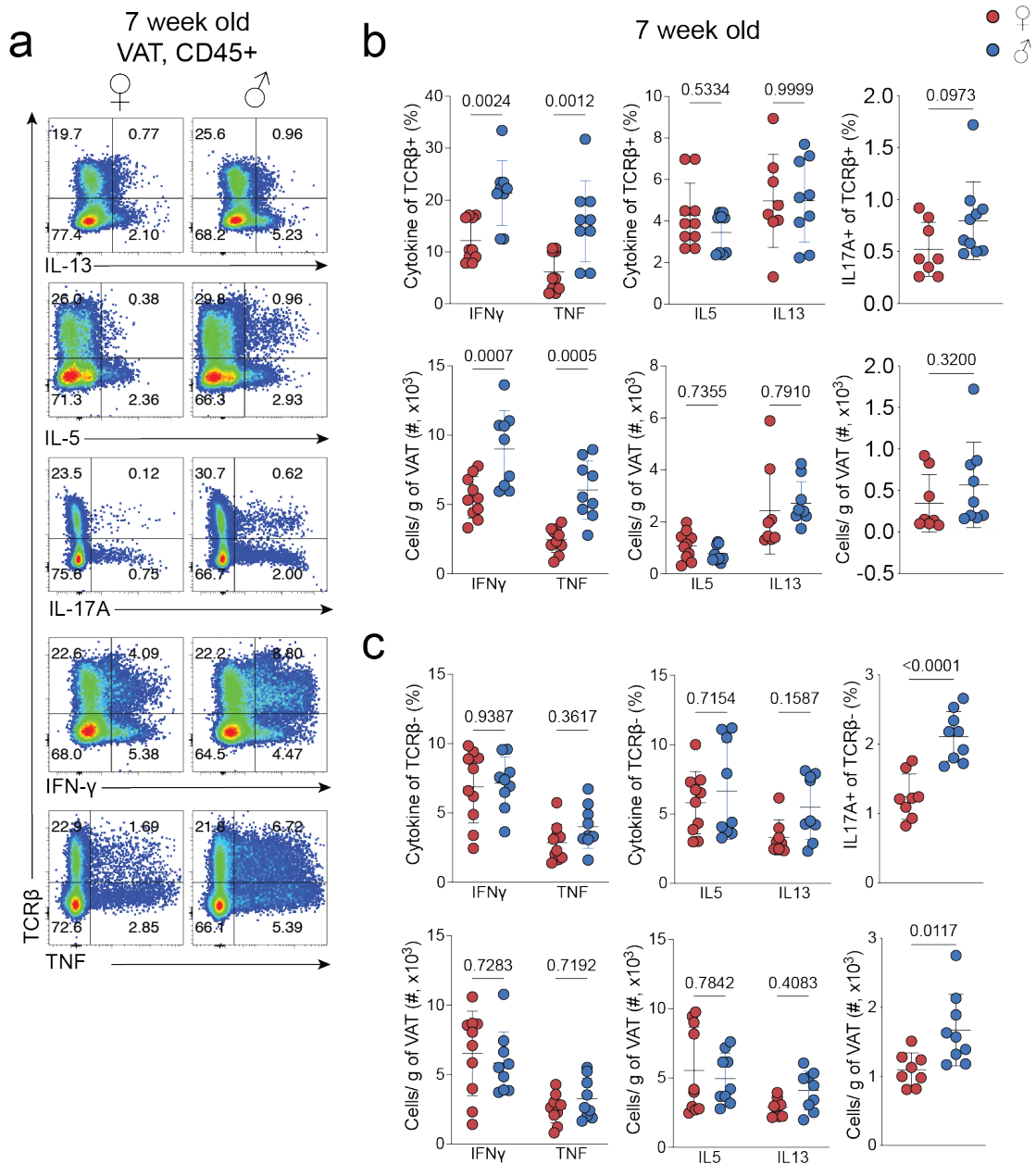


**Figure 37 | Cytokine production in young adult mice is different from mature mice.** VAT SVF from 7-week-old female and male WT mice was restimulated with PMA/Ionomycin for 4 hours to measure cellular cytokine production. Flow cytometric plots displaying TCR $\beta$  versus IL-13, IL-5, IL17A, IFN- $\gamma$  and TNF expression (**a**) in CD45+ cells and quantification of frequencies (top) and cell numbers (bottom) of cytokine producing cells in TCR $\beta$ + (**b**) and TCR $\beta$ - (**c**) cells in male and female mice. Symbols represent individual mice; horizontal lines indicate means. Data are representative (**a**) or pooled (**b**, **c**) from a minimum of two independent experiments. Error bars indicate the standard deviation. Statistical analyses were performed using two-way ANOVA.

IFN- $\gamma$  could provide important signals for CXCR3<sup>+</sup> VAT Treg cell differentiation yet no migratory cues. Therefore, REX3 mice with *Cxcl9*<sup>RFP</sup> and *Cxcl10*<sup>BFP</sup> modifications were analysed that report for RNA expression of the CXCR3 ligands, CXCL9 and CXCL10, respectively (Groom et al., 2012). Through flow cytometric analysis RFP<sup>+</sup> (CXCL9<sup>+</sup>) and BFP (CXCL10<sup>+</sup>) cells were detected in the VAT. Analysis showed that proportions and numbers of CXCL10 expressing CD45<sup>+</sup> cells were higher in female mice compared to male mice (**Figure 38a, b**). Levels of CXCL9<sup>+</sup> cells were also higher in female mice compared to male (**Figure 38c, d**). Interestingly, CXCL9 was co-expressed with CXCL10 in all measured samples. To determine the source of chemokine expression in T cells and innate immune cells we employed the gating strategy shown in **Figure 38e**. FACS analysis revealed that a large proportion for CXCL10 originates from macrophages (M $\Phi$ ) whose contribution is higher in male mice compared to female mice. (**Figure 38f**). Furthermore, CXCL10 expression was measurable in B and NK cells at low levels, while the majority of T cell generated CXCL10 was from CD4<sup>+</sup> T cells (**Figure 38f**). The majority of RFP (CXCL9) signal was derived from M $\Phi$  and DCs and could not be detected in other cell types. Overall, our results show significant differences in IFN- $\gamma$  and CXCR3 ligand production that potentially affects VAT Treg cell composition and ultimately local inflammation, adipocyte and immune cell composition and function.

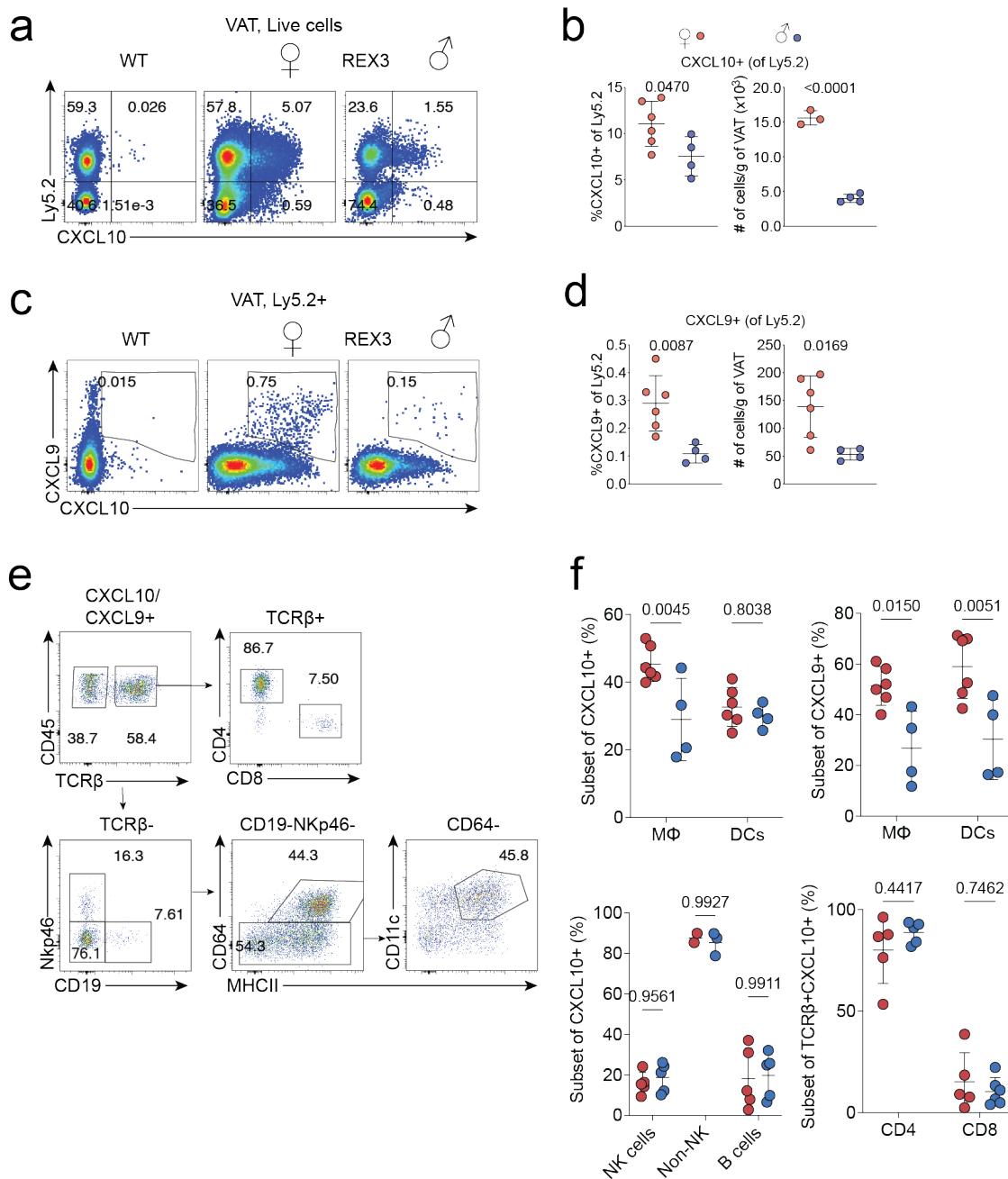


**Figure 38 | CXCR3 ligands CXCL9 and CXCL10 production is higher in female mice compared to male mice.** VAT SVF from 25-30-week-old female and male REX3 mice was restimulated with PMA/Ionomycin for 4 hours to measure cellular cytokine production. **a, b**, Flow cytometry plots displaying CD45 against CXCL0 expression (**a**) in Live cells and quantification (**b**) of frequencies and numbers of CXCL10+ cells in female and male mice. **c, d**, Flow cytometry plots displaying CXCL9 against CXCL0 expression (**c**) in CD45+ cells and quantification (**d**) of frequencies and numbers of CXCL9+ cells in female and male mice. **e**, Gating strategy to identify different cell subsets producing CXCL10. **f**, Frequencies of macrophages (M $\Phi$ ), DCs, NK cells, B cells, CD4+, CD8+ T cells among CXCL10 and CXCL9 producing cells in male and female mice. Symbols represent individual mice; horizontal lines indicate means. Data are

representative (**a, c, e**) or pooled (**b, d, f**) from a minimum of two independent experiments. Error bars indicate the standard deviation. Statistical analyses were performed using two-way ANOVA (**f**) or unpaired, two-tailed Student's *t*-test (**b, d**).

## 5.2 IFN- $\gamma$ deficiency leads to ST2+ VAT Treg cell expansion and T cell infiltration

Considering the differences in IFN- $\gamma$  production between male and female mice, experiments were conducted to investigate VAT immune cells in mice lacking IFN- $\gamma$ . Therefore, the VAT of female and male *Ifng*<sup>-/-</sup> and control mice was analysed. Analysis of the total VAT Treg cell population showed no difference between *Ifng*<sup>-/-</sup> and control mice of both sexes (**Figure 39a, b**). More detailed analysis showed an increased proportions of ST2+ VAT Treg cells in male and female mice. However, only female mice had more ST2+ Treg cells per g of VAT (**Figure 39c, d**). In contrast, CXCR3+ VAT Treg cells were significantly reduced in proportion and numbers in male and female mice. Furthermore, GATA3 expression, which is important for ST2+ VAT Treg cells, was altered in absence of IFN- $\gamma$ . Measurements of GATA3 MFI in DN, ST2+ and CXCR3+ VAT Treg cells showed enhanced GATA3 expression levels in ST2+ cells of male *Ifng*<sup>-/-</sup> mice when compared to controls. All other comparisons did not reveal any differences (**Figure 39e**).

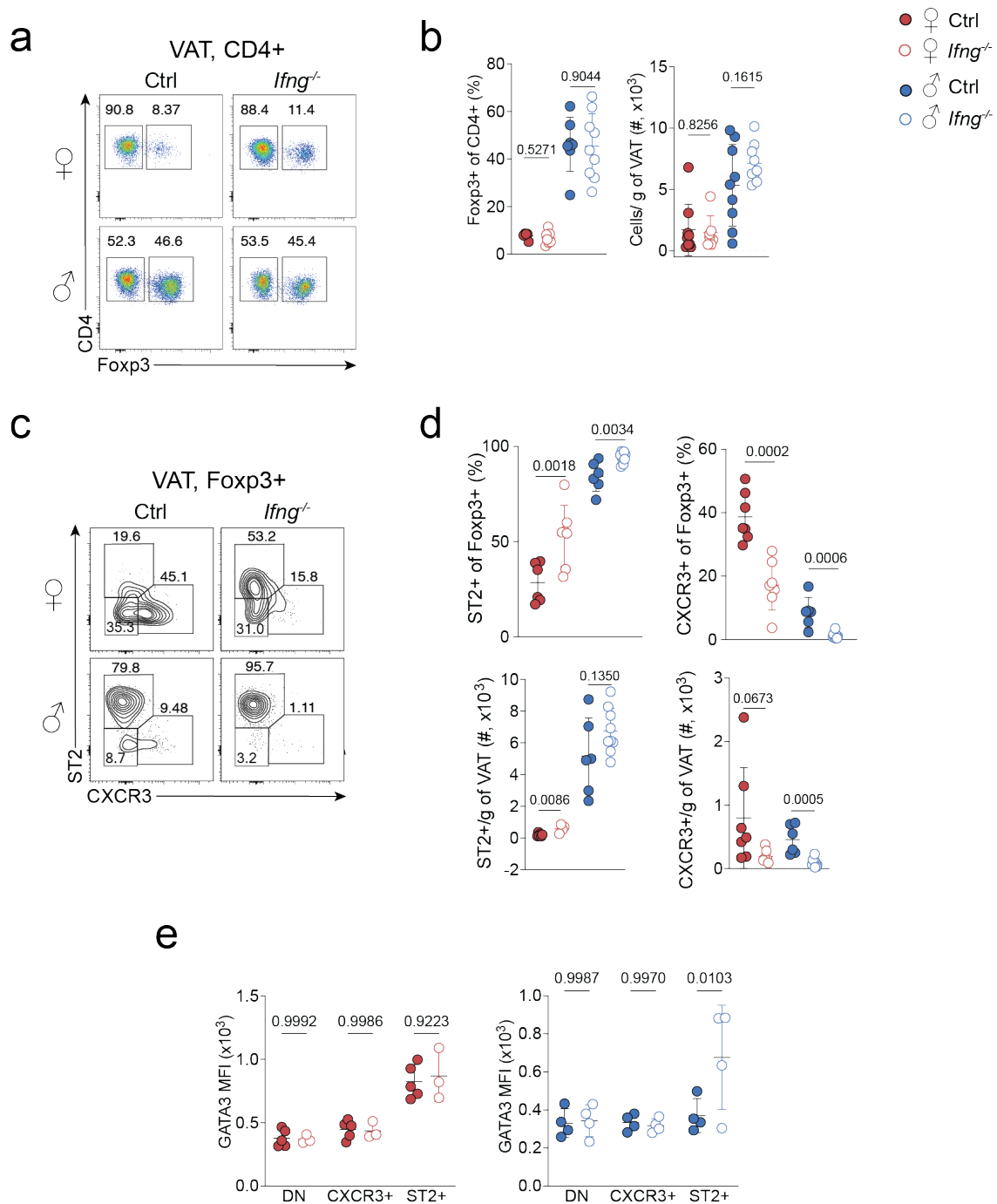


**Figure 39 | IFN- $\gamma$  depletion induces expansion of ST2+ VAT Treg cells in female and male mice.** VAT from 27–32-week-old *Ifng*<sup>-/-</sup> and WT mice were analysed and compared. **a, b**, Flow cytometry plots showing CD4 versus Fopx3 expression (**a**) and quantification (**b**) of frequencies and numbers of total VAT Treg cells in *Ifng*<sup>-/-</sup> and control mice. **c, d**, Flow cytometry plots showing ST2 versus CXCR3 expression (**c**) and quantification (**d**) of frequencies and numbers of ST2+ and CXCR3+ VAT Treg cells in *Ifng*<sup>-/-</sup> and control mice. **e**, Quantification of GATA3 MFI in VAT Treg cells in *Ifng*<sup>-/-</sup> and control mice. Symbols represent individual mice; horizontal lines indicate means. Data are representative (**a, c**) or pooled (**b, d, e**) from a minimum of two independent experiments. Error bars

indicate the standard deviation. Statistical analyses were performed using two-way ANOVA.

Considering IFN- $\gamma$  contributes to T<sub>H</sub>1 cell fate, T cell numbers and phenotype were assessed in IFN- $\gamma$ -sufficient and -deficient mice. No differences in numbers of CD45<sup>+</sup> or TCR $\beta$ <sup>+</sup> cells in *Ifng*<sup>-/-</sup> mice of either sex compared to their controls was observed (**Figure 40a**). More detailed analysis of the T cell compartment showed that female IFN- $\gamma$ -deficient mice had increased proportion but not numbers of Tconv cells while no difference was detected in male mice (**Figure 40b, c**). In contrast, the CD8<sup>+</sup> T cell compartment was significantly reduced in *Ifng*<sup>-/-</sup> mice compared to their controls in either sex. However, this difference was only discernible in percentages and not numerically (**Figure 40b, c**). Further analysis of the Tconv compartment was conducted. CXCR3 expression was reduced in male *Ifng*<sup>-/-</sup> mice although being similar in numbers (**Figure 40d, e**). Additionally, the results showed an expansion of ST2<sup>+</sup>Tconv cells in both sexes in absence of IFN- $\gamma$  (**Figure 40d, e**). Apart from T cells, ILC2 were also analysed in IFN- $\gamma$ -deficient mice but no substantial difference between *Ifng*<sup>-/-</sup> and control mice of both sexes were detected (**Figure 40f**).

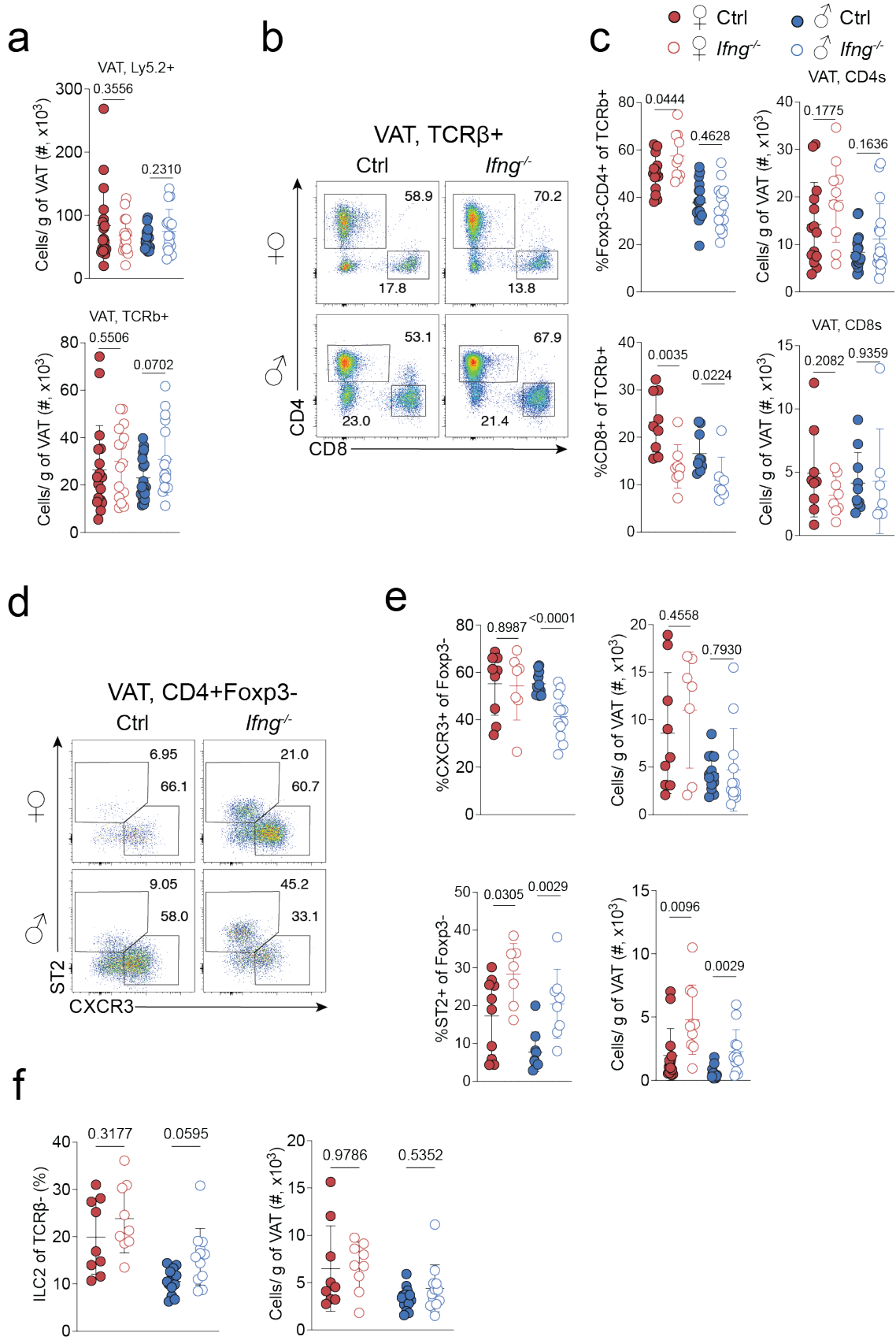


**Figure 40 | ST2+Foxp3<sup>-</sup> cells expand in absence of IFN- $\gamma$  in both sexes.** VAT from 27–32-week-old *Ifng*<sup>-/-</sup> and WT mice were analysed and compared. **a**, Quantification of CD45<sup>+</sup> (top) and TCR $\beta$ <sup>+</sup> (bottom) cell numbers in *Ifng*<sup>-/-</sup> and control mice. **b, c**, Flow cytometry plots showing CD4 versus CD8 expression in TCR $\beta$ <sup>+</sup> cells (**b**) and quantification (**c**) of frequencies and numbers of CD4+Foxp3<sup>-</sup> and CD8<sup>+</sup> T cells in *Ifng*<sup>-/-</sup> and control mice. **d, e**, Flow cytometry plots showing ST2 versus CXCR3 expression in CD4+Foxp3<sup>-</sup> cells (**d**) and quantification (**e**) of frequencies and numbers of ST2<sup>+</sup> and CXCR3<sup>+</sup> cells in *Ifng*<sup>-/-</sup> and control mice. **f**, Quantification of frequencies and cell numbers of ILC2. Symbols represent individual mice; horizontal lines indicate means. Data are representative (**b, d**) or pooled (**a, c, e, f**) from a minimum of two independent experiments. Error bars indicate the standard deviation. Statistical analyses were performed using two-way ANOVA.

Next, the cytokine milieu in *Ifng*<sup>-/-</sup> mice was compared to controls. First, global absence of IFN- $\gamma$  was confirmed. In IFN- $\gamma$  depleted mice, IL-5 expression was enhanced, specifically in T cells when compared to IFN- $\gamma$ -sufficient female and male mice (**Figure 41a-c**). This was not only in proportion but also in numbers. In contrast, IL5 expression was similar in TCR $\beta$ <sup>-</sup> cells of *Ifng*<sup>-/-</sup> and control mice. IL5 expression in CD4+Foxp3<sup>-</sup> T cells was elevated in *Ifng*<sup>-/-</sup> mice compared to controls, both in proportion and in numbers. TNF expression was not different in *Ifng*<sup>-/-</sup> mice compared to control in TCR $\beta$ <sup>+</sup> or TCR $\beta$ <sup>-</sup> cells of either sex (**Figure 41a-c**). However, further analysis revealed that TNF expression was proportionally higher in CD8<sup>+</sup> but not CD4<sup>+</sup> T cells in absence of IFN- $\gamma$  (**Figure 41d, e**).

Taken together, our results show that absence of IFN- $\gamma$  induces ST2 expression in Foxp3<sup>+</sup> and Foxp3<sup>-</sup> VAT T cells and is accompanied by elevated IL5 expression.

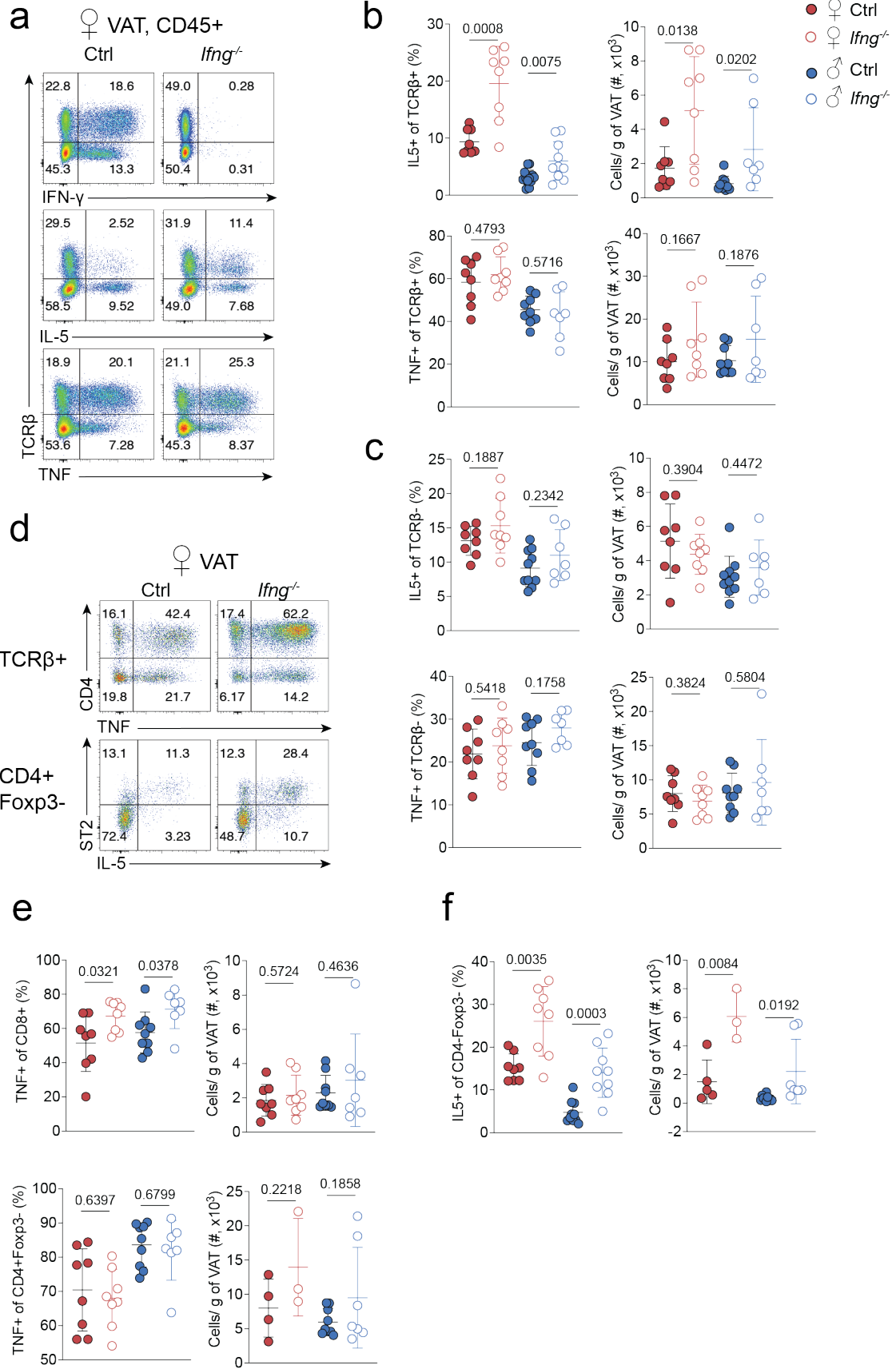


**Figure 41 | IL-5 production is significantly enhanced in *Ifng*<sup>-/-</sup> mice.** VAT from 27–32-week-old *Ifng*<sup>-/-</sup> and WT mice were analysed and compared. **a-c**, Flow cytometric plots displaying TCR $\beta$  versus IL-5, IFN- $\gamma$  and TNF expression (**a**) in CD45<sup>+</sup> cells and quantification of frequencies (top) and cell numbers (bottom) of cytokine producing cells in TCR $\beta$ <sup>+</sup> (**b**) and TCR $\beta$ <sup>-</sup> (**c**) cells in male and female mice. **d**, Flow cytometric plots displaying TCR $\beta$  versus TNF and ST2 versus IL-5 in TCR $\beta$ <sup>+</sup> and CD4<sup>+</sup>Foxp3<sup>-</sup> cells, respectively. **e, f**, Quantification of frequencies and cell numbers of TNF (**e**) and IL-5 (**f**) producing cells among CD4<sup>+</sup>Foxp3<sup>-</sup> and CD8<sup>+</sup> T cells. Symbols represent individual mice; horizontal lines indicate means. Data are representative (**a, d**) or pooled (**b, c, e, f**) from a minimum of two independent experiments. Error bars indicate the standard deviation. Statistical analyses were performed using two-way ANOVA.

### 5.3 IFN $\alpha$ R2 deficiency induces minor changes in VAT T cell composition

Like IFN- $\gamma$ , type I interferons promote T<sub>H</sub>1 polarization while inhibiting type 2 immunity. Furthermore, recent reports have shown the involvement of type I interferon signalling in adipose biology (C. Li, G. Wang, et al., 2021). Therefore, mice that lack IFN $\alpha$ R2, a receptor subunit required for type I interferon signalling, were analysed. Flow cytometric analysis of male *Ifnar2*<sup>-/-</sup> and control mice showed no significant difference in VAT Treg cell proportions but increased numbers (**Figure 42a, b**). Furthermore, the proportions of DN, ST2<sup>+</sup> and CXCR3<sup>+</sup> VAT Treg cells were indistinguishable between *Ifnar2*<sup>-/-</sup> and control mice. Only the amount of ST2<sup>+</sup> VAT Treg cells was increased in IFN $\alpha$ R2-deficient mice (**Figure 42c, d**). Phenotypic analysis of VAT Treg also showed no significant difference in CD73 or GATA3 expression between *Ifnar2*<sup>-/-</sup> and control mice (**Figure 42e**).

Further analysis of the T cell compartment showed that CD8<sup>+</sup> cells were proportionally lower in VAT of *Ifnar2*<sup>-/-</sup> male mice when compared to controls (**Figure 43a, b**). While the overall Tconv cells population was not affected by a lack of IFN $\alpha$ R2, CXCR3<sup>+</sup> cells were proportionally reduced while ST2<sup>+</sup> cells were elevated in *Ifnar2*<sup>-/-</sup> males compared to controls (**Figure 43b-d**). Analysis of TCR $\beta$ <sup>-</sup> cells further showed that ILC2 populations were similar in *Ifnar2*<sup>-/-</sup> males compared to controls (**Figure 43e**).

Overall, our results show that ablation of IFN $\alpha$ R2 affects CXCR3 expression in Tconv cells yet has little impact on VAT Treg cell composition in male mice.

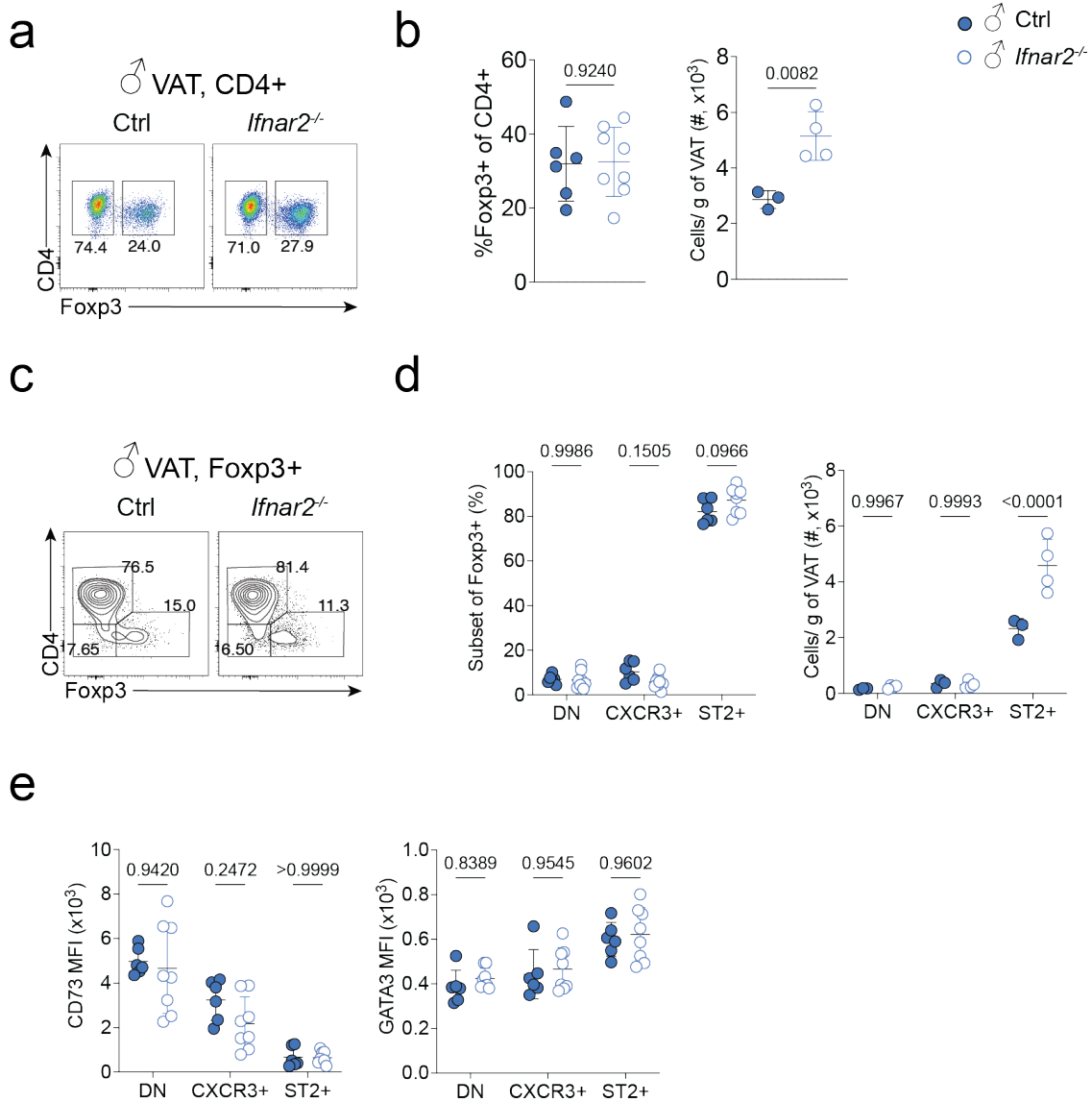


**Figure 42 | VAT Treg cell numbers are increased in *Ifnar2*<sup>-/-</sup> male mice.** VAT from 30–35-week-old *Ifnar2*<sup>-/-</sup> and WT mice were analysed and compared. **a, b**, Flow cytometry plots showing CD4 versus Foxp3 expression (**a**) and quantification (**b**) of frequencies and numbers of total VAT Treg cells in *Ifnar2*<sup>-/-</sup> and control mice. **c, d**, Flow cytometry plots showing ST2 versus CXCR3 expression (**c**) and quantification (**d**) of frequencies and numbers of DN, ST2<sup>+</sup> and CXCR3<sup>+</sup> VAT Treg cells in *Ifnar2*<sup>-/-</sup> and control mice. **e**, Quantification of CD73 and GATA3 MFI in DN, ST2<sup>+</sup> and CXCR3<sup>+</sup> VAT Treg cells of *Ifnar2*<sup>-/-</sup> and control mice. Symbols represent individual mice; horizontal lines indicate means. Data are representative (**a, c**) or pooled (**b, d, e**) from a minimum of two independent experiments. Error bars indicate the standard deviation. Statistical

analyses were performed using two-way ANOVA (b) or unpaired, two-tailed Student's *t*-test (d, e).

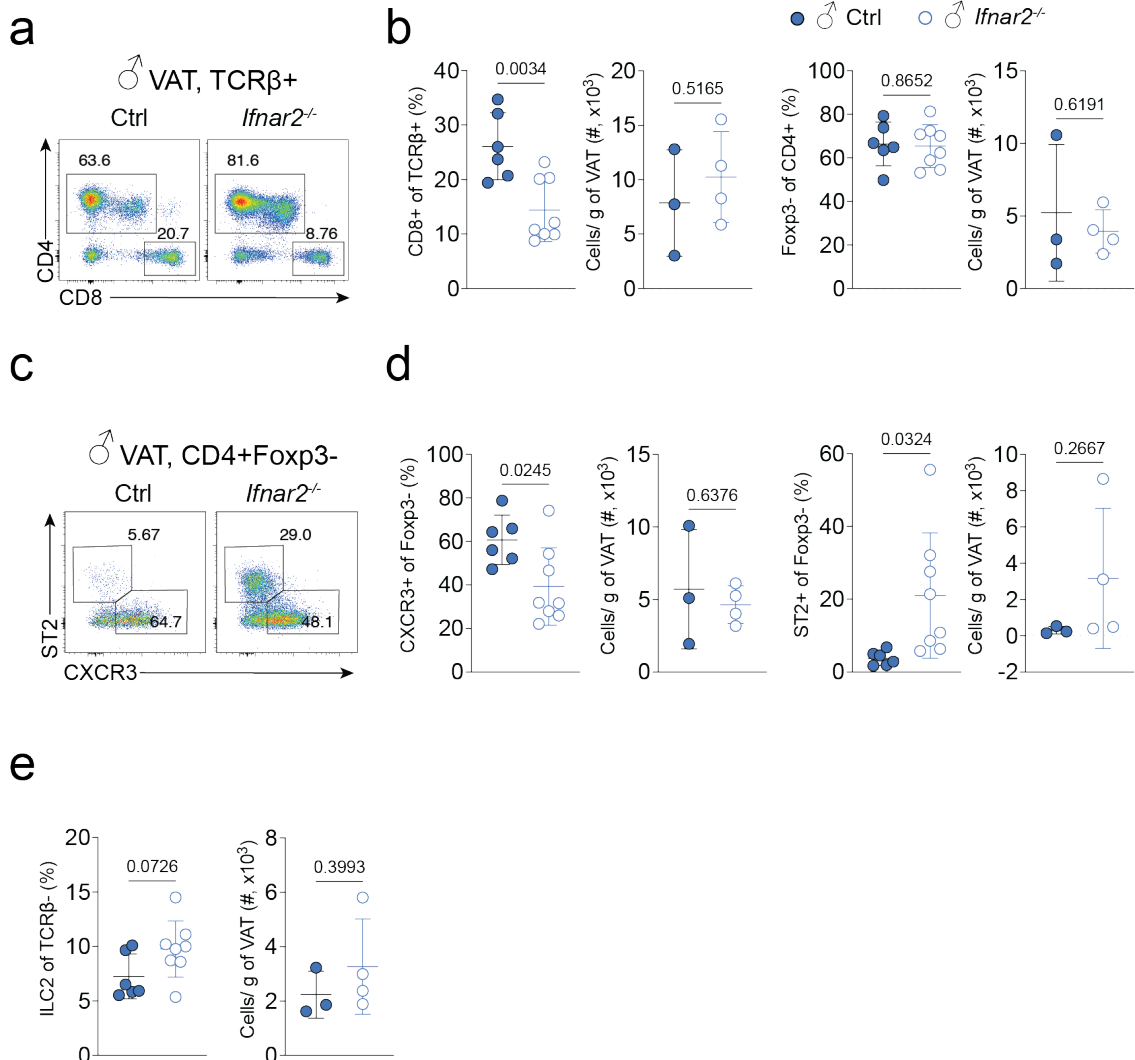


**Figure 43 | IFN $\alpha$ R2 ablation leads to the reduction of CD8<sup>+</sup> and CXCR3<sup>+</sup>Foxp3<sup>-</sup> VAT cells.** VAT from 30–35-week-old *Ifnar2*<sup>-/-</sup> and WT mice were analysed and compared. **a, b**, Flow cytometry plots showing CD4 versus CD8 expression in TCRβ<sup>+</sup> cells (**a**) and quantification (**b**) of frequencies and numbers of CD4<sup>+</sup>Foxp3<sup>-</sup> and CD8<sup>+</sup> T cells in *Ifng*<sup>-/-</sup> and control mice. **c, d**, Flow cytometry plots showing ST2 versus CXCR3 expression in CD4<sup>+</sup>Foxp3<sup>-</sup> cells (**c**) and quantification (**d**) of frequencies and numbers of ST2<sup>+</sup> and CXCR3<sup>+</sup> cells in *Ifng*<sup>-/-</sup> and control mice. **e**, Quantification of frequencies and cell numbers of ILC2. Symbols represent individual mice; horizontal lines indicate means. Data are representative (**a, c**) or pooled (**b, d, e**) from a minimum of two independent experiments. Error bars indicate the standard deviation. Statistical analyses were performed using unpaired, two-tailed Student's *t*-test.

#### 5.4 IL-33 shapes both, ST2<sup>+</sup> and CXCR3<sup>+</sup> VAT Treg cells and regulates CD8<sup>+</sup> T cell infiltration

Several studies have shown the importance of IL-33 in T<sub>H</sub>2 immunity and VAT Treg cell biology (Han et al., 2015; Mathis, 2016; Vasanthakumar et al., 2020; Ajithkumar Vasanthakumar et al., 2015). Hence, we explored how ablation of ST2, and IL-33 affects VAT immunity in female and male mice. As shown in a previous publication from our lab, the proportion of gp38<sup>+</sup> stromal cells that expressed IL-33 was higher in male mice compared to female mice (**Figure 44a**). Further analysis also showed that VAT Treg cells are significantly diminished in male mice of both *Il1r1*<sup>-/-</sup> and *Il33*<sup>-/-</sup> mice, which is in line with previous reports (**Figure 44b**). ST2<sup>+</sup> VAT Treg cells were reduced compared to control, in both ST2<sup>-</sup> and IL33-deficient female and male mice (**Figure 44c, d**). Numerically, however, this was only significant in male mice. In contrast, CXCR3<sup>+</sup> VAT Treg cells expanded in absence of IL-33 signalling in both sexes. This was especially evident in female *Il33*<sup>-/-</sup> mice where higher numbers of CXCR3<sup>+</sup> cells were observed compared to controls (**Figure 44d**). To test whether the increased CXCR3<sup>+</sup> Treg cell population was due to infiltration or proliferation, Ki67 expression in VAT Treg cells was assessed. The results show that Ki67<sup>+</sup> expression was increased within the total Treg cell population of both sexes that lacked either ST2 or IL-33 (**Figure 44e, f**).

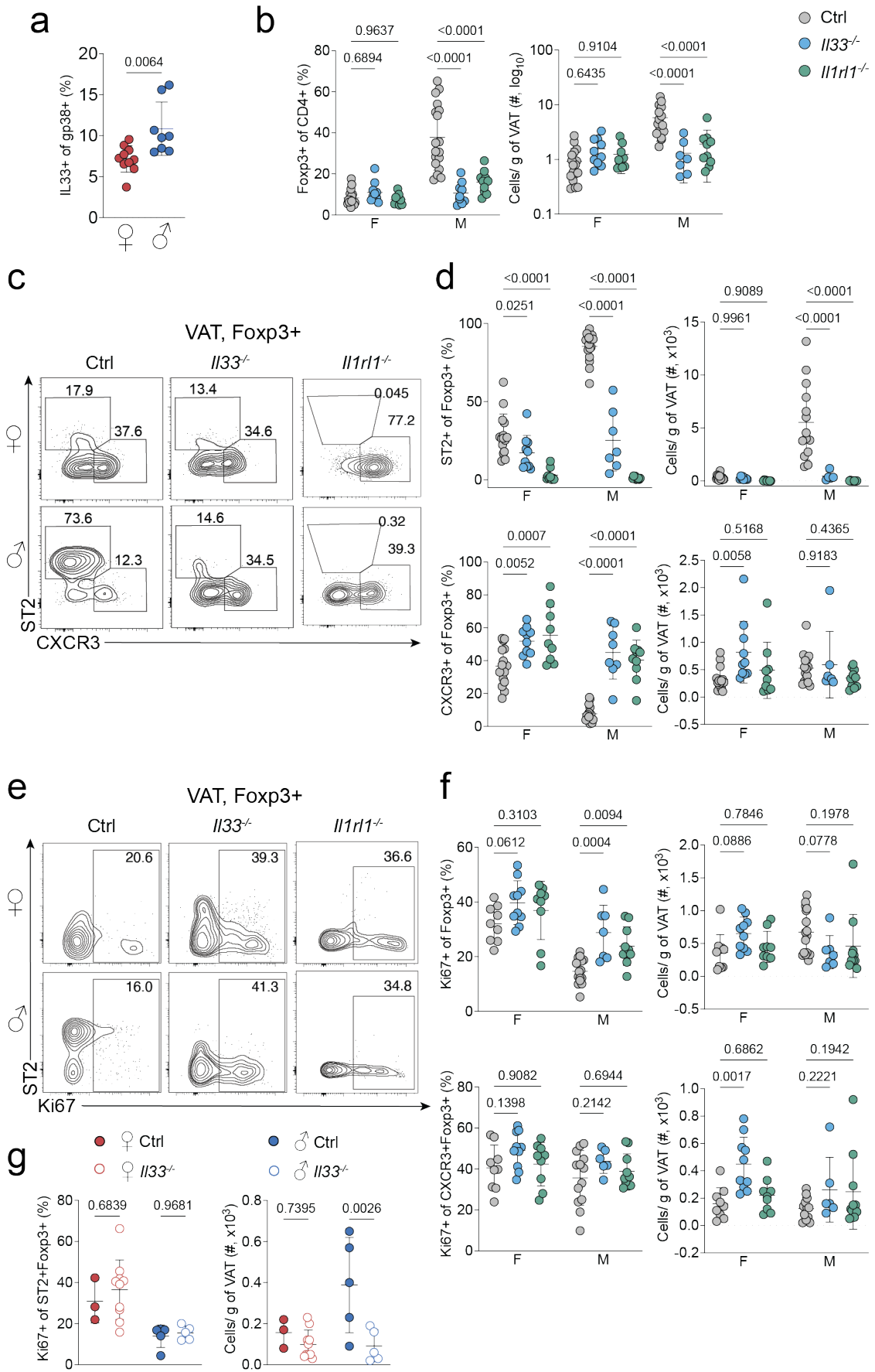
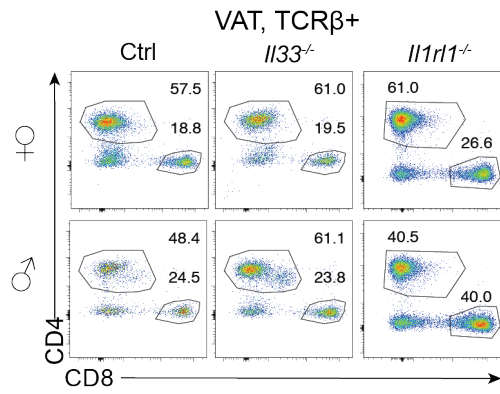


**Figure 44 | IL-33 signalling promotes ST2+ and inhibits CXCR3+ VAT Treg cell differentiation.** **a**, Frequencies of IL-33 producing cells among gp38+ MSCs. **b-g**, VAT from 27–33-week-old *Il33*<sup>-/-</sup>, *Il1rl1*<sup>-/-</sup> and WT mice were analysed and compared. **b**, Quantification of frequencies and numbers of total VAT Treg cells in *Il33*<sup>-/-</sup>, *Il1rl1*<sup>-/-</sup> and WT mice. **c, d**, Flow cytometry plots showing ST2 versus CXCR3 expression (**c**) and quantification (**d**) of frequencies and numbers of ST2+ and CXCR3+ VAT Treg cells in *Il33*<sup>-/-</sup>, *Il1rl1*<sup>-/-</sup> and WT mice. **e-g**, Flow cytometry plots showing ST2 versus Ki67 expression in CD4+Foxp3<sup>-</sup> cells (**e**) and quantification of frequencies and numbers of total, CXCR3+ (**f**) and ST2+ (**g**) cells in *Il33*<sup>-/-</sup>, *Il1rl1*<sup>-/-</sup> and WT mice. Symbols represent individual mice; horizontal lines indicate means. Data are representative (**c, e**) or pooled (**a, b, d, f, g**) from a minimum of two independent experiments. Error bars indicate the standard deviation. Statistical analyses were performed using two-way ANOVA (**b, d, f, g**) or unpaired, two-tailed Student's *t*-test (**a**).

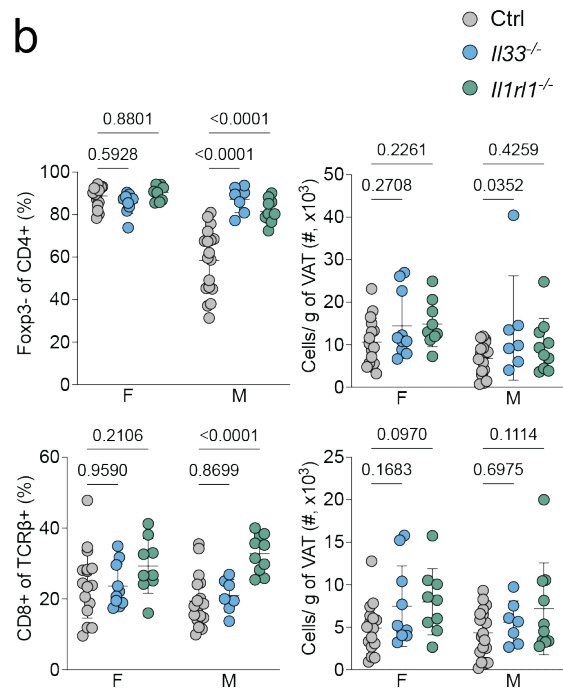
Next, we investigated how lack of IL-33 or ST2 impacts T cell infiltration or phenotype. In females there was no significant difference in proportion or numbers of CD4+Foxp3<sup>-</sup> or CD8<sup>+</sup> T cells of IL-33<sup>-</sup> and ST2-deficient mice compared to controls (**Figure 45a, b**). In contrast, increased proportions of CD8<sup>+</sup> and CD4<sup>+</sup> T cells were detected in male mice, especially in the absence of ST2. While numbers of CD4 T cells were also increased in the absence of IL-33 signalling, numbers of CD8<sup>+</sup> T cells were similar across all comparisons. In females and males, there were higher proportions of CXCR3+CD4+Foxp3<sup>-</sup> T cells in *Il33*<sup>-/-</sup> and *Il1rl1*<sup>-/-</sup> mice, respectively (**Figure 45c, d**). In cell numbers, this made however no difference. Furthermore, the percentage and numbers of Ki67 expressing cells among Foxp3<sup>-</sup> cells was enhanced in *Il33*<sup>-/-</sup> mice compared to controls in both sexes while ablation of ST2 did not have an impact. Furthermore, ILC2 populations were significantly reduced in absence of IL-33 or ST2 in both sexes, although a much stronger phenotype was observed in *Il1rl1*<sup>-/-</sup> mice when compared to controls (**Figure 45e**). However, the proportion of Ki67<sup>+</sup> cells in the TCRβ<sup>-</sup> population was elevated in female but not in male mice in both knockout models.

In summary, IL-33 signalling is crucial for ST2+ VAT Treg cell formation, inhibition of CXCR3+ VAT Treg cells and affects T cell infiltration and proliferation.

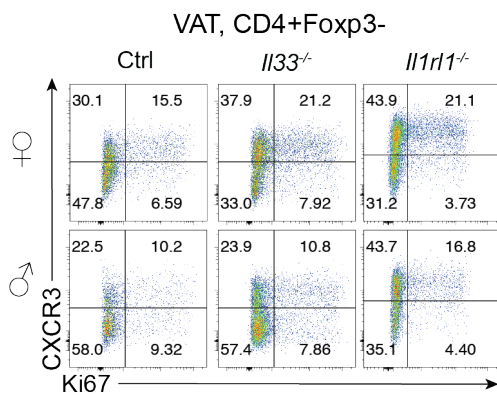
**a**



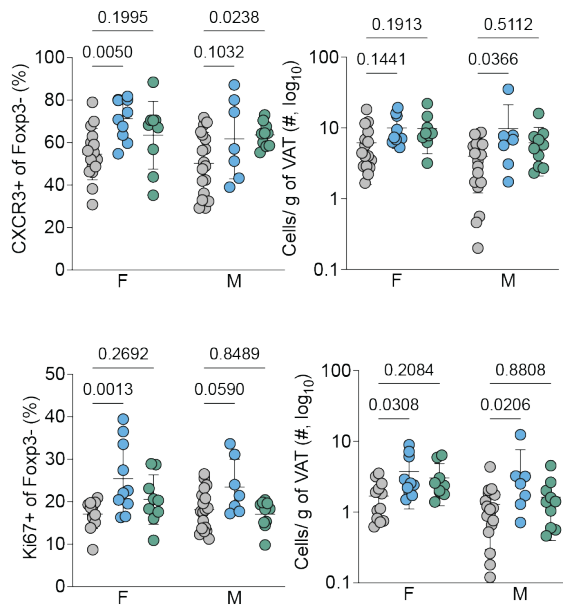
**b**



**c**



**d**



**e**

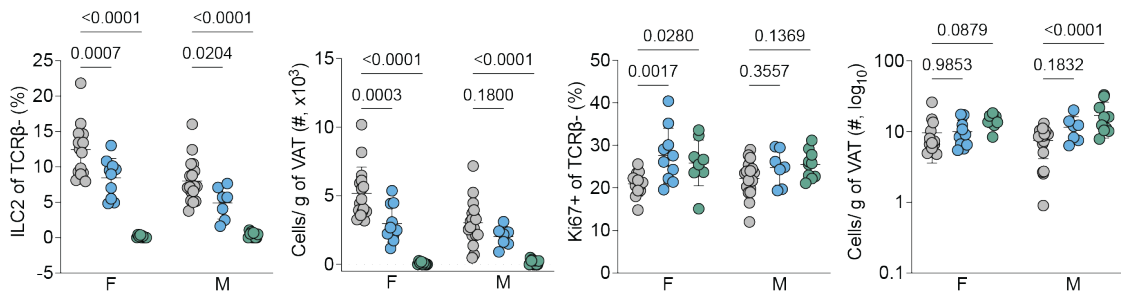


**Figure 45 | CD8+ T cells expand in absence of IL-33-dependent signalling.** VAT from 27–33-week-old *Il33*<sup>-/-</sup>, *Il1rl1*<sup>-/-</sup> and WT mice were analysed and compared. **a, b**, Flow cytometry plots showing CD4 versus CD8 expression in TCRβ<sup>+</sup> cells (**a**) and quantification (**b**) of frequencies and numbers of CD4<sup>+</sup>Foxp3<sup>-</sup> and CD8<sup>+</sup> T cells in *Il33*<sup>-/-</sup>, *Il1rl1*<sup>-/-</sup> and WT mice. **c, d**, Flow cytometry plots showing CXCR3 versus Ki67 expression in CD4<sup>+</sup>Foxp3<sup>-</sup> cells (**c**) and quantification (**d**) of frequencies and numbers of Ki67<sup>+</sup> and CXCR3<sup>+</sup> cells in *Il33*<sup>-/-</sup>, *Il1rl1*<sup>-/-</sup> and WT mice. **e**, Quantification of frequencies and cell numbers of ILC2 (left) and Ki67<sup>+</sup> cells (right) in TCRβ<sup>-</sup> cells. Symbols represent individual mice; horizontal lines indicate means. Data are representative (**a, c**) or pooled (**b, d, e**) from a minimum of two independent experiments. Error bars indicate the standard deviation. Statistical analyses were performed using two-way ANOVA.

## 5.8 High-fat diet induces TNF and IFN-γ production in males but not T cell infiltration

Increased infiltration of inflammatory immune cells such as CD8 T cells, Th1 cells and pro-inflammatory macrophages is a hallmark of obesity and metabolic disease (Grant & Dixit, 2015). Therefore, infiltration of CD4 and CD8 T cells was assessed. Firstly, numbers of CD45<sup>+</sup> and T cells (TCRβ<sup>+</sup>) were analysed, but no significant difference was detected between ND and HFD mice (**Figure 46a**). Secondly, proportion and numbers of ST2<sup>+</sup> and CXCR3<sup>+</sup> conventional CD4 cells were assessed also showing no difference between ND and HFD fed mice of both sexes (**Figure 46b, c**). And finally, analysis of CD8 T cell and ILC2 proportion and cell numbers revealed no HFD-induced changes in female or male mice.

Next, cytokine production was measured through re-stimulation of VAT SVF with PMA/Ionomycin. IFN-γ and TNF levels were reduced in T cells from HFD fed males compared to ND controls while female proportion and numbers of IFN-γ- and TNF-producing T cells remained unchanged (**Figure 47a**). Furthermore, no significant difference between ND and HFD fed mice was observed in T cell derived IL-5, IL-13, IL-17A, IFN-γ and TNF (**Figure 47b, c**). In TCRβ<sup>-</sup> cells, the IL-5 expression levels HFD fed mice were increased in females but decreased in males when compared to controls (**Figure 47d**). The proportion of IL13 and IL17A expressing cells in HFD fed mice was similar to ND controls. However, the

number of IL13<sup>+</sup> and IL17A<sup>+</sup> cells was reduced in male HFD mice when compared to ND controls.

Overall, the results unexpectedly showed no induction of inflammatory cell infiltration upon feeding a HFD and reduced levels of T<sub>H</sub>1 associated cytokines IFN- $\gamma$  and TNF and T<sub>H</sub>2 associated cytokines IL5 and IL13 in male HFD mice when compared to ND controls. Any differences could have been potentially masked by the significant variation across experiments. Data analysis from a different angle might help explain the variation across experiments and resolve potential differences which was unfortunately not possible in the limited time and will be further elaborated on in the discussion.

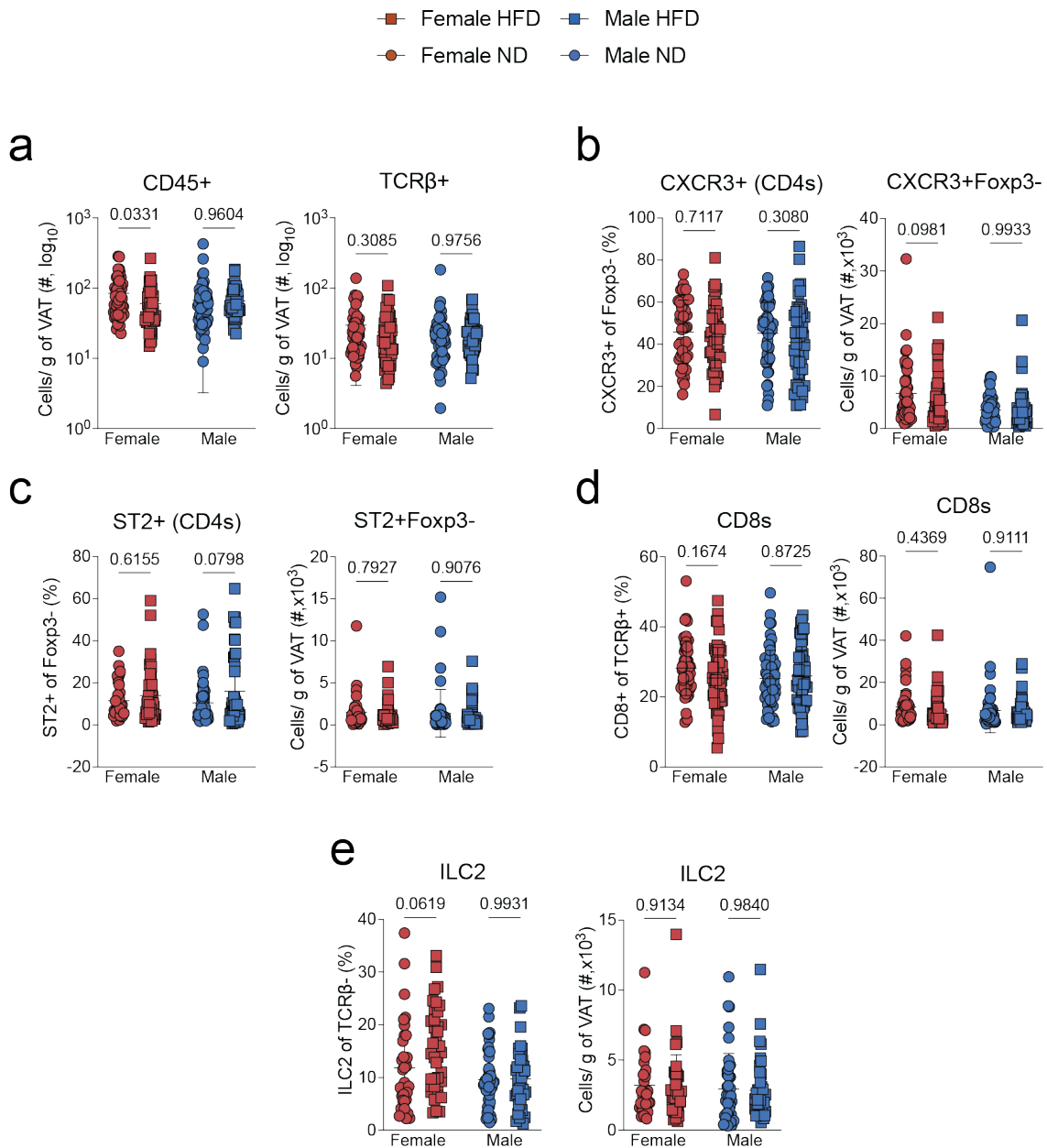


**Figure 46 | Cellular infiltration is not substantially altered in high-fat diet fed mice.** C57BL/6 female and male mice were subjected to high-fat diet for 25 weeks and the VAT was analysed. **a**, Quantification of numbers of CD45<sup>+</sup> and TCRβ<sup>+</sup> cells. **b**, **c**, Quantification of frequencies and cell numbers of CXCR3<sup>+</sup> (**b**) and ST2<sup>+</sup> (**c**) cells among CD4<sup>+</sup>Foxp3<sup>-</sup> populations. **d**, **e**, Quantification of frequencies and cell numbers of CD8<sup>+</sup> (**d**) and ILC2 (**e**) cells among TCRβ<sup>+</sup> and TCRβ<sup>-</sup> populations, respectively. Symbols represent individual mice. Data are pooled from a minimum of two independent experiments. Error bars indicate the standard deviation. Statistical analyses were performed using two-way ANOVA.

Female HFD Male HFD  
 Female ND Male ND

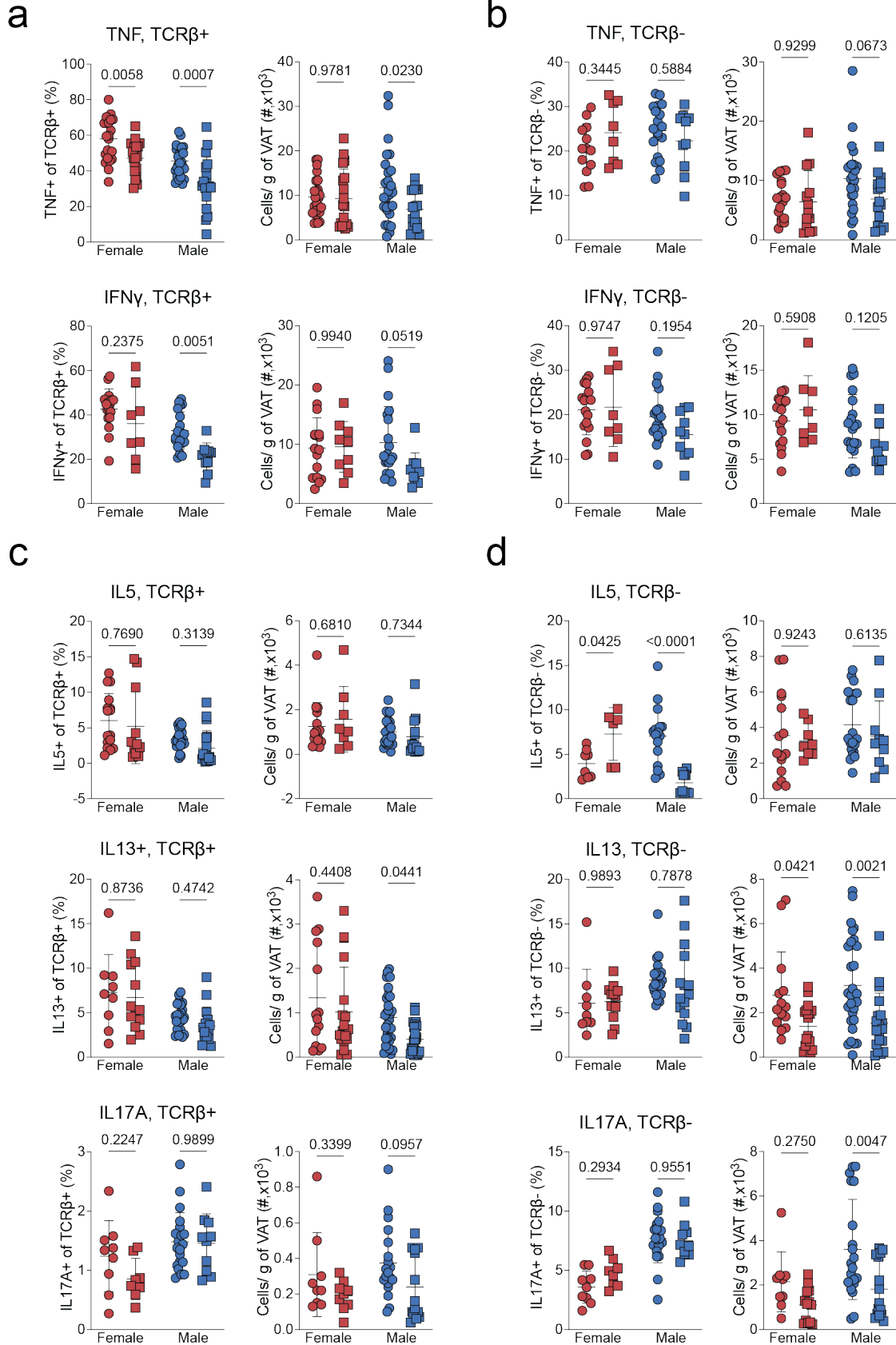


**Figure 47 | TNF, IL5 and IL13 cytokine production is reduced upon high-fat diet.** C57BL/6 female and male mice were subjected to high-fat diet for 25 weeks. VAT SVF was re-stimulated for 4hrs and cytokine measure intracellularly. **a, b**, Quantification of frequencies and cell numbers of TNF and IFN- $\gamma$  producing cells among TCR $\beta$ <sup>+</sup> (**a**) and TCR $\beta$ <sup>-</sup> (**b**) populations, respectively. **c, d**, Quantification of frequencies and cell numbers of IL5, IL13 and IL17A producing cells among TCR $\beta$ <sup>+</sup> (**c**) and TCR $\beta$ <sup>-</sup> (**d**) populations, respectively. Symbols represent individual mice. Data are pooled from a minimum of two independent experiments. Error bars indicate the standard deviation. Statistical analyses were performed using two-way ANOVA.

## Chapter 6 – Functions of ST2<sup>+</sup> and CXCR3<sup>+</sup> VAT Treg cells

### 6.1 Elevated T cell infiltration and IFN- $\gamma$ expression in the VAT after systemic Treg depletion

Findings listed in the previous chapters have revealed the influence of VAT microenvironment on Treg cells. We sought to understand the impact of Treg ablation on VAT Treg cell microenvironment. First, Treg cells were depleted systemically using *Foxp3<sup>DTR</sup>* mice as described previously in this study (see **Figure 6b**) and analysed the impact of Treg cell loss 10 days post-depletion. The results showed substantial T cell infiltration in proportion and numbers after Treg cell depletion in both sexes (**Figure 48a**). This was unique to T cells as numbers and proportion of TCR $\beta$ - cells remained unchanged in male and female mice that were devoid of Treg cells. Further analysis of the T cell compartment showed that numbers of CD4<sup>+</sup>Foxp3<sup>-</sup> T cells were substantially increased in female, but not male Treg-depleted mice compared to controls (**Figure 48b**). The proportion of CD4<sup>+</sup>Foxp3<sup>-</sup> T cells, however, remained unchanged in both sexes. Moreover, the CD8<sup>+</sup> T cell population expanded significantly in absence of VAT Treg cells in both sexes when compared to controls (**Figure 48b**). This was at least partly due to increased proliferation as evidence by elevated numbers and proportion of Ki67<sup>+</sup> cells in the CD8<sup>+</sup> T cell compartment (**Figure 48c**). A similar observation was made in CD4<sup>+</sup>Foxp3<sup>-</sup> T cells that harboured increased numbers of Ki67-expressing cells. CXCR3 expression remained largely unaltered 10 days post Treg cell depletion (**Figure 48d, e**). Additionally, assessment of cytokine production in Treg cell depleted female mice revealed strikingly increased levels of IFN- $\gamma$  and TNF production in CD45<sup>+</sup> cells compared to controls (**Figure 48f, g**). In contrast, numbers of IFN- $\gamma$ <sup>+</sup> and TNF<sup>+</sup> lymphocytes were similar in male DT- and PBS-treated mice while the proportion of IFN- $\gamma$ <sup>-</sup> and TNF-expressing cells was up- and downregulated, respectively. Furthermore, IL-5 production in females did not change in proportion but only increased numerically in DT treated mice compared to controls. However, numbers of IL-5 expressing CD45<sup>+</sup> cells were significantly reduced in Treg cell depleted male mice compared to controls (**Figure 48h**).

Overall, the results demonstrate that Treg cells are critical to limit proliferation of the T cell in the VAT and control the production of IFN- $\gamma$ , TNF and IL-5.

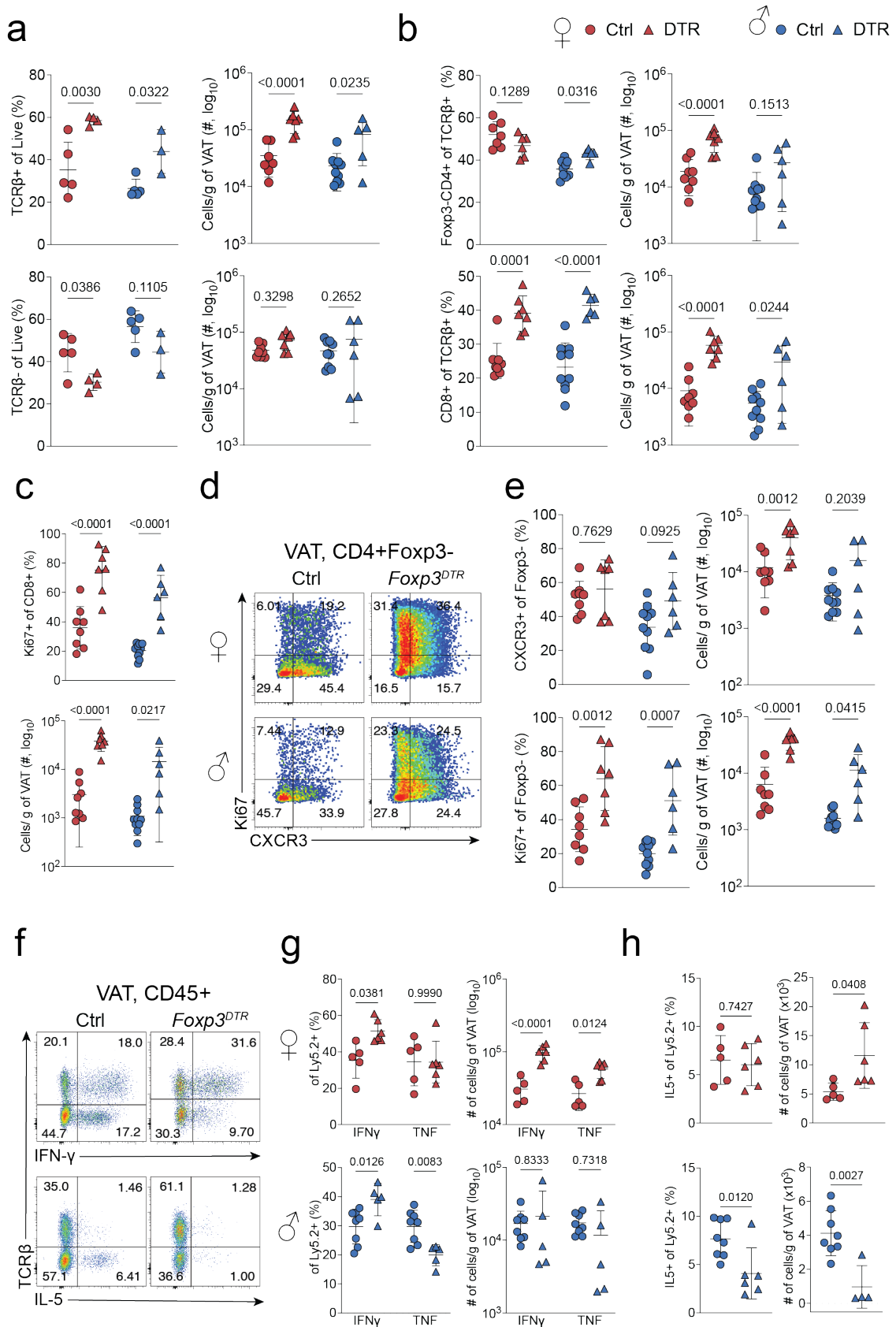


**Figure 48 | T cell infiltration and IFN- $\gamma$  production is substantially increased in the VAT after Treg cell depletion. Male and female *Foxp3<sup>DTR</sup>* mice were**

treated with either a single dose of diphtheria toxin (DT) or PBS and analysed 10 days post-treatment at 28-30-weeks of age. **a**, Quantification of frequencies and numbers of TCR $\beta$ <sup>+</sup> and TCR $\beta$ <sup>-</sup> cells among live cells in DT and PBS treated *Foxp3<sup>DTR</sup>* mice. **b**, Quantification of frequencies and numbers of Foxp3-CD4<sup>+</sup> and CD8<sup>+</sup> T cells among TCR $\beta$ <sup>+</sup> cells in DT and PBS treated *Foxp3<sup>DTR</sup>* mice. **c**, Quantification of frequencies and numbers of Ki67<sup>+</sup> cells among CD8<sup>+</sup> T cells. **d, e**, Flow cytometry plots showing CXCR3 versus Ki67 expression (**d**) and quantification (**e**) of frequencies and numbers of Ki67<sup>+</sup> and CXCR3<sup>+</sup> cells among Foxp3-CD4<sup>+</sup> T cells in DT and PBS treated *Foxp3<sup>DTR</sup>* mice. **f-h**, Flow cytometry plots showing TCR $\beta$  versus IFN- $\gamma$  and IL-5 expression in CD45<sup>+</sup> cells (**f**) and quantification of frequencies and numbers of IFN- $\gamma$ <sup>+</sup>, TNF<sup>+</sup> (**g**) and IL-5<sup>+</sup> (**h**) cells among CD45<sup>+</sup> cells in male DT and PBS treated *Foxp3<sup>DTR</sup>* mice. Symbols represent individual mice; horizontal lines indicate means. Data are representative (**d, f**) or pooled (**a-c, e, g, h**) from a minimum of two independent experiments. Error bars indicate the standard deviation. Statistical analyses were performed using two-way ANOVA (**a-c, e, g**) or unpaired, two-tailed Student's *t*-test (**h**).

## 6.2 GATA3 dependent ST2<sup>+</sup> VAT Treg cells are required to regulate T cell infiltration and cytokine production

Given the essential role of GATA3 in ST2<sup>+</sup> Treg cell differentiation, we assessed the local immune cell composition and cytokine production in *Gata3<sup>fl/fl</sup>Foxp3<sup>Cre</sup>* mice. The numbers of CD4<sup>+</sup> T cells in *Gata3<sup>fl/fl</sup>Foxp3<sup>Cre</sup>* mice were substantially elevated yet displayed no difference or modest decrease in proportions in male and female mice, respectively (**Figure 49a**). Analysis of the CD8<sup>+</sup> T cell compartment showed a striking proportional and numerical increase in *Gata3<sup>fl/fl</sup>Foxp3<sup>Cre</sup>* mice compared to controls in both sexes. In contrast, the proportion of TCR $\beta$ <sup>-</sup> cells in *Gata3<sup>fl/fl</sup>Foxp3<sup>Cre</sup>* remained unchanged in female or were significantly reduced in male mice compared to controls. Yet numbers of TCR $\beta$ <sup>-</sup> cells were elevated in female GATA3-deficient mice compared to controls and unaltered in their male counterparts (**Figure 49b**). The ILC2 population also remained unchanged in *Gata3<sup>fl/fl</sup>Foxp3<sup>Cre</sup>* mice when compared to controls. More detailed analysis of the CD4<sup>+</sup>Foxp3<sup>-</sup> compartment revealed substantial phenotypic changes. While the proportion of CXCR3<sup>+</sup> cells dropped in male *Gata3<sup>fl/fl</sup>Foxp3<sup>Cre</sup>* mice, CXCR3<sup>+</sup> cell numbers were elevated in their female counterparts when compared to control mice (**Figure 49c, d**). Furthermore, a substantial increase of ST2<sup>+</sup> Treg cells was observed within the CD4<sup>+</sup>Foxp3<sup>-</sup> T

cell compartment of *Gata3<sup>fl/fl</sup>Foxp3<sup>Cre</sup>* male but not female mice. Cytokine analysis of *Gata3<sup>fl/fl</sup>Foxp3<sup>Cre</sup>* mice revealed elevated IFN- $\gamma$  production in male but not female T cells and TCR $\beta$ - cells. In female *Gata3<sup>fl/fl</sup>Foxp3<sup>Cre</sup>* mice, the proportion of IFN- $\gamma$ -expressing cells was unchanged in TCR $\beta$ <sup>+</sup> population, whereas it dropped in TCR $\beta$ - cells (**Figure 49e-g**). While TNF expression remained unchanged in GATA3-deficient male mice, it was substantially reduced in T cells of female mice compared to controls. TNF production in TCR $\beta$ - cells was comparable between *Gata3<sup>fl/fl</sup>Foxp3<sup>Cre</sup>* and control mice of both sexes (**Figure 49g**). IL-5 expression in T cells was slightly enhanced in males while displaying no significant changes in female *Gata3<sup>fl/fl</sup>Foxp3<sup>Cre</sup>* mice. In TCR $\beta$ - cells, however, the amount of IL-5 expressing cells was substantially reduced in female *Gata3<sup>fl/fl</sup>Foxp3<sup>Cre</sup>* mice, while only displaying a proportional decrease in males when compared to controls.

In summary, Treg cell specific deletion of GATA3 and associated loss of ST2<sup>+</sup> VAT Treg cells resulted in increased T cell infiltration in both sexes, altered CD4<sup>+</sup>Foxp3<sup>-</sup> T cell phenotype and cytokine production, both of which are however pronounced in male mice.

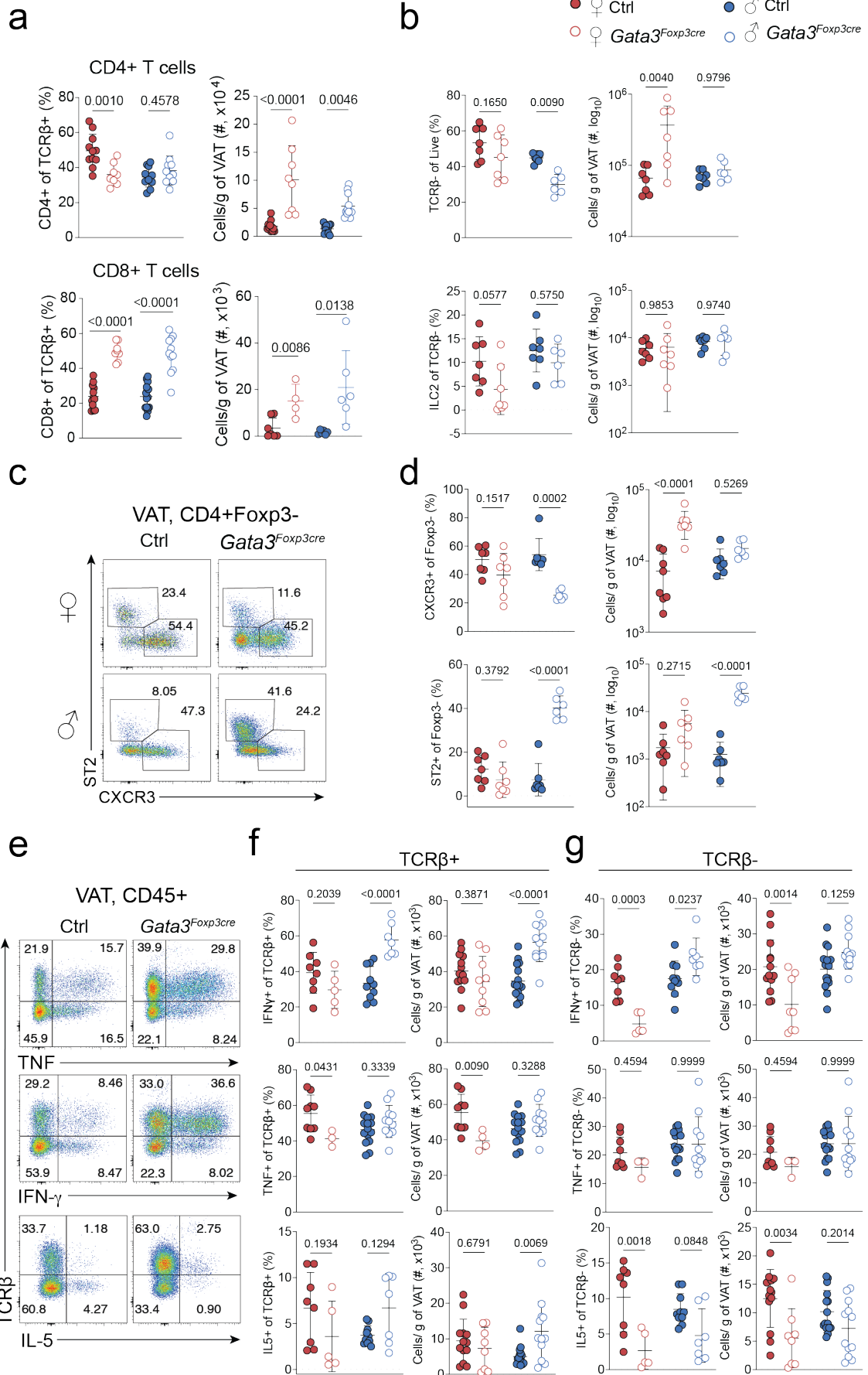


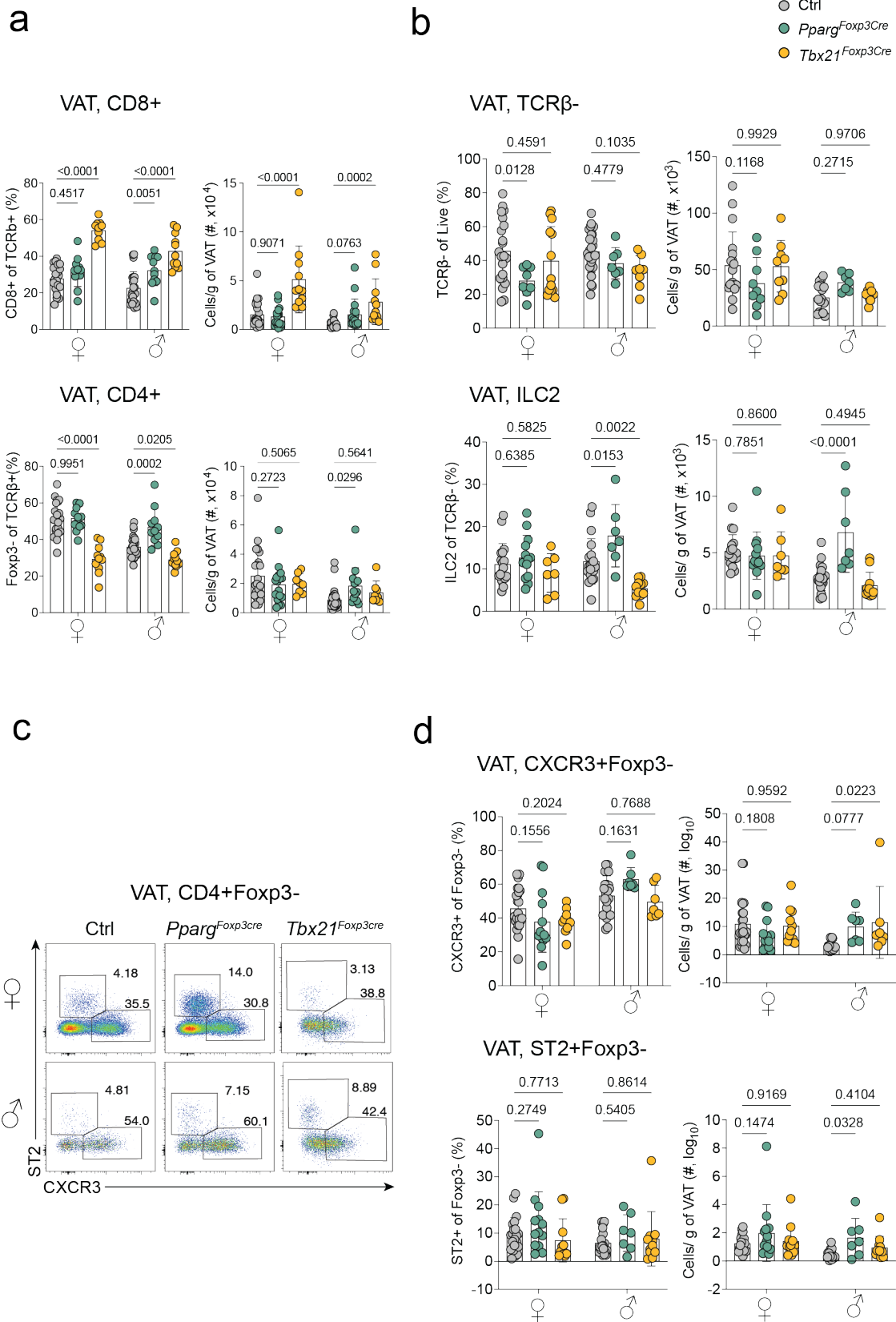
**Figure 49 | Treg cell specific ablation of GATA3 leads to increased T cell infiltration and inflammatory cytokine production.** Analysis of VAT from 29-32-week-old male and female *Gata3<sup>fl/fl</sup>Foxp3<sup>Cre</sup>*, wildtype (n=20) and *Foxp3<sup>Cre</sup>* (n=4) mice. **a**, Quantification of frequencies and numbers of CD4+ and CD8+ T cells among TCRβ+ cells. **b**, Quantification of ILC2 and TCRβ- cells in *Gata3<sup>fl/fl</sup>Foxp3<sup>Cre</sup>* and control mice. **c, d**, Flow cytometry plots showing ST2 versus CXCR3 expression in CD4+Foxp3- cells (**c**) and quantification (**d**) of frequencies and numbers of ST2+ and CXCR3+ cells in *Gata3<sup>fl/fl</sup>Foxp3<sup>Cre</sup>* and control mice. **e-h**, Flow cytometry plots showing TCRβ versus TNF, IFN-γ and IL-5 expression in CD45+ cells (**e**) and quantification of frequencies and numbers of IFN-γ, TNF and IL-5 producing cells among TCRβ+ (**f**) and TCRβ- (**g**) *Gata3<sup>fl/fl</sup>Foxp3<sup>Cre</sup>* and control mice. Symbols represent individual mice; horizontal lines indicate means. Data are representative (**c, e**) or pooled (**a, b, d, f, g**) from a minimum of two independent experiments. Error bars indicate the standard deviation. Statistical analyses were performed using two-way ANOVA.

### 6.3 Depletion of CXCR3+ but not ST2+ VAT Treg cells significantly impact T cell and cytokine homeostasis in the VAT.

Given the molecular differences of the VAT Treg cell subsets and their differential enrichment in male and female mice, we hypothesized that ST2+ and CXCR3+ Treg cells contribute to the suppression of VAT inflammation and maintenance of organismal homeostasis in a distinct and sex-specific manner.

To test this hypothesis, the immune cell composition in the VAT that lacked either ST2+ or CXCR3+ VAT Treg cells was compared. Analysis of *Pparg<sup>fl/fl</sup>Foxp3<sup>Cre</sup>* mice revealed a modestly increased T cell (CD4+ and CD8+) compartment in male mice. Both, CD4+ and CD8+ T cells were increased in male mice deficient of ST2+ VAT Treg cells in proportion and numbers compared to controls. Female mice did not display this phenotype and were indistinguishable from control mice (**Figure 50a**). Analysis of *Tbx21<sup>fl/fl</sup>Foxp3<sup>Cre</sup>* mice revealed a different picture. A substantial increase of CD8+ T cells was observed in both sexes, even to a higher magnitude than in *Pparg<sup>fl/fl</sup>Foxp3<sup>Cre</sup>* (**Figure 50a**). This was both in proportion and numbers. In contrast, only the proportion of CD4+ T cells was reduced in female and male *Tbx21<sup>fl/fl</sup>Foxp3<sup>Cre</sup>* mice compared to controls. Analysis of TCRβ- cells showed, with exception of a proportional drop in *Pparg<sup>fl/fl</sup>Foxp3<sup>Cre</sup>* female mice, no significant alterations when compared to controls. However, a closer look revealed that ILC2 expanded in *Pparg<sup>fl/fl</sup>Foxp3<sup>Cre</sup>* male mice when compared to

controls (**Figure 50b**). Depletion of CXCR3<sup>+</sup> VAT Treg cells resulted only in a proportional reduction of the ILC2 compartment in male mice. In females, however, no significant changes in ILC2 were observed. More detailed analysis of the CD4<sup>+</sup>Foxp3<sup>-</sup> T cell compartment showed no substantial differences in ST2 or CXCR3 expression between PPAR $\gamma$  or T-bet-deficient mice and their respective controls (**Figure 50c, d**). Thus, loss of CXCR3<sup>+</sup> VAT Treg cells leads to CD8<sup>+</sup> T cell infiltration in both sexes while ST2<sup>+</sup> VAT Treg cell depletion results in selective expansion of Tconv and ILC2 cells in male mice only.



*Tbx21<sup>fl/fl</sup>Foxp3<sup>Cre</sup>* and *Foxp3<sup>Cre</sup>* control mice. **a**, Frequencies (left) and absolute numbers (right) of CD8 T cells (top) and Foxp3-CD4+ cells (bottom). **c**, Frequencies (left) and absolute numbers (right) of TCRβ- cells (top) and ILC2 (bottom). **c, d**, Flow cytometry plots showing ST2 versus CXCR3 expression in CD4+Foxp3- cells (**c**) and quantification (**d**) of frequencies and numbers of ST2+ and CXCR3+ cells in *Pparg<sup>fl/fl</sup>Foxp3<sup>Cre</sup>*, *Tbx21<sup>fl/fl</sup>Foxp3<sup>Cre</sup>* and *Foxp3<sup>Cre</sup>* control mice. Symbols represent individual mice; horizontal lines indicate means. Data are representative (**c**) or pooled (**a, b, d**) from a minimum of two independent experiments. Error bars indicate the standard deviation. Statistical analyses were performed using two-way ANOVA.

Additionally, cytokine production of VAT immune cells in these mice was measured by intracellular cytokine staining after PMA/Ionomycin re-stimulation *ex vivo*. Mice devoid of ST2+ VAT Treg cells did not display significant changes in either IL-5, TNF or IFN-γ production by T cells (**Figure 51a**). This was the case for both sexes. In contrast, depletion of CXCR3+ VAT Treg cells resulted in increased IFN-γ expression compared to control mice, particularly in female mice. Furthermore, proportions of TNF+ were reduced in both sexes while cell numbers remained unchanged (**Figure 51a**). Loss of CXCR3+ VAT Treg cells did not affect the proportion of IL-5+ T cells in female and male mice compared to controls, while elevated IL-5+ T cell numbers were found in both sexes. With exception of reduced IFN-γ production in females, reduction of ST2+ VAT Treg cells did not affect IL-5, IFN-γ or TNF expression in TCRβ- cells (**Figure 51b**). In a similar way, IFN-γ expression was unaltered in *Tbx21<sup>fl/fl</sup>Foxp3<sup>Cre</sup>* mice across all comparisons (**Figure 51b**). However, TNF expression was reduced in proportion and numbers in TCRβ- cells of female and male mice lacking CXCR3+ VAT Treg cells when compared to controls (**Figure 51b**). However, only male but not female mice lacking CXCR3+ Treg cells had reduced proportion and numbers of IL-5+ TCRβ- cells.

Taken together, ablation of CXCR3+ and ST2+ VAT Treg cells affects VAT immunity in different ways. The data showed that diminishing CXCR3+ VAT Treg cells results in CD8+ T cell expansion, increased IFN-γ and reduced TNF production while the absence of ST2+ VAT Treg cells had little to no impact on immune cell composition or cytokine production.

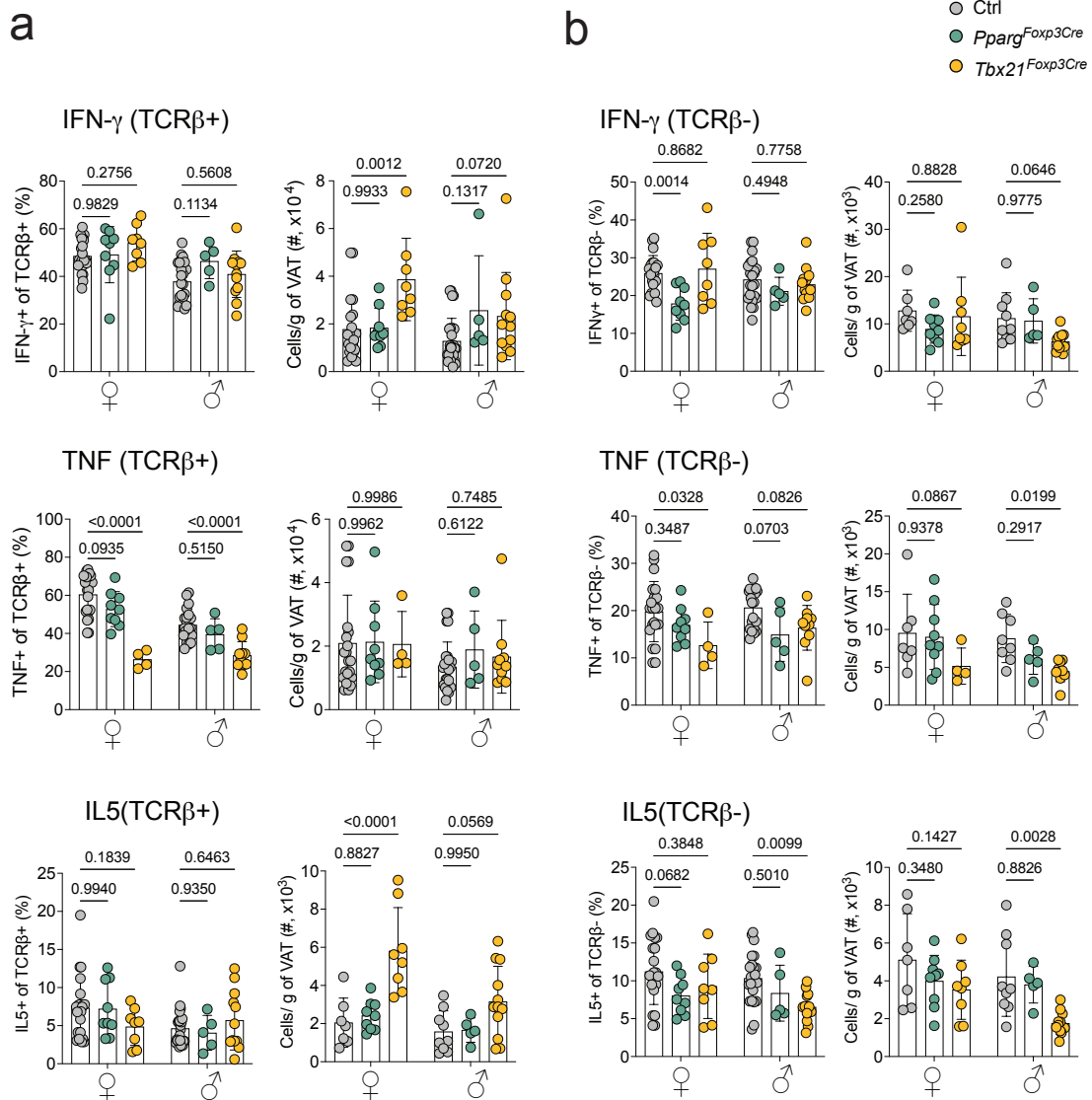


**Figure 51 | TNF production is reduced in *Tbx21*<sup>fl/fl</sup>*Foxp3*<sup>Cre</sup> mice.** Analysis of VAT of 25–30-week-old *Pparg*<sup>fl/fl</sup>*Foxp3*<sup>Cre</sup>, *Tbx21*<sup>fl/fl</sup>*Foxp3*<sup>Cre</sup> and *Foxp3*<sup>Cre</sup> control mice. **a, b**, Quantification of frequencies and numbers of TNF+, IL-5+ and IFN- $\gamma$ + among TCR $\beta$ + (**a**) and TCR $\beta$ - (**b**) cells. Symbols represent individual mice; horizontal lines indicate means. Data are pooled from a minimum of two independent experiments. Error bars indicate the standard deviation. Statistical analyses were performed using two-way ANOVA.

## 6.4 CXCR3<sup>+</sup> but not ST2<sup>+</sup> VAT Treg cell depletion results in exacerbated VAT inflammation

To further analyse the different impact of CXCR3<sup>+</sup> and ST2<sup>+</sup> VAT Treg cells on inflammation, RNASeq of total VAT from male and female *Pparg<sup>fl/fl</sup>Foxp3<sup>Cre</sup>*, *Tbx21<sup>fl/fl</sup>Foxp3<sup>Cre</sup>* and *Foxp3<sup>Cre</sup>* mice was performed.

Surprisingly, RNASeq analysis of VAT showed only 135 genes differentially expressed (DE) in male *Pparg<sup>fl/fl</sup>Foxp3<sup>Cre</sup>* mice compared to sex matched control, whereas more >700 DE genes were detected in female *Pparg<sup>fl/fl</sup>Foxp3<sup>Cre</sup>* mice (**Figure 52a, b**). Furthermore, genes associated with metabolic dysfunction (*Gpr18*, *Scnn1b*) were upregulated and genes involved in lipid metabolism (*Cck*, *Fgfbp3*) and BAT differentiation (*Slc22a12*, *Pex5l*, *Mettl*) were downregulated in *Pparg<sup>fl/fl</sup>Foxp3<sup>Cre</sup>* male mice compared to controls (Matson & Ritter, 1999; W. Y. Park et al., 2022; Y. Wang et al., 2020). Additionally, elevated *Trdc* transcript levels, encoding for T cell receptor  $\delta$  constant subunit, were detected suggesting increased numbers of  $\gamma\delta$  T cells, which are known to promote insulin resistance. Strikingly the number of DE genes detected (FDR 0.1) was substantially lower in the male comparison (150 genes) related to female comparison from *Tbx21<sup>fl/fl</sup>Foxp3<sup>Cre</sup>* mice (>1300 genes; **Figure 52c, d**). In both, male and female *Tbx21<sup>fl/fl</sup>Foxp3<sup>Cre</sup>* mice insulin degrading enzyme (*Ide*) was downregulated compared to controls. Apart from that, only a few genes involved in adipogenesis (*Cxcr4*), insulin metabolism (*Depp1*, *Thbd*) and lipid metabolism (*Apoc2*) were deregulated in the VAT of male T-bet-deficient mice compared to controls (Gil-Ortega et al., 2013; Girusse et al., 2019; Lontchi-Yimagou et al., 2020) (**Figure 52c**). Consistent with the important role of CXCR3<sup>+</sup> VAT Treg cells in females, several genes involved in lipid metabolism (*Abcg1*, *Scd1*), adipogenesis (*Mest*, *Me1*) and cellular metabolism (*Tkt*) were deregulated in *Tbx21<sup>fl/fl</sup>Foxp3<sup>Cre</sup>* mice compared to control mice (Al-Dwairi, Pabona, Simmen, & Simmen, 2012; Karbiener et al., 2015; Takahashi, Kamei, & Ezaki, 2005) (**Figure 52d**). Pathway analysis showed significant enrichment of genes involved in metabolism (KEGG) and increased levels of interferon induced transcripts (*Ifit2*, *Stat1*, *Cd40*, *Irf1*, *Irf8*,

*Irf5*) and genes encoding proinflammatory chemokines (*Ccl5*, *Ccl6* and *Ccl9*) in female *Tbx21<sup>fl/fl</sup>Foxp3<sup>Cre</sup>* mice compared to controls (**Figure 52e**).

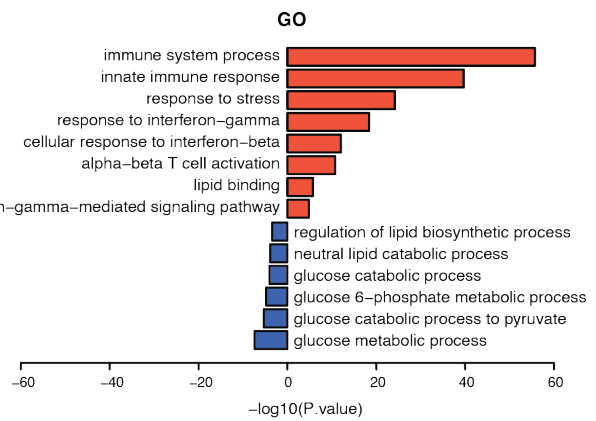
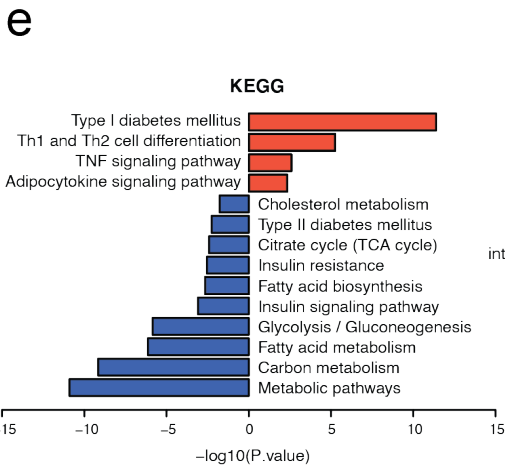
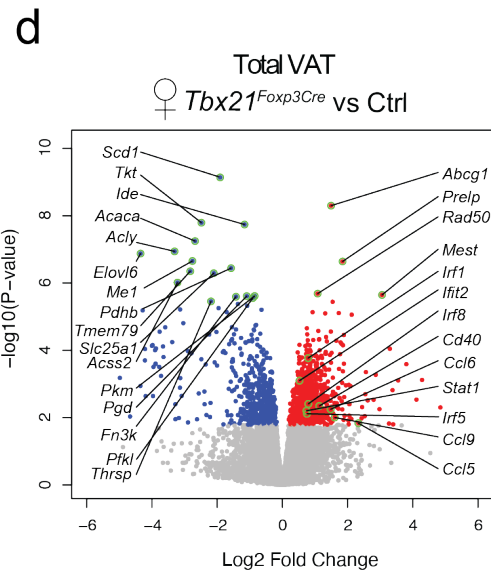
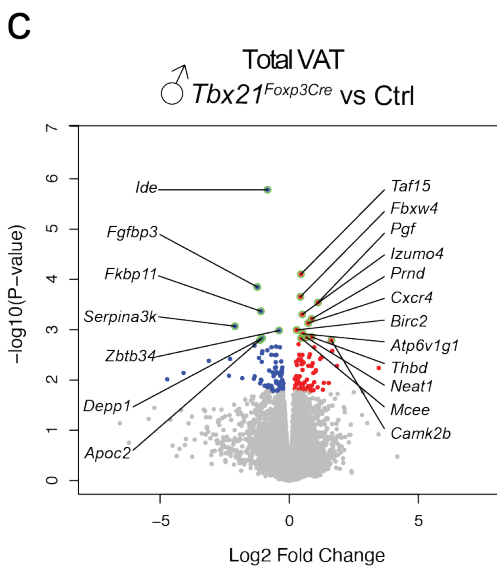
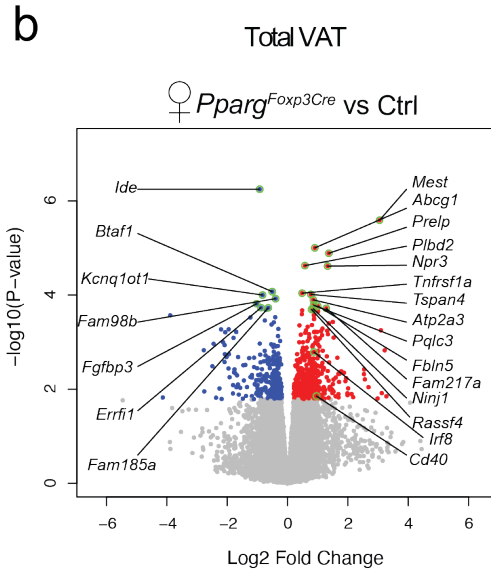
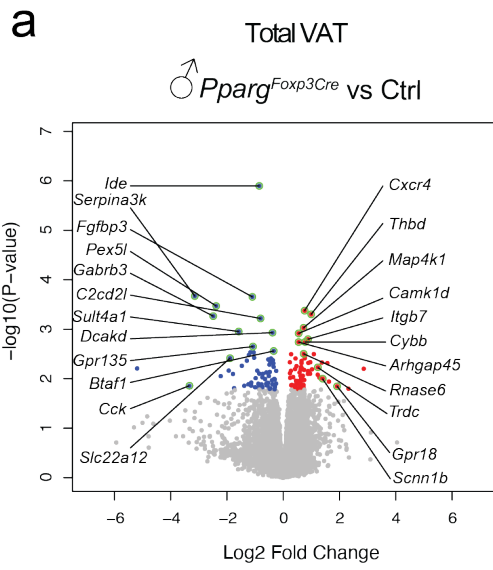
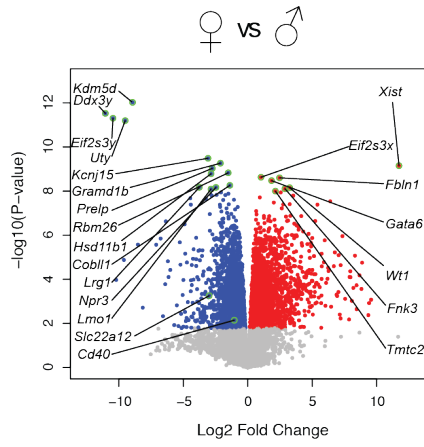


**Figure 52 | CXCR3+ but not ST2+ VAT Treg depletion leads to increased VAT inflammation.** RNASeq of total VAT of *Pparg<sup>fl/fl</sup>Foxp3<sup>Cre</sup>* and *Tbx21<sup>fl/fl</sup>Foxp3<sup>Cre</sup>* and control mice was performed. **a-d**, Volcano plots showing genes differentially expressed between total VAT of male (**a**) and female (**b**) *Pparg<sup>fl/fl</sup>Foxp3<sup>Cre</sup>* and male (**c**) and female (**d**) *Tbx21<sup>fl/fl</sup>Foxp3<sup>Cre</sup>* vs control mice. Each dot represents a gene; genes highlighted in red are up-regulated and genes highlighted in blue are down-regulated. **e**, KEGG (left) and GO (right) pathway enrichment analysis for differentially expressed genes in female VAT of *Tbx21<sup>fl/fl</sup>Foxp3<sup>Cre</sup>* vs control mice. Positive values refer to pathways upregulated (red), negative values refer to pathways downregulated (blue) in the VAT of *Tbx21<sup>fl/fl</sup>Foxp3<sup>Cre</sup>* vs control mice.

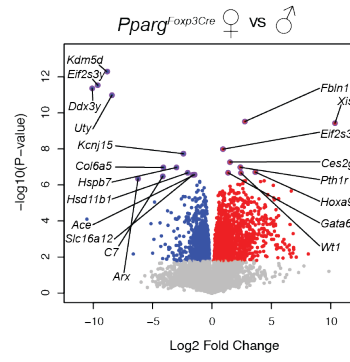
Furthermore, several genes deregulated in female VAT of *Pparg<sup>fl/fl</sup>Foxp3<sup>Cre</sup>* mice (*Ide*, *Mest*, *Abcg1*, *Cd40*, *Irf8*) overlapped with deregulated genes observed in the VAT of female *Tbx21<sup>fl/fl</sup>Foxp3<sup>Cre</sup>*. That includes upregulation of genes in the VAT of female *Tbx21<sup>fl/fl</sup>Foxp3<sup>Cre</sup>* and *Pparg<sup>fl/fl</sup>Foxp3<sup>Cre</sup>* mice that are usually downregulated in WT females when compared to WT males. These includes genes that have been positively linked to insulin resistance (*Prelp*, *Npr3*), obesity (*Lrg1*) and adipogenesis (*Kdm5d*, *Slc22a12*) potentially blunting sex-specific differences of the VAT transcriptome (**Figure 53a**). Indeed, female versus male comparison of *Tbx21<sup>fl/fl</sup>Foxp3<sup>Cre</sup>* and *Pparg<sup>fl/fl</sup>Foxp3<sup>Cre</sup>* VAT RNAseq data detected <2400 and <2500 DE genes, respectively, which is significantly lower to the number of DE genes detected when comparing WT male and female mice (>4800 DE genes; **Figure 53b, c**). Gene expression changes that occurred in the absence of T-bet also suggested that the transcriptional profile of female *Tbx21<sup>fl/fl</sup>Foxp3<sup>Cre</sup>* mice shifted towards a male-like phenotype (**Figure 53d**).

Taken together the results show that CXCR3+ but not ST2+ VAT Treg cells are crucial to restrain VAT inflammation. In keeping with this finding, absence of CXCR3+ Treg cells (T-bet deficient) changed the inflammatory phenotype and transcriptome of female VAT to resemble WT males.

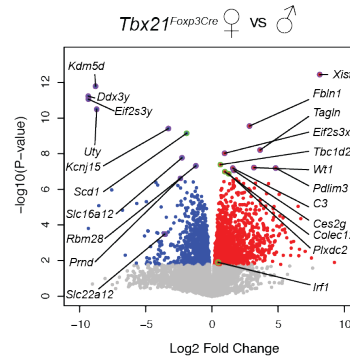
a



b



c



d

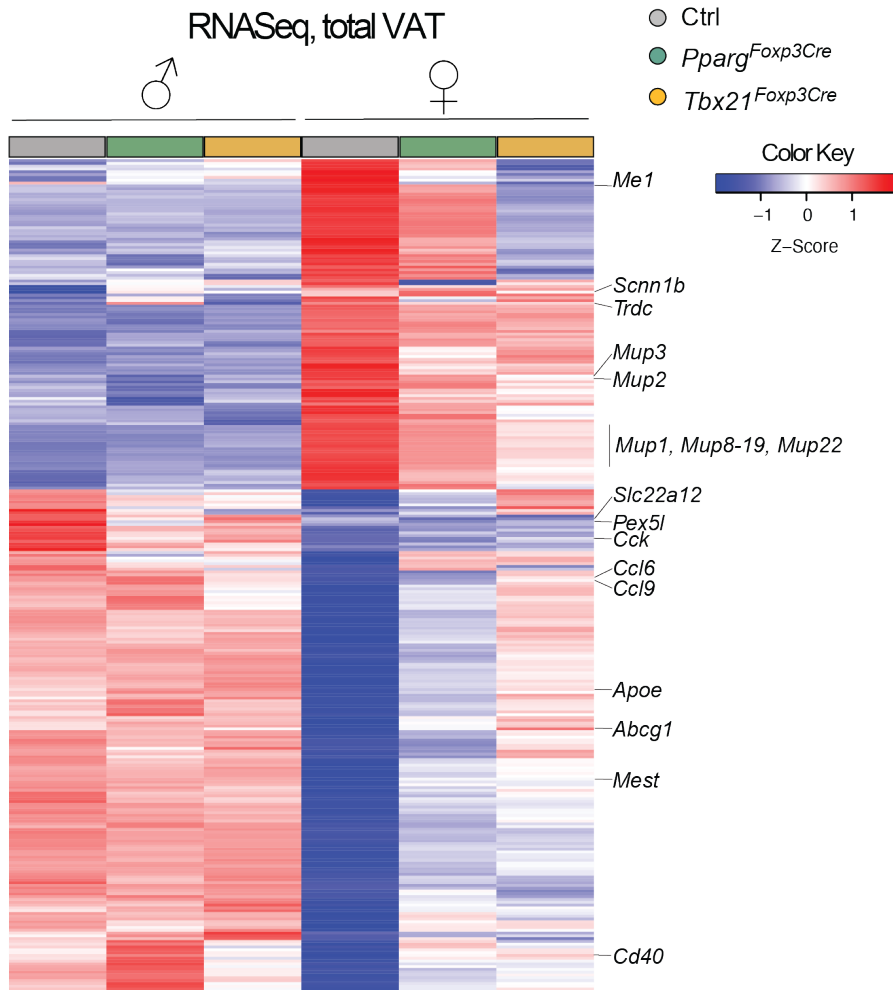


**Figure 53 | Depletion of CXCR3+ Treg cells blunt the sex-specific transcriptional differences in VAT a-e**, Volcano plots shows genes differentially expressed between total VAT of female vs male control (**a**), female vs male *Pparg<sup>fl/fl</sup>Foxp3<sup>Cre</sup>* (**b**), female vs male *Tbx21<sup>fl/fl</sup>Foxp3<sup>Cre</sup>* (**c**) mice. **d**, Heatmap shows top 500 genes that are DE in the female vs male comparison of control VAT that are also DE in either *Pparg<sup>fl/fl</sup>Foxp3<sup>Cre</sup>* or *Tbx21<sup>fl/fl</sup>Foxp3<sup>Cre</sup>* vs *Foxp3<sup>Cre</sup>* control comparisons.

## 6.5 Loss of IFN- $\gamma$ impacts adiposity but not metabolism in males

Our results have shown that depletion CXCR3+ VAT Treg cells has a substantial impact on immune cell infiltration and local cytokine production. To test the link between immune phenotype and metabolism, *Ifng<sup>-/-</sup>* and *Tbx21<sup>fl/fl</sup>Foxp3<sup>Cre</sup>* mice were weighed, subjected to metabolic testing and gene expression analysis. Body and VAT weight were substantially reduced in male but not female *Ifng<sup>-/-</sup>* mice compared to controls and so was adiposity (**Figure 54a, b**). Assessment of glucose metabolism revealed no significant difference between *Ifng<sup>-/-</sup>* and control mice in both sexes (**Figure 54c**). Next HFD fed mice from the same groups were analysed. Substantially lower body and VAT weight was observed in *Ifng<sup>-/-</sup>* mice from both sexes that were fed a HFD (**Figure 54d**). The same trend was observable after calculation of adiposity, yet it did only reach statistical significance in female mice (**Figure 54e**). Assessment of glucose tolerance showed no significant difference between *Ifng<sup>-/-</sup>* and WT mice (**Figure 54f**).

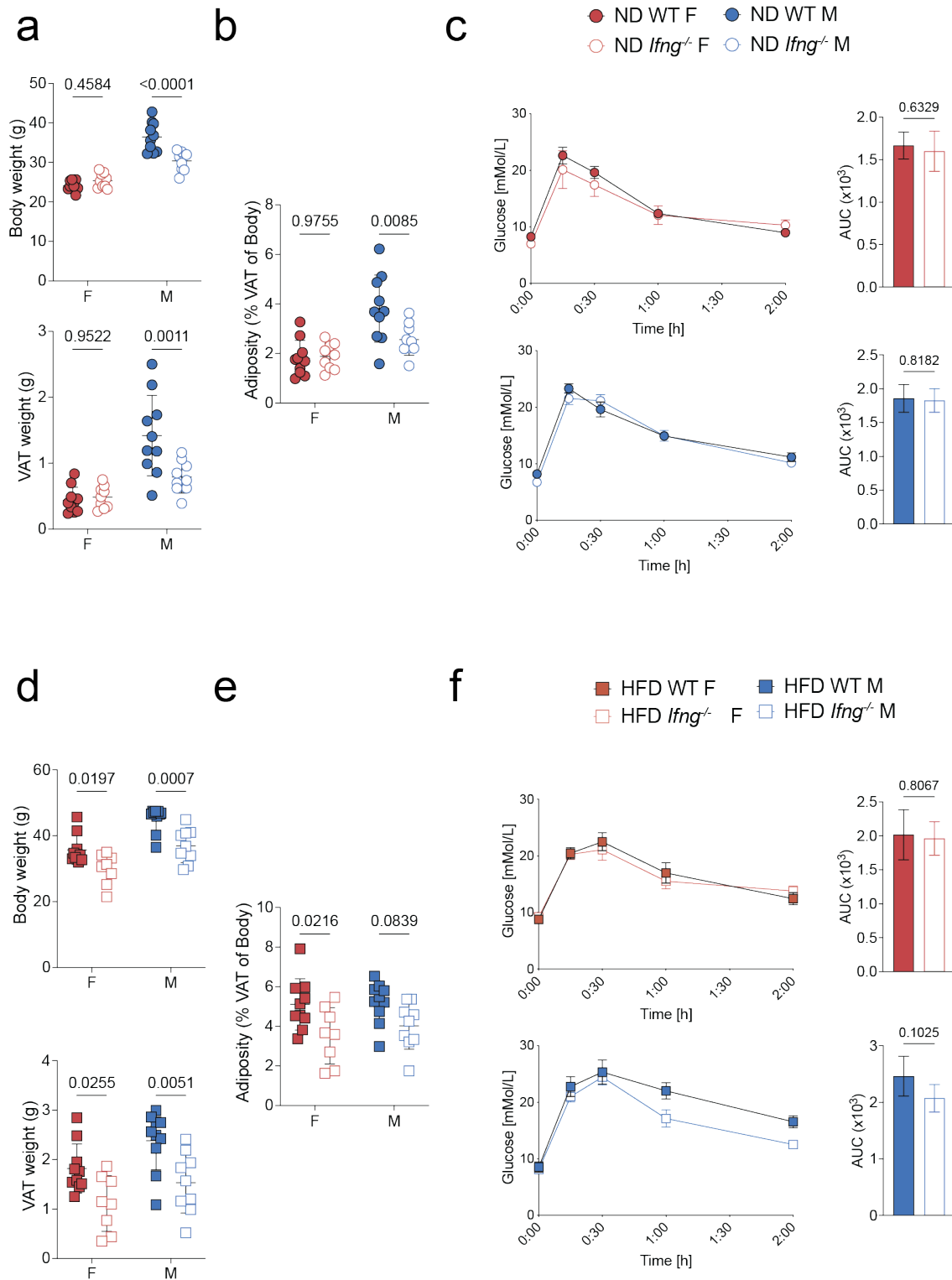


**Figure 54 | Male *lfng*<sup>-/-</sup> mice have reduced VAT and body weight compared to controls.** C57BL/6 and *lfng*<sup>-/-</sup> mice on normal chow (a-c) or high-fat diet (d-f) were subjected to metabolic testing and body and VAT weight was measured. Body and VAT weight (a, d) was measured, adiposity calculated (b, e) and glucose tolerance tests (c, f) performed on female and male mice. Symbols

represent individual mice (**a, b, d, e**) or mean of 3-5 mice (**c, f**); horizontal lines indicate means (**a, b, d, e**). Data are pooled (**a, b, d, e**) or representative (**c, f**) from two separate experiments. Error bars indicate the standard deviation (**a, b, d, e**) or s.e.m. (**c, f**). Statistical analyses were performed using two-way ANOVA (**a, b, d, e**) or unpaired, two-tailed Student's *t*-test (**c, f**).

To further expand the metabolic analysis, magnetic resonance imaging (MRI) and metabolic cages were utilised. Body composition analysis with the MRI revealed that ND male *Ifng*<sup>-/-</sup> mice have reduced lean mass compared to WT counterparts while no difference was observed in female mice or in fat mass from both sexes (**Figure 55a**). Furthermore, with the use of metabolic cages respiratory exchange ratio (RER), locomotion and food intake were measured over the course of a 24h period (**Figure 55b-d**). The RER value is calculated by dividing the volume of CO<sub>2</sub> produced by the volume of O<sub>2</sub> consumed and indicates what fuel is used for energy production. An RER of 1.0 means that carbon is primarily used and a value of 0.7 indicates that fat is used as an energy source (Marvyn, 2016, Ramos-Jimenez, 2008). Values in between mean that it's a mix of carbon and fat. Analysis of the curves and averages showed that RER was equivalent in *Ifng*<sup>-/-</sup> and WT mice (**Figure 55b**). Interestingly, regardless of sex or diet, the RER was notably lower during daytime and increased at night-time. Pedestrian locomotion measurement showed that *Ifng*<sup>-/-</sup> mice moved less during the night compared to WT while there was no difference during daytime (**Figure 55c**). Furthermore, no difference in food intake was observed between female *Ifng*<sup>-/-</sup> and WT mice. However, male IFN- $\gamma$ -deficient mice ingested significantly less food compared to their WT counterparts (**Figure 55d**).

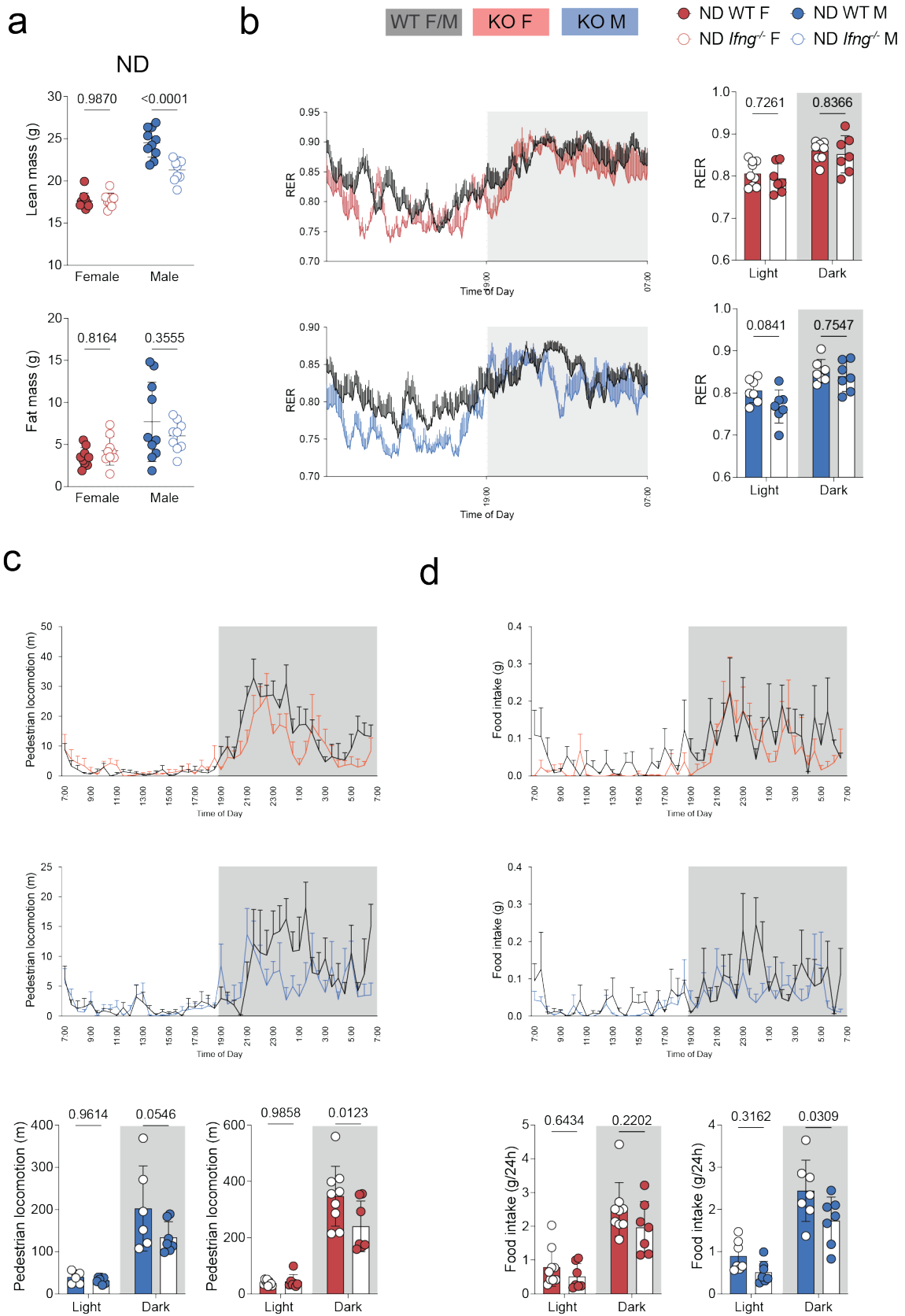


**Figure 55 | Male *Ifng*<sup>-/-</sup> mice have reduced lean mass compared to controls. Body composition and various metabolic parameters were measured from**

C57BL/6 and *Ifng*<sup>-/-</sup> female and male mice on normal chow. **a**, Body composition analysis of lean and fat mass from WT and *Ifng*<sup>-/-</sup> mice. **b-d**, RER (**b**), pedestrian locomotion (**c**) and food consumption (**d**) are depicted over a 24h time period or as an average from metabolic cage analysis. Symbols represent individual mice (**a**) or mean of 3-5 mice (**b-d**); horizontal lines indicate means (**a**). Data are representative (**b-d**) or pooled (**a**) from two separate experiments. Error bars indicate the standard deviation (**a**) or s.e.m. (**b-d**). Statistical analyses were performed using two-way ANOVA.

Body composition analysis showed that HFD fed *Ifng*<sup>-/-</sup> mice had reduced lean and fat mass compared to WT mice in both sexes (**Figure 56a**). Determination of RER did not show any significant difference between IFN- $\gamma$ -deficient and -sufficient mice in either sex (**Figure 56b**). However, unlike ND mice where RER is higher during night-time, RER in HFD mice stayed on average between 0.7-0.75 and did not increase at night-time. Finally, analysis of locomotion and food intake did not show any striking difference between *Ifng*<sup>-/-</sup> and WT mice of either sex (**Figure 56c, d**).

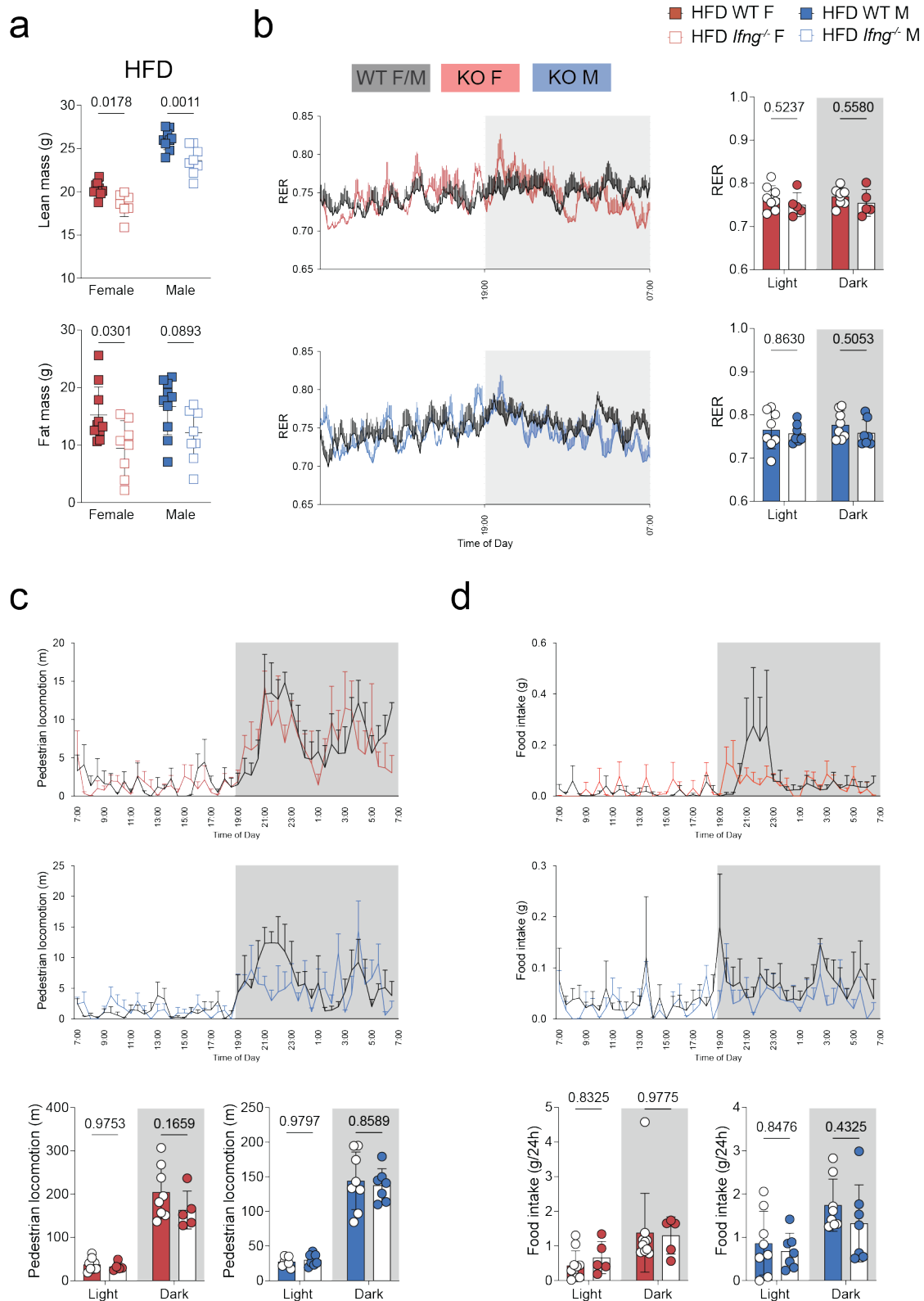


**Figure 56 | *Ifng*<sup>-/-</sup> mice have reduced lean and fat mass compared to controls on a high-fat diet.** Body composition and various metabolic parameters were measured from C57BL/6 and *Ifng*<sup>-/-</sup> female and male mice which were fed a HFD. **a**, Body composition analysis of lean and fat mass from WT and *Ifng*<sup>-/-</sup> mice. **b-d**,

RER (**b**), pedestrian locomotion (**c**) and food consumption (**d**) are depicted over a 24h time period or as an average from metabolic cage analysis. Symbols represent individual mice (**a**) or mean of 3-5 mice (**b-d**); horizontal lines indicate means (**a**). Data are representative (**b-d**) or pooled (**a**) from two separate experiments. Error bars indicate the standard deviation (**a**) or s.e.m. (**b-d**). Statistical analyses were performed using two-way ANOVA.

## 6.6 Treg cell specific PPAR $\gamma$ and GATA-3 but not T-bet depletion results in impaired glucose tolerance in male mice

Previous reports have shown that Treg specific PPAR $\gamma$  expression is important for glucose metabolism (Cipolletta et al., 2012). In line with this, body and VAT weight were significantly reduced in male, but not female *Pparg<sup>fl/fl</sup>Foxp3<sup>Cre</sup>* mice compared to controls (**Figure 57a**). Adiposity remained unchanged in both sexes (**Figure 57b**). Assessment of glucose tolerance showed that male *Pparg<sup>Foxp3Cre</sup>* mice were strikingly glucose intolerant compared to controls (**Figure 57c**). In females, PPAR $\gamma$ -deficient mice had improved glucose tolerance yet the difference, although statistically significant, was small. Next *Tbx21<sup>fl/fl</sup>Foxp3<sup>Cre</sup>* and control mice were analysed. Determination of body, VAT weight and adiposity did not show any significant difference between *Tbx21<sup>fl/fl</sup>Foxp3<sup>Cre</sup>* and control mice of either sex (**Figure 57d, e**). Glucose tolerance was increased in female, but not male *Tbx21<sup>fl/fl</sup>Foxp3<sup>Cre</sup>* mice compared to controls (**Figure 57f**). Yet the difference in female mice was very small.

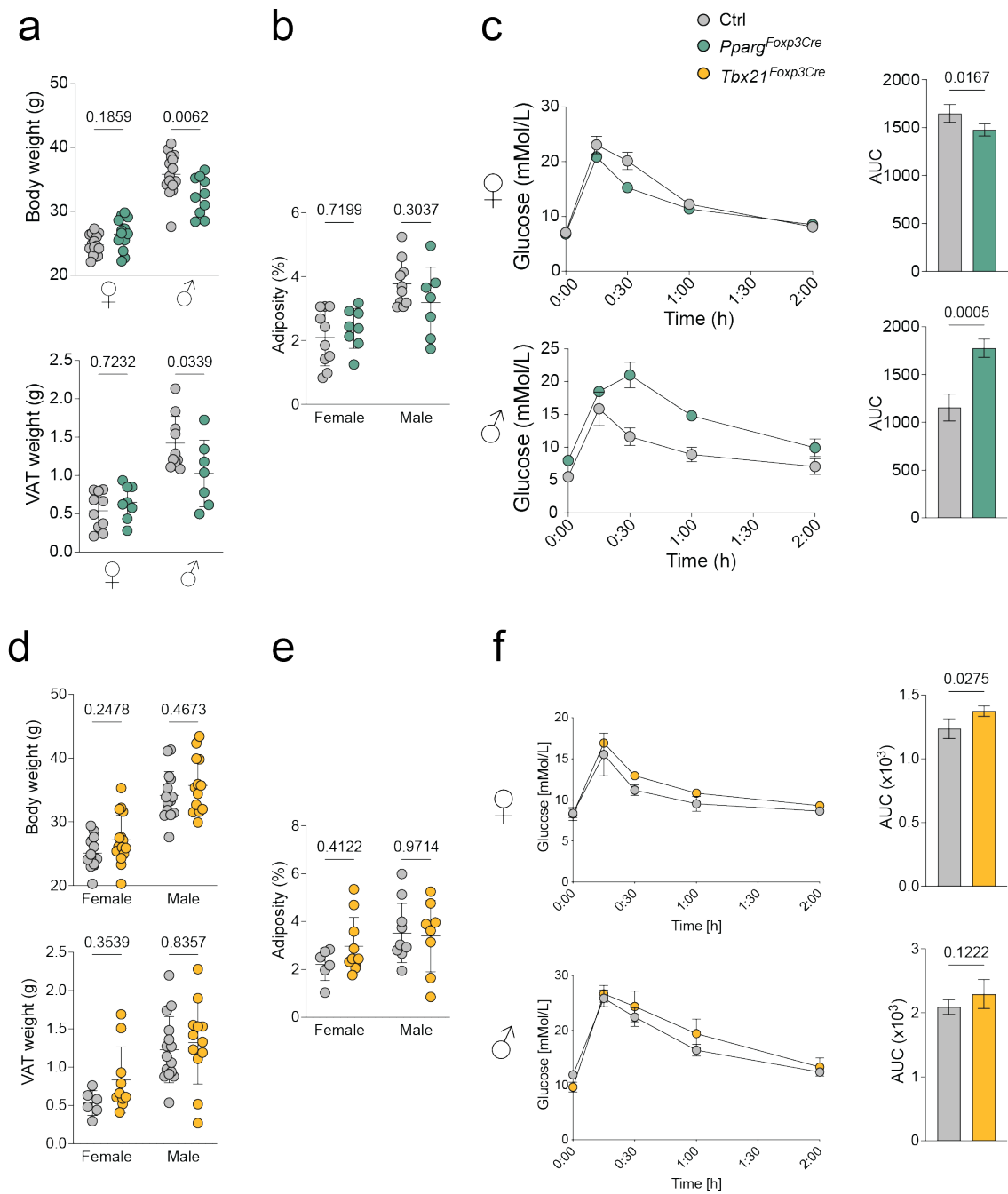


**Figure 57 | ST2+ and CXCR3+ VAT Treg cells regulate different aspects of VAT physiology and metabolism.** **a-c**, Analysis of 25–30-week-old *Pparg<sup>fl/fl</sup>Foxp3<sup>Cre</sup>* (**a-c**), *Tbx21<sup>fl/fl</sup>Foxp3<sup>Cre</sup>* (**d-f**) and *Foxp3<sup>Cre</sup>* control mice. Body and VAT weight (**a, d**) was measured, adiposity calculated (**b, e**) and glucose tolerance tests (**c, f**) performed on female and male mice. Symbols represent individual mice (**a, b, d, e**) or mean of 3–5 mice (**c, f**); horizontal lines indicate means (**a, b, d, e**). Data are pooled (**a, b, d, e**) from at least two independent experiments; GTT are representative. Error bars indicate the standard deviation (**a, b, d, e**) or s.e.m. (**c, f**). Statistical analyses were performed using unpaired, two-tailed Student's *t*-test.

To fully understand role of ST2+ VAT Treg cells in glucose metabolism, further metabolic tests were performed with mice that have substantially reduced ST2+ Treg cell populations. In line with the male-specific immune phenotype in the VAT, *Gata3<sup>fl/fl</sup>Foxp3<sup>Cre</sup>* male mice only showed reduced body, VAT weight and adiposity compared to controls (**Figure 58a, b**). Surprisingly however, both, female and male, *Gata3<sup>fl/fl</sup>Foxp3<sup>Cre</sup>* mice displayed improved glucose tolerance compared to control mice (**Figure 58c**). In contrast analysis of *Tgfb2<sup>fl/fl</sup>Foxp3<sup>Cre</sup>* mice showed no significant difference in body weight. However, VAT weight and adiposity were significantly reduced in male mice only (**Figure 58d, e**). Furthermore, no significant difference was observed in glucose tolerance in *Tgfb2<sup>fl/fl</sup>Foxp3<sup>Cre</sup>* mice when compared to controls (**Figure 58f**).

Overall, the data indicated that depletion of ST2+ but not CXCR3+ VAT Treg cells impact glucose metabolism. Depletion of PPAR $\gamma$ , GATA-3 and TGF $\beta$ R2 potentially affects different ST2+ subpopulations which might explain the different outcomes in glucose metabolism. Further analyses with metabolic cages and HFD will be required to further evaluate their role, which was not possible in this study due to time-constraints.

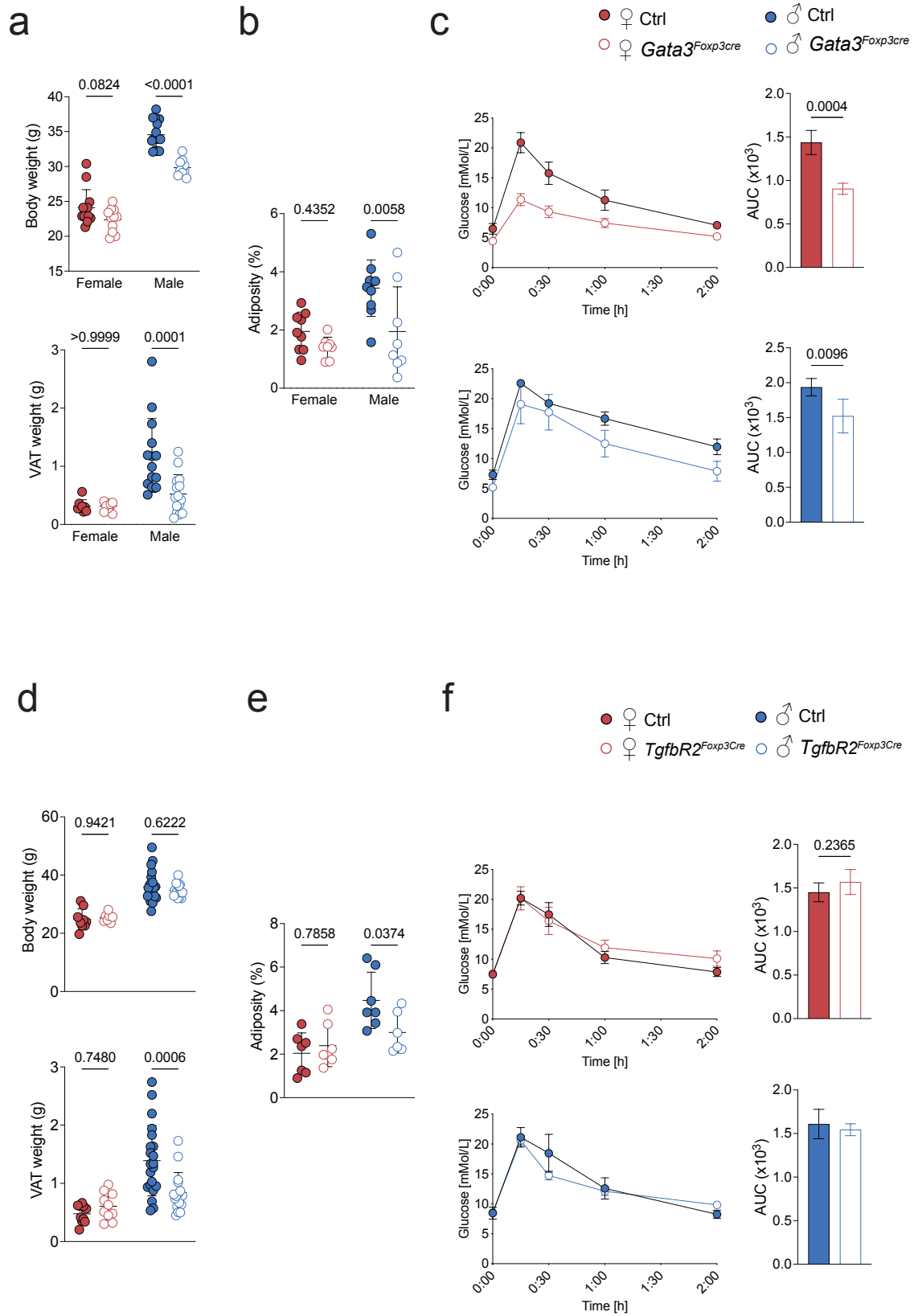


**Figure 58 | GATA-3 but not TGF $\beta$ R2 depletion affects glucose metabolism.** *Gata3<sup>fl/fl</sup>Foxp3<sup>Cre</sup>* (a-c), *TgfbR2<sup>fl/fl</sup>Foxp3<sup>Cre</sup>* (d-f) and control mice were subjected

to metabolic testing and body and VAT weight was measured. Body and VAT weight (**a, d**) was measured, adiposity calculated (**b, e**) and glucose tolerance tests (**c, f**) performed on female and male mice. Symbols represent individual mice (**a, b, d, e**) or mean of 3-5 mice (**c, f**); horizontal lines indicate means (**a, b, d, e**). Data are pooled (**a, b, d, e**) or representative (**c, f**) of at least two independent experiments. Error bars indicate the standard deviation (**a, b, d, e**) or s.e.m. (**c, f**). Statistical analyses were performed using two-way ANOVA (**a, b, d, e**) or unpaired, two-tailed Student's *t*-test (**c, f**).

## Chapter 7 – Discussion

A large body of work has uncovered the important role Treg cells play in preserving the health and function of VAT (Cipolletta et al., 2012; M. Feuerer et al., 2009; A. B. Molofsky et al., 2015; A. Vasanthakumar et al., 2015). Until the last few years, ST2<sup>+</sup> Treg cells have been described as the main population in the VAT. However, recent publications have shown evidence for Treg cell heterogeneity across several organs including the VAT (Michael Delacher et al., 2017; C. Li et al., 2018; Y. Li et al., 2021; Zemmour et al., 2018). The discovery of sex-based differences in VAT Treg cells and inflammation in our recent publication also strongly suggested the existence of other VAT Treg cell subsets. Yet a comprehensive understanding of mechanisms that control differentiation and function of ST2<sup>+</sup> VAT Treg cells and other potential subsets is still missing. In this study, two new VAT Treg cell populations that dominated the female VAT was identified and characterised. CXCR3<sup>+</sup> VAT Treg cells depend on T-bet and local IFN- $\gamma$  expression. ST2-CXCR3<sup>-</sup> (DN) Treg cells display a naïve-like phenotype and constitute potential precursor to both, ST2<sup>+</sup> and CXCR3<sup>+</sup> VAT Treg cells. Functionally, CXCR3<sup>+</sup> VAT Treg cells were required for inflammation control while ST2<sup>+</sup> VAT Treg cells are crucial to maintain glucose metabolism in a sex-specific manner. Thus, this study expands current knowledge of VAT Treg cell phenotype, function and regulation and underpins the importance of sex- and tissue-specific signals that define cell fate and function as discussed below.

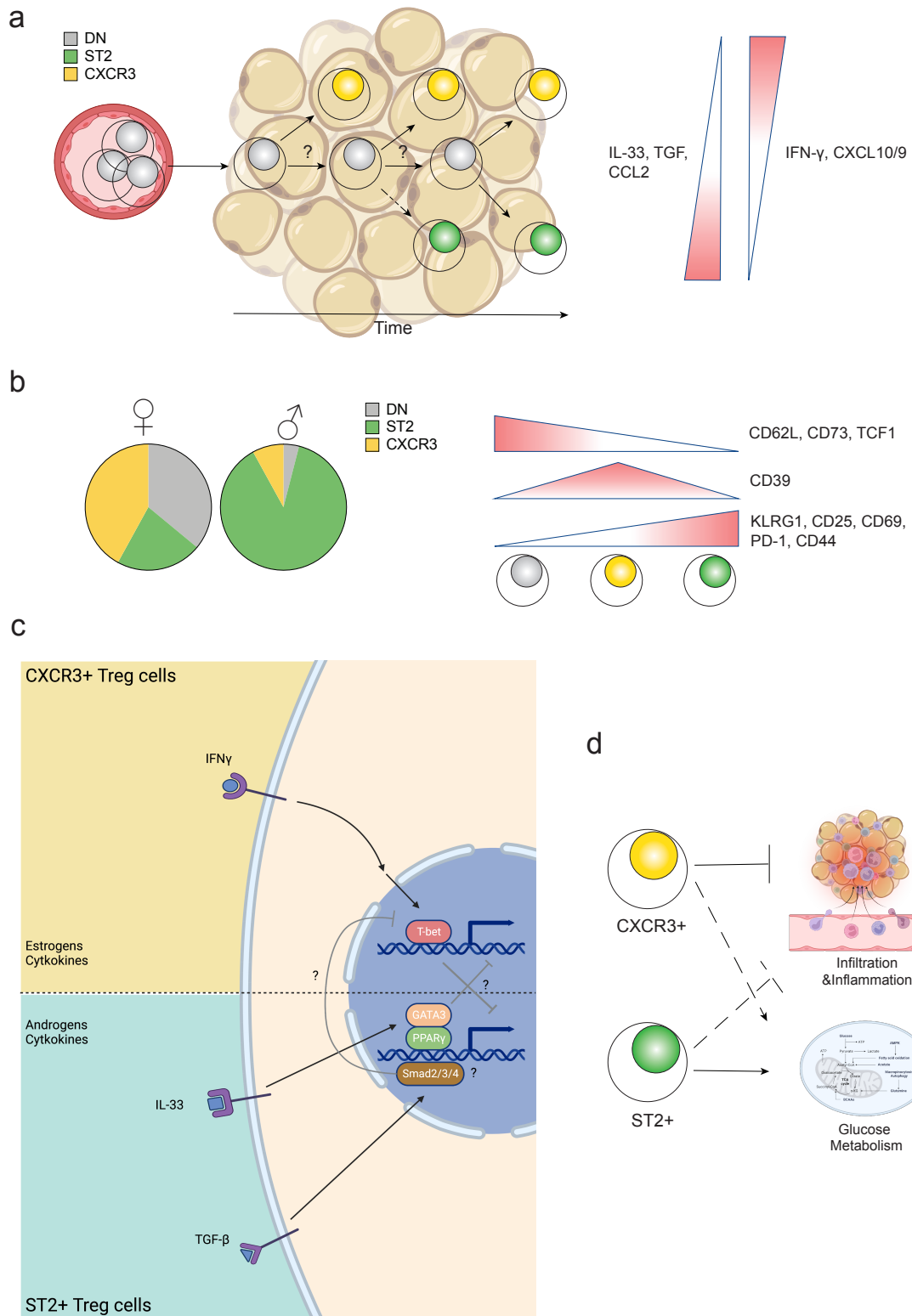


**Figure 59 | VAT Treg cell development, phenotype, and function.** **a**, DN (CD62L+) Treg cells seed the VAT at early age and quickly differentiate into CXCR3+ Treg cells in a IFN $\gamma$ -dependent manner. ST2+ Treg cells seed the VAT later in life in an IL-3e-depednet manner. **b**, Differences in the VAT microenvironment (incl. IL-33 and IFN $\gamma$  expression) results in dominance of

phenotypically distinct ST2<sup>+</sup> or CXCR3<sup>+</sup> Treg cells in male and female VAT, respectively. **c**, Differences in VAT microenvironment, incl. sex hormones and cytokines, drive activation of transcriptional machinery that induces either ST2<sup>+</sup> (PPAR $\gamma$ , GATA3) or CXCR3<sup>+</sup> (T-bet) VAT Treg cell fate. **d**, The predominant function of ST2<sup>+</sup> and CXCR3<sup>+</sup> Treg cells appear to be regulation of glucose metabolism and suppression of inflammation and cell infiltration, respectively.

## 7.1 VAT Treg cell heterogeneity

Our recent publication has suggested significant Treg cell heterogeneity in the VAT which has also been reported in other studies (C. Li et al., 2018; Vasanthakumar et al., 2020). Indeed, five different VAT Treg cell clusters were identified using sc-RNASeq from male and female mice, of which three expressed characteristic VAT (or tissue) Treg cell genes encoding for ST2, KLRG1 and CCR2. Experiments in this thesis could confirm high CCR2, KLRG1 and CD44 expression in ST2<sup>+</sup> VAT Treg cells. However, only a fraction of ST2<sup>+</sup> VAT Treg cells showed IL-10 expression on protein and transcriptional level. This could be indicative of different activation states of cells based on *Areg*, *Il10* and *Gzmb* expression which is in line with the findings from a recent study (C. Li et al., 2018). Additionally, this could be functional segregation of ST2<sup>+</sup> VAT Treg cells. *Areg* expression (highest in cluster 4) is usually associated with tissue homeostasis although it has been recently linked to macrophage-mediated insulin resistance (S. Cao et al., 2022). Expression of *Cxcl2* (highest in cluster 4) leads to recruitment of neutrophils which have been linked to promote obesity induced inflammation (Rouault et al., 2013; Watanabe et al., 2019), yet, their role in steady state is unclear considering there is only a small number of neutrophils in the VAT (Elgazar-Carmon, Rudich, Hadad, & Levy, 2008). On the other hand, previous reports have shown that Treg cells expressing *Gzmb* (highest in cluster 5) are capable to kill effector T cells and NK cells in a tumour or infection setting (X. Cao et al., 2007; C. Li, Jiang, Wei, Xu, & Wang, 2020; Loebbermann et al., 2012). Thus, cluster 5 Treg cells could protect from inflammation while cluster 4 Treg cells potentially promote it which would partly explain elevated VAT inflammation in males compared to females and the contradicting results about the role of Treg cells in the context of obesity (Sagar P. Bapat et al., 2015; Cipolletta et al., 2015; Han et al., 2015; Vasanthakumar et al., 2020; A. Vasanthakumar et al., 2015). In

lean mice, however, cluster 4 and 5 likely play a minor role, as they were underrepresented in male VAT and our results showed no significant changes in inflammation upon loss of ST2<sup>+</sup> Treg cells. The characterization of this subtypes is yet very superficial in this study and requires further investigation in the context of obesity and metabolic disease parallel with GzmB and IL-10 staining to decipher any differences in ST2<sup>+</sup> VAT Treg cell phenotype. Alternatively, sc-RNASeq of CD4<sup>+</sup> T cells in HFD fed mice could be performed to better understand the cellular changes in the context of obesity.

Unlike, ST2<sup>+</sup> cells, CXCR3<sup>+</sup> VAT Treg cells were the dominant population in female VAT. They can be further characterized by high CD39 expression and fall in the CD73<sup>+</sup> population. These membrane-bound enzymes can convert extracellular ATP, an indicator for inflammation and cell death, into adenosine, a strong immunosuppressant (Borsellino et al., 2007). Thus, CXCR3<sup>+</sup> VAT Treg cells potentially compensate their lack in IL-10 expression by producing the anti-inflammatory nucleotide adenosine to keep VAT inflammation in check. Compared to ST2<sup>+</sup> VAT Treg cells, CXCR3<sup>+</sup> VAT Treg cells had low CD25 and CD69 expression which are popular markers for early and immediately activated T cells, respectively (Ferenczi et al., 2000). Supporting this, it has been documented that TCR signalling is required for ST2<sup>+</sup> Treg cell transcriptional program (Levine et al., 2014). Supporting this, it has been documented that TCR signalling is required for ST2<sup>+</sup> Treg cell transcriptional program (Levine et al., 2014; Ajithkumar Vasanthakumar et al., 2015). Thus, CXCR3<sup>+</sup> cells potentially encounter antigen less frequently compared to ST2<sup>+</sup> cells. In line with this, recent studies have shown that CXCR3 expression negatively correlates with TCR signalling intensity in splenic and VAT Treg cells (Zemmour et al., 2018). Furthermore, a recent report has shown that ST2<sup>+</sup> Treg cells had a different TCR specificity from CXCR3 expressing cells and displayed elevated TCR activity (C. Li et al., 2018). Hence, differences in TCR usage would add another layer of regulation in ST2<sup>+</sup> and CXCR3<sup>+</sup> VAT Treg cell differentiation. Experiments such as TCR sequencing could be performed to test this hypothesis. Alternatively, *in vitro* activation of OT-II Treg cells with IL-12 and IFN- $\gamma$  (CXCR3<sup>+</sup>) or IL-33 (ST2) and varying doses/strength of OT-II specific peptide could be performed to

determine differences in TCR signalling that determine CXCR3<sup>+</sup> or ST2<sup>+</sup> Treg cell differentiation.

TCR signalling is likely less important for DN VAT Treg cells as they displayed a more naïve phenotype as measured by CD62L and CD73 expression. Moreover, intravascular staining showed that a large fraction of DN Treg cells were from circulatory origin, thus representing a population of cells *en route* or recently arrived at the VAT. Their potential role as precursors and their role in VAT Treg cell developmental trajectory is discussed in a later section.

## 7.2 Environmental factors that affect VAT Treg cell composition

### *Cytokines*

Various factors in the VAT microenvironment such as IL-33, sex-hormones and IL-17 have been shown to impact VAT Treg cell maintenance and survival (Kohlgruber et al., 2018; Vasanthakumar et al., 2020; A. Vasanthakumar et al., 2015). Increased IL-33 and IL-17A expression were found in male mice compared to female mice in gp38<sup>+</sup> MSCs and TCR $\beta$ <sup>-</sup> cells, respectively. However, our results did not show whether IL-17 in males is derived from  $\gamma\delta$  T cells, as reported by Kohlgruber and colleagues, which could be confirmed through further flow cytometric analysis (Kohlgruber et al., 2018). Depletion of IL-33 or its receptor substantially reduced ST2<sup>+</sup> VAT Treg cells in both sexes suggesting that IL-33 acts in a sex independent manner. Sex-dependent differences in androgen and IL17 availability more likely drive the sexual dichotomy through IL-33. Simultaneously, our analyses showed that IL-33 signalling interferes with CXCR3<sup>+</sup> VAT Treg cell differentiation but not proliferation. Indeed, previous studies have shown that IL-33 can induce the expression of BATF and ST2, to push the ‘tissue Treg’ transcriptional program (M. Delacher et al., 2020). Additionally, GATA-3 is inducible via IL-33 signalling and known to actively suppress IFN- $\gamma$  production thus inhibiting CXCR3<sup>+</sup> Treg cell differentiation (Ouyang et al., 1998; Usui et al., 2006).

Our experiments indeed have shown a correlation between IFN- $\gamma$  expression and CXCR3<sup>+</sup> VAT Treg cell numbers. Depletion of IFN- $\gamma$  resulted in reduction of CXCR3<sup>+</sup> VAT Treg cells in both sexes. Additionally, enhanced IFN- $\gamma$  expression in Treg depleted mice (*Foxp3<sup>DTR</sup>*) correlated with increased CXCR3<sup>+</sup> VAT Treg cell levels in females and males. This suggests that there must be a different environmental factor that drives the sex-specific difference. A significant body of work has shown that estrogens can induce IFN- $\gamma$  expression in adipocytes, DCs and iNKT cells (Gourdy et al., 2005; H. M. Lee et al., 2009; Panchanathan, Shen, Zhang, Ho, & Choubey, 2010; Siracusa, Overstreet, Housseau, Scott, & Klein, 2008). The results in this study have shown that IFN- $\gamma$  expression predominantly derived from NK1.1+TCR $\beta$ - cells and CD4<sup>+</sup> T cells, which could potentially be identified as NKT cells with additional flow cytometry experiments. Estrogen driven sex-specific differences in adipose tissue biology and autoimmune diseases such as systemic lupus erythematosus have been described in several studies and it is likely that Estrogen could promote the differentiation of CXCR3<sup>+</sup> Treg cells (Bynote et al., 2008; Cohen-Solal, Jeganathan, Grimaldi, Peeva, & B, 2006; Davis et al., 2013). This could be tested using *Er $\alpha$ <sup>-/-</sup>* mice as well as by performing mixed bone marrow chimera experiments to assess if the function of ER $\alpha$  in this instance is intrinsic to Treg cells

TGF $\beta$  is a known regulator of Treg cell development. This pleiotropic cytokine also controls multiple immunological processes including the suppression of T<sub>H</sub>1 differentiation and CXCR3 expression (Batlle & Massague, 2019). In line with this notion, Treg cell specific depletion of TGF $\beta$  signalling resulted in expansion of CXCR3<sup>+</sup> VAT Treg cells while conventional T cells (CD4<sup>+</sup>Foxp3<sup>-</sup>) remained unchanged. Mechanistically, TGF $\beta$  seems to regulate the differentiation or recruitment of Treg cells since proliferation was not affected when TGF $\beta$  signalling was perturbed in Treg cells. Furthermore, Treg cell function is disturbed partially in absence of TGF $\beta$  as shown by the expansion of CD8 T cells in males. Given CXCR3<sup>+</sup> Treg cells are enriched in females, TGF $\beta$  signalling could also be regulated by female sex hormones as reported in the female reproductive tract (Sanjabi, Oh, & Li, 2017). Considering this study focuses on perigonadal VAT, a significant impact by sex hormones, male or female is expected.

Our previous work has shown that VAT inflammation is higher in males compared to female mice which contributes to the sexual dichotomy (Vasanthakumar et al., 2020). Comparison of newly generated total VAT RNASeq data revealed sex-specific differences in gene expression of transcripts associated with tissue specific processes such as adipocyte and BAT differentiation (*Kdm5* and *Slc22a12*). The combined suppression of fibrosis promoting (*Prelp*) and insulin desensitizing (*Npr3*, *Lrg1*) and upregulation of angiogenesis and adipogenesis regulating genes (*Gata6*, *Wt1*) likely affects local VAT inflammation, oxygenation and thereby also VAT Treg cell composition.

### *Nutrients*

There is increasing evidence that tissue-specific nutrients play a significant role in regulating function and differentiation of cancer and immune cells (Kedia-Mehta & Finlay, 2019; Kumar et al., 2019). Reports have shown that Treg cell function and differentiation is impacted by e.g. vitamin, salt and oxygen levels. VAT is abundant in lipids and numerous reports have shown CD36 expression in Treg cells in the VAT, liver and tumours. CD36 is a scavenger receptor able to transport lipids across the membrane, activate PPAR $\gamma$  and thus potentially activate tissue-specific functions in ST2<sup>+</sup> VAT Treg cells (Y. Chen, Zhang, Cui, & Silverstein, 2022). Furthermore, our single cell data showed increased expression of *Hilpda* in ST2<sup>+</sup> cell which is a lipolysis promoting protein induced by hypoxia (Liu, Zhou, Zeng, Wu, & Liu, 2021). Hypoxia inducible factor (HIF) 1 $\alpha$  is required for ST2<sup>+</sup> VAT Treg cells and together with abundant lipid availability could be a mechanism by which ST2<sup>+</sup> Treg cells adapt to the VAT microenvironment (Y. Li et al., 2021). Lower ST2<sup>+</sup> VAT Treg cell levels in females could be explained by difference in local oxygen levels as estrogen promotes angiogenesis therefore preventing a hypoxic environment (Elias in & (Palmer & Clegg, 2015). Furthermore, estrogen promotes HIF1 $\alpha$  degradation and potentially intervenes with ST2<sup>+</sup> Treg cell maintenance.

The involvement of ST2<sup>+</sup> Treg cells in lipid metabolism could be assessed by measuring CD36 expression or intracellular lipid levels. Additionally, metabolomic profiling of total male and female VAT could provide more insight into sex-specific

differences in nutrient availability. To test the role of oxygen in Treg cell differentiation the proximity of ST2<sup>+</sup> and CXCR3<sup>+</sup> cells to blood vessels can be assessed. A recent study used vascular perfusion dye to determine the distance of tumour cells from the blood vessel and thereby group them into metabolic zones based on oxygen levels (Kumar et al., 2019). If successful in VAT, this method can be used to determine the relative location of Treg cells to the vascular system but also make predictions about their cellular metabolism which in turn can be expanded via detailed metabolic profiling with methods such as SCENITH on a single cell level (Arguello et al., 2020).

#### *Age and adiposity*

The VAT microenvironment and therefore local Treg cells are influenced by multiple extrinsic factors such as age, diet and sex (Grant & Dixit, 2015; Vasanthakumar et al., 2020). Our results, indeed, confirmed that the enrichment of ST2<sup>+</sup> and CXCR3<sup>+</sup> VAT Treg cells in both sexes change over time. CXCR3<sup>+</sup> VAT Treg cell levels were similar in young adult mice (7 weeks) of both sexes suggesting that sex hormone mediated differences are not in effect at this age. IFN- $\gamma$  and TNF levels were higher in young male mice compared to females supporting the notion that VAT inflammation is significantly different in early life. In females CXCR3<sup>+</sup> VAT Treg cell enrichment increases over time but not significantly. Increased IFN- $\gamma$  expression with increasing age and the ability of CXCR3<sup>+</sup> VAT Treg cells to inhibit IFN- $\gamma$ , potentially creates a balance that is sufficient to promote a T<sub>H</sub>1-like transcriptional program in Treg cells without leading to exacerbated inflammation. In contrast, the proportion of CXCR3<sup>+</sup> VAT Treg cells decreased in males over time as a consequence of ST2<sup>+</sup> cell enrichment with increasing age that has also been reported in previous studies (Cipolletta et al., 2015). Indeed, our results showed that the number of ST2<sup>+</sup> VAT Treg cells increases along with body and VAT weight in male mice. In females however, ST2<sup>+</sup> Treg cell populations rapidly declined despite accumulation of weight over time. This is likely due to missing IL-33 in mature female mice which is maybe expressed in younger females that can be determined through analysis of young *Il33<sup>Gfp</sup>* reporter mice. It is documented that IL-33 protein levels are lower

in the VAT of younger males compared to mature male mice (Ajithkumar Vasanthakumar et al., 2015). Hence, the combination of similar or even higher levels of IL-33 and no estrogen signalling is likely sufficient to maintain ST2<sup>+</sup> Treg cells in young females.

### 7.3 Development of VAT Treg cells

Several studies have investigated the differentiation pathways of VAT Treg cells (Cipolletta et al., 2012; M. Delacher et al., 2020; D Kolodin et al., 2015; C. Li et al., 2018; Y. Li et al., 2021; A. Vasanthakumar et al., 2015). The current model describes the precursors of mature VAT Treg cells as Nfil3<sup>+</sup>KLRG1<sup>+</sup>Blimp1<sup>+</sup>PPAR $\gamma$ <sup>lo</sup> effector Treg cells that develop in a IRF4 and BATF dependent manner. Upon development, these precursors migrate via a CCR2-CCL2 axis to the VAT where they adjust their transcriptional programme and expand in an IL-33 dependent manner (Cipolletta et al., 2012; M. Delacher et al., 2020; D Kolodin et al., 2015; C. Li et al., 2018; Y. Li et al., 2021; A. Vasanthakumar et al., 2015). In line with this, our results show substantial reduction of KLRG1<sup>+</sup> splenic Treg cells in PPAR $\gamma$ -depleted mice. Furthermore, Treg-specific depletion of GATA-3 has the same effect. Therefore, GATA-3 likely has an important role in regulating splenic precursor formation. Indeed, a recent study reported progressive increase in GATA-3 levels in different stages of tissue Treg cell precursors destined to colonize the VAT, colon, lung and skin (M. Delacher et al., 2020). While this model is supported by multiple lines of evidence, recent data suggested another mode of differentiation. Li and colleagues showed that peripheral CD73<sup>+</sup> Treg cells were recruited into the VAT where they developed into ST2<sup>+</sup>CD73<sup>lo</sup> Treg cells in an insulin dependent manner (Y. Li et al., 2021). Yet these studies only provide mechanisms by which ST2<sup>+</sup> VAT Treg cells migrate and populate the VAT.

Our findings offer at least two distinct pathways by which Treg cells can populate the VAT. In the first pathway, KLRG1<sup>+</sup> Treg cell precursors migrate to the VAT under homeostatic conditions where they expand proportional to increasing age and weight in an IL-33 dependent manner. Alternatively, DN Treg cells enter the

VAT still expressing CD73 but change their cellular and transcriptional profile in response to tissue specific cues to become ST2<sup>+</sup> or CXCR3<sup>+</sup> Treg cells. Our results showed that DN cells expressed low amounts of KLRG1 which could be the potential precursors for ST2<sup>+</sup> VAT Treg cells. In adoptively transferred mice there is a very high proportion of CD62L<sup>+</sup> and CD73<sup>+</sup> cells suggesting that CXCR3<sup>+</sup> and ST2<sup>+</sup> VAT Treg cells derive from DN VAT Treg cells and differentiate *in situ*. CXCR3<sup>+</sup> VAT Treg cell precursor are recruited via inflammatory cues such as IFN- $\gamma$  and CXCR3 ligand secretion to arrive the in VAT and counteract local inflammation. Thus, CXCR3<sup>+</sup> and ST2<sup>+</sup> VAT Treg cells are recruited by an inflammatory and non-inflammatory pathway, respectively, which is a concept that has been described in the generation of iTreg cells in other tissues before (Curotto de Lafaille et al., 2008).

Trajectory analysis showed that ST2<sup>+</sup> and CXCR3<sup>+</sup> VAT Treg cells derive from the same cluster, but it is unclear whether it is one or more progenitor populations that fall into the same cluster. Their vast differences in phenotype, function and molecular regulation would argue against one CXCR3<sup>+</sup> and ST2<sup>+</sup> Treg cell progenitor with single TCR specificity. Supporting this notion, recent studies have shown that resting T cells bifurcate into splenic VAT precursor populations with different TCR usage. In the TCR Tg mice expressing ST2<sup>+</sup> VAT Treg TCR, CXCR3<sup>+</sup> VAT Treg cells were significantly reduced (C. Li et al., 2018; C. Li, A. R. Munoz-Rojas, et al., 2021). Furthermore, the transcriptional profile of these precursors alluded to their potential fate as expression of *Klrg1* and *Cxcr3* transcripts were detected, respectively, suggesting that they are poised in the spleen before arriving to the VAT (C. Li, A. R. Munoz-Rojas, et al., 2021). Importantly, however, trajectory inference analysis does not guarantee that pseudotime and chronological time have a linear relationship and the analysis does not specify whether the cells maintain plasticity or not, which should be considered in the interpretation of these results (van den Berge et al, 2020).

The transcriptional profile that defines a specific set of precursor cells might be conserved in different types of T cells. Recent studies have associated higher CD62L, CD73 and TCF1 expression with progenitor or stem-like cells (Y. Li et al., 2021; J. M. Sullivan, Hollbacher, & Campbell, 2019; Tsui et al., 2022). In fact, DN

VAT Treg cells in this study expressed genes (*S1pr1*, *Itgb1*, *Nt5e*, *Sell*, *Slamf6*, *Tcf7*) that are part of the transcriptional signature of CD62L<sup>+</sup> effector CD8 T cell progenitors during chronic infection (Tsui et al., 2022).

Further analyses are required to determine how these different concepts of cell progenitors fit into our model. Most proposed models are based on male T cell biology or a combination of both sexes, hence the knowledge about female specific precursor development and TCR clonality is missing. Single cell TCR sequencing combined with lineage tracing or TCR transgenic mouse models could be used to further delineate the developmental trajectory of ST2<sup>+</sup> and CXCR3<sup>+</sup> VAT Treg cells.

## 7.4 Molecular regulation and function of VAT (tissue) Treg cells

### *PPAR $\gamma$*

A large body of work has shown that ST2 expressing VAT Treg cells are essential to maintain a healthy metabolism and restrict inflammation via IL10 (D Kolodin et al., 2015; A. Vasanthakumar et al., 2015). Surprisingly, our results show that ST2<sup>+</sup> VAT Treg depletion not always dysregulates metabolism or inflammation. PPAR $\gamma$ -mediated depletion, for example, only resulted in impaired glucose tolerance in males while no significant alteration in inflammation or T cell infiltration was detected. This contradicts previous research that has shown the significant impact of VAT Treg cell loss on VAT inflammation (C. Li, G. Wang, et al., 2021; Wu et al., 2019). A potential explanation for this could be ST2<sup>+</sup> Treg cell heterogeneity in the VAT. Apart from DN and CXCR3<sup>+</sup> VAT Treg cells, our results show three separate clusters of ST2<sup>+</sup> VAT Treg cells. PPAR $\gamma$  deletion could just affect one of these subclusters as ST2<sup>+</sup> Treg cells can still be detected in *Pparg*<sup>Foxp3cre</sup> mice. Thus, PPAR $\gamma$  promotes a subset that specializes in regulating VAT specific functions such as metabolism and adipogenesis. In line with this notion, our results showed that the most prominent genes deregulated (*Thbd*, *Cxcr4*, *Fgfbp3*, *Gpr18*, *Mettl*) in male *Pparg*<sup>Foxp3cre</sup> mice are involved in adipose tissue biology, carbohydrate and lipid metabolism (Kotanska et al., 2021; Matson & Ritter, 1999; W. Y. Park et al., 2022; Tassi et al., 2018; Y. Wang et al.,

2020). Analysis of IL-33- and ST2-deficient mice showed that ST2<sup>+</sup> VAT Treg cells are needed to prevent CD8 T cell infiltration. Both, mouse models affect the entire ST2<sup>+</sup> Treg cell population suggesting that there is a fraction of ST2<sup>+</sup> VAT Treg cells capable to suppress T cell influx in a PPAR $\gamma$ -independent manner. It is likely that PPAR $\gamma$  expressing Treg cells play a more prominent role in the context of disease. Several reports have shown that PPAR $\gamma$  expression in gut and VAT Treg cells are essential to ameliorate colitis and obesity-induced insulin resistance, respectively (Cipolletta et al., 2015; C. Li, G. Wang, et al., 2021; H. J. Park, Park, Lee, Bothwell, & Choi, 2016). Evidently, Treg specific PPAR $\gamma$  deletion was sufficient to reduce ROR $\gamma$ t<sup>+</sup> Treg cell population, important in regulating gut inflammation, yet experiments with high-fat, high-fibre diets and metabolic cage analyses are required to better understand the role of PPAR $\gamma$ <sup>+</sup> VAT Treg cells in both sexes. Furthermore, splenic PPAR $\gamma$ -depleted mice displayed sex-specific downregulation of GATA-3 in female Treg cells which opposes the dependence of PPAR $\gamma$  in male VAT. Previous reports have shown that PPAR $\gamma$  can be regulated by female hormones and impacts T cell differentiation, which should be considered when analysing multiple organs in this mouse model and assessing its impact on organismal metabolism (Park et al., 2016a; Park et al. 2016b; Klotz et al., 2009).

### *GATA-3*

Treg specific depletion of GATA-3 significantly affected Treg cells across multiple tissues which is in line with previous reports showing the involvement of GATA-3 in differentiation and function of intestinal, skin and lung Treg cells (Michael Delacher et al., 2017; Miragaia et al., 2019; Ohnmacht et al., 2015; Wohlfert et al., 2011). Indeed, decreased KLRG1 and ST2 expression was found in spleen, lung, small intestine and VAT highlighting the role of GATA-3 in the tissue Treg cell specific signature. It is well reported that GATA-3 can interact with T-bet and thereby inhibit T<sub>H</sub>1 cell differentiation which explains increased proliferation and differentiation of CXCR3<sup>+</sup> Treg cells in lung and VAT (Tindemans, Serafini, Di Santo, & Hendriks, 2014). Alternatively, this could also be CXCR3<sup>+</sup> Treg cells filling the niche that was left empty by ST2<sup>+</sup> Treg cells. Our experiments also

showed that GATA3 specific depletion induced increased CD8<sup>+</sup> T cell infiltration in both sexes and elevated IFN- $\gamma$  expression in male VAT. This contrasted the PPAR $\gamma$  phenotype suggesting that, like IL-33, GATA-3 is involved in regulating differentiation and function of all ST2<sup>+</sup> VAT Treg cells and not a specialized subset. The global impact of GATA-3 in Treg cell differentiation could also explain why *Gata3<sup>fl/fl</sup>Foxp3<sup>Cre</sup>* mice had significantly improved glucose tolerance in both sexes, despite substantially increased inflammation in the VAT. Apart from VAT and lung Treg cells, GATA3 depletion resulted in significant alterations in SI Treg cell composition including the appearance of ROR $\gamma$ t<sup>+</sup>Helios<sup>+</sup> cells that are not existent during homeostatic conditions. This likely affects the ability of local Treg cells to restrict inflammation, prevent tissue damage and thereby preventing appropriate nutrient uptake which is evidenced by lower body and VAT weight in *Gata3<sup>Foxp3cre</sup>* males. Although mice are leaner and have better glucose tolerance it does not imply that they are healthy. To evaluate this RNASeq of total VAT, blood insulin levels, intestine immunohistochemistry and measurement of inflammatory cytokines in gut, lung and other organs would be required.

### *T-bet*

Type 1 responses have been usually associated with increased VAT inflammation and insulin resistance in obesity, thus it was surprising to detect increased IFN- $\gamma$  and T-bet expression levels in female mice, considering they are typically protected from obesity-induced metabolic dysfunction (Kautzky-Willer et al., 2016; Tramunt et al., 2020). In previous studies T<sub>H</sub>1-like Treg cells have been described in pancreas, intestine, lung, and brain (Koch et al., 2009; McPherson et al., 2015; Tan et al., 2016; Yu et al., 2015). Our study shows that CXCR3<sup>+</sup>/T-bet<sup>+</sup> VAT Treg cells play a significant role in regulating VAT inflammation in both sexes by preventing expression of interferon-induced transcripts or encoding proinflammatory chemokines suggesting their role in inhibiting inflammation is sex-independent. Their function could not be replaced by expanding ST2<sup>+</sup> VAT Treg cells in *Tbx21<sup>fl/fl</sup>Foxp3<sup>Cre</sup>* mice supporting the idea that CXCR3<sup>+</sup> and ST2<sup>+</sup> VAT Treg cells have non-overlapping functions. Absence of CXCR3<sup>+</sup> VAT Treg cells had no impact on glucose tolerance in either sex. A previous study exploring

the role of pancreatic CXCR3<sup>+</sup> Treg cells showed increased insulin resistance and development of diabetes in mice lacking CXCR3<sup>+</sup> Treg cells (Tan et al., 2016). The mice analysed, however, were on a NOD (non-obese diabetic) background suggesting that CXCR3<sup>+</sup> Treg cells might have a more prominent role in glucose homeostasis in context of disease and not during homeostasis.

There are conflicting reports about the role of T<sub>H</sub>1-like Treg cells in immune responses. In line with our findings intra-tumoral T<sub>H</sub>1-like Treg cells display high suppressive capacity and are also characterized by high CTLA-4 expression. Depletion of these Treg cells in *Tbx21<sup>fl/fl</sup>Foxp3<sup>Cre</sup>* mice resulted in increased T cell activation and IFN- $\gamma$  expression which our study also showed (Colbeck et al., 2015). Furthermore, CXCR3<sup>+</sup> VAT Treg cells also express CD73 that can produce immunosuppressive adenosine. This notion is supported by recent reports showing that CD73<sup>+</sup> Treg cells have a higher suppressive capacity compared to ST2<sup>+</sup> Treg cells (Li et al., 2021). In contrast, several studies have shown that T<sub>H</sub>1-like Treg cells have impaired inhibitory functions and have been associated with autoimmune diseases such as T1D and autoimmune hepatitis (Shi & Chi, 2019).

These differences might likely depend on the context, be sex-specific and requires further investigation. To further assess the role of CXCR3<sup>+</sup> VAT Treg cells in context of disease, high-fat diet experiments are currently underway combined with metabolic cage analysis, glucose tolerance test and measurement of immune cell infiltration and cytokine production. Furthermore, Treg suppression assays combined with flow cytometry of inhibitory receptors such as GITR, CTLA-4 or PD-L1 would help determine the inhibitory capacity of CXCR3<sup>+</sup> and ST2<sup>+</sup> Treg cells in both sexes. Analysis of other organs such as pancreas, lung, small intestine and colon would likely be helpful to uncover any changes in immune cell composition or inflammation in these tissues that could impact metabolic or physiologic parameters measured in metabolic cages.

## 7.5 ST2+ and CXCR3+ VAT Treg cells in obesity

The role of VAT Treg cells in obesity has been extensively studied but their role in obesity and its associated morbidities have remained controversial (S. P. Bapat et al., 2015; Beppu et al., 2021; Cipolletta et al., 2012; M. Feuerer et al., 2009; Man et al., 2022; Wu et al., 2020). Unfortunately, the results in this study are not clear enough to evaluate the impact of VAT Treg cells on HFD and vice versa. Unlike reported in numerous studies, ST2+ VAT Treg cells are not depleted in male mice after HFD and, surprisingly, TNF and IFN- $\gamma$  expression is reduced in HFD fed mice compared to ND controls. In females and in males, correlation between ST2+, CXCR3+ VAT Treg cells and body weight is similar in ND and HFD fed mice. Meaning that changes in ST2+ or CXCR3+ VAT Treg cell composition is a function of weight gain independent of the diet. Combined with the substantial variation in cellular and metabolic phenotype across the experiments no reasonable conclusions could be made about the role of HFD in CXCR3+ and ST2+ VAT Treg cell differentiation and function. However, more extensive analysis of the data from a different angle could help resolve the experimental variation. Correlation between glucose tolerance test outcomes weight gain to determine the mice in which HFD consumption has led to impairment of glucose homeostasis. In this context, the occurrence of metabolically healthy obesity (MHO) will have to be taken into consideration which is characterized by low adipose stress and inflammation compared to pathogenic obesity (Bluher, 2020). One way to exclude MHO would be to compare immune cell infiltration and cytokine levels in mice on a HFD to ND controls and filter them accordingly. The combined correlation of cellular and metabolic data could help separate metabolically healthy and unhealthy animals which was not achievable any more in this study.

Although no significant changes were observed during HFD, the current results do not fit to the T<sub>H</sub>1/T<sub>H</sub>2 paradigm of obesity. While a type 2 cytokine environment is necessary to maintain a healthy metabolic phenotype in males, IFN- $\gamma$ , a type 1 cytokine, is prominent in the microenvironment of healthy female mice. Indeed, women display increased production of IFN and more robust T<sub>H</sub>1 and estrogens

are capable to induce IFN- $\gamma$  production (Gourdy et al., 2005; Lee et al., 2009; Panchanathan, Shen, Zhang, Ho, & Choubey, 2010; Siracusa, Overstreet, Housseau, Scott, & Klein, 2008). Hence this relationship – male (Type 2) vs female (Type 1) – might be preserved yet requires further experiments in human and mice to validate.

ST2<sup>+</sup> and CXCR3<sup>+</sup> VAT Treg cells are likely relevant in obesity considering the functional data presented in this study. Furthermore, in omental adipose tissue from human subjects both, *Tbx21* and *I1r11* transcripts, encoding for T-bet and ST2, respectively, have been detected suggesting conserved VAT Treg cell heterogeneity in mice and human (A. Vasanthakumar et al., 2015; Wu et al., 2019)

## 7.6 Conclusion

In this study a novel population of VAT Treg cell has been identified and characterised. The newly identified CXCR3<sup>+</sup> Treg cells are dominant in female VAT as opposed to the canonical ST2<sup>+</sup> Treg cells, which are enriched in male VAT. Our experiments have shown that the two VAT Treg cell populations have different developmental trajectory but derive from a population of naïve CD62L<sup>+</sup>CD73<sup>hi</sup> VAT Treg cells. Furthermore, the data revealed higher expression of type 1 cytokines, especially IFN- $\gamma$ , in females that contribute to CXCR3<sup>+</sup> VAT Treg cell differentiation. ST2<sup>+</sup> VAT Treg cells on the other hand require IL-33 and TGF $\beta$  signalling. Mechanistically, ST2<sup>+</sup> VAT Treg cell differentiation was regulated by PPAR $\gamma$  and GATA-3 and competes with CXCR3<sup>+</sup> VAT Treg cells and its transcriptional regulator T-bet. Additionally, loss-of-function experiments show that CXCR3<sup>+</sup> VAT Treg cells are crucial to prevent excessive inflammation and T cell infiltration. ST2<sup>+</sup> VAT Treg cells are more important for regulating glucose and lipid metabolism. Overall, this study has helped to discover and characterize a new VAT Treg cell subset and characterize female and male inflammatory landscape that will help have a superior understanding of adipose biology and immunity in a sex-specific manner and

move forward development of tailored treatments for diabetes and metabolic syndrome.

## References

- Al-Dwairi, A., Pabona, J. M., Simmen, R. C., & Simmen, F. A. (2012). Cytosolic malic enzyme 1 (ME1) mediates high fat diet-induced adiposity, endocrine profile, and gastrointestinal tract proliferation-associated biomarkers in male mice. *PLoS One*, *7*(10), e46716. doi:10.1371/journal.pone.0046716
- Ali, N., Zirak, B., Rodriguez, R. S., Pauli, M. L., Truong, H.-A., Lai, K., . . . Rosenblum, M. D. (2017). Regulatory T Cells in Skin Facilitate Epithelial Stem Cell Differentiation. *Cell*, *169*(6), 1119-1129.e1111. doi:10.1016/j.cell.2017.05.002
- Anderson, K. G., Mayer-Barber, K., Sung, H., Beura, L., James, B. R., Taylor, J. J., . . . Masopust, D. (2014). Intravascular staining for discrimination of vascular and tissue leukocytes. *Nat Protoc*, *9*(1), 209-222. doi:10.1038/nprot.2014.005
- Arguello, R. J., Combes, A. J., Char, R., Gigan, J. P., Baaziz, A. I., Bousiquot, E., . . . Pierre, P. (2020). SCENITH: A Flow Cytometry-Based Method to Functionally Profile Energy Metabolism with Single-Cell Resolution. *Cell Metab*, *32*(6), 1063-1075 e1067. doi:10.1016/j.cmet.2020.11.007
- Arnetz, L., Rajamand Ekberg, N., & Alvarsson, M. (2014). Sex differences in type 2 diabetes: focus on disease course and outcomes. *Diabetes, Metabolic Syndrome and Obesity: Targets and Therapy*, 409. doi:10.2147/dms.o.s51301
- Atarashi, K., Tanoue, T., Shima, T., Imaoka, A., Kuwahara, T., Momose, Y., . . . Honda, K. (2011). Induction of colonic regulatory T cells by indigenous Clostridium species. *Science*, *331*(6015).
- Bapat, S. P., Myoung Suh, J., Fang, S., Liu, S., Zhang, Y., Cheng, A., . . . Zheng, Y. (2015). Depletion of fat-resident Treg cells prevents age-associated insulin resistance. *Nature*, *528*(7580), 137-141. doi:10.1038/nature16151
- Bapat, S. P., Myoung Suh, J., Fang, S., Liu, S., Zhang, Y., Cheng, A., . . . Zheng, Y. (2015). Depletion of fat-resident Treg cells prevents age-associated insulin resistance. *Nature*, *528*(7580), 137-141. doi:10.1038/nature16151
- Battle, E., & Massague, J. (2019). Transforming Growth Factor-beta Signaling in Immunity and Cancer. *Immunity*, *50*(4), 924-940. doi:10.1016/j.immuni.2019.03.024
- Belkaid, Y., & Tarbell, K. (2009). Regulatory T cells in the control of host-microorganism interactions (\*). *Annu Rev Immunol*, *27*, 551-589. doi:10.1146/annurev.immunol.021908.132723
- Bennett, C., Christie, J., Ramsdell, F., Brunkow, M., Ferguson, P., Whitesell, L., . . . Ochs, H. (2001). The immune dysregulation, polyendocrinopathy, enteropathy, X-linked syndrome (IPEX) is caused by mutations of FOXP3. *Nature Genetics*.

- Beppu, L. Y., Mooli, R. G. R., Qu, X., Marrero, G. J., Finley, C. A., Fooks, A. N., . . . D'Cruz, L. M. (2021). Tregs facilitate obesity and insulin resistance via a Blimp-1/IL-10 axis. *JCI Insight*, *6*(3). doi:10.1172/jci.insight.140644
- Bertola, A., Ciucci, T., Rousseau, D., Bourlier, V., Duffaut, C., Bonnafous, S., . . . Wakkach, A. (2012). Identification of Adipose Tissue Dendritic Cells Correlated With Obesity-Associated Insulin-Resistance and Inducing Th17 Responses in Mice and Patients. *Diabetes*, *61*(9), 2238-2247. doi:10.2337/db11-1274
- Bin Dhuban, K., Kornete, M., Mason, E., & Piccirillo, C. (2014). Functional dynamics of Foxp3<sup>+</sup> regulatory T cells in mice and humans. *Immunological Reviews*, *259*(1).
- Bluher, M. (2020). Metabolically Healthy Obesity. *Endocr Rev*, *41*(3). doi:10.1210/edrv/bnaa004
- Bonilla, W. V., Fröhlich, A., Senn, K., Kallert, S., Fernandez, M., Johnson, S., . . . Pinschewer, D. D. (2012). The Alarmin Interleukin-33 Drives Protective Antiviral CD8<sup>+</sup> T Cell Responses. *Science*, *335*(6071), 984-989. doi:10.1126/science.1215418
- Borsellino, G., Kleinewietfeld, M., Di Mitri, D., Sternjak, A., Diamantini, A., Giometto, R., . . . Falk, K. (2007). Expression of ectonucleotidase CD39 by Foxp3<sup>+</sup> Treg cells: hydrolysis of extracellular ATP and immune suppression. *Blood*, *110*(4), 1225-1232. doi:10.1182/blood-2006-12-064527
- Boulenouar, S., Michelet, X., Duquette, D., Alvarez, D., Hogan, A. E., Dold, C., . . . Lynch, L. (2017). Adipose Type One Innate Lymphoid Cells Regulate Macrophage Homeostasis through Targeted Cytotoxicity. *Immunity*, *46*(2), 273-286. doi:10.1016/j.immuni.2017.01.008
- Brestoff, J. R., Kim, B. S., Saenz, S. A., Stine, R. R., Monticelli, L. A., Sonnenberg, G. F., . . . Artis, D. (2015). Group 2 innate lymphoid cells promote beiging of adipose and limit obesity. *Nature*, *519*(7542), 242-246. doi:10.1038/nature14115
- Brunkow, M., Jeffery, E., Hjerrild, K., Paepfer, B., Clark, L., Yasayko, S., . . . Ramsdell, F. (2001). Disruption of a new forkhead/winged-helix protein, scurfy, results in the fatal lymphoproliferative disorder of the scurfy mouse. *Nature Genetics*.
- Brussaard, H. E., Leuven, J. A. G., Fr, X000F, Lich, M., Kluft, C., & Krans, H. M. J. (1997). Short-term oestrogen replacement therapy improves insulin resistance, lipids and fibrinolysis in postmenopausal women with NIDDM. *Diabetologia*, *40*(7), 843-849. doi:10.1007/s001250050758
- Bunis, D. G., Andrews, J., Fragiadakis, G. K., Burt, T. D., & Sirota, M. (2020). dittoSeq: Universal User-Friendly Single-Cell and Bulk RNA Sequencing Visualization Toolkit. *Bioinformatics*. doi:10.1093/bioinformatics/btaa1011
- Burzyn, D., Benoist, C., & Mathis, D. (2013). Regulatory T cells in nonlymphoid tissues. *Nat Immunol*, *14*(10), 1007-1013. doi:10.1038/ni.2683
- Bynote, K. K., Hackenberg, J. M., Korach, K. S., Lubahn, D. B., Lane, P. H., & Gould, K. A. (2008). Estrogen receptor-alpha deficiency attenuates autoimmune disease in (NZB x NZW)F1 mice. *Genes Immun*, *9*(2), 137-152. doi:10.1038/sj.gene.6364458
- Camhi, S. M., Bray, G. A., Bouchard, C., Greenway, F. L., Johnson, W. D., Newton, R. L., . . . Katzmarzyk, P. T. (2011). The Relationship of Waist Circumference and BMI

- to Visceral, Subcutaneous, and Total Body Fat: Sex and Race Differences. *Obesity*, 19(2), 402-408. doi:10.1038/oby.2010.248
- Cao, J., Spielmann, M., Qiu, X., Huang, X., Ibrahim, D. M., Hill, A. J., . . . Shendure, J. (2019). The single-cell transcriptional landscape of mammalian organogenesis. *Nature*, 566(7745), 496-502. doi:10.1038/s41586-019-0969-x
- Cao, S., Pan, Y., Tang, J., Terker, A. S., Arroyo Ornelas, J. P., Jin, G. N., . . . Zhang, M. Z. (2022). EGFR-mediated activation of adipose tissue macrophages promotes obesity and insulin resistance. *Nat Commun*, 13(1), 4684. doi:10.1038/s41467-022-32348-3
- Cao, X., Cai, S. F., Fehniger, T. A., Song, J., Collins, L. I., Piwnica-Worms, D. R., & Ley, T. J. (2007). Granzyme B and perforin are important for regulatory T cell-mediated suppression of tumor clearance. *Immunity*, 27(4), 635-646. doi:10.1016/j.immuni.2007.08.014
- Cayrol, C., & Girard, J.-P. (2018). Interleukin-33 (IL-33): A nuclear cytokine from the IL-1 family. *Immunological Reviews*, 281(1), 154-168. doi:10.1111/imr.12619
- Chaudhry, A., & Rudensky, A. Y. (2013). Control of inflammation by integration of environmental cues by regulatory T cells. *Immunity*, 38(3), 939-944. doi:10.1016/j.immuni.2013.02.001
- Chen, J.-Q., Cammarata, P. R., Baines, C. P., & Yager, J. D. (2009). Regulation of mitochondrial respiratory chain biogenesis by estrogens/estrogen receptors and physiological, pathological and pharmacological implications. *Biochim Biophys Acta*, 1793(10), 1540-1570. doi:10.1016/j.bbamcr.2009.06.001
- Chen, S., Fan, J., Zhang, M., Qin, L., Dominguez, D., Long, A., . . . Zhang, B. (2019). CD73 expression on effector T cells sustained by TGF-beta facilitates tumor resistance to anti-4-1BB/CD137 therapy. *Nat Commun*, 10(1), 150. doi:10.1038/s41467-018-08123-8
- Chen, Y., Zhang, J., Cui, W., & Silverstein, R. L. (2022). CD36, a signaling receptor and fatty acid transporter that regulates immune cell metabolism and fate. *J Exp Med*, 219(6). doi:10.1084/jem.20211314
- Chensue, S. W., Lukacs, N. W., Yang, T.-Y., Shang, X., Frait, K. A., Kunkel, S. L., . . . Lira, S. A. (2001). Aberrant in Vivo T Helper Type 2 Cell Response and Impaired Eosinophil Recruitment in Cc Chemokine Receptor 8 Knockout Mice. *J Exp Med*, 193(5), 573-584. doi:10.1084/jem.193.5.573
- Chusyd, D. E., Wang, D., Huffman, D. M., & Nagy, T. R. (2016). Relationships between Rodent White Adipose Fat Pads and Human White Adipose Fat Depots. *Front Nutr*, 3, 10. doi:10.3389/fnut.2016.00010
- Cildir, G., Akincilar, S. C., & Tergaonkar, V. (2013). Chronic adipose tissue inflammation: all immune cells on the stage. *Trends Mol Med*, 19(8), 487-500. doi:10.1016/j.molmed.2013.05.001
- Cinti, S. (2012). The adipose organ at a glance. *Cell*, 150(5), 588-594. doi:10.1016/j.cell.2012.05.001
- Cipolletta, D., Cohen, P., Spiegelman, B. M., Benoist, C., & Mathis, D. (2015). Appearance and disappearance of the mRNA signature characteristic of Treg cells in visceral adipose tissue: age, diet, and PPARgamma effects. *Proc Natl Acad Sci U S A*, 112(2), 482-487. doi:10.1073/pnas.1423486112

- Cipolletta, D., Feuerer, M., Li, A., Kamei, N., Lee, J., Shoelson, S. E., . . . Mathis, D. (2012). PPAR-gamma is a major driver of the accumulation and phenotype of adipose tissue Treg cells. *Nature*, *486*(7404), 549-553. doi:10.1038/nature11132
- Clegg, D. J., Brown, L. M., Woods, S. C., & Benoit, S. C. (2006). Gonadal Hormones Determine Sensitivity to Central Leptin and Insulin. *55*(4), 978-987. doi:10.2337/diabetes.55.04.06.db05-1339
- Cohen-Solal, J., Jeganathan, V., Grimaldi, C., Peeva, E., & B, D. (2006). Sex hormones and SLE: influencing the fate of autoreactive B cells. *Current Topic Microbiology Immunology*.
- Colbeck, E., Hindley, J., Smart, K., Jones, E., Bloom, A., Bridgeman, H., . . . Gallimore, A. (2015). Eliminating roles for T-bet and IL-2 but revealing superior activation and proliferation as mechanisms underpinning dominance of regulatory T cells in tumors. *Oncotarget*, *6*(28).
- Coombes, J. L., Siddiqui, K. R., Arancibia-Carcamo, C. V., Hall, J., Sun, C. M., Belkaid, Y., & Powrie, F. (2007). A functionally specialized population of mucosal CD103+ DCs induces Foxp3+ regulatory T cells via a TGF-beta and retinoic acid-dependent mechanism. *J Exp Med*, *204*(8), 1757-1764. doi:10.1084/jem.20070590
- Corbould, A. (2007). Chronic testosterone treatment induces selective insulin resistance in subcutaneous adipocytes of women. *Journal of Endocrinology*, *192*(3), 585-594. doi:10.1677/joe.1.07070
- Cretney, E., Kallies, A., & Nutt, S. L. (2013a). Differentiation and function of Foxp3+ effector regulatory T cells. *34*(2), 74-80. doi:10.1016/j.it.2012.11.002
- Cretney, E., Kallies, A., & Nutt, S. L. (2013b). Differentiation and function of Foxp3+ effector regulatory T cells. *Trends in Immunology*, *34*(2), 74-80. doi:10.1016/j.it.2012.11.002
- Cretney, E., Xin, A., Shi, W., Minnich, M., Masson, F., Miasari, M., . . . Kallies, A. (2011). The transcription factors Blimp-1 and IRF4 jointly control the differentiation and function of effector regulatory T cells. *Nat Immunol*, *12*(4), 304-311. doi:10.1038/ni.2006
- Curotto de Lafaille, M. A., Kutchukhidze, N., Shen, S., Ding, Y., Yee, H., & Lafaille, J. J. (2008). Adaptive Foxp3+ regulatory T cell-dependent and -independent control of allergic inflammation. *Immunity*, *29*(1), 114-126. doi:10.1016/j.immuni.2008.05.010
- Dalmas, E., Venteclef, N., Caer, C., Poitou, C., Cremer, I., Aron-Wisnewsky, J., . . . Guerre-Millo, M. (2014). T Cell-Derived IL-22 Amplifies IL-1 $\beta$ -Driven Inflammation in Human Adipose Tissue: Relevance to Obesity and Type 2 Diabetes. *Diabetes*, *63*(6), 1966-1977. doi:10.2337/db13-1511
- Davis, K. E., M, D. N., Sun, K., W, M. S., J, D. B., J, A. Z., . . . Clegg, D. J. (2013). The sexually dimorphic role of adipose and adipocyte estrogen receptors in modulating adipose tissue expansion, inflammation, and fibrosis. *Mol Metab*, *2*(3), 227-242. doi:10.1016/j.molmet.2013.05.006
- DeFuria, J., Belkina, A. C., Jagannathan-Bogdan, M., Snyder-Cappione, J., Carr, J. D., Nersesova, Y. R., . . . Nikolajczyk, B. S. (2013). B cells promote inflammation in

- obesity and type 2 diabetes through regulation of T-cell function and an inflammatory cytokine profile. *Proc Natl Acad Sci U S A*, 110(13), 5133-5138. doi:10.1073/pnas.1215840110
- Deiuliis, J., Shah, Z., Shah, N., Needleman, B., Mikami, D., Narula, V., . . . Rajagopalan, S. (2011). Visceral Adipose Inflammation in Obesity Is Associated with Critical Alterations in Tregulatory Cell Numbers. *PLoS One*, 6(1), e16376. doi:10.1371/journal.pone.0016376
- Delacher, M., Imbusch, C. D., Hotz-Wagenblatt, A., Mallm, J. P., Bauer, K., Simon, M., . . . Feuerer, M. (2020). Precursors for Nonlymphoid-Tissue Treg Cells Reside in Secondary Lymphoid Organs and Are Programmed by the Transcription Factor BATF. *Immunity*, 52(2), 295-312 e211. doi:10.1016/j.immuni.2019.12.002
- Delacher, M., Imbusch, C. D., Weichenhan, D., Breiling, A., Hotz-Wagenblatt, A., Träger, U., . . . Feuerer, M. (2017). Genome-wide DNA-methylation landscape defines specialization of regulatory T cells in tissues. *Nature Immunology*, 18(10), 1160-1172. doi:10.1038/ni.3799
- Derry, J., Wiedemann, P., Blair, P., Wang, Y., Kerns, J., Lemahieu, V., . . . Francke, U. (1995). The mouse homolog of the Wiskott-Aldrich syndrome protein (WASP) gene is highly conserved and maps near the scurfy (sf) mutation on the X chromosome. *Genomics*, 29(2).
- Ding, E. L., Song, Y., Malik, V. S., & Liu, S. (2006). Sex Differences of Endogenous Sex Hormones and Risk of Type 2 Diabetes. *JAMA*, 295(11), 1288. doi:10.1001/jama.295.11.1288
- DiSpirito, J. R., & Mathis, D. (2015). Immunological contributions to adipose tissue homeostasis. *Semin Immunol*, 27(5), 315-321. doi:10.1016/j.smim.2015.10.005
- Dispirito, J. R., & Mathis, D. (2015). Immunological contributions to adipose tissue homeostasis. *Seminars in Immunology*, 27(5), 315-321. doi:10.1016/j.smim.2015.10.005
- Dobin, A., Davis, C. A., Schlesinger, F., Drenkow, J., Zaleski, C., Jha, S., . . . Gingeras, T. R. (2013). STAR: ultrafast universal RNA-seq aligner. *Bioinformatics*, 29(1), 15-21. doi:10.1093/bioinformatics/bts635
- Dombrowski, Y., O'Hagan, T., Dittmer, M., Penalva, R., Mayoral, S. R., Bankhead, P., . . . Fitzgerald, D. C. (2017). Regulatory T cells promote myelin regeneration in the central nervous system. *Nat Neurosci*, 20(5), 674-680. doi:10.1038/nn.4528
- Duhen, T., Duhen, R., Lanzavecchia, A., Sallusto, F., & Campbell, D. J. (2012). Functionally distinct subsets of human FOXP3+ Treg cells that phenotypically mirror effector Th cells. *119*(19), 4430-4440. doi:10.1182/blood-2011-11-392324
- Duhen, T., Duhen, R., Montler, R., Moses, J., Moudgil, T., de Miranda, N. F., . . . Weinberg, A. D. (2018). Co-expression of CD39 and CD103 identifies tumor-reactive CD8 T cells in human solid tumors. *Nat Commun*, 9(1), 2724. doi:10.1038/s41467-018-05072-0
- Elbers, J. M. H., Asscheman, H., Seidell, J. C., Megens, J. A. J., & Gooren, L. J. G. (1997). Long-Term Testosterone Administration Increases Visceral Fat in Female to Male Transsexuals 1. *The Journal of Clinical Endocrinology & Metabolism*, 82(7), 2044-2047. doi:10.1210/jcem.82.7.4078

- Elgazar-Carmon, V., Rudich, A., Hadad, N., & Levy, R. (2008). Neutrophils transiently infiltrate intra-abdominal fat early in the course of high-fat feeding. *J Lipid Res*, *49*(9), 1894-1903. doi:10.1194/jlr.M800132-JLR200
- Eller, K., Kirsch, A., Wolf, A. M., Sopper, S., Tagwerker, A., Stanzl, U., . . . Eller, P. (2011). Potential Role of Regulatory T Cells in Reversing Obesity-Linked Insulin Resistance and Diabetic Nephropathy. *Diabetes*, *60*(11), 2954-2962. doi:10.2337/db11-0358
- Evans, M. J., Eckert, A., Lai, K., Adelman, S. J., & Harnish, D. C. (2001). Reciprocal Antagonism Between Estrogen Receptor and NF- $\kappa$ B Activity In Vivo. *Circ Res*, *89*(9), 823-830. doi:doi:10.1161/hh2101.098543
- Ferenczi, K., Burack, L., Pope, M., Krueger, J., & Austin, L. (2000). CD69, HLA-DR and the IL-2R identify persistently activated T cells in psoriasis vulgaris lesional skin: blood and skin comparisons by flow cytometry. *Journal of Autoimmunity*, *14*(1).
- Ferrante, A. W. (2013). Macrophages, fat, and the emergence of immunometabolism. *Journal of Clinical Investigation*, *123*(12), 4992-4993. doi:10.1172/jci73658
- Feuerer, M., Herrero, L., Cipolletta, D., Naaz, A., Wong, J., Nayer, A., . . . Mathis, D. (2009). Lean, but not obese, fat is enriched for a unique population of regulatory T cells that affect metabolic parameters. *Nature Medicine*, *15*(8), 930-939. doi:10.1038/nm.2002
- Feuerer, M., Herrero, L., Cipolletta, D., Naaz, A., Wong, J., Nayer, A., . . . Mathis, D. (2009). Lean, but not obese, fat is enriched for a unique population of regulatory T cells that affect metabolic parameters. *Nat Med*, *15*(8), 930-939. doi:10.1038/nm.2002
- Finotto, S., Neurath, M. F., Glickman, J. N., Qin, S., Lehr, H. A., Green, F. H. Y., . . . Glimcher, L. H. (2002). Development of Spontaneous Airway Changes Consistent with Human Asthma in Mice Lacking T-bet. *Science*, *295*(5553), 336-338. doi:10.1126/science.1065544
- Fontana, L., Eagon, J. C., Trujillo, M. E., Scherer, P. E., & Klein, S. (2007). Visceral Fat Adipokine Secretion Is Associated With Systemic Inflammation in Obese Humans. *Diabetes*, *56*(4), 1010-1013. doi:10.2337/db06-1656
- Fontenot, J. D., Gavin, M. A., & Rudensky, A. Y. (2003). Foxp3 programs the development and function of CD4+CD25+ regulatory T cells. *Nature Immunology*, *4*(4), 330-336. doi:10.1038/ni904
- Fuente-Martín, E., Argente-Arizón, P., Ros, P., Argente, J., & Chowen, J. A. (2013a). Sex differences in adipose tissue. *Adipocyte*, *2*(3), 128-134. doi:10.4161/adip.24075
- Fuente-Martín, E., Argente-Arizón, P., Ros, P., Argente, J., & Chowen, J. A. (2013b). Sex differences in adipose tissue. *Adipocyte*, *2*(3), 128-134. doi:10.4161/adip.24075
- Gabriely, I., Ma, X. H., Yang, X. M., Atzmon, G., Rajala, M. W., Berg, A. H., . . . Barzilai, N. (2002). Removal of Visceral Fat Prevents Insulin Resistance and Glucose Intolerance of Aging: An Adipokine-Mediated Process? , *Diabetes*, *51*(10), 2951-2958. doi:10.2337/diabetes.51.10.2951
- Galic, S., Oakhill, J. S., & Steinberg, G. R. (2010). Adipose tissue as an endocrine organ. *Mol Cell Endocrinol*, *316*(2), 129-139. doi:10.1016/j.mce.2009.08.018
- Gavin, K. M., Cooper, E. E., & Hickner, R. C. (2013). Estrogen receptor protein content is different in abdominal than gluteal subcutaneous adipose tissue of overweight-

- to-obese premenopausal women. *Metabolism*, 62(8), 1180-1188.  
doi:10.1016/j.metabol.2013.02.010
- Gavin, K. M., Cooper, E. E., Raymer, D. K., & Hickner, R. C. (2013). Estradiol effects on subcutaneous adipose tissue lipolysis in premenopausal women are adipose tissue depot specific and treatment dependent. *Am J Physiol Endocrinol Metab*, 304(11), E1167-1174. doi:10.1152/ajpendo.00023.2013
- Geuking, M. B., Cahenzli, J., Lawson, M. A., Ng, D. C., Slack, E., Hapfelmeier, S., . . . Macpherson, A. J. (2011). Intestinal bacterial colonization induces mutualistic regulatory T cell responses. *Immunity*, 34(5), 794-806.  
doi:10.1016/j.immuni.2011.03.021
- Gil-Ortega, M., Garidou, L., Barreau, C., Maumus, M., Breasson, L., Tavernier, G., . . . Sengenès, C. (2013). Native adipose stromal cells egress from adipose tissue in vivo: evidence during lymph node activation. *Stem Cells*, 31(7), 1309-1320.  
doi:10.1002/stem.1375
- Giordano, A., Frontini, A., & Cinti, S. (2016). Convertible visceral fat as a therapeutic target to curb obesity. *Nat Rev Drug Discov*, 15(6), 405-424.  
doi:10.1038/nrd.2016.31
- Girousse, A., Gil-Ortega, M., Bourlier, V., Bergeaud, C., Sastourne-Arrey, Q., Moro, C., . . . Sengenès, C. (2019). The Release of Adipose Stromal Cells from Subcutaneous Adipose Tissue Regulates Ectopic Intramuscular Adipocyte Deposition. *Cell Rep*, 27(2), 323-333 e325. doi:10.1016/j.celrep.2019.03.038
- Glimcher, L. H., Townsend, M. J., Sullivan, B. M., & Lord, G. M. (2004). Recent developments in the transcriptional regulation of cytolytic effector cells. 4(11), 900-911. doi:10.1038/nri1490
- Goodman-Gruen, D., & Barrett-Connor, E. (1996). Sex Differences in Measures of Body Fat and Body Fat Distribution in the Elderly. *American Journal of Epidemiology*, 143(9), 898-906. doi:10.1093/oxfordjournals.aje.a008833
- Gourdy, P., Araujo, L. M., Zhu, R., Garmy-Susini, B., Diem, S., Laurell, H., . . . Herbelin, A. (2005). Relevance of sexual dimorphism to regulatory T cells: estradiol promotes IFN-gamma production by invariant natural killer T cells. *Blood*, 105(6), 2415-2420. doi:10.1182/blood-2004-07-2819
- Grant, R. W., & Dixit, V. D. (2015). Adipose tissue as an immunological organ. *Obesity*, 23(3), 512-518. doi:10.1002/oby.21003
- Groom, J. R., Richmond, J., Murooka, T. T., Sorensen, E. W., Sung, J. H., Bankert, K., . . . Luster, A. D. (2012). CXCR3 chemokine receptor-ligand interactions in the lymph node optimize CD4+ T helper 1 cell differentiation. *Immunity*, 37(6), 1091-1103. doi:10.1016/j.immuni.2012.08.016
- Hafemeister, C., & Satija, R. (2019). Normalization and variance stabilization of single-cell RNA-seq data using regularized negative binomial regression. *Genome Biol*, 20(1), 296. doi:10.1186/s13059-019-1874-1
- Halim, L., Romano, M., McGregor, R., Correa, I., Pavlidis, P., Grageda, N., . . . Lombardi, G. (2017). An Atlas of Human Regulatory T Helper-like Cells Reveals Features of Th2-like Tregs that Support a Tumorigenic Environment. *Cell Rep*, 20(3), 757-770. doi:10.1016/j.celrep.2017.06.079

- Han, J. M., Wu, D., Denroche, H. C., Yao, Y., Verchere, C. B., & Levings, M. K. (2015). IL-33 Reverses an Obesity-Induced Deficit in Visceral Adipose Tissue ST2+ T Regulatory Cells and Ameliorates Adipose Tissue Inflammation and Insulin Resistance. *194*(10), 4777-4783. doi:10.4049/jimmunol.1500020
- Heine, P. A., Taylor, J. A., Iwamoto, G. A., Lubahn, D. B., & Cooke, P. S. (2000). Increased adipose tissue in male and female estrogen receptor-alpha knockout mice. *Proceedings of the National Academy of Sciences*, *97*(23), 12729-12734. doi:10.1073/pnas.97.23.12729
- Heinzel, F., Sadick, M., Holaday, B., Coffman, R., & Locksley, R. (1989). Reciprocal expression of interferon gamma or interleukin 4 during the resolution or progression of murine leishmaniasis. Evidence for expansion of distinct helper T cell subsets. *Journal of Experimental Medicine*, *169*(1).
- Hill, J. A., Feuerer, M., Tash, K., Haxhinasto, S., Perez, J., Melamed, R., . . . Benoist, C. (2007). Foxp3 transcription-factor-dependent and -independent regulation of the regulatory T cell transcriptional signature. *Immunity*, *27*(5), 786-800. doi:10.1016/j.immuni.2007.09.010
- Ho, I. C., Lo, D., & Glimcher, L. H. (1998). c-maf Promotes T Helper Cell Type 2 (Th2) and Attenuates Th1 Differentiation by Both Interleukin 4-dependent and -independent Mechanisms. *188*(10), 1859-1866. doi:10.1084/jem.188.10.1859
- Hori, S., Nomura, T., & Sakaguchi, S. (2003). Control of regulatory T cell development by the transcription factor Foxp3. *Science*, *299*(5609).
- Hotamisligil, G., Shargill, N., & Spiegelman, B. (1993). Adipose expression of tumor necrosis factor-alpha: direct role in obesity-linked insulin resistance. *Science*, *259*(5091), 87-91. doi:10.1126/science.7678183
- Hovhannisyan, Z., Treatman, J., Littman, D. R., & Mayer, L. (2011). Characterization of interleukin-17-producing regulatory T cells in inflamed intestinal mucosa from patients with inflammatory bowel diseases. *Gastroenterology*, *140*(3), 957-965. doi:10.1053/j.gastro.2010.12.002
- Hsieh, C., Macatonia, S., O'Garra, A., & Murphy, K. (1995). T cell genetic background determines default T helper phenotype development in vitro. *Journal of Experimental Medicine*, *181*(2).
- Hu, W., Wang, Z. M., Feng, Y., Schizas, M., Hoyos, B. E., van der Veecken, J., . . . Rudensky, A. Y. (2021). Regulatory T cells function in established systemic inflammation and reverse fatal autoimmunity. *Nat Immunol*, *22*(9), 1163-1174. doi:10.1038/s41590-021-01001-4
- Hwang, E. S., Szabo, S. J., Schwartzberg, P. L., & Glimcher, L. H. (2005). T Helper Cell Fate Specified by Kinase-Mediated Interaction of T-bet with GATA-3. *Science*, *307*(5708), 430-433. doi:10.1126/science.1103336
- Ichikawa, T., Hirahara, K., Kokubo, K., Kiuchi, M., Aoki, A., Morimoto, Y., . . . Nakayama, T. (2019). CD103(hi) Treg cells constrain lung fibrosis induced by CD103(lo) tissue-resident pathogenic CD4 T cells. *Nat Immunol*, *20*(11), 1469-1480. doi:10.1038/s41590-019-0494-y
- Ioan-Facsinay, A., Kwekkeboom, J. C., Westhoff, S., Giera, M., Rombouts, Y., Van Harmelen, V., . . . Toes, R. E. M. (2013). Adipocyte-derived lipids modulate

- CD4+T-cell function. *European Journal of Immunology*, 43(6), 1578-1587.  
doi:10.1002/eji.201243096
- Ito, M., Komai, K., Mise-Omata, S., Iizuka-Koga, M., Noguchi, Y., Kondo, T., . . . Yoshimura, A. (2019). Brain regulatory T cells suppress astrogliosis and potentiate neurological recovery. *Nature*, 565(7738), 246-250.  
doi:10.1038/s41586-018-0824-5
- Jackson-Jones, L. H., Duncan, S. M., Magalhaes, M. S., Campbell, S. M., Maizels, R. M., McSorley, H. J., . . . Benezech, C. (2016). Fat-associated lymphoid clusters control local IgM secretion during pleural infection and lung inflammation. *Nat Commun*, 7, 12651. doi:10.1038/ncomms12651
- Jaensson-Gyllenback, E., Kotarsky, K., Zapata, F., Persson, E. K., Gundersen, T. E., Blomhoff, R., & Agace, W. W. (2011). Bile retinoids imprint intestinal CD103+ dendritic cells with the ability to generate gut-tropic T cells. *Mucosal Immunol*, 4(4), 438-447. doi:10.1038/mi.2010.91
- Jensen, M. D., Haymond, M. W., Rizza, R. A., Cryer, P. E., & Miles, J. M. (1989). Influence of body fat distribution on free fatty acid metabolism in obesity. *Journal of Clinical Investigation*, 83(4), 1168-1173. doi:10.1172/jci113997
- Ji, Z., & Ji, H. (2016). TSCAN: Pseudo-time reconstruction and evaluation in single-cell RNA-seq analysis. *Nucleic Acids Res*, 44(13), e117. doi:10.1093/nar/gkw430
- Jin, H. S., Park, Y., Elly, C., & Liu, Y. C. (2013). Itch expression by Treg cells controls Th2 inflammatory responses. *J Clin Invest*, 123(11), 4923-4934.  
doi:10.1172/JCI69355
- Jones, E. A., & Flavell, R. A. (2005). Distal Enhancer Elements Transcribe Intergenic RNA in the IL-10 Family Gene Cluster. *The Journal of Immunology*, 175(11), 7437-7446. doi:10.4049/jimmunol.175.11.7437
- Josefowicz, S. Z., Lu, L. F., & Rudensky, A. Y. (2012). Regulatory T cells: mechanisms of differentiation and function. *Annu Rev Immunol*, 30, 531-564.  
doi:10.1146/annurev.immunol.25.022106.141623
- Kalekar, L., Cohen, J., Prevel, N., Sandoval, P., Mathur, A., Moreau, J., . . . Rosenblum, M. (2019). Regulatory T cells in skin are uniquely poised to suppress profibrotic immune responses. *Science Immunology*, 39(4).
- Kang, S. G., Lim, H. W., Andrisani, O. M., Broxmeyer, H. E., & Kim, C. H. (2007). Vitamin A metabolites induce gut-homing FoxP3+ regulatory T cells. *J Immunol*, 179(6), 3724-3733. doi:10.4049/jimmunol.179.6.3724
- Kanhere, A., Hertweck, A., Bhatia, U., Gökmen, M. R., Perucha, E., Jackson, I., . . . Jenner, R. G. (2012). T-bet and GATA3 orchestrate Th1 and Th2 differentiation through lineage-specific targeting of distal regulatory elements. *Nat Commun*, 3, 1268. doi:10.1038/ncomms2260
- Karastergiou, K., Fried, S. K., Xie, H., Lee, M.-J., Divoux, A., Rosencrantz, M. A., . . . Smith, S. R. (2013). Distinct Developmental Signatures of Human Abdominal and Gluteal Subcutaneous Adipose Tissue Depots. *The Journal of Clinical Endocrinology & Metabolism*, 98(1), 362-371. doi:10.1210/jc.2012-2953
- Karastergiou, K., Smith, S. R., Greenberg, A. S., & Fried, S. K. (2012). Sex differences in human adipose tissues – the biology of pear shape. *Biology of Sex Differences*, 3(1), 13. doi:10.1186/2042-6410-3-13

- Karbiener, M., Glantschnig, C., Pisani, D. F., Laurencikiene, J., Dahlman, I., Herzig, S., . . . Scheideler, M. (2015). Mesoderm-specific transcript (MEST) is a negative regulator of human adipocyte differentiation. *Int J Obes (Lond)*, *39*(12), 1733-1741. doi:10.1038/ijo.2015.121
- Kautzky-Willer, A., Harreiter, J., & Pacini, G. (2016). Sex and Gender Differences in Risk, Pathophysiology and Complications of Type 2 Diabetes Mellitus. *Endocrine Reviews*, *37*(3), 278-316. doi:10.1210/er.2015-1137
- Kedia-Mehta, N., & Finlay, D. K. (2019). Competition for nutrients and its role in controlling immune responses. *Nat Commun*, *10*(1), 2123. doi:10.1038/s41467-019-10015-4
- Kershaw, E. E., & Flier, J. S. (2004). Adipose tissue as an endocrine organ. *J Clin Endocrinol Metab*, *89*(6), 2548-2556. doi:10.1210/jc.2004-0395
- Kim, J. M., Rasmussen, J. P., & Rudensky, A. Y. (2007). Regulatory T cells prevent catastrophic autoimmunity throughout the lifespan of mice. *Nat Immunol*, *8*(2), 191-197. doi:10.1038/ni1428
- Kim, K., Hong, S., Han, D., Yi, J., Jung, J., Yang, B., . . . Surh, C. (2016). Dietary antigens limit mucosal immunity by inducing regulatory T cells in the small intestine. *2016*, *35*(6275).
- Kleinjan, A., Klein Wolterink, R. G. J., Levani, Y., De Bruijn, M. J. W., Hoogsteden, H. C., Van Nimwegen, M., & Hendriks, R. W. (2014). Enforced Expression of Gata3 in T Cells and Group 2 Innate Lymphoid Cells Increases Susceptibility to Allergic Airway Inflammation in Mice. *The Journal of Immunology*, *192*(4), 1385-1394. doi:10.4049/jimmunol.1301888
- Koch, M. A., Tucker-Heard, G. S., Perdue, N. R., Killebrew, J. R., Urdahl, K. B., & Campbell, D. J. (2009). The transcription factor T-bet controls regulatory T cell homeostasis and function during type 1 inflammation. *Nature Immunology*, *10*(6), 595-602. doi:10.1038/ni.1731
- Kohlgruber, A. C., Gal-Oz, S. T., Lamarche, N. M., Shimazaki, M., Duquette, D., Koay, H.-F., . . . Lynch, L. (2018).  $\gamma\delta$  T cells producing interleukin-17A regulate adipose regulatory T cell homeostasis and thermogenesis. *Nature Immunology*, *19*(5), 464-474. doi:10.1038/s41590-018-0094-2
- Kolodin, D., van Panhuys, N., Li, C., Magnuson, A., Cipolletta, D., Miller, C., . . . Mathis, D. (2015). Antigen- and Cytokine-Driven Accumulation of Regulatory T Cells in Visceral Adipose Tissue of Lean Mice. *21*(4), 543-557. doi:10.1016/j.cmet.2015.03.005
- Kolodin, D., van Panhuys, N., Li, C., Magnuson, A. M., Cipolletta, D., Miller, C. M., . . . Mathis, D. (2015). Antigen- and cytokine-driven accumulation of regulatory T cells in visceral adipose tissue of lean mice. *Cell Metab*, *21*(4), 543-557. doi:10.1016/j.cmet.2015.03.005
- Komatsu, N., Mariotti-Ferrandiz, M. E., Wang, Y., Malissen, B., Waldmann, H., & Hori, S. (2009). Heterogeneity of natural Foxp3<sup>+</sup> T cells: a committed regulatory T-cell lineage and an uncommitted minor population retaining plasticity. *Proc Natl Acad Sci U S A*, *106*(6), 1903-1908. doi:10.1073/pnas.0811556106
- Konkel, J. E., Zhang, D., Zanvit, P., Chia, C., Zangarle-Murray, T., Jin, W., . . . Chen, W. (2017). Transforming Growth Factor-beta Signaling in Regulatory T Cells

- Controls T Helper-17 Cells and Tissue-Specific Immune Responses. *Immunity*, 46(4), 660-674. doi:10.1016/j.immuni.2017.03.015
- Korn, T., Reddy, J., Gao, W., Bettelli, E., Awasthi, A., Petersen, T. R., . . . Kuchroo, V. K. (2007). Myelin-specific regulatory T cells accumulate in the CNS but fail to control autoimmune inflammation. *Nat Med*, 13(4), 423-431. doi:10.1038/nm1564
- Koster, A., Stenholm, S., Alley, D. E., Kim, L. J., Simonsick, E. M., Kanaya, A. M., . . . Harris, T. B. (2010). Body Fat Distribution and Inflammation Among Obese Older Adults With and Without Metabolic Syndrome. *Obesity*, 18(12), 2354-2361. doi:10.1038/oby.2010.86
- Kotanska, M., Mika, K., Szafarz, M., Kubacka, M., Muller, C. E., Sapa, J., & Kiec-Kononowicz, K. (2021). Effects of GPR18 Ligands on Body Weight and Metabolic Parameters in a Female Rat Model of Excessive Eating. *Pharmaceuticals (Basel)*, 14(3). doi:10.3390/ph14030270
- Kraakman, M. J., Kammoin, H. L., Allen, T. L., Deswaerte, V., Henstridge, D., Estevez, E., . . . A., M. (2015). Blocking IL-6 trans-Signaling Prevents High-Fat Diet-Induced Adipose Tissue Macrophage Recruitment but Does Not Improve Insulin Resistance. 21(3), 403-416. doi:10.1016/j.cmet.2015.02.006
- Kraakman, M. J., Kammoun, H. L., Allen, T. L., Deswaerte, V., Henstridge, D. C., Estevez, E., . . . Febbraio, M. A. (2015). Blocking IL-6 trans-signaling prevents high-fat diet-induced adipose tissue macrophage recruitment but does not improve insulin resistance. *Cell Metab*, 21(3), 403-416. doi:10.1016/j.cmet.2015.02.006
- Krishnamoorthy, N., Khare, A., Oriss, T. B., Raundhal, M., Morse, C., Yarlagadda, M., . . . Ray, P. (2012). Early infection with respiratory syncytial virus impairs regulatory T cell function and increases susceptibility to allergic asthma. *Nat Med*, 18(10), 1525-1530. doi:10.1038/nm.2896
- Kumar, S., Sharife, H., Kreisel, T., Mogilevsky, M., Bar-Lev, L., Grunewald, M., . . . Keshet, E. (2019). Intra-Tumoral Metabolic Zonation and Resultant Phenotypic Diversification Are Dictated by Blood Vessel Proximity. *Cell Metab*, 30(1), 201-211 e206. doi:10.1016/j.cmet.2019.04.003
- Kuswanto, W., Burzyn, D., Panduro, M., Wang, K. K., Jang, Y. C., Wagers, A. J., . . . Mathis, D. (2016). Poor Repair of Skeletal Muscle in Aging Mice Reflects a Defect in Local, Interleukin-33-Dependent Accumulation of Regulatory T Cells. *Immunity*, 44(2), 355-367. doi:10.1016/j.immuni.2016.01.009
- Kuswanto, W., Burzyn, D., Panduro, M., Wang, K. K., Jang, Y. C., Wagers, A. J., . . . Mathis, D. (2016). Poor Repair of Skeletal Muscle in Aging Mice Reflects a Defect in Local, Interleukin-33-Dependent Accumulation of Regulatory T Cells. *Immunity*, 44(2), 355-367. doi:10.1016/j.immuni.2016.01.009
- Law, C. W., Chen, Y., Shi, W., & Smyth, G. K. (2014). Voom: precision weights unlock linear model analysis tools for RNA-seq read counts. *Genome Biol*, 15(2), R29. doi:10.1186/gb-2014-15-2-r29
- Lazarevic, V., Chen, X., Shim, J.-H., Hwang, E.-S., Jang, E., Bolm, A. N., . . . Glimcher, L. H. (2011). T-bet represses TH17 differentiation by preventing Runx1-mediated activation of the gene encoding ROR $\gamma$ t. 12(1), 96-104. doi:10.1038/ni.1969

- Lee, C. C., Kasa-Vubu, J. Z., & Supiano, M. A. (2003). Differential Effects of Raloxifene and Estrogen on Insulin Sensitivity in Postmenopausal Women. *Journal of American Geriatrics Society*, *51*(5), 683-688. doi:10.1034/j.1600-0579.2003.00214.x
- Lee, H. M., Mima, T., Sugino, H., Aoki, C., Adachi, Y., Yoshio-Hoshino, N., . . . Nishimoto, N. (2009). Interactions among type I and type II interferon, tumor necrosis factor, and beta-estradiol in the regulation of immune response-related gene expressions in systemic lupus erythematosus. *Arthritis Res Ther*, *11*(1), R1. doi:10.1186/ar2584
- Levine, A. G., Arvey, A., Jin, W., & Rudensky, A. Y. (2014). Continuous requirement for the TCR in regulatory T cell function. *Nat Immunol*, *15*(11), 1070-1078. doi:10.1038/ni.3004
- Levine, A. G., Mendoza, A., Hemmers, S., Moltedo, B., Niec, R. E., Schizas, M., . . . Rudensky, A. Y. (2017). Stability and function of regulatory T cells expressing the transcription factor T-bet. *Nature*, *546*(7658), 421-425. doi:10.1038/nature22360
- Li, C., DiSpirito, J. R., Zemmour, D., Spallanzani, R. G., Kuswanto, W., Benoist, C., & Mathis, D. (2018). TCR Transgenic Mice Reveal Stepwise, Multi-site Acquisition of the Distinctive Fat-Treg Phenotype. *Cell*, *174*(2), 285-299 e212. doi:10.1016/j.cell.2018.05.004
- Li, C., Jiang, P., Wei, S., Xu, X., & Wang, J. (2020). Regulatory T cells in tumor microenvironment: new mechanisms, potential therapeutic strategies and future prospects. *Mol Cancer*, *19*(1), 116. doi:10.1186/s12943-020-01234-1
- Li, C., Munoz-Rojas, A. R., Wang, G., Mann, A. O., Benoist, C., & Mathis, D. (2021). PPARgamma marks splenic precursors of multiple nonlymphoid-tissue Treg compartments. *Proc Natl Acad Sci U S A*, *118*(13). doi:10.1073/pnas.2025197118
- Li, C., Wang, G., Sivasami, P., Ramirez, R. N., Zhang, Y., Benoist, C., & Mathis, D. (2021). Interferon-alpha-producing plasmacytoid dendritic cells drive the loss of adipose tissue regulatory T cells during obesity. *Cell Metab*, *33*(8), 1610-1623 e1615. doi:10.1016/j.cmet.2021.06.007
- Li, M. O., Wan, Y. Y., Sanjabi, S., Robertson, A.-K. L., & Flavell, R. A. (2006). TRANSFORMING GROWTH FACTOR- $\beta$  REGULATION OF IMMUNE RESPONSES. *Annual Review of Immunology*, *24*(1), 99-146. doi:10.1146/annurev.immunol.24.021605.090737
- Li, Y., Lu, Y., Lin, S. H., Li, N., Han, Y., Huang, Q., . . . Li, B. (2021). Insulin signaling establishes a developmental trajectory of adipose regulatory T cells. *Nat Immunol*, *22*(9), 1175-1185. doi:10.1038/s41590-021-01010-3
- Liao, Y., Smyth, G. K., & Shi, W. (2013). The Subread aligner: fast, accurate and scalable read mapping by seed-and-vote. *Nucleic Acids Res*, *41*(10), e108. doi:10.1093/nar/gkt214
- Liao, Y., Smyth, G. K., & Shi, W. (2014). featureCounts: an efficient general purpose program for assigning sequence reads to genomic features. *Bioinformatics*, *30*(7), 923-930. doi:10.1093/bioinformatics/btt656

- Licona-Limón, P., Kim, L. K., Palm, N. W., & Flavell, R. A. (2013). TH2, allergy and group 2 innate lymphoid cells. *Nat Rev Immunol*, *14*(6), 536-542. doi:10.1038/ni.2617
- Liew, F. Y., Girard, J.-P., & Turnquist, H. R. (2016). Interleukin-33 in health and disease. *Nature Reviews Immunology*, *16*(11), 676-689. doi:10.1038/nri.2016.95
- Lindberg, M., Weihua, Z., Andersson, N., Movérare, S., Gao, H., Vidal, O., . . . Ohlsson, C. (2002). Estrogen receptor specificity for the effects of estrogen in ovariectomized mice. *Journal of Endocrinology*, *174*(2).
- Liston, A., & Gray, D. H. D. (2014). Homeostatic control of regulatory T cell diversity. *Nature Reviews Immunology*, *14*(3), 154-165. doi:10.1038/nri3605
- Liu, C., Zhou, X., Zeng, H., Wu, D., & Liu, L. (2021). HILPDA Is a Prognostic Biomarker and Correlates With Macrophage Infiltration in Pan-Cancer. *Front Oncol*, *11*, 597860. doi:10.3389/fonc.2021.597860
- Loebbermann, J., Thornton, H., Durant, L., Sparwasser, T., Webster, K. E., Sprent, J., . . . Openshaw, P. J. (2012). Regulatory T cells expressing granzyme B play a critical role in controlling lung inflammation during acute viral infection. *Mucosal Immunol*, *5*(2), 161-172. doi:10.1038/mi.2011.62
- Lohning, M., Stroehmann, A., Coyle, A. J., Grogan, J. L., Lin, S., Gutierrez-Ramos, J. C., . . . Kamradt, T. (1998). T1/ST2 is preferentially expressed on murine Th2 cells, independent of interleukin 4, interleukin 5, and interleukin 10, and important for Th2 effector function. *95*(12), 6930-6935. doi:10.1073/pnas.95.12.6930
- Lontchi-Yimagou, E., Kang, S., Goyal, A., Zhang, K., You, J. Y., Carey, M., . . . Hawkins, M. (2020). Insulin-sensitizing effects of vitamin D repletion mediated by adipocyte vitamin D receptor: Studies in humans and mice. *Mol Metab*, *42*, 101095. doi:10.1016/j.molmet.2020.101095
- Lord, G. M., Rao, R. M., Choe, H., Sullivan, B. M., Lichtman, A. H., Luscinskas, S. W., & Glimcher, L. H. (2005). T-bet is required for optimal proinflammatory CD4+ T-cell trafficking. *106*(10), 3432-3439. doi:10.1182/blood-2005-04-1393
- Lowe, M. M., Boothby, I., Clancy, S., Ahn, R. S., Liao, W., Nguyen, D. N., . . . Rosenblum, M. D. (2019). Regulatory T cells use arginase 2 to enhance their metabolic fitness in tissues. *JCI Insight*, *4*(24). doi:10.1172/jci.insight.129756
- Lu, Y. P., Lou, Y. R., Bernard, J. J., Peng, Q. Y., Li, T., Lin, Y., . . . Conney, A. H. (2012). Surgical removal of the parametrial fat pads stimulates apoptosis and inhibits UVB-induced carcinogenesis in mice fed a high-fat diet. *109*(23), 9065-9070. doi:10.1073/pnas.1205810109
- Lumeng, C. N., Bodzin, J. L., & Saltiel, A. R. (2007). Obesity induces a phenotypic switch in adipose tissue macrophage polarization. *Journal of Clinical Investigation*, *117*(1), 175-184. doi:10.1172/jci29881
- Lumeng, C. N., Deyoung, S. M., Bodzin, J. L., & Saltiel, A. R. (2007). Increased Inflammatory Properties of Adipose Tissue Macrophages Recruited During Diet-Induced Obesity. *Diabetes*, *56*(1), 16-23. doi:10.2337/db06-1076
- Lun, A. T. L., Riesenfeld, S., Andrews, T., Dao, T. P., Gomes, T., participants in the 1st Human Cell Atlas, J., & Marioni, J. C. (2019). EmptyDrops: distinguishing cells from empty droplets in droplet-based single-cell RNA sequencing data. *Genome Biol*, *20*(1), 63. doi:10.1186/s13059-019-1662-y

- Macotela, Y., Boucher, J., Tran, T. T., & Kahn, C. R. (2009). Sex and Depot Differences in Adipocyte Insulin Sensitivity and Glucose Metabolism. *Diabetes*, *58*(4), 803-812. doi:10.2337/db08-1054
- Malhotra, N. L.-C., Juan Manuel; Jadhav, Unmesh; Barreiro, Olga; Kam, Christy; O'Neill, Nicholas K. (2018). ROR $\alpha$ -expressing T regulatory cells restrain allergic skin inflammation. *Science Immunology*, *3*.
- Man, K., Kallies, A., & Vasanthakumar, A. (2022). Resident and migratory adipose immune cells control systemic metabolism and thermogenesis. *Cell Mol Immunol*, *19*(3), 421-431. doi:10.1038/s41423-021-00804-7
- Manolopoulos, K. N., Karpe, F., & Frayn, K. N. (2010). Gluteofemoral body fat as a determinant of metabolic health. *International Journal of Obesity*, *34*(6), 949-959. doi:10.1038/ijo.2009.286
- Mathis, D. (2013). Immunological Goings-on in Visceral Adipose Tissue. *17*(6), 851-859. doi:10.1016/j.cmet.2013.05.008
- Mathis, D. (2013). Immunological goings-on in visceral adipose tissue. *Cell Metab*, *17*(6), 851-859. doi:10.1016/j.cmet.2013.05.008
- Mathis, D. (2016). IL-33, Imprimatur of Adipocyte Thermogenesis. *166*(4), 794-795. doi:10.1016/j.cell.2016.07.051
- Matson, C. A., & Ritter, R. C. (1999). Long-term CCK-leptin synergy suggests a role for CCK in the regulation of body weight. *Am J Physiol*, *276*(4), R1038-1045. doi:10.1152/ajpregu.1999.276.4.R1038
- Mauvais-Jarvis, F., Clegg, D. J., & Hevener, A. L. (2013). The Role of Estrogens in Control of Energy Balance and Glucose Homeostasis. *Endocrine Reviews*, *34*(3), 309-338. doi:10.1210/er.2012-1055
- McCarthy, D. J., & Smyth, G. K. (2009). Testing significance relative to a fold-change threshold is a TREAT. *Bioinformatics*, *25*(6), 765-771. doi:10.1093/bioinformatics/btp053
- McGillicuddy, F. C., Chiquoine, E. H., Hinkle, C. C., Kim, R. J., Shah, R., Roche, H. M., . . . Reilly, M. P. (2009). Interferon Attenuates Insulin Signaling, Lipid Storage, and Differentiation in Human Adipocytes via Activation of the JAK/STAT Pathway. *Journal of Biological Chemistry*, *284*(46), 31936-31944. doi:10.1074/jbc.m109.061655
- McHugh, R., Whitters, M., Piccirillo, C., Young, D., Shevach, E., Collins, M., & Byrne, M. (2002). CD4(+)CD25(+) immunoregulatory T cells: gene expression analysis reveals a functional role for the glucocorticoid-induced TNF receptor. *Immunity*, *16*(2).
- McPherson, R. C., Turner, D. G., Mair, I., O'Connor, R. A., & Anderton, S. M. (2015). T-bet Expression by Foxp3(+) T Regulatory Cells is Not Essential for Their Suppressive Function in CNS Autoimmune Disease or Colitis. *Front Immunol*, *6*, 69. doi:10.3389/fimmu.2015.00069
- Miller, A. M., Asquith, D. L., Hueber, A. J., Anderson, L. A., Holmes, W. M., McKenzie, A. N., . . . Liew, F. Y. (2010). Interleukin-33 induces protective effects in adipose tissue inflammation during obesity in mice. *Circ Res*, *107*(5), 650-658. doi:10.1161/circresaha.110.218867

- Miragaia, R. J., Gomes, T., Chomka, A., Jardine, L., Riedel, A., Hegazy, A. N., . . . Teichmann, S. A. (2019). Single-Cell Transcriptomics of Regulatory T Cells Reveals Trajectories of Tissue Adaptation. *Immunity*, *50*(2), 493-504 e497. doi:10.1016/j.immuni.2019.01.001
- Molofsky, A. B., Nussbaum, J. C., Liang, H.-E., Van Dyken, S. J., Cheng, L. E., Mohapatra, A., . . . Locksley, R. M. (2013). Innate lymphoid type 2 cells sustain visceral adipose tissue eosinophils and alternatively activated macrophages. *Journal of Experimental Medicine*, *210*(3), 535-549. doi:10.1084/jem.20121964
- Molofsky, A. B., Van Gool, F., Liang, H. E., Van Dyken, S. J., Nussbaum, J. C., Lee, J., . . . Locksley, R. M. (2015). Interleukin-33 and Interferon-gamma Counter-Regulate Group 2 Innate Lymphoid Cell Activation during Immune Perturbation. *Immunity*, *43*(1), 161-174. doi:10.1016/j.immuni.2015.05.019
- Moreau, J., Dhariwala, M., Gouirand, V., Boda, D., Boothby, I., Lowe, M., . . . MD, R. (2021). Regulatory T cells promote innate inflammation after skin barrier breach via TGF- $\beta$  activation. *Science Immunology*, *6*(62).
- Morita, H., Arae, K., Unno, H., Miyauchi, K., Toyama, S., Nambu, A., . . . Nakae, S. (2015). An Interleukin-33-Mast Cell-Interleukin-2 Axis Suppresses Papain-Induced Allergic Inflammation by Promoting Regulatory T Cell Numbers. *Immunity*, *43*(1), 175-186. doi:10.1016/j.immuni.2015.06.021
- Moro, K., Yamada, T., Tanabe, M., Takeuchi, T., Ikawa, T., Kawamoto, H., . . . Koyasu, S. (2010). Innate production of T(H)2 cytokines by adipose tissue-associated c-Kit(+)/Sca-1(+) lymphoid cells. *Nature*, *463*(7280), 540-544. doi:10.1038/nature08636
- Morrison, S. F., Madden, C. J., & Tupone, D. (2014). Central neural regulation of brown adipose tissue thermogenesis and energy expenditure. *Cell Metab*, *19*(5), 741-756. doi:10.1016/j.cmet.2014.02.007
- Munoz-Rojas, A. R., & Mathis, D. (2021). Tissue regulatory T cells: regulatory chameleons. *Nat Rev Immunol*, *21*(9), 597-611. doi:10.1038/s41577-021-00519-w
- Murano, I., Barbatelli, G., Parisani, V., Latini, C., Muzzonigro, G., Castellucci, M., & Cinti, S. (2008). Dead adipocytes, detected as crown-like structures, are prevalent in visceral fat depots of genetically obese mice. *J Lipid Res*, *49*(7), 1562-1568. doi:10.1194/jlr.M800019-JLR200
- Muzumdar, R., Allison, D. B., Huffman, D. M., Ma, X., Atzmon, G., Einstein, F. H., . . . Barzilai, N. (2008). Visceral adipose tissue modulates mammalian longevity. *7*(3), 438-440. doi:10.1111/j.1474-9726.2008.00391.x
- Nishimura, S., Manabe, I., Takaki, S., Nagasaki, M., Otsu, M., Yamashita, H., . . . Nagai, R. (2013). Adipose Natural Regulatory B Cells Negatively Control Adipose Tissue Inflammation. *Cell Metab*. doi:10.1016/j.cmet.2013.09.017
- Noval Rivas, M., Burton, O. T., Wise, P., Charbonnier, L. M., Georgiev, P., Oettgen, H. C., . . . Chatila, T. A. (2015). Regulatory T cell reprogramming toward a Th2-cell-like lineage impairs oral tolerance and promotes food allergy. *Immunity*, *42*(3), 512-523. doi:10.1016/j.immuni.2015.02.004
- Nutsch, K., Chai, J. N., Ai, T. L., Russler-Germain, E., Feehley, T., Nagler, C. R., & Hsieh, C. S. (2016). Rapid and Efficient Generation of Regulatory T Cells to Commensal

- Antigens in the Periphery. *Cell Rep*, 17(1), 206-220.  
doi:10.1016/j.celrep.2016.08.092
- O'Rourke, R. W., White, A. E., Metcalf, M. D., Winters, B. R., Diggs, B. S., Zhu, X., & Marks, D. L. (2012). Systemic inflammation and insulin sensitivity in obese IFN-gamma knockout mice. *Metabolism*, 61(8), 1152-1161.  
doi:10.1016/j.metabol.2012.01.018
- O'Sullivan, T. E., Rapp, M., Fan, X., Weizman, O.-E., Bhardwaj, P., Adams, N. M., . . . Sun, J. C. (2016). Adipose-Resident Group 1 Innate Lymphoid Cells Promote Obesity-Associated Insulin Resistance. *Immunity*, 45(2), 428-441.  
doi:10.1016/j.immuni.2016.06.016
- Oboki, K., Ohno, T., Kajiwara, N., Arae, K., Morita, H., Ishii, A., . . . Nakae, S. (2010). IL-33 is a crucial amplifier of innate rather than acquired immunity. *Proc Natl Acad Sci U S A*, 107(43), 18581-18586. doi:10.1073/pnas.1003059107
- Odegaard, J. I., Ricardo-Gonzalez, R. R., Goforth, M. H., Morel, C. R., Subramanian, V., Mukundan, L., . . . Chawla, A. (2007). Macrophage-specific PPAR $\gamma$  controls alternative activation and improves insulin resistance. *Nature*, 447(7148), 1116-1120. doi:10.1038/nature05894
- Ohkura, N., Kitagawa, Y., & Sakaguchi, S. (2013). Development and Maintenance of Regulatory T cells. 38(3), 414-423. doi:10.1016/j.immuni.2013.03.002
- Ohnmacht, C., Park, J., Cording, S., Wing, J., Atarashi, K., Obata, Y., . . . Eberl, G. (2015). The microbiota regulates type 2 immunity through ROR $\gamma$ <sup>+</sup> T cells. *Mucosal Immunology*, 28(349), 989-993.
- Osborn, O., & Olefsky, J. M. (2012). The cellular and signaling networks linking the immune system and metabolism in disease. *Nature Medicine*, 18(3), 363-374.  
doi:10.1038/nm.2627
- Ouyang, W., Ranganath, S. H., Weindel, K., Bhattacharya, D., Murphy, T. L., Sha, W. C., & Murphy, K. M. (1998). Inhibition of Th1 Development Mediated by GATA-3 through an IL-4-Independent Mechanism. *Immunity*, 9(5), 745-755.  
doi:10.1016/S1074-7613(00)80671-8
- Palmer, B. F., & Clegg, D. J. (2015). The sexual dimorphism of obesity. *Mol Cell Endocrinol*, 402, 113-119. doi:10.1016/j.mce.2014.11.029
- Panchanathan, R., Shen, H., Zhang, X., Ho, S. M., & Choubey, D. (2010). Mutually positive regulatory feedback loop between interferons and estrogen receptor-alpha in mice: implications for sex bias in autoimmunity. *PLoS One*, 5(5), e10868. doi:10.1371/journal.pone.0010868
- Panduro, M., Benoist, C., & Mathis, D. (2016). Tissue Tregs. *Annu Rev Immunol*, 34, 609-633. doi:10.1146/annurev-immunol-032712-095948
- Park, H. J., Park, H. S., Lee, J. U., Bothwell, A. L., & Choi, J. M. (2016). Sex-Based Selectivity of PPAR $\gamma$  Regulation in Th1, Th2, and Th17 Differentiation. *Int J Mol Sci*, 17(8). doi:10.3390/ijms17081347
- Park, W. Y., Park, J., Lee, S., Song, G., Nam, I. K., Ahn, K. S., . . . Um, J. Y. (2022). PEX13 is required for thermogenesis of white adipose tissue in cold-exposed mice. *Biochim Biophys Acta Mol Cell Biol Lipids*, 1867(1), 159046.  
doi:10.1016/j.bbalip.2021.159046

- Picard, F., Kurtev, M., Chung, N., Topark-Ngarm, A., Senawong, T., Machado De Oliveira, R., . . . Guarente, L. (2004). Sirt1 promotes fat mobilization in white adipocytes by repressing PPAR-gamma. *Nature*, *429*(6993).
- Piconese, S., Valzasina, B., & Colombo, M. P. (2008). OX40 triggering blocks suppression by regulatory T cells and facilitates tumor rejection. *J Exp Med*, *205*(4), 825-839. doi:10.1084/jem.20071341
- Punkosdy, G. A., Blain, M., Glass, D. D., Lozano, M. M., O'Mara, L., Dudley, J. P., . . . Shevach, E. M. (2011). Regulatory T-cell expansion during chronic viral infection is dependent on endogenous retroviral superantigens. *Proc Natl Acad Sci U S A*, *108*(9), 3677-3682. doi:10.1073/pnas.1100213108
- Qiang, L., Wang, L., Kon, N., Zhao, W., Lee, S., Zhang, Y., . . . Accili, D. (2012). Brown remodeling of white adipose tissue by SirT1-dependent deacetylation of Ppargamma. *Cell*, *150*(3), 620-632. doi:10.1016/j.cell.2012.06.027
- Ribas, V., Nguyen, M. T. A., Henstridge, D. C., Nguyen, A. K., Beaven, S. W., Watt, M. J., & Hevener, A. L. (2010). Impaired oxidative metabolism and inflammation are associated with insulin resistance in ER -deficient mice. *AJP Endocrinology and Metabolism*, *298*(2), E304-E319. doi:10.1152/ajpendo.00504.2009
- Ritchie, M. E., Phipson, B., Wu, D., Hu, Y., Law, C. W., Shi, W., & Smyth, G. K. (2015). limma powers differential expression analyses for RNA-sequencing and microarray studies. *Nucleic Acids Res*, *43*(7), e47. doi:10.1093/nar/gkv007
- Rocha, V. Z., Folco, E. J., Sukhova, G., Shimizu, K., Gotsman, I., Vernon, A. H., & Libby, P. (2008). Interferon- $\gamma$ , a Th1 Cytokine, Regulates Fat Inflammation: A Role for Adaptive Immunity in Obesity. *Circ Res*, *103*(5), 467-476. doi:10.1161/circresaha.108.177105
- Rodeheffer, M. S., Birsoy, K., & Friedman, J. M. (2008). Identification of white adipocyte progenitor cells in vivo. *Cell*, *135*(2), 240-249. doi:10.1016/j.cell.2008.09.036
- Rosen, E. D., & Spiegelman, B. M. (2014). What We Talk About When We Talk About Fat. *Cell*, *156*(1-2), 20-44. doi:10.1016/j.cell.2013.12.012
- Rosen, E. D. S., B. M. (2013). What We Talk About When We Talk About Fat: Cell. doi:doi:10.1016/j.cell.2013.12.012
- Rouault, C., Pellegrinelli, V., Schilch, R., Cotillard, A., Poitou, C., Tordjman, J., . . . Lacasa, D. (2013). Roles of chemokine ligand-2 (CXCL2) and neutrophils in influencing endothelial cell function and inflammation of human adipose tissue. *Endocrinology*, *154*(3), 1069-1079. doi:10.1210/en.2012-1415
- Rudra, D., Deroos, P., Chaudhry, A., Niec, R. E., Arvey, A., Samstein, R. M., . . . Rudensky, A. Y. (2012). Transcription factor Foxp3 and its protein partners form a complex regulatory network. *Nature Immunology*, *13*(10), 1010-1019. doi:10.1038/ni.2402
- Rüegg, J., Cai, W., Karimi, M., Kiss, N. B., Swedenborg, E., Larsson, C., . . . Pongratz, I. (2011). Epigenetic Regulation of Glucose Transporter 4 by Estrogen Receptor  $\beta$ . *Molecular Endocrinology*, *25*(12), 2017-2028. doi:10.1210/me.2011-1054
- Sakaguchi, S., Fukuma, K., Kuribayashi, K., & Masuda, T. (1985). Organ-specific autoimmune diseases induced in mice by elimination of T cell subset. I. Evidence for the active participation of T cells in natural self-tolerance; deficit

- of a T cell subset as a possible cause of autoimmune disease. *Journal of Experimental Medicine*, 161(1), 72-87. doi:10.1084/jem.161.1.72
- Sakaguchi, S., Sakaguchi, N., Asano, M., Itoh, M., & Toda, M. (1995). Immunologic self-tolerance maintained by activated T cells expressing IL-2 receptor alpha-chains (CD25). Breakdown of a single mechanism of self-tolerance causes various autoimmune diseases. Retrieved from <http://www.jimmunol.org/content/155/3/1151.long>
- Sakaguchi, S., Yamaguchi, T., Nomura, T., & Ono, M. (2008). Regulatory T Cells and Immune Tolerance. *Cell*, 133(5), 775-787. doi:10.1016/j.cell.2008.05.009
- Sanjabi, S., Oh, S. A., & Li, M. O. (2017). Regulation of the Immune Response by TGF-beta: From Conception to Autoimmunity and Infection. *Cold Spring Harb Perspect Biol*, 9(6). doi:10.1101/cshperspect.a022236
- Schiering, C., Krausgruber, T., Chomka, A., Frohlich, A., Adelman, K., Wohlfert, E. A., . . . Powrie, F. (2014). The alarmin IL-33 promotes regulatory T-cell function in the intestine. *Nature*, 513(7519), 564-568. doi:10.1038/nature13577
- Schmidleithner, L., Thabet, Y., Schönfeld, E., Köhne, M., Sommer, D., Abdullah, Z., . . . Beyer, M. (2019). Enzymatic Activity of HPGD in Treg Cells Suppresses Tconv Cells to Maintain Adipose Tissue Homeostasis and Prevent Metabolic Dysfunction. *Immunity*, 50(5), 1232-1248.e1214. doi:10.1016/j.immuni.2019.03.014
- Schmitz, J., Owyang, A., Oldham, E., Song, Y., Murphy, E., McClanahan, T. K., . . . Kastelein, R. A. (2005). IL-33, an Interleukin-1-like Cytokine that Signals via the IL-1 Receptor-Related Protein ST2 and Induces T Helper Type 2-Associated Cytokines. *Immunity*, 23(5), 479-490. doi:10.1016/j.immuni.2005.09.015
- Schubert, L. A., Jeffery, E., Zhang, Y., Ramsdell, F., & Ziegler, S. F. (2001). Scurfin (FOXP3) acts as a repressor of transcription and regulates T cell activation. *J Biol Chem*, 276(40), 37672-37679. doi:10.1074/jbc.M104521200
- Sefik, E., Geva-Zatorsky, N., Sungwhan, O., Liza, K., David, Z., Abigail, M. M., . . . Christophe, B. (2015). Individual intestinal symbionts induce a distinct population of RORg+regulatory T cells. *Science*.
- Shi, H., & Chi, H. (2019). Metabolic Control of Treg Cell Stability, Plasticity, and Tissue-Specific Heterogeneity. *Front Immunol*, 10, 2716. doi:10.3389/fimmu.2019.02716
- Shime, H., Odanaka, M., Tsuiji, M., Matoba, T., Imai, M., Yasumizu, Y., . . . Yamazaki, S. (2020). Proenkephalin(+) regulatory T cells expanded by ultraviolet B exposure maintain skin homeostasis with a healing function. *Proc Natl Acad Sci U S A*, 117(34), 20696-20705. doi:10.1073/pnas.2000372117
- Shu, C. J., Benoist, C., & Mathis, D. (2012). The immune system's involvement in obesity-driven type 2 diabetes. *Semin Immunol*, 24(6), 436-442. doi:10.1016/j.smim.2012.12.001
- Siracusa, M. C., Overstreet, M. G., Housseau, F., Scott, A. L., & Klein, S. L. (2008). 17beta-estradiol alters the activity of conventional and IFN-producing killer dendritic cells. *J Immunol*, 180(3), 1423-1431. doi:10.4049/jimmunol.180.3.1423

- Smigielski, K. S., Richards, E., Srivastava, S., Thomas, K. R., Dudda, J. C., Klonowski, K. D., & Campbell, D. J. (2014). CCR7 provides localized access to IL-2 and defines homeostatically distinct regulatory T cell subsets. *211*(1), 121-136. doi:10.1084/jem.20131142
- Smith, E. P., Boyd, J., Frank, G. R., Takahashi, H., Cohen, R. M., Specker, B., . . . Korach, K. S. (1994). Estrogen Resistance Caused by a Mutation in the Estrogen-Receptor Gene in a Man. *New England Journal of Medicine*, *331*(16), 1056-1061. doi:10.1056/nejm199410203311604
- Soh, Y. Q., Alfoldi, J., Pyntikova, T., Brown, L. G., Graves, T., Minx, P. J., . . . Page, D. C. (2014). Sequencing the mouse Y chromosome reveals convergent gene acquisition and amplification on both sex chromosomes. *Cell*, *159*(4), 800-813. doi:10.1016/j.cell.2014.09.052
- Spallanzani, R. G., Zemmour, D., Xiao, T., Jayewickreme, T., Li, C., Bryce, P. J., . . . Mathis, D. (2019). Distinct immunocyte-promoting and adipocyte-generating stromal components coordinate adipose tissue immune and metabolic tenors. *Science Immunology*, *4*(35), eaaw3658. doi:10.1126/sciimmunol.aaw3658
- Stolarczyk, E., Vong, C. T., Perucha, E., Jackson, I., Cawthorne, M. A., Wargent, E. T., . . . Howard, J. K. (2013). Improved insulin sensitivity despite increased visceral adiposity in mice deficient for the immune cell transcription factor T-bet. *Cell Metab*, *17*(4), 520-533. doi:10.1016/j.cmet.2013.02.019
- Stuart, T., Butler, A., Hoffman, P., Hafemeister, C., Papalexi, E., Mauck, W. M., 3rd, . . . Satija, R. (2019). Comprehensive Integration of Single-Cell Data. *Cell*, *177*(7), 1888-1902 e1821. doi:10.1016/j.cell.2019.05.031
- Sullivan, B. M., Juedes, A., Szabo, S. J., Von Herrath, M., & Glimcher, L. H. (2003). Antigen-driven effector CD8 T cell function regulated by T-bet. *100*(26), 15818-15823. doi:10.1073/pnas.2636938100
- Sullivan, J. M., Hollbacher, B., & Campbell, D. J. (2019). Cutting Edge: Dynamic Expression of Id3 Defines the Stepwise Differentiation of Tissue-Resident Regulatory T Cells. *J Immunol*, *202*(1), 31-36. doi:10.4049/jimmunol.1800917
- Sun, W. H., Keller, E. T., Stebler, B. S., & Ershler, W. B. (1998). Estrogen Inhibits Phorbol Ester-Induced Ikb $\alpha$  Transcription and Protein Degradation. *Biochemical and Biophysical Research Communications*, *244*(3), 691-695. doi:<https://doi.org/10.1006/bbrc.1998.8324>
- Szabo, S. J., Kim, S. T., Costa, G. L., Zhang, X., Fathman, C. G., & Glimcher, L. H. (2000). A Novel Transcription Factor, T-bet, Directs Th1 Lineage Commitment. *100*(6), 655-669. doi:10.1016/s0092-8674(00)80702-3
- Szabo, S. J., Sullivan, B. M., Peng, S. L., & Glimcher, L. H. (2003). MOLECULAR MECHANISMS REGULATING T H 1 IMMUNE RESPONSES. *21*(1), 713-758. doi:10.1146/annurev.immunol.21.120601.140942
- Takahashi, M., Kamei, Y., & Ezaki, O. (2005). Mest/Peg1 imprinted gene enlarges adipocytes and is a marker of adipocyte size. *Am J Physiol Endocrinol Metab*, *288*(1), E117-124. doi:10.1152/ajpendo.00244.2004
- Tan, T. G., Mathis, D., & Benoist, C. (2016). Singular role for T-BET+CXCR3+regulatory T cells in protection from autoimmune diabetes. *Proceedings of the National Academy of Sciences*, *113*(49), 14103-14108. doi:10.1073/pnas.1616710113

- Tang, Q., & Bluestone, J. A. (2008). The Foxp3+ regulatory T cell: a jack of all trades, master of regulation. *Nature Immunology*, *9*(3), 239-244. doi:10.1038/ni1572
- Tassi, E., Garman, K. A., Schmidt, M. O., Ma, X., Kabbara, K. W., Uren, A., . . . Wellstein, A. (2018). Fibroblast Growth Factor Binding Protein 3 (FGFBP3) impacts carbohydrate and lipid metabolism. *Sci Rep*, *8*(1), 15973. doi:10.1038/s41598-018-34238-5
- Tchkonia, T., Morbeck, D. E., Von Zglinicki, T., Van Deursen, J., Lustgarten, J., Scrable, H., . . . Kirkland, J. L. (2010). Fat tissue, aging, and cellular senescence. *9*(5), 667-684. doi:10.1111/j.1474-9726.2010.00608.x
- Teh, P. P., Vasanthakumar, A., & Kallies, A. (2015). Development and Function of Effector Regulatory T Cells. *Prog Mol Biol Transl Sci*, *136*, 155-174. doi:10.1016/bs.pmbts.2015.08.005
- The Emerging Risk Factors, C. (2010). Diabetes mellitus, fasting blood glucose concentration, and risk of vascular disease: a collaborative meta-analysis of 102 prospective studies. *The Lancet*, *375*(9733), 2215-2222. doi:10.1016/s0140-6736(10)60484-9
- Thornton, A. M., Korty, P. E., Tran, D. Q., Wohlfert, E. A., Murray, P. E., Belkaid, Y., & Shevach, E. M. (2010). Expression of Helios, an Ikaros Transcription Factor Family Member, Differentiates Thymic-Derived from Peripherally Induced Foxp3+ T Regulatory Cells. *184*(7), 3433-3441. doi:10.4049/jimmunol.0904028
- Tindemans, I., Serafini, N., Di Santo, J. P., & Hendriks, R. W. (2014). GATA-3 function in innate and adaptive immunity. *Immunity*, *41*(2), 191-206. doi:10.1016/j.immuni.2014.06.006
- Ting, C.-N., Olson, M. C., Barton, K. P., & Leiden, J. M. (1996). Transcription factor GATA-3 is required for development of the T-cell lineage. *Nature*, *384*(6608), 474-478. doi:10.1038/384474a0
- Townsend, M. J., Weinmann, A. S., Matsuda, J. L., Salomon, R., Farnham, P. J., Biron, C. A., . . . Glimcher, L. H. (2004). T-bet Regulates the Terminal Maturation and Homeostasis of NK and V $\beta$ 14<sup>+</sup> NKT Cells. *Immunity*, *20*(4), 477-494. doi:10.1016/S1074-7613(04)00076-7
- Tramunt, B., Smati, S., Grandgeorge, N., Lenfant, F., Arnal, J. F., Montagner, A., & Gourdy, P. (2020). Sex differences in metabolic regulation and diabetes susceptibility. *Diabetologia*, *63*(3), 453-461. doi:10.1007/s00125-019-05040-3
- Tran, T. T., & Kahn, C. R. (2010). Transplantation of adipose tissue and stem cells: role in metabolism and disease. *Nature Reviews Endocrinology*, *6*(4), 195-213. doi:10.1038/nrendo.2010.20
- Tran, T. T., Yamamoto, Y., Gesta, S., & Kahn, C. R. (2008). Beneficial Effects of Subcutaneous Fat Transplantation on Metabolism. *Cell Metabolism*, *7*(5), 410-420. doi:10.1016/j.cmet.2008.04.004
- Travers, R. L., Motta, A. C., Betts, J. A., Bouloumié, A., & Thompson, D. (2015). The impact of adiposity on adipose tissue-resident lymphocyte activation in humans. *International Journal of Obesity*, *39*(5), 762-769. doi:10.1038/ijo.2014.195

- Tsui, C., Kretschmer, L., Rapelius, S., Gabriel, S. S., Chisanga, D., Knopper, K., . . . Kallies, A. (2022). MYB orchestrates T cell exhaustion and response to checkpoint inhibition. *Nature*. doi:10.1038/s41586-022-05105-1
- Usui, T., Preiss, J. C., Kanno, Y., Yao, Z. J., Bream, J. H., O'Shea, J. J., & Strober, W. (2006). T-bet regulates Th1 responses through essential effects on GATA-3 function rather than on IFNG gene acetylation and transcription. *Journal of Experimental Medicine*, 203(3), 755-766. doi:10.1084/jem.20052165
- van den Brink, S. C., Sage, F., Vertesy, A., Spanjaard, B., Peterson-Maduro, J., Baron, C. S., . . . van Oudenaarden, A. (2017). Single-cell sequencing reveals dissociation-induced gene expression in tissue subpopulations. *Nat Methods*, 14(10), 935-936. doi:10.1038/nmeth.4437
- van Loosdregt, J., Brunen, D., Fleskens, V., Pals, C. E., Lam, E. W., & Coffey, P. J. (2011). Rapid temporal control of Foxp3 protein degradation by sirtuin-1. *PLoS One*, 6(4), e19047. doi:10.1371/journal.pone.0019047
- van Loosdregt, J., Vercoulen, Y., Guichelaar, T., Gent, Y. Y., Beekman, J. M., van Beekum, O., . . . Coffey, P. J. (2010). Regulation of Treg functionality by acetylation-mediated Foxp3 protein stabilization. *Blood*, 115(5), 965-974. doi:10.1182/blood-2009-02-207118
- Varghese, M., Griffin, C., & Singer, K. (2017). The Role of Sex and Sex Hormones in Regulating Obesity-Induced Inflammation. In (pp. 65-86): Springer International Publishing.
- Varlamov, O., White, A. E., Carroll, J. M., Bethea, C. L., Reddy, A., Slayden, O., . . . Roberts, C. T. (2012). Androgen Effects on Adipose Tissue Architecture and Function in Nonhuman Primates. *Endocrinology*, 153(7), 3100-3110. doi:10.1210/en.2011-2111
- Vasanthakumar, A., Chisanga, D., Blume, J., Gloury, R., Britt, K., Henstridge, D. C., . . . Kallies, A. (2020). Sex-specific adipose tissue imprinting of regulatory T cells. *Nature*, 579(7800), 581-585. doi:10.1038/s41586-020-2040-3
- Vasanthakumar, A., Liao, Y., Teh, P., Pascutti, M. F., Oja, A. E., Garnham, A. L., . . . Kallies, A. (2017). The TNF Receptor Superfamily-NF-kappaB Axis Is Critical to Maintain Effector Regulatory T Cells in Lymphoid and Non-lymphoid Tissues. *Cell Rep*, 20(12), 2906-2920. doi:10.1016/j.celrep.2017.08.068
- Vasanthakumar, A., Moro, K., Xin, A., Liao, Y., Gloury, R., Kawamoto, S., . . . Kallies, A. (2015). The transcriptional regulators IRF4, BATF and IL-33 orchestrate development and maintenance of adipose tissue-resident regulatory T cells. *Nat Immunol*, 16(3), 276-285. doi:10.1038/ni.3085
- Vasanthakumar, A., Moro, K., Xin, A., Liao, Y., Gloury, R., Kawamoto, S., . . . Kallies, A. (2015). The transcriptional regulators IRF4, BATF and IL-33 orchestrate development and maintenance of adipose tissue-resident regulatory T cells. *Nature Immunology*, 16(3), 276-285. doi:10.1038/ni.3085
- Vitali, A., Murano, I., Zingaretti, M. C., Frontini, A., Ricquier, D., & Cinti, S. (2012). The adipose organ of obesity-prone C57BL/6J mice is composed of mixed white and brown adipocytes. *J Lipid Res*, 53(4), 619-629. doi:10.1194/jlr.M018846

- Voo, K. S., Wang, Y. H., Santori, F. R., Boggiano, C., Wang, Y. H., Arima, K., . . . Liu, Y. J. (2009). Identification of IL-17-producing FOXP3+ regulatory T cells in humans. *Proc Natl Acad Sci U S A*, *106*(12), 4793-4798. doi:10.1073/pnas.0900408106
- Wang, Q. A., Tao, C., Gupta, R. K., & Scherer, P. E. (2013). Tracking adipogenesis during white adipose tissue development, expansion and regeneration. *Nat Med*, *19*(10), 1338-1344. doi:10.1038/nm.3324
- Wang, Y., Gao, M., Zhu, F., Li, X., Yang, Y., Yan, Q., . . . Chen, Z. (2020). METTL3 is essential for postnatal development of brown adipose tissue and energy expenditure in mice. *Nat Commun*, *11*(1), 1648. doi:10.1038/s41467-020-15488-2
- Wang, Y., Maureen, & Yisong. (2011). An Essential Role of the Transcription Factor GATA-3 for the Function of Regulatory T Cells. *Immunity*, *35*(3), 337-348. doi:10.1016/j.immuni.2011.08.012
- Wang, Y., Misumi, I., Gu, A. D., Curtis, T. A., Su, L., Whitmire, J. K., & Wan, Y. Y. (2013). GATA-3 controls the maintenance and proliferation of T cells downstream of TCR and cytokine signaling. *Nat Immunol*, *14*(7), 714-722. doi:10.1038/ni.2623
- Watanabe, Y., Nagai, Y., Honda, H., Okamoto, N., Yanagibashi, T., Ogasawara, M., . . . Takatsu, K. (2019). Bidirectional crosstalk between neutrophils and adipocytes promotes adipose tissue inflammation. *FASEB J*, *33*(11), 11821-11835. doi:10.1096/fj.201900477RR
- Wei, G., Brian, Yagi, R., Jothi, R., Cui, K., Sharma, S., . . . Zhao, K. (2011). Genome-wide Analyses of Transcription Factor GATA3-Mediated Gene Regulation in Distinct Cell Types. *Immunity*, *35*(2), 299-311. doi:10.1016/j.immuni.2011.08.007
- Weisberg, S. P., McCann, D., Desai, M., Rosenbaum, M., Leibel, R. L., & Ferrante, A. W. (2003). Obesity is associated with macrophage accumulation in adipose tissue. *Journal of Clinical Investigation*, *112*(12), 1796-1808. doi:10.1172/jci19246
- Weiss, J., Bilate, A. M., Gobert, M., Ding, Y., Curotto De Lafaille, M. A., Parkhurst, C. N., . . . Lafaille, J. J. (2012). Neuropilin 1 is expressed on thymus-derived natural regulatory T cells, but not mucosa-generated induced Foxp3 + T reg cells. *209*(10), 1723-1742. doi:10.1084/jem.20120914
- Weiss, J. M., Bilate, A. M., Gobert, M., Ding, Y., Curotto de Lafaille, M. A., Parkhurst, C. N., . . . Lafaille, J. J. (2012). Neuropilin 1 is expressed on thymus-derived natural regulatory T cells, but not mucosa-generated induced Foxp3+ T reg cells. *J Exp Med*, *209*(10), 1723-1742, s1721. doi:10.1084/jem.20120914
- White, U. A., & Tchoukalova, Y. D. (2014). Sex dimorphism and depot differences in adipose tissue function. *Biochimica et Biophysica Acta (BBA) - Molecular Basis of Disease*, *1842*(3), 377-392. doi:10.1016/j.bbadis.2013.05.006
- Winer, S., Chan, Y., Paltser, G., Truong, D., Tsui, H., Bahrami, J., . . . Dosch, H. M. (2009). Normalization of obesity-associated insulin resistance through immunotherapy. *Nat Med*, *15*(8), 921-929. doi:10.1038/nm.2001
- Wing, J. B., & Sakaguchi, S. (2012). Multiple treg suppressive modules and their adaptability. *3*. doi:10.3389/fimmu.2012.00178
- Wing, J. B., Tanaka, A., & Sakaguchi, S. (2019). Human FOXP3(+) Regulatory T Cell Heterogeneity and Function in Autoimmunity and Cancer. *Immunity*, *50*(2), 302-316. doi:10.1016/j.immuni.2019.01.020

- Wohlfert, E. A., Grainger, J. R., Bouladoux, N., Konkell, J. E., Oldenhove, G., Ribeiro, C. H., . . . Belkaid, Y. (2011). GATA3 controls Foxp3<sup>+</sup> regulatory T cell fate during inflammation in mice. *Journal of Clinical Investigation*, *121*(11), 4503-4515. doi:10.1172/jci57456
- Wong, N., Fam, B. C., Cempako, G. R., Steinberg, G. R., Walder, K., Kay, T. W., . . . Andrikopoulos, S. (2011). Deficiency in Interferon- $\gamma$  Results in Reduced Body Weight and Better Glucose Tolerance in Mice. *Endocrinology*, *152*(10), 3690-3699. doi:10.1210/en.2011-0288
- Woods, S. C. G., Koro; Clegg, Deborah. (2003). Gender differences in the control of energy homeostasis. *Exp Biol Med*, *228*(10), 1175 - 1180. doi:10.1177/153537020322801012
- Worthington, J. J., Kelly, A., Smedley, C., Bauché, D., Campbell, S., Marie, J. C. T., & A., M. (2015). Integrin  $\alpha\beta 8$ -Mediated TGF- $\beta$  Activation by Effector Regulatory T Cells Is Essential for Suppression of T-Cell-Mediated Inflammation. *42*(5), 903-915. doi:10.1016/j.immuni.2015.04.012
- Wouters, K., Gaens, K., Bijnen, M., Verboven, K., Jocken, J., Wetzels, S., . . . Schalkwijk, C. G. (2017). Circulating classical monocytes are associated with CD11c<sup>+</sup> macrophages in human visceral adipose tissue. *Scientific Reports*, *7*(1), 42665. doi:10.1038/srep42665
- Wu, D., Han, J. M., Yu, X., Lam, A. J., Hoeppli, R. E., Pesenacker, A. M., . . . Levings, M. K. (2019). Characterization of regulatory T cells in obese omental adipose tissue in humans. *Eur J Immunol*, *49*(2), 336-347. doi:10.1002/eji.201847570
- Wu, D., Wong, C. K., Han, J. M., Orban, P. C., Huang, Q., Gillies, J., . . . Levings, M. K. (2020). T reg-specific insulin receptor deletion prevents diet-induced and age-associated metabolic syndrome. *J Exp Med*, *217*(8). doi:10.1084/jem.20191542
- Xu, H., Barnes, G. T., Yang, Q., Tan, G., Yang, D., Chou, C. J., . . . Chen, H. (2003). Chronic inflammation in fat plays a crucial role in the development of obesity-related insulin resistance. *Journal of Clinical Investigation*, *112*(12), 1821-1830. doi:10.1172/jci19451
- Yamamoto, M., Ko, L. J., Leonard, M. W., Beug, H., Orkin, S. H., & Engel, J. D. (1990). Activity and tissue-specific expression of the transcription factor NF-E1 multigene family. *Genes & Development*, *4*(10), 1650-1662. doi:10.1101/gad.4.10.1650
- Yang, B. H., Hagemann, S., Mamareli, P., Lauer, U., Hoffmann, U., Beckstette, M., . . . Lochner, M. (2016). Foxp3(+) T cells expressing ROR $\gamma$  represent a stable regulatory T-cell effector lineage with enhanced suppressive capacity during intestinal inflammation. *Mucosal Immunol*, *9*(2), 444-457. doi:10.1038/mi.2015.74
- Yang, X. O., Nurieva, R., Martinez, G. J., Kang, H. S., Chung, Y., Pappu, B. P., . . . Dong, C. (2008). Molecular antagonism and plasticity of regulatory and inflammatory T cell programs. *Immunity*, *29*(1), 44-56. doi:10.1016/j.immuni.2008.05.007
- Yu, F., Sharma, S., Edwards, J., Feigenbaum, L., & Zhu, J. (2015). Dynamic expression of transcription factors T-bet and GATA-3 by regulatory T cells maintains immunotolerance. *Nat Immunol*, *16*(2), 197-206. doi:10.1038/ni.3053

- Zemmour, D., Zilionis, R., Kiner, E., Klein, A. M., Mathis, D., & Benoist, C. (2018). Single-cell gene expression reveals a landscape of regulatory T cell phenotypes shaped by the TCR. *Nature Immunology*, *19*(3), 291-301. doi:10.1038/s41590-018-0051-0
- Zhang, D.-H., Cohn, L., Ray, P., Bottomly, K., & Ray, A. (1997). Transcription Factor GATA-3 Is Differentially Expressed in Murine Th1 and Th2 Cells and Controls Th2-specific Expression of the Interleukin-5 Gene. *Journal of Biological Chemistry*, *272*(34), 21597-21603. doi:10.1074/jbc.272.34.21597
- Zhang, H., Chen, X., & Sairam, M. R. (2012). Novel Genes of Visceral Adiposity: Identification of Mouse and Human Mesenteric Estrogen-Dependent Adipose (MEDA)-4 Gene and Its Adipogenic Function. *Endocrinology*, *153*(6), 2665-2676. doi:10.1210/en.2011-2008
- Zheng, W.-P., & Flavell, R. A. (1997). The Transcription Factor GATA-3 Is Necessary and Sufficient for Th2 Cytokine Gene Expression in CD4 T Cells. *Cell*, *89*(4), 587-596. doi:10.1016/s0092-8674(00)80240-8
- Zheng, Y., Chaudhry, A., Kas, A., Deroos, P., Kim, J. M., Chu, T.-T., . . . Rudensky, A. Y. (2009). Regulatory T-cell suppressor program co-opts transcription factor IRF4 to control TH2 responses. *Nature*, *458*(7236), 351-356. doi:10.1038/nature07674
- Zhou, X., Bailey-Bucktrout, S. L., Jeker, L. T., Penaranda, C., Martinez-Llordella, M., Ashby, M., . . . Bluestone, J. A. (2009). Instability of the transcription factor Foxp3 leads to the generation of pathogenic memory T cells in vivo. *Nat Immunol*, *10*(9), 1000-1007. doi:10.1038/ni.1774
- Zhu, J., Jankovic, D., Oler, A. J., Wei, G., Sharma, S., Hu, G., . . . Paul, W. E. (2012). The transcription factor T-bet is induced by multiple pathways and prevents an endogenous Th2 cell program during Th1 cell responses. *Immunity*, *37*(4), 660-673. doi:10.1016/j.immuni.2012.09.007